The Localisation and Regulation of Phosphatidylinositol-4-phosphate 5-Kinase Gamma Splice Variants and the Discovery of a New Mammalian Splice Variant, PIP5KIγ_v6

Yang Xia

PhD Thesis

Trinity College

and

Department of Pharmacology

University of Cambridge

Declaration

All the experiments described in this dissertation were carried out solely by the author unless otherwise stated, in the Department of Pharmacology, University of Cambridge, between January 2008 and September 2010. This dissertation is not substantially identical to any other submitted for a degree, diploma or other qualifications, and no part of it has been, or is currently being, submitted for any such degree, diploma or other qualifications. This dissertation does not exceed the prescribed limit of 60000 words.

Yang Xia

April 2011

Acknowledgments

It has been almost ten years since I first left China to pursue my passion in science. Every single day I miss my parents back at home. As the only child of the family, I was never blamed for not being able to look after them better all these years, nor did I have any pressure stopping me from doing what I loved. They have provided me with a world of freedom, far more than a son could have ever asked for. Thank you, Father and Mother, for you have always had faith in me. I dedicate this thesis to you both, with my sincerest and deepest love.

Summary

Type I PIP kinases (phosphatidylinositol 4-phosphate 5-kinases, PIP5Ks) catalyse the majority of cellular synthesis of $PI(4,5)P_2$. To date, three mammalian isoforms (α, β, γ) have been found. PIP5KIγ is subject to complex C-terminal splice variation, enhancing its transcriptional diversity through evolution and producing at least 5 known spliceoforms in the mammals[*].

This study addresses several important questions. (1) Several remarkable differences have been discovered between the neuronal splice variant PIP5KIγ_i3 and its close variant, Iγ_i2, whose peptide lacks a 26-AA insert near its C-terminus. This study attempts to map these behavioural differences onto motifs within the peptide insert. Furthermore, a site of point mutation is identified near the activation loop, which amplifies the above differences. (2) This study documents properties of the more recently discovered PIP5KIγ_i3, about which relatively little is known, for example, the regulation of its subcellular localisation, kinase activity and post-translational modifications. By site-directed mutagenesis and examining more closely several crucial motifs, insight is gained into the putative relationship between the enzyme's phosphorylation state, cellular localisation, lipid kinase activity and autophosphorylation. (3) The discovery of a new PIP5KIγ splice variant, Iγ_v6, is described. First discovered in rodents, PIP5KIγ_i6 encompasses the 26-AA insert of Iγ_i3, but lacks the common C-terminus of Iγ_i2 and Iγ_i3 which contains peptide motifs that have several roles *in vivo*. A polyclonal antibody against the C-terminus of Iγ_i6 was also developed. Preliminary characterisation of Iγ_i6 demonstrates a similar subcellular localisation, but a wider expression profile than its close relative, Iγ_i3, suggesting potentially differential functions across tissues and at various developmental stages. (4) The existence of Iγ_v3 and Iγ_v6 is also confirmed in humans. In light of recent findings of other novel human spliceoforms, this is shown to be a case of intra-exonic splicing producing "alternative 5' splice site" exons in the human. Overall, this thesis should help to better understand the regulation and physiological roles of PIP5KIγ and, specifically, its different splice variants.

List of Abbreviations

AA   amino acid(s)

ARF   ADP (adenosine diphosphate) ribosylation factor

ATP   adenosine triphosphate

AtT-20   a mouse anterior pituitary epithelial-like tumour cell line

bp   base pair(s)

CaM   calmodulin

cDNA   copied / complementary DNA

COS-7   an African green monkey SV40-transfected kidney fibroblast cell line

DAG   diacyl glycerol

ddH$_2$O   double-distilled H$_2$O

DNA   deoxyribonucleic acid

dsDNA   double-stranded DNA

FAK   focal adhesion kinase

FLAG   a polypeptide tag

FRAP   fluorescence recovery after photobleaching

FYVE   Fab1, YOTB, Vac1 and EEA1 homology domain

GAP   GTPase-activating protein

GFP   green fluorescence protein

GPCR   G-protein-coupled receptor

GTP   guanosine triphosphate

GTPase   GTP hydrolase

HEK-293   a human embryonic kidney cell line

HRP   horseradish peroxidase

IP$_3$ inositol 1,4,5-trisphosphate

LB   Luria-Bertani medium

MARCKS   myristoylated alanine-rich C kinase substrate

mRNA   messenger RNA

MW   molecular weight

nt   nucleotide(s)

PA   phosphatidic acid

PBS   phosphate-buffered saline

PC   phosphatidylcholine

PCR   polymerase chain reaction

PE   phosphatidylethanolamine

PH   pleckstrin homology

PI   phosphatidylinositol

PI(3,4,5)P$_3$ phosphatidylinositol 3,4,5-trisphosphate

PI(3,4)P$_2$ phosphatidylinositol 3,4-bisphosphate

PI(4,5)P$_2$ phosphatidylinositol 4,5-bisphosphate

PI3K   phosphatidylinositol 3-kinase

PI4P   phosphatidylinositol 4-phosphate

PI4K	phosphatidylinositol 4-kinase
PI5P	phosphatidylinositol 5-phosphate
PIP	phosphatidylinositol phosphate
PIP_2	refers only to $PI(4,5)P_2$ in this thesis
PIP_3	see $PI(3,4,5)P_3$
PIP4K	phosphatidylinositol-5-phosphate 4-kinase (*a.k.a.* Type II PIP kinase)
PIP5K	phosphatidylinositol-4-phosphate 5-kinase (*a.k.a.* Type I PIP kinase)
PKA	protein kinase A (*a.k.a.* cAMP-dependent protein kinase)
PKC	protein kinase C
PLC	phospholipase C
PLD	phospholipase D
PM	plasma membrane; *or* palmitoylation and myristoylation tag
PS	phosphatidylserine
RNA	ribonucleic acid
RPM	revolution(s) per minute
RT-PCR	reverse transcription PCR
SDS-PAGE	sodium dodecyl sulfate polyacrylamide gel electrophoresis
SNP	single-nucleotide polymorphism
TBS	Tris-buffered saline
TLC	thin-layer chromatography

List of Tables and Figures

Table of Contents

1. Introduction

1.1. Inositol Derivatives

1.1.1. Inositol and Inositol Phosphates

Inositol and inositol derivatives (inositides) have been an active topic of research for decades[1, 2]. A huge surge of interest in them has occurred in the lst 30 years, particularly since the discovery of IP_3 (inositol 1,4,5-trisphosphate) as a Ca^{2+}-mobilising second messenger[3]. Following this discovery, further exploration took place which led to the discovery of dozens of higher inositol phosphates and lipids.

The inositol phosphates are composed of inositol and phosphates and are therefore water-soluble. The inositol ring can be covalently bonded to a phosphate group at each of its 6 carbon positions, potentially allowing for the existence of more than sixty phosphate derivatives of inositol (see Figure 1 for some of those so far detected in cells). In this study, as with virtually all biological studies on inositol derivatives, I use the D-configuration for numbering the carbon atoms on the inositol ring[4]. The range of inositol phosphates is expanded by the possibility of adding pyrophosphates instead of monophosphates, resulting in derivatives such as IP_7 and IP_8. This thesis addresses the inositol lipids, of which there are, mercifully, fewer.
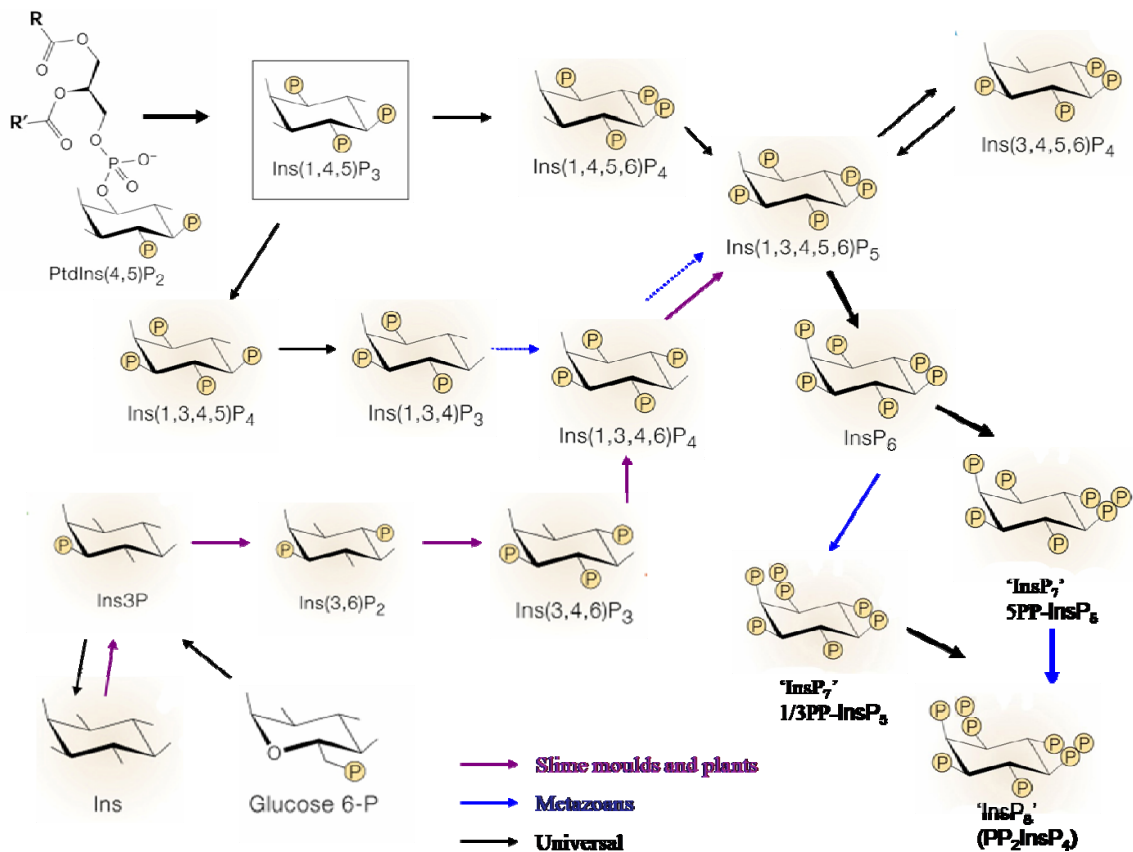
Figure 1 Eukaryotic inositol phosphate metabolism

Courtesy of Professor Robin Irvine (2008). Arrows in black indicate universal eukaryotic pathways, while pathways in purple and blue have only been identified in slime moulds/plants and metazoans, respectively, to date. In this figure, inositol is denoted as Ins (instead of I, which is adopted throughout the rest of this thesis).

1.1.2. Inositol-derived Lipids

It is speculated that inositol 3-phosphate may have been the first eukaryotic inositide to emerge, as a metabolic product from glucose 6-phosphate. Perhaps shortly after, the chemical combination (esterification) happened between inositol and activated phosphatidic acid (CMP-PA), to form the water-insoluble phosphatidylinositol (PI)[5]. In all eukaryotes, as far as we know, PI may be phosphorylated on the D-3, D-4 and

D-5 positions of the inositol ring, giving rise to 7 phosphorylated inositol lipids (Figure 2).

It is now widely appreciated that this diverse family of inositol phosphates and inositol lipids exists as a complex, interconnected metabolic network in the cell, and each member may be converted into others by a spectrum of more than 80 isoforms of kinases, phosphatases, phospholipases and so on. In this way, the inositides form a highly dynamic metabolic and signalling network in the cell, instead of a linear cascade as originally thought. They are important for many aspects of the cellular function, and here I will focus on those most relevant to the topic of this thesis, the phosphatidylinositol-4-phosphate 5-kinases (PIP5Ks).
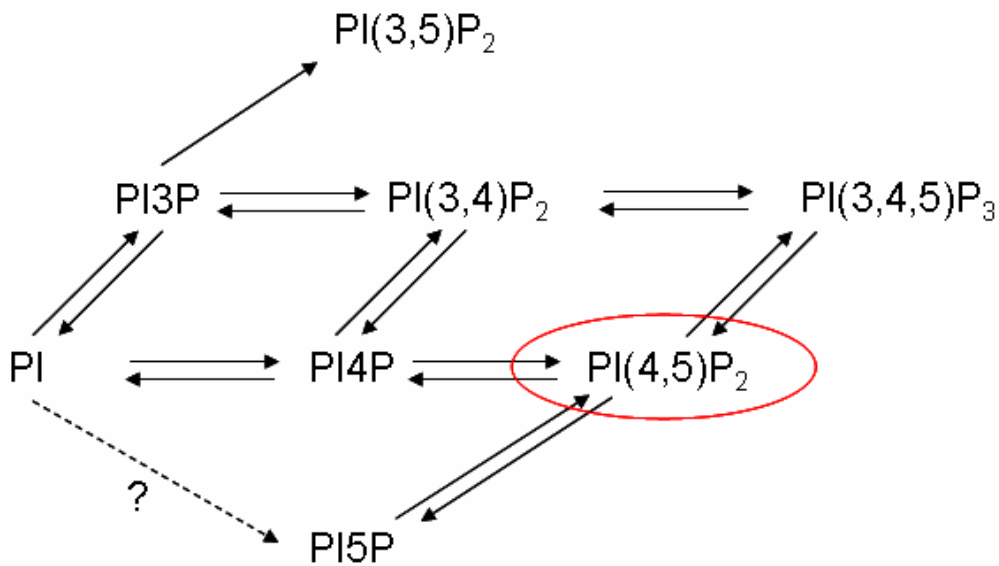
Figure 2 Inter-conversion of phosphorylated phosphatidylinositols
$PI(4,5)P_2$ is emphasised by a red circle in this complex signalling network of phosphoinositides.

1.1.3. Phosphatidylinositol 4,5-bisphosphate

Among the spectrum of inositol lipids (Figure 2), PI(4,5)P$_2$ (hereafter referred to as PIP$_2$) is a remarkably important signalling mediator that fulfils multiple intracellular functions. Its versatile roles are two-fold in principle. Firstly, it is the precursor of many second messengers including IP$_3$, diacylglycerol (DAG) (both generated by phospholipase C isoforms) and PI(3,4,5)P$_3$ (generated by Class I phosphoinositide 3-kinases, PI3Ks). These messengers produced, in turn, are crucial for very important cellular processes. For example, IP$_3$ releases Ca^{2+} from intracellular stores to raise the cytoplasmic concentration of Ca^{2+}[6], DAG activates Ca^{2+}/phospholipid-dependent protein kinase C[7], and PI(3,4,5)P$_3$ is a key player in signalling pathways controlling, for example, the cell cycle[8]. A further proliferation of cell mediators/messengers from PIP$_2$ stems from the conversion of IP$_3$ into the many inositol phosphates shown in Figure 1.

Secondly, PIP$_2$ itself regulates a number of events, such as actin cytoskeletal modelling, membrane vesicle trafficking, motility regulation, process formation, ion channel activity, gene expression and apoptosis. This largely depends on the ability of PIP$_2$ to interact with diverse proteins, for example actin-binding proteins, clathrin-dependent endocytic proteins, signal transduction proteins and enzymes such as phospholipase D and ARF GAP. These proteins contain PIP$_2$-binding domains, such as pleckstrin homology (PH), Fab1, YOTB, Vac1 and EEA1 (FYVE), phox homology (PX) and epsin N-terminal homology (ENTH) domains[9-13]. In the first studies, the importance of such binding properties was implicated in cytoskeleton organisation. Through interactions with actin-binding proteins such as profilin and gelsolin, PIP$_2$ was demonstrated to regulate the free actin monomer concentration[14], and fine-tune the balance between elongation and breakdown of actin filaments[15]. This can result in rapid and local actin polymerisation, subject to Ca^{2+} and pH modulation. PIP$_2$ was later identified as an upstream regulator of actin nucleation and an inducer of actin-based vesicle movement through the WASP-Arp2/3 pathway[16]. In addition, PIP$_2$-binding to vinculin leads to bundling of the distal ends of actin filaments in focal adhesion contacts[17]. Conversely, when cellular PIP$_2$ was reduced (by hydrolysis or protein/peptide sequestration), generally opposite effects were observed[17, 18].

4

More recently, the roles of PIP_2 have expanded into other areas of cell function. PIP_2 can either directly activate a target protein, as in the case of K_{ATP} channels[19] and phospholipase D[20], or help to recruit proteins such as epsin[21], AP180[22] and synaptotagmin-1[23] to PIP_2 pools near the plasma membrane (PM), and thereby affect cellular processes, such as endocytosis (priming for clathrin-coat formation), exocytosis and vesicle motility. Using optical tweezers tether force measurements, it was suggested that PIP_2 could control local adhesion energy between the PM and the underlying cytoskeleton, explaining the membrane dynamics and functional implications through its interactions with several cytoskeletal anchoring proteins, such as talin, vinculin and ERM family proteins[24].

The versatile functions of PIP_2 imply an important role of its synthetic enzymes, phosphatidylinositol-4-phosphate 5-kinases, which will be discussed later as the central object of this study, but first attention will be given to how PIP_2 could fulfil so many discrete roles.

1.1.4. Localisation of PIP_2 and Accummulation in Subcellular Microdomains

PIP_2 (along with PI4P) is the most abundant phosphoinositide at the plasma membrane[25]. Knowledge of PIP_2 localisation can help to further understand its specific local function, *e.g.* [26]. Moreover, the presence of PIP_2 at a specific subcellular location could imply the corresponding localisation of its synthetic enzyme(s), which is one of the main objectives of the present study.

In the classic view, PIP_2 is considered membrane-bound, primarily due to the hydrophobic nature of its phosphatidyl group on the D-1-position of inositol, which is a phosphoglycerol moiety linked to two long fatty acid chains. However, the overall level of intracellular PIP_2 does not usually seem to change greatly, as a result of the dynamic equilibrium between its upstream and downstream metabolic pathways. Instead, it is usually local changes that mediate distinct effects and convey salient

information[27]. PIP$_2$ is found in a variety of subcellular pools, serving a spectrum of functions that are potentially differentially regulated by various metabolic and signalling pathways. The local accumulation of PIP$_2$ is therefore important, and can be achieved by two mechanisms: lateral sequestration and local synthesis. I will discuss local PIP$_2$ synthesis later in Section 1.2.2, and here I focus on the former mechanism.

The lateral sequestration by either lipids, phosphoinoside-binding effectors and/or selective, reversible phosphoinositide-sinks relies largely on the intrinsic property of the membrane heterogeneity, as opposed to that described by the classic fluid mosaic model[28]. In 1973, phospholipids were found by spin-label measurements to be present in a quasicrystalline halo, which enclosed the relevant enzyme system[29]. Supporting evidence was soon added by various means such as X-ray diffraction, electron microscopy, lateral diffusion measurements, differential partitioning of lipid probes and differential scanning calorimetry (*e.g.* [30, 31]). These types of clusters or glycolipoprotein microdomains of lipids and proteins were later formalised into the concept of "lipid rafts"[32, 33], putative planar or caveolar structures with uncommon lipid composition (enriched in cholesterol and sphingolipids), which are themselves free floating in the membrane but are supposed to be more ordered and tightly packed than the surrounding phospholipid bilayer.

These structures exhibit locally regulated PIP$_2$ turnover and restricted diffusion-mediated exchanges with their environment. However, since inositol lipids typically contain polyunsaturated fatty acid tails (*e.g.* arachidonic acid), it is unlikely for them to partition in these rafts just through hydrophobic interactions. Indeed, variations in the cholesterol content alone seemed to have a dramatic modulatory effect on the membrane structure, which in turn influenced the mobility and function of the phosphoinositide kinases[34, 35]. Experimental techniques are starting to be able to isolate and discern the fine print of the content of these heterogeneous endomembrane systems, leading to useful structural and functional insight into the composition and signalling capacity of lipid rafts[36-42].

With the enriched lipids and associated proteins, the putative lipid rafts should not be regarded as mere sites for phosphoinositide storage, but rather as critical dynamic

membrane compartments for PIP_2 turnover and generation of derived second messengers in response to various agonists. We should, however, note that there are key controversies and caveats with the lipid raft theory. For example, the use of model systems *in vitro* implies inherent oversimplifications and limitations. A line tension that should in theory exist between the two postulated phases has never been directly observed in the cell system. There is no consensus on the size of the rafts, which currently is thought to span across a huge range of options (*e.g.* [43, 44]). The time scale of their existence is not known, therefore the rafts may not necessarily be relevant to biological processes. Furthermore, it is unclear how lipid rafts in the outer leaflet of the membrane bilayer could organise signal-transducing molecules in the inner leaflet[45]. Therefore, it may be more helpful to consider the rafts not as generalised, loosely defined structures, but as a helpful experimental system and thought framework that may be useful for addressing certain questions in appropriate contexts. Meanwhile, other plausible mechanisms were also proposed to support membrane heterogeneity, such as the trapping by the actin cytoskeleton[46], which would still be compatible with observations on phosphoinositide mobility[47].

In addition, through electrostatic interactions, PIP_2 can also be sequestered by proteins with a highly basic cluster of amino acids, such as MARCKS (myristoylated alanine-rich C kinase substrate)[48, 49]. These proteins are thought to be present at a high enough local concentration, and possess a high affinity for PIP_2, in order to sequester it[50]. Indeed, a recent study suggested that a major fraction of PIP_2 *in vivo* was bound by slow or immobile membrane components[51], which could be polybasic proteins interacting electrostatically with the phosphoinositide's head group. MARCKS, for instance, is myristoylated at its N-terminus, which anchors it into the plasma membrane in addition to other mechanisms such as a positively charged phosphorylation site domain[52]. It is itself reversibly controlled by PKC-mediated phosphorylation and binding to CaM, a mechanism for releasing the pre-formed PIP_2 pool following the appropriate signal[53]. It is hence possible for MARCKS to bind PIP_2 globally, but release it locally upon PKC activation or a rise in Ca^{2+}/CaM. Therefore, as well as being simple lipid backbones, phosphoinositides could often serve signalling functions, capable of rapidly interacting and recruiting specific effectors to help generate signals reliably.

Indeed, according to confocal microscopy using a GFP-conjugated pleckstrin-homology (PH) domain which preferentially binds to PIP_2, PIP_2 is mostly enriched in highly dynamic, actin-rich regions[54] or unidentified clusters in the PM[55-59]. The localisation of PIP_2 in caveolin-enriched membrane domains is supported by biochemical data[60]. In addition to the PM, there has been accumulating evidence confirming its presence (at low levels) also in the Golgi apparatus[58, 61-63], endosomes[58], the endoplasmic reticulum (ER)[58, 64] and the nucleus[58, 65]. The existence of such multiple, metabolically distinct subcellular PIP_2 pools means that different microenvironments (consisting of both proteins and lipids) may cater for differential metabolic and signalling reactions, in spite of the usually unchanging *total* cellular PIP_2 concentration[56, 66-69].

1.1.5. Localisation of PI4P

The localisation of PI4P has been perhaps even more controversial. After the early stages when PI4P was considered only an intermediate in the PIP_2 synthetic pathway, pioneering work showed that some processes regulated by PI4P could be dissociated from PIP_2, and that PI4P could also be a signalling molecule in its own right. Interestingly, most of the early discovered PI4P-binding proteins were localised to the Golgi complex[70]. This led to the initial assumption that PI4P was mostly present at the Golgi. However, more recent investigations into this phosphorylated inositol lipid and its binding proteins suggested a far wider distribution of PI4P, compartmentalised into metabolically distinct pools, including the PM, trans-Golgi-network, ER, endosomes, synapse and exocytic vesicles[68, 71-73].

A large number of metabolic regulators and effectors of PI4P have been investigated. Importantly, PI4P has a central role in anterograde membrane trafficking at the exit of the Golgi complex, as well as sphingomyelin and glycosphingolipid metabolism[74]. Therefore, PI4P appears to be a crucial regulator of the protein and lipid flux towards the cell surface, and hence it is in charge of the PM composition itself. Meanwhile, its presence at the PM has been directly demonstrated by immunocytochemistry using

carefully designed experimental protocols to visualise the PM[68]. As parallel evidence, a fraction of both PI4KIIα and IIβ were found at the PM, and this fraction (in the case of IIβ) increased upon Rac-dependent stimulation with growth factor[75]. In addition, PI4KIIIα was also implicated in the control of a plasma membrane pool of PI4P, with itself residing in the ER, at sites of close apposition to the PM[72]. A similar case of ER-localised Sac1-mediated PI4P break down at the plasma membrane was recently reported, activated by Osh3 proteins located at the ER/PM contact sites[76]. So the majority of PI4P is now suggested to reside in the PM[68], and this makes sense, as local pools of PI4P must serve as synthetic precursors for the conversion by PIP5Ks into membrane-bound PIP_2[77].

Having briefly described our present knowledge of the substrate and product of PIP5Ks, we need to bear in mind several caveats with the direct imaging of inositol lipids. **First**, the choice of inositide-binding domain from different proteins may possess additional targeting motifs that bias the detection. For example, the PH domain from PLCδ1 localises with the PIP_2 on the PM but fails to label the Golgi[78]. **Secondly**, low binding-specificity can cause an issue when a protein needs to distinguish among several morphologically similar inositol lipid species. PH domains fall into four categories based on their phosphoinositide binding specificity[79, 80], and despite those that specifically bind to PIP_3 and $PI(3,4)P_2$, exclusive $PI(4,5)P_2$-binding domains are not seen, although some do have high preference towards PIP_2. Multi-specific binding actually accounts for 85% of PH domains, some with significant regulatory roles, *e.g.* increasing affinity through oligomerisation[81]. As another example, PLCδ1-PH binds to IP_3 with at least 10 times higher affinity than to PIP_2 *in vitro*[82]. In fact, the PH domain of PLCδ initially binds PIP_2 with high affinity and specificity, leading to substrate recognition, which is then released due to competition from the IP_3 product formed during the catalytic reaction. It was initially observed using reporter PLCδ1-PH-GFP, that PIP_2 concentration at the PM could decrease transiently following PAF receptor stimulation[55]; however, this apparent translocation was more likely to be a reflection of the cytosolic increase in IP_3[83]. Therefore, proteins containing other phosphoinositide-binding domains may also be

explored that possess a suitable specificity (*e.g.* GAP1(IP4BP)[84, 85] and the transcription factor tubby[86]), as well as the antibiotic neomycin[87]. Another method used especially for cells not amenable to GFP-tagged probe transfection was by low temperature staining with a specific monoclonal antibody[65, 88]. Other methods such as fluorescence resonance energy transfer (FRET), total internal reflection fluorescence (TIRF), single molecule fluorescence microscopy, laser tweezer, nuclear magnetic resonance (NMR) and fluorescence correlation spectroscopy have also been used (for a review see [48]). **Thirdly**, binding of reporters may mask or distort the inositol lipid interaction with other endogenous proteins and/or interfere with regular cellular metabolism, thereby affecting its apparent physiological function[89, 90]. **Finally**, there may be a dependence of binding specificity on coincident factors *e.g.* ARF1[91, 92] or generally the *in vivo* environment[71].

Therefore, although it is informative and reassuring to have examined PI4P and PIP$_2$ localisation in the cell (particularly the PM-bound pools), this must be complemented by the direct detection of the actual PIP kinase protein.

1.2. Phosphatidylinositol Phosphate Kinases

1.2.1. The Spectrum of PIP Kinases

According to the canonical phosphoinositide pathway, PIP$_2$ synthesis is achieved through sequential phosphorylation of D-4 and D-5 positions of inositol, by PI 4-kinase (PI4K) and PI4P 5-kinase (PIP5K). Two PIP5Ks were originally isolated from erythrocytes by chromatographic procedures, and were found to have distinct immunological and biochemical properties[93]. The Type I PIP kinase had a 20 fold lower K$_m$ for PI4P than Type II, and was stimulated by phosphatidic acid, heparin and spermine[94]. It is now known that the "Type II PIP5K" had actually been misnamed, and was in fact a PI5P 4-kinase[95].

Therefore, the synthesis of $PI(4,5)P_2$ from PIP is mediated by two independent PIP kinase pathways. Type I PIP kinases (phosphatidylinositol 4-phosphate 5-kinases, hereafter referred to as PIP5K) phosphorylate PI4P on the D-5 position of the inositol ring, whereas Type II PIP kinases (phosphatidylinositol 5-phosphate 4-kinases, PIP4K) catalyse the phosphorylation of PI5P on the D-4 position. It is worth mentioning that PIP_2 could also be generated by specific dephosphorylation of D-3 position of $PI(3,4,5)P_3$ by the lipid phosphatase PTEN, but it is largely considered to terminate the PIP_3 signal instead of contributing to the functional PIP_2 pool, as it was from PIP_2 that the PIP_3 was largely synthesised.

Both types of PIP kinase actually possess broader substrate specificity than initially expected. For example, both types could phosphorylate PI3P, and Type I kinases can even phosphorylate PI3P on both D-4 and D-5 positions in a concerted double phosphorylation, leading to $PI(3,4,5)P_3$[96, 97]. Moreover, the Type I kinases can also use $PI(3,4)P_2$ and PI (though to a lesser extent) as the substrate *in vitro*[96]. In fact, the PIP kinase family has been through quite a few duplication events, and different paralogues have been divergently evolved to produce a whole array of related enzymes. Their kinase core domain have conserved catalytic residues for ATP and Mg^{2+} binding, spatially organised in a similar fashion to other lipid and protein kinases, implying a common phosphotransfer mechanism[98]. However, although PIP kinases are related between themselves, they share little sequence homology to other known phosphatidylinositide kinases or protein kinases[94, 99]. For example, another type of D-5 kinase preferably uses PI3P (and, to a much less extent, PI) as the substrate and shares no homology with Type I and II, so that the mammalian PIKfyve gene (orthologous to the yeast Fab1p) is proposed to be designated Type III.

PIP5KIα has a conserved kinase homology domain that is, for example, 35% identical to PIP4KIIα. A more stringent alignent between PIP4KIIβ (the only PIP kinase whose structure has been solved[98]) and other families of protein kinases (*e.g.* Fab1p, PI3K, PI4K, PKA[98], PK and ATP-grasp[100]) revealed structural similarity and short motifs reminiscent of protein kinases, despite the lack of significant primary sequence homology. Three residues were absolutely conserved across the kinases tested, *i.e.*, Lys^{150}, Asp^{278} and Asp^{369} (based on human IIβ)[98]. These residues were identified as

responsible for ATP-binding, weak base transfer and Mg^{2+}/Mn^{2+}-binding, respectively, just as in PKA. The rest of the enzyme also contained a flat membrane attachment site and a dimerisation interface[98, 101].

In intact cells, pulse-radiolabelling experiments suggest that PIP_2 is mostly synthesised via the Type I PIP kinase route[102]. This is consistent with the fact that PIP_2 and its main precursor PI4P are ubiquitous in eukaryotes, and PI4P is the most abundant monophosphorylated derivative of PI, compared to PI5P which only accounts for about 2% of cellular PIP[25, 95, 103, 104]. Functional interactions between Type I and II PIP kinases have been observed – for instance, Type IIα PIP kinase associates with the PM via interaction with Type I isoforms[105].

It has long been observed that all PIP5Ks are mainly localised to the plasma membrane (as well as to a lesser extent Golgi, vesicles and internal nuclear matrix), while PIP4Ks are typically cytosolic or nucleus-targeted[105-110], though the γ isoform associates with cellular vesicles[111]. It is clear that the nuclear phosphoinositide pools are independent of the cytosolic ones, likely to be regulating a unique set of cellular events. In this study I focus on the PIP5Ks outside the nucleus, which are typically found on the plasma membrane.

1.2.2. Physiological Regulation of PIP5K

I mentioned earlier in Section 1.1.4 that in addition to lateral sequestration by membrane microdomains, local synthesis of PIP_2 by PIP5Ks is another mechanism for obtaining differentially regulated PIP_2 pools. For example, transient accumulation of PIP_2 at phagosomes is attributable to local synthesis by PIP5Ks, where PIP5KIβ is recruited to produce a local, transient PIP_2 pool that in turn leads to negative feedback on the kinase through PLC[112].

Indeed, a coincidence detection mechanism was postulated for PIP5K to localise to the membrane and its specific compartments, by the electrostatic interactions with both its substrate (PI4P) and the negatively charged membrane[113]. Both PI4P-

binding and polycationic surfaces (formed by polybasic amino acid residues in PIP5K) are necessary for membrane localisation, while neither is sufficient on itself (also see later in Sections 1.3.3 and 1.3.4). In this way, the enzyme can be translocated to a membrane microdomain through a number of differentially regulated, low-affinity interactions. The membrane-binding energies of the domains often simply add in parallel, while the binding constants multiply[114]. At least three advantages are suggested to associate with such multi-motif interactions. 1) It promotes lateral organisation/sequestration; 2) It offers greater possibilities for reversible binding and adds extra layers of modulation; 3) It may underly synergistic, coincidence detection.

The anchoring of PIP5K to the membrane is physiologically important, as it then brings the enzyme into the surface phase, a few nm adjacent to the membrane, where the catalytic site can experience an approximately 1000x higher *effective* concentration of PIP$_2$, than if it was diffusing randomly through the cytoplasm[115-117]. Such a rise in local concentration is termed reduction in dimensionality[118]. This must also mean that the regulation of PIP5K localisation would have been critically implicated in determining their K$_m$ for substrate through evolution.

Additionally, membrane recruitment of PIP5K as a functional effector by the phosphoinositides is well supported by the mobility of other inositol lipid effectors. These were shown to have a relatively fast diffusion coefficient (~1 μm^2/s) and short membrane dissociation time (2–7 s), which meant that the lipid-protein complex could rapidly explore the membrane once recruited, and make thorough, functional interactions, yet not stray too far from the site of locally directed lipid synthesis[47].

The accurate and timely localisation of the kinase is hugely important for achieving the appropriate specific function, and is tightly regulated in addition to direct modulation of the kinase activity itself. *In vivo*, spatially and temporally organised PIP$_2$ synthesis by PIP5Ks is under sophisticated regulation of membrane receptors, phosphorylation and small Rho and ARF GTPases (both of the Ras superfamily), amongst other potential regulatory partners. Here I briefly touch upon these regulatory mechanisms in turn.

1) Membrane receptors. Upon pharmacological receptor activation, the formation of IP_3 by PLC can lower the cellular PIP_2 by as much as 80%[119], which then has to be regenerated in time to allow for reliable signalling through membrane receptors. Traditionally, modulation of PIP_2 synthesis by GPCR was investigated in platelets, where thrombin stimulation resulted in elevated PIP_2 formation and increased PIP5K association with the cytoskeleton[120]. Indeed, radiolabelling experiments suggested that PIP_2 synthesis (through strong and long-lasting potentiation of repeated PLC activation) can be stimulated by GPCR and receptor tyrosine kinases[121, 122].

In addition, PIP5K is found to associate during B cell receptor activation in lymphocytes with Btk, a Tec family non-receptor tyrosine kinase which is recruited onto the membrane (through its PH domain and independent of its kinase activity) and which ultimately joins PLC-γ2 to enable sustained calcium signalling[123]. Both Btk and PLC-γ2 are anchored by the PIP_3 produced by coincident activation of PI3K also docked in the complex, and the presence of PIP5K can therefore obviously ensure the local availability of PIP_2 as a common substrate for both PLC-γ2 and PI3K.

Both PI4K and PIP5K are also found to interact with the activated EGF receptor[124, 125]. Such stimulation and association could be a mechanism where PIP5K becomes assembled into signalling complexes in order to allow for efficient regulation, *e.g.* by PLC. Another example is the Wnt3A ligand, which activates PIP5KIβ through Frizzled and Dishevelled, both part of the Wnt receptor complex on the cell surface[126].

2) Phosphorylation. Some phosphoinositide enzymes (including PIP5Ks) possess intrinsic protein kinase activity, which can lead to the phosphorylation of amino acid residues on the kinase molecule itself and, ultimately, changes in its catalytic activity that is largely shared between the two related catalytic mechanisms[127].

Phosphorylation is generally seen to negatively affect the enzyme's kinase activity[127-129]. For instance, inactivation of PIP5Ks was observed with phosphorylation by PKA, and, in contrast, PIP5KIβ activity was stimulated by its dephosphorylation through protein phosphatase 1[129]. Key positive residues were demonstrated to be necessary for the interaction with the phospho-head group of the

substrate, and serine phosphorylation near these residues was proposed to perturb substrate binding, hence reducing the catalytic activity[130]. However, another study on the *Schizosaccharomyces pombe* Type I homologue implicated a decrease in catalytic activity to a lower V_{max} but no change in K_m[128], somewhat in conflict with the above hypothesis.

Alternatively, phosphorylation can also up-regulate the PIP5K in certain scenarios. As such potential regulatory mechanisms by protein phosphorylation are directly relevant to the present study, a more Iγ-related discussion will be presented in detail in Section 1.3.1, as well as Results I (Section 3.2.5).

3) Rho family GTPases. These small GTPases (such as Rho, Rac and Cdc42) control a wide spectrum of signalling pathways and have profound effects on cell morphology and the dynamics of the actin cytoskeleton, possibly partly through modulating phosphoinositide metabolism. Specific inactivation of Rho (which enhances PIP_2 synthesis) prevents the stimulation of PIP5K by GTP[131]. Dominant negative RhoA does not affect stress fibre induction by PIP5KIβ, demonstrating that PIP5K functions downstream of RhoA in actin organisation[132], later shown to be mediated by the RhoA effector, Rho-kinase[133]. This transduction pathway was more recently demonstrated in neurons, where neurite retraction induced by receptor agonists, RhoA and Rho-kinase was completely blocked by a kinase-inactive PIP5K mutant[134].

In contrast, a stimulatory effect on PIP5K activity by Cdc42 and Rac1 was specific, and independent of RhoA and Rho-kinase. Rac, for example, is a stimulator of PIP_2 synthesis, and PIP5Ks are critical mediators of Rac-dependent actin remodelling, leading to isoform-specific uncapping and polymerisation of actin filaments[135]. Catalytically-inactive PIP5KIβ blocked Rac-induced actin filament assembly[136] and membrane ruffle formation[137], again, functioning downstream of Rac. Rac has also been shown to contribute to targeting of PIP5Ks to the plasma membrane[138, 139], and this is explored in some detail later in this thesis. Interestingly, PIP5KIα was reciprocally proposed to be an upstream regulator of Rac1, controlling its integrin-induced translocation and activation[139]. Meanwhile, PI4KIIβ was also found to be activated by Rac and translocate to the plasma membrane[75]. Rac can therefore recruit and activate the enzymes responsible for colocalised PIP_2 synthesis at

the membrane, allowing for functions in specific cellular compartments (such as pollen tube elongation[140]).

All three PIP5K isoforms were also demonstrated to associate physically with RhoA and Rac1, but not Cdc42 or Rac2, both *in vivo* and *in vitro*[141]. Importantly, this association is independent of the nucleotide-binding state[142], while most other Rho GTPase effectors (*e.g.* PI3K) bind to the active, GTP-bound form exclusively[143]. It is important to note that such regulations of PIP5K by Rho GTPases can be under the control of membrane receptors and adhesion signals, allowing for *e.g.* receptor-mediated PIP5K activation and translocation, involving sequential activation of G_α, Rac1 and RhoA.

4) ARF family GTPases. ADP-ribosylation factor (ARF) GTPases regulate intracellular vesicle trafficking. PIP5K can be directly activated by ARF proteins in the presence of phosphatidic acid (PA)[144]. For example, PIP5K is recruited by ARF1 to the Golgi complex as its direct effector[62, 63]. ARF6 also colocalises with PIP5K in ruffling membranes and endosomal structures[145], and the regulation of PIP5K activity and localised PIP_2 turnover are critical for ARF6-induced membrane trafficking[145, 146].

During integrin-mediated phagocytosis, focal and transient accumulation of PIP_2 by PIP5K revealed efficient collaboration between Rac1 and ARF6, where Rac1 regulated the early recruitment of PIP5K, and ARF6 controlled the activity of membrane-docked kinase[147].

5) Other proteins. Many other factors regulate PIP5K too, besides the cases mentioned above. This is not surprising, since the cellular signalling pathways form a vast and complex network, in which PIP5K is an important node due to the versatile functions of PIP_2. For instance, PIP5K can associate with pRB (a master regulator of cell cycle progression from G1 into S-phase), and this induces its own activation and hence PIP_2 synthesis[148]. This can have important functions, since fractionation studies have demonstrated PIP5K activity in the inner nuclear matrix[106], later proposed to be nuclear speckles containing pre-mRNA processing factors[149]. Upon inhibition of mRNA transcription, both kinases and PIP_2 reorganise along with other

speckle components. Notably, the nuclear phosphoinositides are presented to their enzymes in a non-membranous form[150], perhaps bound to proteins by the hydrophobic tail, exposing the head group for interactions with other targets[151].

Another example is the Phospholipase D (PLD). PLD catalyses the hydrolysis of phosphatidylcholine (PC) into PA, as an alternative PA-generating route to 1,2-DAG conversion by diacylglycerol kinase (DGK). Both DGK- and PLD-generated PA is able to stimulate PIP5K activity *in vivo*[26]. On the other hand, PLD is crucially dependent on PIP5K and PIP_2[11, 152], and PLD1 is also directly regulated by Rho and ARF GTPases[153]. This interesting relationship between PIP5K and PLD of reciprocal stimulation and common regulation by the same GTPases allows for concerted positive feedback and feed-forward mechanisms leading to acute, localised PIP_2-synthesis.

1.2.3. Type I PIP Kinase Isoforms

To date, three mammalian Type I PIP kinase (PIP5K) genes (α, β, γ) have been found (Figure 4)[108, 154], sharing about 60% peptide sequence identity overall, and approximately 80% in the conserved central catalytic core. The amino- or carboxyl-terminal sequences, on the other hand, are less homologous between PIP5Ks, potentially underlying isoform-specific functions. The C-terminus exhibits alternative splicing and adds diversity to the versatile signalling potentials of the enzyme, *e.g.* interaction with talin (see Section 1.3.5 below). The N-terminus, on the other hand, is responsible for other regulatory mechanisms, *e.g.* Rac-binding[138]. In this study, I will investigate detailed C-terminal variations of PIP5KIγ, and also build upon the knowledge of this N-terminal Rac-interaction site on PIP5KIγ.

PIP5KIα and Iβ have an apparent MW of 68 kDa, while Iγ has several splice variants ranging from 87 to 100 kDa (see next Section). Figure 3 depicts the divergent evolution through gene duplication (resulting in paralogues) and speciation (resulting in orthologues in other organisms), using Iγ as an example. Note that the more distant proteins such as MSS4 (*Saccharomyces cerevisiae*), ppk-1 (*Caenorhabditis elegans*),

PIP5K59B and sktl (*Drosophila melanogaster*) are also homologous to the mammalian PIP5Ks (Figure 3). The yeast MSS4, for instance, is membrane-localised and is required for cell-cycle-dependent actin reorganisation and cell wall integrity, which is not complemented by Type II PIP4Ks[155, 156].
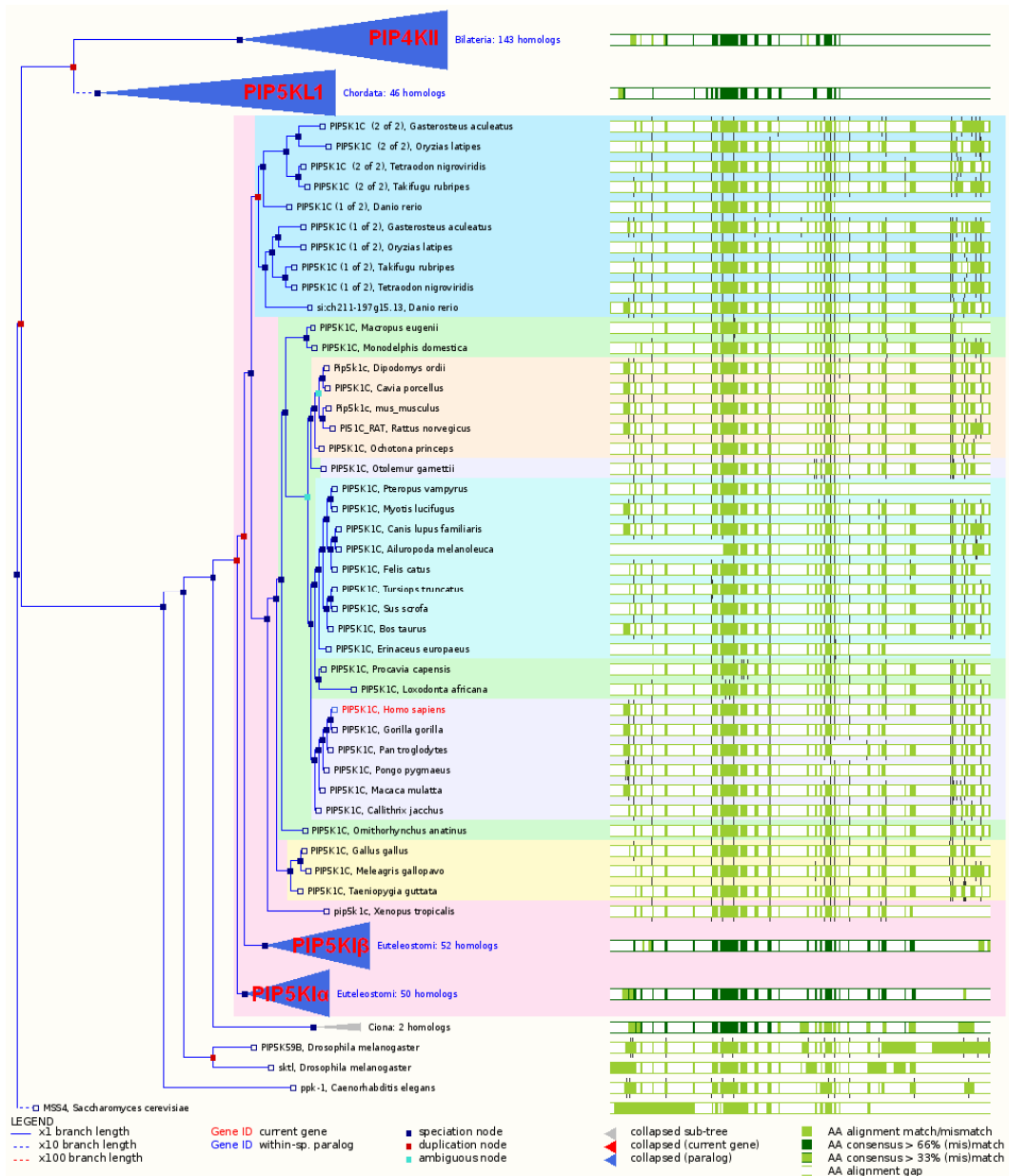
Figure 3 Gene tree illustrating the divergent evolution of PIP5KIγ

Image adapted from Ensembl. PIP5KIγ is denoted "PIP5K1C" by consensus. Orthologues of PIP5KIγ are expanded, while nodes corresponding to other paralogues of Iγ within the PIP kinase family are collapsed. Note that "PIP5KL1" is a class of generally non-active homologues to PIP kinases, whose physiological functions are still poorly understood.

Due to historical reasons, the names of Iα and Iβ genes were once reversed between humans and rodents. The human Iβ, at the time of naming by Loijens and Anderson, happened to be orthologous to the murine Iα as named by Ishihara and Shibasaki, and the human Iα to the murine Iβ[94, 154]. This unfortunate mismatch of isoform names caused considerable confusion, which accumulated in the literature until more recently (between April 2006 and October 2007), when the gene names of rodent (mouse and rat) isoforms were swopped to be consistent with those of the human counterparts (Table 1). Notably, the human PI5KIβ was in fact previously known as the STM7 gene, implicated in Friedreich's ataxia, which was later discovered to possess PIP5K activity[157].

For clarity, all names in the original literature are updated in this thesis to be consistent with the human system, based on the species used and the date of publication. Iγ, in contrast, was discovered later[108] and its naming has been consistent across the species (Figure 3).

PIP5K isoform	Gene name	Mouse (*Mus musculus*)	Rat (*Rattus norvegicus*)	Human (*Homo sapiens*)
Type I α	PIP5K1a	ENSMUSG00000028126 P70182	ENSRNOG00000021068 D3ZSI8	ENSG00000143398 Q99755
Type I β	PIP5K1b	ENSMUSG00000024867 P70181	ENSRNOG00000015232 Q5CZZ9	ENSG00000107242 O14986
Type I γ	PIP5K1c	ENSMUSG00000034902 O70161	ENSRNOG00000020577 Q5I6B8	ENSG00000186111 O60331

Table 1 Identity of Type I PIP5K genes in bioinformatic databases of the mouse, rat and human

For every gene isoform entry, the upper row denotes the Ensembl identifier, while the lower row shows the most representative UniProtKB/Swiss-Prot identifier. The table above quotes the current, updated names of all genes.

To a large extent, the three isoforms of Type I PIP5K appeared to share similar regulatory properties. For example, they are all stimulated by PA[108, 158], and negatively regulated by PI-dependent autophosphorylation[127] and PKA[129]. Moreover, they all show specific interactions with binding partners, such as Rho GTPases[141] and PIP4KIIα[105].

However, the presence of various isoforms certainly implies differential regulation by multiple signal transduction components, leading to various non-redundent PIP_2-modulated processes, likely dependent on the subcellular distribution of isoform-specific binding partners and discrete membrane microdomains. For example, it was suggested that ruffle formation in response to PDGF depended exclusively on the PIP_2 produced by translocated PIP5KIα, but not Iβ[137]. Iα was identified to be an upstream regulator of Rac1 in its integrin-induced translocation, a function not shared with other isoforms[139]. In contrast, only Iβ mediated Rac-dependent actin filament uncapping in permeabilised platelets, although both Iα and Iβ associated with Rac1 *in vitro*[136]. Knockdown of PIPKIβ (but no other isoforms) blocked adhesion turnover leading to the inhibition of cell migration[159]. In CV-1 cells, constitutive endocytosis specifically required the Iβ subtype, but not Iα or Iγ[160]. This is paralleled by the observation that the central kinase domain of Iα and Iγ (but not Iβ) was sufficient to prime endocytosis, correlated with their intrinsic lipid kinase activity[161]. Recently, a parallel study of all PIP5K isoforms revealed a striking redundancy of Iα and Iβ functions in the rapid synthesis of discrete pools of PIP_2, required for second messenger formation after GPCR stimulation of platelets. The presence of Iγ did not rescue the phenotype of a Iβ knockout. In contrast, Iγ knockout impaired the connection between cytoskeleton and PM in murine megakaryocytes, which was not reversed by Iβ overexpression[162]. Furthermore, a single allele of Iγ was sufficient to support life to adulthood in the absence of Iα and Iβ, and Iα (but not Iβ) supported prenatal development, while Iβ alone was implicated in neuronal differentiation[163]. The PIP_2 pools generated by different PIP kinase isoforms may therefore be differentially compartmentalised, and distinguished by the local membrane composition in which they are embedded.

Different isoforms can collaborate too. For instance, during phagocytosis, PIP5KIα regulates actin polymerisation and bacterial internalisation, and localises to the forming phagosome by electrostatic interactions with the phagocytic membrane, while Iγ is required for clustering receptors that interact with bacteria, both isoforms increasing the local PIP_2 concentration in the pseudopods[113].

Type I α and β isoforms are expressed in a relatively wide and partially overlapping range of tissues[94], implying ubiquitous functions in different cell types. Nevertheless, their differential localisation is also thought to be of functional significance. Type I γ expression, on the other hand, is largely confined to the kidney, the lung, and especially the brain[108] (highly expressed in focal adhesion sites[164] and nerve terminals[165]). This makes sense in light of neurobiology, that Iγ has been shown as the major PIP_2-synthesising enzyme at the synapse, and is probably crucial for clathrin-mediated endocytosis following synaptic vesicle secretion[165, 166], the maintenance of neuronal processes[167], adhesion junction formation and neuronal cell migration[168], as well as life from conception till at least before adulthood[163]. In other systems, knockdown of Iγ also suggested other functions, for example, in cardiovascular development[168]. Interestingly, many of its functions seemed to be splice variant-dependent.

1.2.4. Alternative Splicing of PIP5KIγ

Alternative splicing of pre-mRNA gives rise to more variability at the protein level, potentially a mechanism for increasing the diversity of inositol signalling and its regulation[169]. PIP5KIγ has 19 known exons and three splice variants identified in rodents prior to this study (Figure 5), namely γ90, γ87 and γ93 according to their apparent molecular weight (in kDa). These spliceoforms are also known as γ661, γ635 and γ687, respectively, indicating their (mouse) polypeptide length in amino acid residues. However, a recent publication reported two further splice variants of PIP5KIγ specific to humans, both with the Iγ87 core but unique C-termini largely unrelated to any of the above variants[170]. The authors named their novel splice

variants γ4 and γ5, while allowing for γ87, γ90 and γ93 to be renamed γ1, γ2 and γ3, respectively (Figure 4). According to the guidelines of the HUGO Genetic Nomenclature Committee, the mRNA of Iγ3, for example, is now denoted by Iγ_v3 and the protein Iγ_i3.

HUGO name (mRNA)	HGVS name (protein)	Corresponding exons (murine)	Previous names
Iγ_v1	Iγ_i1	1 – 16, 19	Iγ87, Iγ635, PIP5KIγb
Iγ_v2	Iγ_i2	1 – 16, 18, 19	Iγ90, Iγ661, PIP5KIγa
Iγ_v3	Iγ_i3	1 – 16, 17, 18, 19	Iγ93, Iγ687, PIP5KIγc
Iγ_v4	Iγ_i4	1 – 16, 16b*, 16c*	
Iγ_v5	Iγ_i5	1 – 16, 16c*	
Iγ_v6	Iγ_i6	1 – 16, 17, 19	#

Table 2 Summary of synonymous nomenclature of PIP5KIγ splice variants in the literature

* exists only in humans, not in the rodents where the corresponding inter-exonic region is much shorter and therefore homology cannot be established. # is discovered in the present study (see Results III and IV), and therefore has no previous names.

Table 2 provides a concise summary of synonymous names of PIP5KIγ splice variants in different naming systems. Hereafter, this thesis will consistently adopt the HUGO/HGVS nomenclature, when referring to the earlier literature and naming other newly discovered splice variants.

Among these spliceoforms, Iγ_v1 and Iγ_v2 were cloned earlier, at the time when PIP5KIγ was initially discovered[108]. Both contain the initial 16 exons (and end with Exon 19 that has a stop codon at its 5' end), with Iγ_i2 having an additional 26 amino acid "tail" at the C-terminus, corresponding to Exon 18 (Figure 5). To date, a significant amount is known about them, and their functions seem to be spliceoform-specific. For example, only Iγ_i2 interacts functionally with talin and is targeted to focal adhesion[171, 172] under the regulation of Src phosphorylation[164]. This ability to bind talin and other proteins *e.g.* AP-2 also leads to other roles, for example, in EGF-stimulated directional cell migration[173], integrity of membrane cytoskeleton in megakaryocytes[162], and endocytosis regulation[174, 175]. Moreover, Iγ_i2 binds directly to both E-cadherin and clathrin-adaptor protein complexes, enabling E-cadherin trafficking, whereas Iγ_i1 only binds to E-cadherin and is not sufficient to support trafficking on its own[176, 177]. While acting as a signalling scaffold for the adherens junction formation, Iγ_i2 also regulates trafficking events via the spatial generation of PIP_2. On the other hand, Iγ_i1 (but not Iγ_i2) is involved in PLD2 stimulation of integrin-mediated adhesion[11]. This clearly demonstrates in the specific case of PIP5KIγ, that alternative splicing is indeed a powerful way of generating functional diversity and regulatory complexity[178].
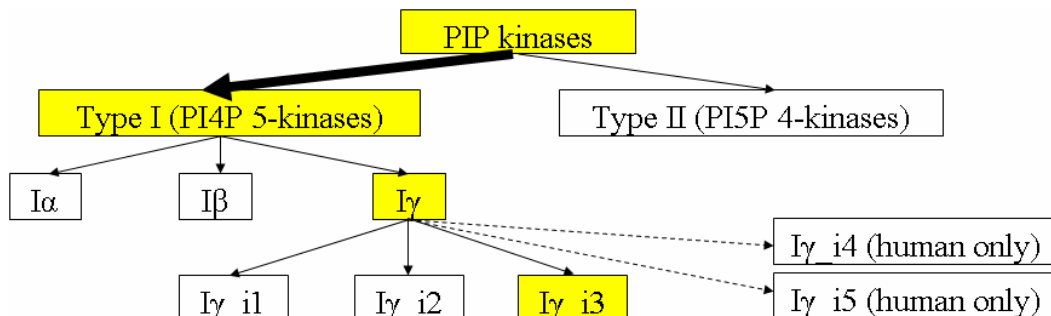
Figure 4 Schematic illustration of the Iγ_i3 splice variant in the PIP kinase family.

The third splice variant, Iγ_i3, was discovered more recently in our lab from the amplification of a rat hippocampal cDNA library (Figure 4)[167, 179]. It is similar to Iγ_i2, but has an additional 26 amino acid insert near the C-terminus, coded by Exon 17. This exon has a plausible counterpart in the human genome[138], implying that the Iγ_v3 spliceoform may also be present in humans, which we shall address later (see Results IV).

In the majority of this study, Iγ_i3 will be the focus of investigation, and in particular its tissue expression profiles and the regulation of its localisation, phosphorylation, lipid kinase activity and putative autophosphorylation.

Figure 5 Sequence of rat PIP5KIγ and schematic illustration of peptide features of its three splice variants

(**a**) Exon map of the rat PIP5KIγ gene, where the distances between available exons are drawn to scale. (**b**) Corresponding amino acid residue numbers (of the rat gene) are noted below Iγ_v3 as landmarks. The conserved kinase domain containing ATP-binding (Lys[188]) and weak base catalytic (Asp[316]) sites, as well as the conserved activation loop, constitutes the kinase homology domain. Another conserved site responsible for Mg^{2+}/Mn^{2+}-binding (Asp[398]) is not shown. Detailed sequence alignment of this region is presented in Figure 6. The 26-AA-long insert in Iγ_i3 and the 26-AA-long Iγ_i2 tail are also illustrated. (**c**) Sequence of the rat PIP5KIγ_v3 mRNA, illustrating exon junctions and numbering.

1.3. PIP5KIγ_i3

1.3.1. Phosphorylation

When detected by Western blot, wild type Iγ_i3 appeared as two bands, the slower running upper band completely disappearing after phosphatase treatment *in vitro* (unpublished observation by Dr Luisa Giudici; also see Results I). This mobility shift was also seen with Iγ_i2. Therefore, the presence of such two (or possibly more) bands in Western blot indicates, and conveniently assays, post-translational phosphorylation at one or multiple residues.

So far, several important residues have been implicated in talin-binding in focal adhesion assembly, which are under transient Src and MEK phosphorylation (see Section 1.3.5). However, these phosphorylation sites were dependent on the specific kinase involved, and, in the PIP kinase pulldown of mutants that were not phosphorylated by Src and MEK, the overall phosphorylation was not altered, indicating the importance of phosphorylation at other unidentified residues[164]. To date, these putative phosphorylation sites remain to be discovered.

Many lipid kinases (including all three PIP5K isoforms) have been demonstrated to show protein kinase activities, a classic example being PI3Ks[180]. It is still unclear whether the Iγ_i3's *in vivo* phosphorylation observed is entirely due to interactions with other proteins kinases, or partly as a result of its own autophosphorylation, as exemplified by the putative protein kinase activity of PIP5KIγ demonstrated *in vitro*[127]. Autophosphorylation is a widely observed phenomenon whereby a kinase can regulate its own activity, by inducing a conformational change through phosphorylation of the molecule itself (*cis*) or a dimerising partner (*trans*). Indeed, the crystal structure of PIP4KIIβ interacted with membranes over a large flat patch of positively charged interface, formed jointly by two subunits assembling a homodimer[98]. Two of such dimerisation domains were also later identified in PIP5KIβ[101]. Whether PIP5Ks autophosphorylate as monomers or crossphosphorylate as dimers is beyond the scope of the current study. In this study, I use the term autophosphorylation to mean the protein kinase activity of PIP kinases on

themselves without regard to mechanisms; whether they phosphorylated other protein substrates is also not a subject for investigation or discussion here.

Autophosphorylation could potentially be a mechanism for autoinhibition. Autoinhibition has been structurally demonstrated in the Src, Abl, ZAP-70, and FAK families of cytoplasmic protein tyrosine kinases, AGC serine/threonine kinases (such as PKA), receptor tyrosine kinases, and calcium/calmodulin-dependent protein kinases (CaMK). It can be mediated in unique ways, for instance, by a pseudosubstrate sequence in the case of PKA[181], a juxtamembrane segment in the receptor tyrosine kinases that occupies the catalytic cleft[182], or a C-terminal autoinhibitory helix-loop-helix segment in the case of CaMKI[183]. A classic case was seen where serine phosphorylation in the catalytic or associated regulatory subunit of PI3K down-regulated the enzyme[180].

Indeed, relevant to the current study, PI-dependent autophosphorylation of PIP5KIγ_i2 decreased its lipid kinase activity by ten-fold, indicating the possibility of PIP5K autophosphorylation inhibiting PIP_2 synthesis *in vivo*[127]. Depolarisation-dependent dephosphorylation of neuronal PIP5KIγ in synaptosomes was accompanied by an increase in phosphoinositide turnover[165]. In addition, it has been known that the binding of talin to PIP5KIγ_i2 activates the latter, probably by releasing autoinhibitory constraints in Iγ_i2's C-terminal tail[184]. In other words, the talin-binding site of Iγ (see Section 1.3.5) probably contributes to autoinhibitory interactions in the unactivated kinase.

On the other hand, phosphorylation on other motifs of PIP5K may well enhance its activity. For instance, PIP5K was suggested to be up-regulated by WASP-Arp2/3-mediated tyrosine phosphorylation[16], and focal adhesion kinase (FAK) phosohorylation on certain tyrosine residues of PIP5KIγ led to increased lipid kinase activity[164], either directly or via altered interactions with talin[171] (more discussion in Section 1.3.5).

1.3.2. Localisation

When we investigate the detailed localisation of PIP5KIγ_i3, it may be interesting to reflect on some insights given by its product PIP₂ and its substrate PI4P (see Sections 1.1.4 and 1.1.5 above). Logically, it would make sense for PIP5KIγ to localise to where its substrate is most available, and hence where its product is abundant as a result. Besides the discussions above on the localisation of PIP5Ks in general (Section 1.2.2), here we focus on the PIP5KIγ_i3-specific perspectives.

In situ hybridisation has shown that Iγ_v3 expression is confined to certain groups of neurons in the brain, such as the cortex, cerebellum and especially some major excitatory output neurons in the forebrain *e.g.* hippocampus and olfactory bulb[167]. *In situ* signals were also detected in the pituitary, primarily in the anterior part (adenohypophysis) (unpublished), although this is somewhat puzzling since it is the posterior pituitary that has a more typical neuronal origin. Overall, this neuronal and even class-specific expression pattern is in contrast to the other two spliceoforms, especially Iγ_i2 which is much more widely expressed. This suggests possibly unique functions of Iγ_i3 in the brain.

Since Iγ_i2 and Iγ_i3 share the same C-terminal 26 AA (*i.e.*, the Iγ_i2 tail), an antibody raised against their common C-terminus would not produce specific staining. This adds complexity to the earlier literatures (prior to Iγ_i3 discovery) on endogenous Iγ_i2 distribution that were based on antibody-binding. Therefore, in the present study, I use overexpression of GFP- or FLAG-tagged vectors in HEK-293 and COS-7 cells to provide a way of specifically detecting the spliceoform of interest. Despite the obvious caveat that Iγ_i3 is naturally expressed in neurons, the data obtained can shine indirect but informative light on the endogenously expressed Iγ_i3.

A fascinating finding was obtained in an earlier paper[179], from expression of the wild type Iγ_i3 and two different dominant negative (kinase-inactive) constructs. With both Iγ_i2 and Iγ_i3, the active enzyme was primarily at the PM. However, it was observed that the inactive Iγ_i3 was completely cytosolic, while the inactive Iγ_i2 counterpart remained largely membrane-bound, more similar to its active wild type. In

terms of how Iγ_i3's additional 26-AA insert might have produced this difference between inactive Iγ_i2 and Iγ_i3, one could imagine that the insert disrupts some important interaction required for membrane localisation (see next Section). However, even so, why this effect was uncovered only when the enzymes were inactive was not easily understood. The two inactivating mutations used, K188A and D316K, impaired the enzyme's ability to bind ATP and transfer proton via weak base, respectively, both independently required for its kinase activity[98]. Therefore, it was unlikely that the common cytosolic presence observed was due to a non-specific disruption of protein structure.

In addition, such different localisations also depended on the catalytic activity of the individual kinase molecule, instead of the overall intracellular PIP_2 produced. In an elegant control using cotransfection of active and inactive Iγ_i3, the inactive Iγ_i3 was still cytosolic as if transfected on its own[179]. In other words, the capability of active Iγ_i3 molecules to make PIP_2 in the cell did not rescue the non-membrane localisation of inactive Iγ_i3. Importantly, neither K118A nor D316K should affect the binding of the enzyme to its lipid substrate, PI4P, and therefore the effects on localisation observed should be independent of PI4P-binding at the membrane and genuinely activity-dependent.

1.3.3. Iγ_i3-specific Insert

Such activity- and insert-dependent differences in localisation required further investigation. What could the Iγ_i3-insert do that affects only the inactive Iγ_i3, but neither active Iγ_i3 nor active/inactive Iγ_i2, at least in its apparent membrane-targeting?

I thought that there might be a simple explanation for the difference. The 26-AA insert in Iγ_i3 may serve as a *PIP₂*-binding site. Indeed, this is consistent with the fact that the insert actually has a run of four arginine residues ($R^{648} - R^{651}$, shown in Figure 6c), whose positive charge may very well bind PIP_2 and enhance PM-association[185-188]. Such basic residues and consensus motifs were identified in

other phospholipid binding sequences such as PH, FYVE, PX and ENTH domains[9, 189-195], and other PI(3,4,5)P$_3$- and PIP$_2$-binding proteins could be targeted to the PM by their characteristic polybasic clusters[196]. Therefore, suppose there is an added mechanism in Iγ_i3, where the insert is (or is part of) a PIP$_2$-binding site which holds its own catalytic *product* in place once it is produced, and this conformational change in turn helps its localisation to the PM either directly or by interacting with other proteins. Inability to produce PIP$_2$ will at this level impair the interaction, and therefore make inactive Iγ_i3 (but not Iγ_i2) cytosolic.

As described later in this thesis, I generated a mutant "4R", which has all the four arginine residues within the insert mutated into glutamate, *i.e.*, RRRR(648,649,650,651)EEEE (Figure 6c) to address this issue. Also I used another mutant, "5P", which has all five potential phosphorylation targets in the insert abolished, hence preventing any phosphorylation happening within this peptide insert of Iγ_i3.

1.3.4. Activation Loop

Type I and Type II PIP kinases (*i.e.*, PIP5K and PIP4K) share sequence similarity clustered in the catalytic core, and little homology outside this region, potentially a mechanism allowing for distinct regulation. They also share 20–25 amino acids nearer to the C-terminus (Figure 5b), topologically corresponding to the activation loop in other kinases. The activation loops are highly conserved within the same PIP kinase subfamily, but are divergent between subfamilies (Figure 6a). Although the activation loop seems to be disordered in the crystal structure of IIβ, it spans the active site of the kinase and therefore implies an important role in substrate recognition, phosphate coordination on the inositol ring, and, ultimately, second messenger generation[98]. Meanwhile, the loop is adjacent to critical membrane-interaction interfaces (Figure 6b), potentially strategically positioned for subcellular targeting.

Earlier studies from Anderson's group showed that mutagenesis in the activation loop revealed crucial information regarding the localisation and substrate specificity of PIP

kinases. When the activation loop of PIP kinases Type Iβ and IIβ were swopped, the localisation appeared to correspond to the activation loop present, but not the remaining backbone of the enzyme[197]. Even more strikingly, a single amino acid substitution in the loop (A381E in IIβ and the reciprocal E362A in Iβ) changed the stero-specific substrate recognition[130]. It was suggested that Glu^{362} in the Iβ activation loop conferred selectivity by preventing interaction with the D-5 phosphate on inositol, either through electrostatic repulsion, or interaction with a positively charged residue. In addition, Glu^{362} also helped to orient the substrate in the catalytic core for specific phosphotransfer to the correct hydroxyl, demonstrated by moderate PIP kinase-chimera activity (V_{max}/K_m) arising from the Type I activation loop[130].

Meanwhile, the entire activation loop consensus of PIP5K seemed to be both necessary and sufficient for targeting PIP4KIIβ to the PM (when combined with the IIβ backbone), and PIP5KIβ with the IIβ loop appeared cytosolic. In contrast, while Iβ E362A was no longer membrane-bound, the reciprocal A381E point mutation above did not manage to target IIβ to the PM, despite the same binding affinity to PI4P and kinase activity to produce PIP$_2$ as that of the Iβ loop. This portion of the loop was implicated in high-affinity substrate-binding, and these data imply that efficient substrate binding by the activation loop alone is necessary, but not sufficient, for anchoring PIP5K to the PM[197]. For instance, a conserved dilysine motif is present in the N-terminus of the Type I activation loop (KK in Figure 6a), whose positive charge is likely to contribute to PM localisation. In fact, the membrane-attachment interface on a PIP5K dimer is a highly basic, exceptionally flat (and large) surface that extends right across the dimer interface[98]. In order to realise total PIP5K functions, additional features outside the activation loop must also be required (*e.g.* [198]).

These interesting roles of the activation loop raised one important question – previously, the absence of protein kinase activity in a lipid kinase-inactive PIP5KIβ mutant suggested the same catalytic mechanism in both activities[127], so the above inactive mutants should also have impaired autophosphorylation activity. Was it possible that an impaired general catalytic mechanism led to the dislocation from the membrane, instead of the inability to produce PIP$_2$? That is, the enzyme might require a conformational change upon binding ATP to expose further interaction sites[199],

or indeed undergo autophosphorylation (involving the general catalytic mechanism), which then brings it to the PM. As an alternative mechanism, binding to PI4P (and ARF) was shown to be able to enhance the Golgi-to-PM translocation of FAPP[92], potentially a mechanism for PM-targeting. To address this, Dr Luisa Giudici (unpublished) designed two rat PIP5KIγ mutants based on the human PIP5KIβ E362A in Kunz *et al.*[130], E410A and EH(410,411)AE, impairing the enzyme's ability to bind its PI4P substrate, while leaving the ATP-binding and general base catalysis intact.

Interestingly, preliminary studies by Giudici revealed a reduction in phosphorylation with EH(410,411)AE compared to E410A, and therefore, it was plausible that His^{411} might be adjacent to some phosphorylation site. An obvious candidate was residue Thr^{412}, right next to His^{411}(Figure 6a), therefore mutations T412D and T412A will also be generated in this study to explore further the regulatory mechanisms (Section 4.2).

a   Activation loop

```
IIDILQSYRFVKKLEHSWKALVHDGDT-----VSVHRP    H. sapiens Iα

IIDILQSYRLMKKLEHSWKALVYDGDT-----VSVHRP    H. sapiens Iβ

IIDILQSYRFIKKLEHTWKALVHDGDT-----VSVHRP    H. sapiens Iγ

IIDILQNYRLLKKMEHSWKAILHDGDT-----ISVHNP    C. elegans Type I

IIDILQSYRLEKKLEHTFKSILYNGDT-----VSVCRP    D. melanogaster skittles

IIDFLTSYSVMKKLETFWRSLRHDTKL-----VSAIPP    S. pombe MSS4

IIDLLTKYSYVKRVEHLWKGINHSDSV-----ISAVPP    S. cerevisae MSS4


IIDILTHYDAKKKAAHAAKTVKHGAGAE----ISTVNP    H. sapiens IIα

IIDILTPYDAKKKAAHAAKTVKHGAGAE----ISTVNP    H. sapiens IIβ

LIDILTQYDAKKKAAHAAKTVKHGAGAE----ISTVHP    H. sapiens IIγ

IIDVLTQYGVKKQAAKAAKTVKYGSNVDG---ISTCDP    D. melanogaster Type II


IIDFIRTFTWDKKLESWVKEKGLVGGASVIKQPTVVTP    S. cerevisiae Fab1

IIDYIRTFTWDKKLEMVVKSTGILGGQGKM--PTVVSP    M. musculus PIKfyve

IIDFMRQYTWDKHLETWVKASGILGGPKNAS-PTIVSP    A. thaliana Fab1

IVDYMRTYTLDKKLESWVKIVAIPGAHL----PTILSP    C. elegans Fab1
```

b

Activation loop

←

```
DTVSVHRPGFYAERFQRFMCNTVFKKIP---LKP          M. musculus Iα

DTVSVHRPSFYADRFLKFMNSRVFKKIQA--LKA          M. musculus Iβ

DTVSVHRPSFYAERFFKFMSSTVFRKSSS--LKS          M. musculus Iγ

DTVSVCRPSFYAKRFQDAMGKQVFKKTPTFPLKH          D. melanogaster

DTISVHNPNFYASRFLTFMTEKVFKKGTA--LKQ          C. elegans

KLVSAIPPRDYANRFYEFIEDSVDPLPQ---KKT          S. cerevisiae

. :*.   *   **.**   : . *           *
```

c

```
...STDIYFFAHGRYWLFSPRRRRLRAVTPSHTGAPTDERSWVYSPLHYSARPASDGESDT
631                                                       688
```

Figure 6 Segments from PIP kinase peptide sequences, illustrating important features
For an alignment of the complete peptide sequences of rat, mouse and human PIP5KIγ, as well as different human PIP kinase homologues, refer to the Appendix. (**a**) Multiple alignment of PIP kinase peptide sequences around the activation loop. Sequences are obtained from GenBankTM, alignement generated by ClustalW. Identical and similar amino acids conserved in all PIP kinase subfamilies are shaded in gray. Conserved residues within the activation loop of Type I PIP kinase and close relatives are shaded in green. Glu[410], His[411] and Thr[412] in Iγ_i3 are labelled by a box. (**b**) Site of Val[443] in Type I and related PIP kinases, shown in red, just downstream of the activation loop. Dibasic residues are shaded in grey. The relevance of this site will be discussed in Section 3.1. (**c**) Amino acid sequence of the C-terminal region of Iγ_i3, where the 26-AA insert specific to Iγ_i3 is underlined, followed by the 26-AA Iγ_i2 tail. Residue numbers (as in the rat version of Iγ_i3) are noted below the sequence. Note that the mouse numbering for residues in this C-terminal region is smaller by 1 than for the rat, *i.e.*, ending with Thr[687]. Within the insert, five putative phosphorylation sites are shaded in blue, and four adjacent arginine residues in red. SPLH domain in the tail is shaded in yellow, flanked by Tyr[671] and Tyr[676].

1.3.5. C-terminal tail

The 26-AA C-terminus shared by Iγ_i2 and Iγ_i3 is also an interesting region (Figure 6c). Research has shown that the SPLH domain is a talin-binding site, explaining why Iγ_i2 binds talin in an activity-independent fashion in focal adhesions[164, 171, 172] and Iγ_i1 does not, as it lacks Iγ_i2's 26-AA tail. Moreover, overexpression of this C-terminal tail results in loss of talin from focal contacts. This binding is competitive with the NPXY motif in β-integrin, whose interaction with talin is disrupted by Src phosphorylation. Meanwhile, Src phosphorylation also phosphorylates Iγ on the Tyr^{644} (numbering based on mouse Iγ_i2, equivalent to Tyr^{671} of rat Iγ_i3 as in Figure 6c) immediately preceding SPLH, enhancing its interaction with talin[164, 200]. Other tyrosine residues[201], *e.g.* the Tyr^{634}[173] and Tyr^{649}[184], have also been implicated, although they are perhaps less crucial. This provides a novel, non-NPXY-based phosphotyrosine recognition mode that outcompetes integrin-binding to talin FERM domain[202] upon Src phosphorylation. Such a molecular switch serves to enrich PIP_2 production for the regulation of focal adhesion assembly and integrin signalling. On the other hand, p35/Cdk5- and MAPK-mediated phosphorylation targets the Ser^{645} residue of the SPLH motif itself (mouse numbering, equivalent to Ser^{650} in humans), disrupting the PIP5KIγ binding to talin at the synapse[203]. Importantly, the phosphorylations of Tyr^{644} and the adjacent Ser^{645} antagonise each other, forming a crosstalking point between two independent signalling pathways, which is potentially critical for the balance between cell adhesion and cell motility at the synapse.

Interestingly, talin-binding activates Iγ_i2, probably by releasing autoinhibitory constraints due to the otherwise consititutively phosphorylated Ser^{645}[184]. Therefore, the C-terminal talin-binding region may be implicated in autoinhibitory interactions in the unactivated kinase, presumably acting as a pseudosubstrate (also see Section 1.3.1 above).

1.3.6. Other Functional Observations

Besides the above-mentioned localisation differences, functionally Iγ_i3 is also dramatically different from its close relative Iγ_i2. Expression of both dominant negative (kinase-inactive) constructs independently produced a detrimental effect on cellular morphology of rat cerebellar granule cells, including greatly shortened processes and increased cell death[167]. Again, interestingly, this striking effect of inactive enzymes appeared spliceoform-specific to Iγ_i3, since the two corresponding kinase-inactive mutants of Iγ_i2 did not produce a similar effect[167]. It was therefore suggested that Iγ_i3 may be responsible for the synthesis of a separate pool of PIP_2, required for the trafficking of cellular components, and hence essential in the maintenance of neuronal processes.

1.4. Aim of This Study

Despite the achievements described above, the regulation of Iγ_i3 and its differences compared to Iγ_i2 (and Iγ_i1) are still relatively poorly understood. This study builds upon the previous studies on PIP5KIγ_i3, and some emphasis is given to its 26-AA insert (which supposedly causes the difference between Iγ_i3 and Iγ_i2). With a natural mutation that is discovered in our previously used Iγ_v3 constructs, I turn it into a useful tool for investigating the fine details of the enzymes' various properties (Results I).

Meanwhile, a series of mutageneses is performed in an attempt to identify the crucial sites implicated in a range of properties, such as substrate binding, kinase activity and membrane association. Using these tools, I endeavour to understand further the relationship between its localisation, phosphorylation state, lipid kinase activity and putative autophosphorylation (Results II).

I also try to confirm the alternative splicing pattern of the PIP5KIγ gene in various rodent tissues (Results III), and investigate for the first time whether these are also present in humans (Results IV). As we shall see, a novel Iγ splice variant was

discovered from these studies. This potentially completes our knowledge base of PIP5KIγ's alternative splicing profile, and shines useful light onto the alternative splicing in rodents and especially humans.

An antibody developed against a Iγ_i3-specific peptide will be tested and optimised, as well as a co-immunoprecipitation protocol for PIP5K and Rac, which will become useful tools for further studies on the endogenous protein of the novel splice variant.

2. Materials and Methods

2.1. Plasmid Constructs

FLAG-constructs were based on the expression vector pCMV-2B, where a FLAG epitope tag (DYKDDDDK) was expressed at the N-terminus. GFP-constructs were based on pEGFP-C1, where an EGFP gene was fused upstream to the gene of interest. Gene expression in both vectors was driven by a pCMV promoter. The initial constructs containing PIP5KIγ were obtained as described in [167] and [179].

Both FLAG- and GFP-tagged vectors were selected by kanamycin resistance. Plasmids were amplified in XL10-Gold cells grown in Luria-Bertani (LB) Medium containing 50 μg/ml kanamycin.

2.2. RNA Extraction and Purification

Prior to the experiment, glass equipment was incubated in diethyl pyrocarbonate (DEPC) (Sigma) overnight at 37 °C, followed by autoclaving. Other non-disposal equipment was cleaned using RNaseZAP (Sigma). Fresh or frozen (in RNAlater RNA stabilization reagent, QIAGEN) tissues were homogenised in a Dounce homogeniser, using the RNeasy mini kit (QIAGEN).

2.3. DNA/RNA Quantification

The yield of nucleic acid was determined on a diode-array UV/vis spectrophotometer (S2000, WPA lightwave). The light path was 10 mm. dsDNA concentration (in μg/ml) = OD_{260} x 50. RNA concentration (in μg/ml) = OD_{260} x 44.

2.4. Polymerase Chain Reaction

Polymerase Chain Reaction (PCR) was performed using Taq DNA polymerase (Sigma) together with Pfu Turbo DNA polymerase (Stratagene), in a 4:1 molar ratio. For a 50 μl reaction, 1 μl (5 units) of enzyme was supplemented with 50 ng DNA template, 0.2 μM of each primer, 200μM each dNTPs and 1x reaction buffer (50 mM KCl, 10 mM Tris-HCl, 1.5 mM $MgCl_2$, pH 8.3). A typical thermal cycle consisted of 2 min at 95 °C, 25–30 cycles of 30 sec at 95 °C, 1 min at 55 °C and 1 min at 72 °C.

This was followed by 5 min at 72 °C, and 4 °C thereafter. Typical primer pairs were designed to be 18–22 bp in length, with a GC content of 50–60% and similar T_m, between 55–60 °C.

The rat hippocampal cDNA library was a gift from Dr Hilmar Bading. For the amplification from human tissues, the templates were obtained commercially (First Strand cDNA of human tissues, OriGene). The custom primers (Sigma) used are listed in Table 8 and Table 9 in the Results.

2.5. Reverse-transcription PCR

Access RT-PCR system (Promega) was used, with specific primers, to amplify the region of interest from RNA. Basic PCR and RT-PCR were carried out in one thermal reaction to produce double-stranded DNA fragments. RNA templates were obtained either from tissue extraction (see above, in the cases of rat pituitary and AtT-20) or commercially (mouse total RNA, Ambion). Primers were designed to span the junctions of two adjacent exons of the target, where possible, in order to avoid any potential contamination from genomic DNA. The pair of primers are designed to have similar GC content (> 40%) and T_m (> 78 °C). For a list of custom primers (Sigma) used, see Table 8 in the Results.

2.6. Site-directed Mutagenesis

Mutations were generated in the FLAG- and GFP-tagged vectors, using the QuikChange™ Site-Directed Mutagenesis kit (Stratagene). Typical PCR procedure included a 5 min hot start at 95 °C, followed by 16–18 cycles consisting of 30 sec denaturation at 95 °C, 1 min annealing at 55 °C, and 14 min elongation at 68 °C. Generally, primers were designed to anneal to the plasmid 10–15 bp on either side of the mutation site, with predicted T_m > 78 °C and GC content > 40%. For a list of custom primers (Sigma) used, refer to Table 3, Table 5, Table 6 and Figure 39 in the Results.

Amplified product was analysed on 0.7% (w/v, g/ml) agarose gel containing 0.5 µg/ml ethidium bromide, and the sample was digested for 1 hr in *DpnI* before proceeding to transformation. Vectors were selected to contain the desired mutation by sequencing of 2–3 single colonies on the transformation plates.

2.7. Agarose Gel Electrophoresis

0.7–1 g of agarose was resuspended in 100 ml Tris-buffer saline (TBS, containing 50 mM Tris, 140 mM NaCl, pH 7.5), heated to dissolve, topped up with 0.5 µg/ml ethidium bromide, and left to set in the gel tank at room temperature. DNA samples were loaded near the cathode in the loading dye (2.5% Ficoll-400, 11 mM EDTA, 3.3 mM Tris-HCl, 0.017% SDS, 0.015% bromophenol blue, pH 8.0). A voltage of typically 80 V was applied till the blue front line of the dye ran out of the gel. The separation pattern of the DNA bands could then be visualised and digitalised under the UV light.

2.8. Gel Extraction, Nucleotide Removal and PCR Purification

Gel extraction, nucleotide removal and PCR purification were performed using the corresponding QIAquick kits (QIAGEN).

2.9. Restriction Digestion and Ligation of DNA Vectors

Commercially available restriction enzymes (NEB) were used to linearise circular plasmid vectors following their recommended protocol. In cases where a linear piece of DNA was to be inserted between the restriction sites, shrimp alkaline phosphatase (NEB) was used to treat the linearised vector, prior to ligation using the Rapid DNA Ligation Kit (Roche) containing T4 DNA ligase.

2.10. Plasmid Purification

Plasmid was harvested from bacteria growing in LB medium at 37 °C, 24 hr after transformation, using either the QIAprep miniprep kit or the EndoFree plasmid maxi kit (QIAGEN). The latter method was preferentially used for plasmids that were subsequently used for transfection.

2.11. Competent Bacteria Preparation

E. coli XL10-Gold strain was grown in starting LB culture at 37 °C overnight. 1% was inoculated into 250 ml SOB medium (20 g/l tryptone, 5 g/l yeast extract, 8.6 mM NaCl, 2.5 mM KCl, 10 mM $MgCl_2$, pH7.0) plus 1% glycine, where the culture was left shaken at 18 °C until the OD_{600} reaches 0.5–0.6. Cells were washed twice with

ice-cold Transformation Buffer (10 mM PIPES, 55 mM $MnCl_2$, 15 mM $CaCl_2$, 250 mM KCl, pH 6–7), harvested at 2500 g, and resuspended in 40:3 (v/v) Transformation Buffer/DMSO. Aliquots were snap-frozen in liquid nitrogen, and stored at -80 °C.

2.12. Bacterial Transformation

A 200 μl aliquot of XL10-Gold competent cells were taken from -80 °C to thaw on ice. Typically, 1 μl of plasmid (or, in the case of site-directed mutagenesis, the *DpnI*-treated PCR product) was added to the cells, and allowed to sit on ice for 30 min. Heat shock was delivered as a 45 sec pulse at 42 °C. Cells were immediately put back on ice for 2 min, and then 500 μl of 37 °C SOC media was added (20 g/l tryptone, 5 g/l yeast extract, 8.6 mM NaCl, 2.5 mM KCl, 10 mM $MgCl_2$, 20 mM glucose, pH7.0). Samples were shaken at 37 °C for 1 hr, before being spread onto LB/Agar selection plates containing 50 μg/ml kanamycin, and left overnight at 37 °C. Single colonies were amplified by growth in LB at 37 °C for another 24 hr, and plasmids extracted for analysis or transfection.

2.13. Mammalian Cell Culture

HEK-293, COS-7 and AtT-20 cells were maintained in Dulbecco's Modified Eagles Medium (DMEM) (Invitrogen) containing 10% foetal bovine serum (Invitrogen), 50 U/ml penicillin and 50 U/ml streptomycin at 37 °C, 5% CO_2. When cells were 90–95% confluent, they were washed once by phosphate-buffered saline (PBS, containing 2.67 mM KCl, 1.47 mM KH_2PO_4, 137.93 mM NaCl, 8.06 mM Na_2HPO_4), resuspended by Trypsin/EDTA/PBS, and plated onto new flasks in fresh growth medium at an appropriate density. In order to maintain a consistent condition for overexpression, cells were split from Passage 6 up to 23.

For subsequent transfection, the resuspended cells could be quantified on a haemocytometer, and seeded at an appropriate density, *e.g.* 3 x 10^6 per ml, onto either polystyrene cell culture dishes (Corning) for experiments involving protein extraction, or glass-bottom dishes (WillCo) for live confocal imaging. In the case of immunofluorescence staining, cells were seeded onto 1.5 cm diameter glass coverslips in 6 well dishes. Before seeding, dishes and glass coverslips were pre-coated with

0.07 mg/ml poly-D-lysine (Sigma) in 20 mM H_3BO_3/NaOH pH 8.4, washed with ddH$_2$O, and left to dry.

2.14. Mammalian Cell Stock Maintenance

To use the HEK-293, COS-7 and AtT-20 stock, cells from -80 °C were warmed up at 37 °C, pelleted at 1000 RPM, and resuspended in warm growth medium. Cells were immediately plated onto a poly-D-lysine-coated culture flask, and the medium was changed the next day.

To make the stock, early passage cells were resuspended, pelleted at 1000 RPM, and supplemented with fresh growth medium and 10% sterile DMSO. Aliquots were left in -80 °C in an isopropanol-surrounded chamber, and transferred into liquid nitrogen the next day.

2.15. Transfection

Transient transfection of HEK-293 cells in 10 cm diameter polystyrene dishes for protein extraction was performed by the calcium phosphate precipitation technique. Growth medium was changed 3–4 hr before transfection. Meanwhile, for each transfection, 20 µg DNA and 36 µl of 2 M CaCl$_2$ were made up to 300 µl in an Eppendorf tube. This was added slowly and dropwise to 300 µl 2x HBSS (Hank's Balanced Salt Solution, containing 274 mM NaCl, 10 mM KCl, 1.4 mM Na$_2$HPO$_4$, 15 mM D-glucose, 42 mM HEPES, pH 7.07) while bubbling through another pipette in the solution. The calcium phosphate/DNA precipitate mixture was incubated at room temperature for 30 min, and was added to the cells. Cells were incubated overnight, followed by a glycerol shock (4 ml of 15% glycerol, 2 min) the next morning. Then the cells were washed with PBS and kept in fresh growth medium for another 24 hr.

HEK-7 and COS-7 cells in 3 cm/6 cm diameter polystyrene dishes, 6-well plates and WillCo dishes were transiently transfected using FuGene6 transfection reagent (Roche Molecular Biochemicals), 24 hr before imaging, at 80–90% confluence.

No discernible difference was observed in cellular morphology or expression level using the two methods above.

2.16. Protein Extraction

After transfection, the lysates were made by freezing (over dry ice) and thawing the cells, scraped from their dishes in 1% (v/v) Triton X-100, 5 mM EDTA, 5 mM EGTA plus 1:200 protease inhibitor cocktail (Sigma). The homogenates were then passed three times through a 0.4 mm diameter needle (Terumo) and centrifuged at 14000 g for 10 min at 4 °C. The supernatants were stored at -80 °C. Lysates used for direct comparison in lipid kinase activity and autophosphorylation activity assays were frozen and thawed in parallel each time, in order to control for temperature-dependent protein denaturation, even if not all lysates from the same batch were used in one particular experiment.

2.17. Protein Dephosphorylation

Protein lysate was incubated with shrimp alkaline phosphatase (NEB) in its buffer. Typically, a 0.5–1 hr incubation at 30 °C was stopped by transferring samples to 4 °C, in order to minimise potential impairment of the native structure.

2.18. SDS-PAGE

The sodium dodecyl sulfate polyacrylamide gel electrophoresis (SDS-PAGE) running gel (6%, w/v, g/ml) was made up of 2.5 ml 30% acrylamide, 6.25 ml 0.75 M Tris/0.2% SDS pH 8.8, 45 μl ammonium persulphate (AMPS), 15 μl N, N, N', N'-tetramethylethylenediamine (TEMED) in a total volume of 12.5 ml. For the 15% (w/v, g/ml) running gel, 6.25 ml acrylamide was added instead. After settling under a thin layer of tertiary alcohol, the upper surface of the running gel was rinsed by ddH$_2$O, and 4% stacking gel was added on top and allowed to set (1 ml 30% acrylamide, 3.75 ml 0.75 M Tris/0.2% SDS pH 8.8, 27 μl AMPS, 9 μl TEMEM in a total volume of 7.5 ml). Samples were made to contain 1x sample buffer (80 mM Tris-HCl pH 6.8, 10% glycerol, 2% SDS, 50 μg/ml bromophenol blue and 5% β-mercaptoethanol) and boiled for 3 min immediately before loading.

The running buffer contained 24.8 mM Tris, 19.2 mM glycine and 3.5 mM SDS. For experiments concerning the phosphorylation states, good separation was achieved by running samples (from cathode to anode) under 100 V through the stacking gel, and then 200 V until 5 min after the dye front ran out of the running gel. A gentler running

condition, *e.g.* 5 mA throughout, gave a flatter shape of the dye front, but sometimes a less clear separation between the phosphorylation states.

Because only the enzyme of interest needed to be visualised on the gel, gels were Western blotted in order to detect the enzyme over a low background.

2.19. Western Blotting

Proteins separated by SDS-PAGE were transferred to nitrocellulose membranes (Schleicher & Schuell) at 4 °C, under either 20 V overnight, or 1 A for 1 hr. Blotting buffer contained 25 mM Tris, 190 mM glycine and 20% methanol. Blots were blocked at room temperature with 5% (w/v, g/ml) non-fat dried milk and 0.05% (v/v) Tween-20, and then probed with the primary antibody (diluted in the blocking buffer). Blots were washed 5 times within 30 min by TBS containing 0.05% (v/v) Tween-20, and then incubated in the secondary antibody (diluted in the blocking buffer) for 1 hr. After another 5 washes in TBS/Tween-20 as above, blots were washed once in TBS and visualised by SuperSignal West Femto chemiluminescent substrate (Pierce).

Images were then either developed using high performance chemiluminescence film (GE Healthcare), or acquired digitally. In the latter case, acquisition was done by GeneSnap (SynGene), and subsequent analysis was performed in the GeneTool (SynGene) software.

Where the primary antibody was mouse anti-FLAG monoclonal antibody (1:10000 from 1 mg/ml, Strategene) or mouse anti-Rac monoclonal antibody (1:1000 from 0.25 mg/ml, BD Transduction), the secondary used was horseradish peroxidase (HRP)-linked goat anti-mouse (1:2500 from 10 μg/ml, Pierce) or, in the case of Rac-detection, HRP-linked goat anti-mouse-heavy-chain (1:7500, Pierce). Where the primary antibody was rabbit E2139 (1:7500), HRP-linked goat anti-rabbit antibody was used as the secondary (1:1000 from 10 μg/ml, Pierce).

2.20. Immunoprecipitation

The FLAG-tagged enzymes were immunoprecipitated by incubation of the cell lysate with the monoclonal M2 anti-FLAG antibody (4 μg/ml) in 500 μl PBS overnight at 4 °C, and subsequent incubation with 25 μl Protein G-Sepharose beads (Amersham

Biosciences) for 3 hr at 4 °C. The immunoprecipitates were washed twice in TBS and then resuspended in the PIP kinase assay buffer (80 mM KCl, 10 mM MgCl$_2$, 2 mM EGTA, 50 mM Tris-HCl, pH 7.4) at 4 °C.

2.21. Lipid Kinase Assay

The lipid kinase assay was performed on immunoprecipitates obtained from HEK-293 cells, transiently transfected with FLAG-tagged PIP kinases by the calcium phosphate precipitation technique described above.

The lipid kinase activity was assayed in a final volume of 100 μl at 30 °C in PIP kinase assay buffer, by using 10 μM ATP (plus 50 μCi/ml [γ-^{32}P]ATP) and the liposome mixture (or lipid micelle) as substrates. The lipid micelle contained 9.57 mg/l PI4P and 7.25 mg/l PA. The liposome mixture contained 3.44 mg/l PIP$_2$, 3.2 mg/l PI4P, 0.027 mg/ml PI, 0.11 mg/ml PE, 0.44 mg/ml PC, 0.126 mg/ml PS and 2.4 mg/l PA. The lipid mix was ultrasonicated for 10 min (Decon F5 Minor). Recombinant PIP4KIIα was run alongside as a control for identifying the [^{32}P]PIP$_2$ product, using PI5P as the substrate instead of PI4P. The linearity of the lipid kinase assay for each PIP kinase was determined by allowing the reaction to proceed for variable time courses (see individual figures).

The reaction was stopped by transferring the samples to 4 °C. 500 μl of chloroform/methanol (1:1, v/v) and subsequently 125 μl of 2.4 M HCl were added. After spinning at 10000 g and removal of the upper phase, the lower phase was washed once with 490 μl of chloroform/methanol/1 M HCl (3:47:49, by volume) and then dried down in vacuum. Lipids were separated by thin-layer chromatography (TLC) on silica-gel plates (Merck) impregnated with 1% potassium oxalate and containing 4 mM EGTA, and pre-conditioned at 110 °C for 1 hr. The lipids extracted from each sample were dissolved in chloroform/methanol/water (2:1:0.01, by volume), loaded on to plates and separated by ethanol/chloroform/water/saturated ammonium hydroxide solution (40:28:10:6, by volume). The plates were dried and exposed to an imaging plate (Fujifilm) at room temperature for 24 hr. The imaging plate was read by a phosphoimager, and PIP$_2$ was identified by comparison with a radioactive standard (see above) run on the same plate.

The relative activity of the PIP kinases was measured on immunoprecipitates containing similar amounts of recombinant enzyme. This was carefully determined by prior analysis of the immunoprecipitates with SDS-PAGE and Western blotting. A serial dilution of $[\gamma\text{-}^{32}P]$ATP was also included on the TLC plate, to ensure that the phosphoimager readings were within the linear range.

During image analysis, regions of interest were selected containing the PIP_2 produced. The mean pixel intensity was measured for each sample, and plotted against its reaction time. The non-linear curve for each PIP kinase construct was fitted by the equation $y = A \times (1 - e^{-kx})$. The lipid kinase activity was then taken as the initial slope of the reaction profile at time 0, for relative comparison within the same set of experiments.

2.22. Autophosphorylation Assay

The autophosphorylation assay was performed on immunoprecipitates obtained from HEK-293 cells, transiently transfected with FLAG-tagged PIP kinases by the calcium phosphate precipitation technique described above.

The assay mixture contained 50 μM PI, 10 μM ATP, and 10 μCi of $[\gamma\text{-}^{32}P]$ATP (3000 Ci/mmol, 10 mCi/ml as of the delivery date, Perkin Elmer) per sample in the PIP kinase assay buffer. If the assay was to be visualised by Western blot to see the overall phosphorylation pattern (instead of the ^{32}P incorporation), 200 μM non-radiolabelled ATP was added instead. The protein kinase activity was assayed by adding 80 μl assay mixture to the enzyme at 30 °C for 3 hr. The samples were mixed repeatedly during the incubation.

The reaction was stopped by transferring the samples to 4 °C . Samples were centrifuged at 13000 g for 1 min, and washed with ice-cold TBS for 6–7 times. This was to remove the majority of remaining $[\gamma\text{-}^{32}P]$ATP that would otherwise contribute to the background noise and preclude detection of the phosphorylated protein.

25 μl of 2x protein loading buffer was added to each sample, and 6% SDS-PAGE was performed. Attention was given to ensure the dye front to run out, so that little $[\gamma\text{-}^{32}P]$ATP remained trapped in the gel. The gel was overlaid on top of a filter paper, wrapped by parafilm and dried over vacuum suction. When dry, the gel was then

exposed to an imaging plate (Fujifilm) at room temperature for 24 hr, and the imaging plate was read by a phosphoimager.

The relative activity of the PIP kinases was measured on immunoprecipitates containing similar amounts of recombinant enzyme. This was carefully determined by prior analysis of the immunoprecipitates with SDS-PAGE and Western blotting.

During analysis, regions of interest on the gel image were selected containing the phosphorylated PIP kinase of interest. The mean pixel intensity was measured for each sample, for relative comparison within the same set of experiments.

2.23. Live Confocal Imaging

Immediately prior to the experiment, HEK-293 cells transfected with GFP-tagged constructs were incubated for 1 min at room temperature, in 1 ml of DMEM supplemented with 25 mM D-glucose, 4 mM L-glutamine and 25 mM HEPES (Invitrogen), with or without 0.5 μl Cellmask (Molecular Probes). Experiments were then conducted in fresh DMEM, either at room temperature or 37 °C. No temperature-dependent effects were observed on subcellular localisation.

Images were acquired using a Leica CTR6500 confocal microscope and Leica Application Suite software (2.4.1 build 6384). An Argon laser at 28 mW and a HeNe 543 laser provided the sources of illumination at 488 and 543 nm, respectively. A 40x, 1.25 NA oil-immersion objective was used. GFP-fused kinases were visualised through a 495–535 nm filter, and the Cellmask signal was filtered between 586–617 nm. Images were collected in 1024 x 1024 pixels, each line as an average of 4 consecutive scans, sampling bidirectionally at 1400 Hz. Experimental results with each construct were saved as LIF files for offline analysis.

2.24. Quantification of Plasma Membrane Fraction

Single confocal sections (in the form of LIF files) were analysed in ImageJ. The original brightness and contrast were unaltered during quantitative measurement. For each cell imaged, five regions of interest were randomly selected in the cytosol (while care was taken to exclude the nucleus). The average of their fluorescent signal intensity, minus the extracellular background, served as the cytosolic reference. Five

other regions were randomly taken within the plasma membrane (labelled by the Cellmask) to give the membrane fluorescent intensity (after subtracting the extracellular background). The ratio of the membrane signal over the cytosolic reference gave the membrane fraction index. For each construct examined, typically 6 cells were imaged, producing 30 raw data points. Unpaired t-test was performed between two comparable constructs to determine the statistical significance, where $p < 0.05$ and $p < 0.001$ were denoted * and **, respectively, in corresponding figures.

2.25. Fluorescence Recovery after Photobleaching

Fluorescence Recovery after Photobleaching (FRAP) was performed using a Leica CTR6500 confocal microscope and Leica Application Suite software (2.4.1 build 6384). A 40x, 1.25 NA oil-immersion objective was used. Illumination was provided by an Argon laser at 28 mW, filtered at 488 nm. The GFP signal was visualised through a 495–535 nm filter, frames sampled every 0.366 sec on average. The photobleach was performed by turning the 488 nm illumination to 100% intensity (280mW) for 100 msec, with the pinhole open. Typically, 15 frames were collected before the photobleach, and 300 frames afterwards. Bleach spot intensity (minus the background) was plotted, after compensating for the time-dependent, non-specific decrease in the whole cell signal throughout the observation.

Data were only used where the initial bleach was more than 70% and the recovering signal stabilised to a plateau.

2.26. Immunocytochemistry

Paraformaldehyde was heated to 60–70 °C and depolymerised with 1-2 drops of NaOH, allowed to cool, and dissolved 4% (w/v, g/ml) in 0.1 M NaH_2PO_4 buffer (pH 7.4) to make the fixative solution. Cells on glass coverslips were washed with PBS/0.9 mM $CaCl_2$/0.52 mM $MgCl_2$/0.16 mM $MgSO_4$, and incubated in fixative at 4 °C for 1 hr. All subsequent steps were performed at room temperature. The cells were washed 5 times in PBS, permeabilised with 0.1% (v/v) Triton X-100 in PBS for 5 min at room temperature, and washed again 4 times with PBS. Cells were then blocked with 4% fish skin gelatin (Sigma)/2% normal goat serum (Sigma) in PBS for 1 hr. The glass coverslips were incubated on parafilm for 1 hr with 100 µl blocking buffer

containing mouse monoclonal M2 anti-FLAG antibody (1:500 from 1 mg/ml, Stratagene), mouse monoclonal anti-GFP (1:250 from 0.2 mg/ml, Molecular Probes), or E2139 at a 1:750 dilution. Cells were washed 4 times in PBS over 15 min, and re-blocked with gelatine/serum for 15 min. Immunofluorescence detection was made possible by incubation for 30 min in the dark with the secondary antibody (goat anti-mouse or anti-rabbit) conjugated to Alexa Fluor dyes (1:100 from 2 mg/ml, Invitrogen), usually 555 nm (red) or 548 nm (green). Stained and PBS-washed coverslips were mounted in the Prolong antifade reagent (Molecular Probes). For long-term storage, coverslips were sealed with adhesive polymers (*e.g.* resin) dissolved in acetone and stored at 4 °C. Images were acquired with a Leica CTR6500 confocal microscope and Leica Application Suite software (2.4.1 build 6384), through appropriate filters corresponding to the staining.

2.27. Immunohistochemistry

Sagittal mouse brain slices (perfused animal, 4% paraformaldehyde-fixed, 10% sucrose-impregnated, cryostat-sectioned and mounted on glass slides, frozen at -80 °C) were obtained by courtesy of Dr Jon Clarke[204]. The slide was incubated in $NaBH_4$ (26 mM fresh in PBS) at room temperature for 10 min and repeated 2–3 times. It was washed 3 times in PBS for 5 min each and blocked at room temperature for 2 hr (or overnight at 4 °C) in PBS with 0.3% Triton X-100 and 1% fish gelatine, followed by primary incubation with E2139. Longer incubations were generally performed in a humidified chamber. After 3 times of 10 min washes in PBS, the slide was incubated for 4 hr at room temperature with secondary antibodies. The donkey anti-rabbit antibody (conjugated to 555 nm Alexa Fluor, 1 mg/ml, Invitrogen) was used at a 1:1000 dilution. Meanwhile, NeuroTrace 535 nm Nissl stain (Invitrogen) was added where necessary at a dilution of 1:3000. Stained and PBS-washed slides were mounted in the Prolong antifade reagent (Molecular Probes). For long-term storage, coverslips were sealed with adhesive polymers (*e.g.* resin) dissolved in acetone and stored at 4 °C. High magnification images were acquired with a Leica CTR6500 confocal microscope and Leica Application Suite software (2.4.1 build 6384), through appropriate filters corresponding to the staining. Low magnification images of the 535

nm NeuroTrace green signal were acquired on a fluorescence microscope with 488 nm illumination.

2.28. Generation of Iγ_i6-specific Antibody, E2139

The custom polyclonal rabbit antibody E2139 was produced by NeoMPS (San Diego, USA), > 96% pure by high-performance liquid chromatography (HPLC). It was against the 16 amino acids on the C-terminus of the unique 26-AA peptide of Iγ_i3/6. The epitope sequence was CRRRRLRAVTPSHTGA.

3. Results I – Behaviour of Iγ_i3 Compared to Iγ_i1 and Iγ_i2

3.1. V443A Found in Iγ_i3 Clones Previously Used

At the beginning of this study, relevant plasmid constructs from Dr Giudici's previous studies were sequenced, covering the full length of Iγ_v3. The linker/multiple cutting site sequences flanking the fusion protein within both the pEGFP-C1 and pCMV-2B vectors were determined, and integrated into corresponding plasmid maps (Figure 7a and b).

A mutation of thymidine-1328 into cytosine was found to have occurred since the initial cloning of Iγ_v3 from the rat hippocampal cDNA library in our lab[167], which corresponded to a non-synonymous conversion from valine-443 into alanine after translation (Figure 7c). This T1328C (*i.e.* V443A) mutation has accumulated in all subsequent Iγ_v3 constructs generated by site-directed mutagenesis.
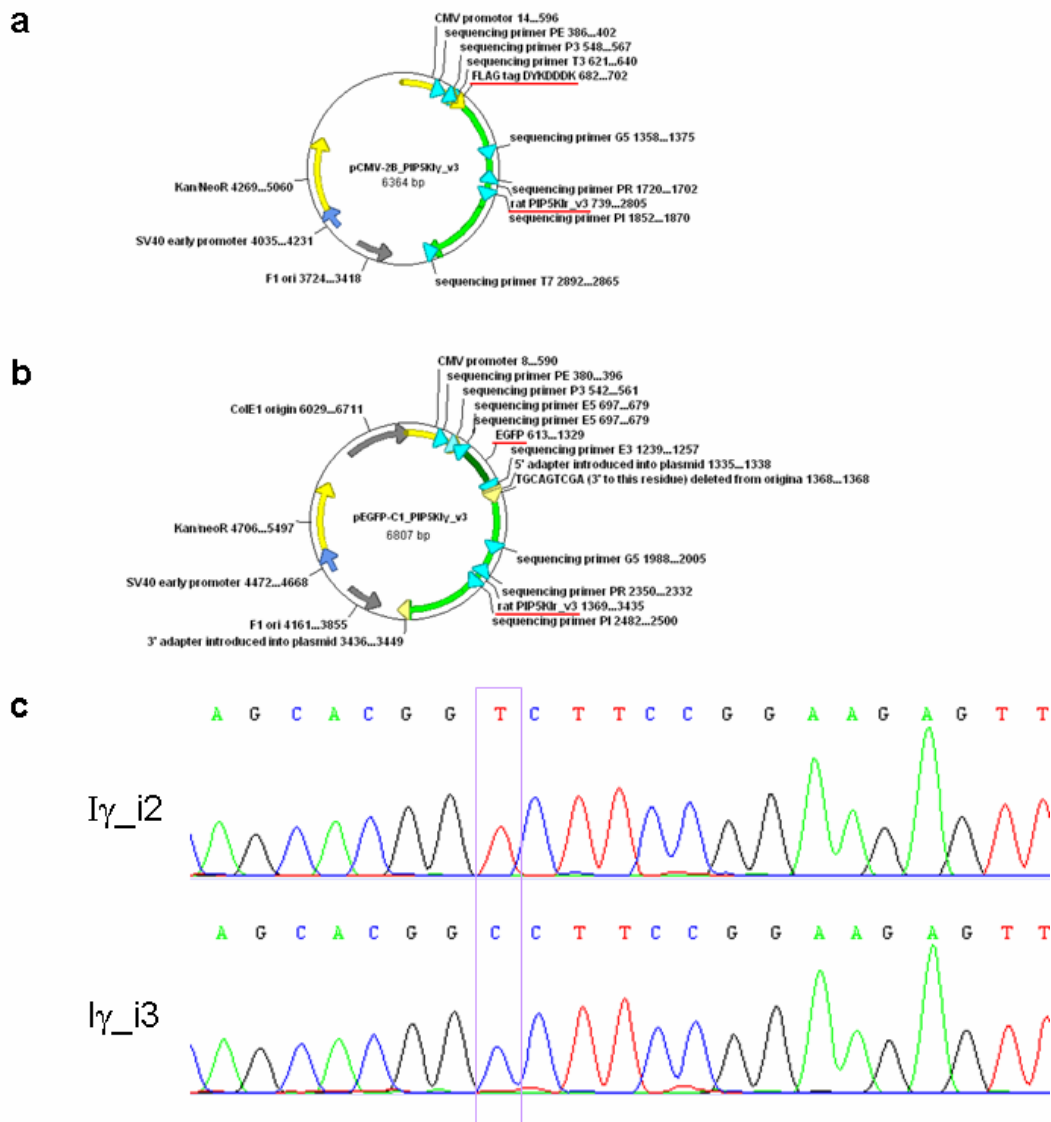
Figure 7 Discovery of the T1328C mutation in Iγ_v3 construct previously used
Plasmid map and sequencing scheme of Iγ_v3 in the (**a**) pCMV-2B (FLAG) plasmid and (**b**) pEGFP-C1 plasmid. (**c**) T1328C discovered in Iγ_v3 constructs used, compared to wild type Iγ_v2.

In comparison, the Iγ_v1 and Iγ_v2 constructs both had the correct, wild type thymidine-1328 within Exon 11 (Figure 6b), as expected from the Ensembl database of the rat genome.

In the PIP5KIγ entry of the Ensembl database (Table 1), this mutation did not show up as a naturally occurring genetic variation. In fact, 90% of the natural variations listed were single-nucleotide polymorphism (SNP), which could be either synonymous (where specific point mutations of DNA did not alter the amino acid it coded for, due to the degeneracy of the codon table), or non-synonymous.

This means that the non-SNP mutation observed in our Iγ_v3(A) construct was not likely to be frequent enough to be considered physiologically representative, despite the fact that it may have been a genuine, natural mutation from the particular mRNA/cDNA template during the initial cloning, which was amplified and preserved in all subsequent PCR steps.

In this thesis, Iγ_v3 with V443A is hereafter referred to as Iγ_v3(A), while the true wide type Iγ_v3 containing Val^{443} is denoted Iγ_v3(V). Such a convention is also applied to other splice variants, with (V) representing the wild type and (A) for the mutant with V443A in place.

Since Val^{443} is in proximity to a crucial dibasic motif implicated in membrane targeting, and just downstream of the activation loop that is central to lipid substrate binding and catalysis (Figure 6b, see Introduction), its mutation into alanine could potentially have an effect on many aspects of the enzyme property, including its subcellular localisation, phosphorylation state and kinase activity.

Some of the previous studies (*e.g.* [167, 179]) used constructs based on Iγ_i1(V), Iγ_i2(V) and Iγ_i3(A). Therefore, some of the special characteristics attributed to Iγ_i3 could have been partially due to the intrinsic presence of V443A in γ_i3, but not γ_i1 or γ_i2. In other words, previous comparisons between γ_i1, γ_i2 and γ_i3 may not have been strictly valid.

Therefore, Iγ_v3(A) "wild type" and mutants generated earlier were mutated back into the Iγ_v3(V) version, with Val^{443} in place. Meanwhile, the Iγ_v2(V) wild type and some of its mutants were also purposely mutated to generate the corresponding Iγ_v2(A) enzyme, *i.e.*, to include V443A (Table 3).

Primer	Note	Sequence
For sequencing the plasmid		
E3	to sequence downstream of EGFP	CAAAGACCCCAACGAGAAG
E5	to sequence upstream of EGFP	TGAACTTGTGGCCGTTTAC
G5	to sequence downstream of the shared middle part of PIP5KIγ	TGAACCTCAACCAGAACC
P3	to sequence downstream of CMV-IE promoter	CGGTGGGAGGTCTATATAAG
PE	to sequence downstream of the middle of CMV-IE promoter	CAGTACATCAATGGGCG
PI	to sequence downstream of the shared middle part of PIP5KIγ	GAGACAGATGACACGATGG
PR	to sequence upstream of the shared middle part of PIP5KIγ	GGTCAATGTTGTGCACACC
T3	to sequence downstream into the FLAG tag	ATTAACCCTCACTAAAGGGA
T7	to sequence upstream into the inserted gene in pCMV-2B	TAATACGACTCACTATAGGG
For correction of T1328C (V443A) from Iγ_v3		
TCback_f	SDM forward	GAGCAGCACGG *T* CTTCCGGAAGAGTTCC
TCback_r	SDM reverse	CTTCCGGAAG *A* CCGTGCTGCTCATGAAC
For introduction of T1328C (V443A) into Iγ_v1 and Iγ_v2		
V443A_f	SDM forward	GTTCATGAGCAGCACGG *C* CTTCCGGAAGAG
V443A_r	SDM reverse	GGAACTCTTCCGGAAG *G* CCGTGCTGCTC

Table 3 Primers designed for plasmid sequencing and mutagenesis regarding V443A

The nucleotides in the *underlined and Italic* font refer to the mismatching region with the template, *i.e.*, the sequence desired after site-directed mutagenesis.

This would allow for direct comparison between equivalent Iγ_v2 and Iγ_v3 constructs, and hence more accurately deduce the role of the 26-AA insert itself in Iγ_i3.

3.2. Revisiting Genuine Behavioural Differences Between Iγ_i3 and Other Spliceoforms

We now re-examine some of the previously observed differences between Iγ_i3 and Iγ_i2/1, as well as a range of their mutant counterparts. This is to correct for any effect potentially attributable to V443A, and therefore deduce the remaining, genuine behavioural differences between PIP5KIγ_i3 and its splicing relatives, Iγ_i2 and Iγ_i1. Therefore, when observing the behaviours of γ_i3(V), we shall bear in mind two important dimensions in this Chapter: (1) Val^{443} *vs.* Ala^{443}; (2) Iγ_i3 *vs.* Iγ_i2/1.

3.2.1. *In Vivo* Phosphorylation

In a Western blot, overexpressed PIP5KIγ could typically be observed as several bands, as opposed to a singlet. The slower mobility in SDS-PAGE of the additional upper band(s) likely resulted from post-translational modifications such as protein phosphorylation, compared to the unphosphorylated molecules. When treated with alkaline phosphatase *in vitro*, the upper band completely collaspsed into the lower band (Figure 8a), confirming that the upper and lower bands indeed corresponded to the phosphorylated and unphosphorylated versions of the same PIP5KIγ protein, respectively. This provided us with a convenient way of observing the enzyme's phosphorylation pattern *in vivo*. In this thesis, typical phosphorylation patterns of various constructs from many experiments are shown below, in which a wild type enzyme was always included as a control (as well as, often, a kinase-inactive mutant). When aligned, the relative intensities of the major bands could be assessed and compared between different constructs.

It had been previously observed that Iγ_i3(A) was less phosphorylated than Iγ_i2(V). In re-examining this, I observed that with the wild type Val[443], both Iγ_i2 and Iγ_i3 were in fact phosphorylated to a comparable extent (Figure 8b). Interestingly, when V443A was introduced into Iγ_i2, it also became less phosphorylated (Figure 8b). Therefore, the V443A mutation itself appeared to be mostly responsible for shifting the equilibrium towards unphosphorylated PIP5KIγ.

D316K, the kinase-inactive mutation, dramatically decreased phosphosphorylation (compare Figure 8b and c). However, while the previously reported Iγ_i3(A) D316K was completely unphosphorylated, Iγ_i3(V) D316K was now partially phosphorylated (Figure 8c). A similar reduction in phosphorylation by V443A was observed with Iγ_i2(V) D316K compared with its V443A mutant (Figure 8c). Consequently, the presence of the double mutation V443A/D316K was able to completely abolish phosphorylation *in vivo*, for both Iγ_i3 and Iγ_i2 (Figure 8c).
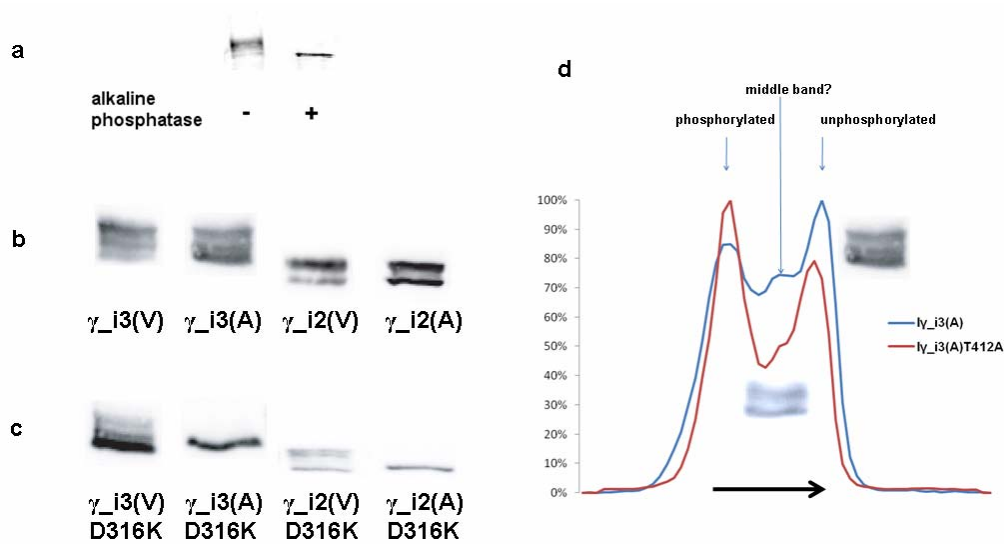
Figure 8 Phosphorylation patterns of Iγ_i3 and Iγ_i2
Lysate from HEK-293 cells overexpressing each FLAG-tagged enzyme was extracted, and subjected to SDS-PAGE. The phosphorylation pattern *in vivo* was visualised by anti-FLAG staining of the Western blot. (**a**) Alkaline phosphatase treatment *in vitro* collapsed the upper band of Iγ_i3 into the lower one completely, indicating that the upper band consisted of

phosphorylated molecules. (**b**) Comparison of Iγ_i2 and Iγ_i3, adjusting for V443A. (**c**) Comparison of the kinase-inactive D316K constructs of Iγ_i2 and Iγ_i3, adjusting for V443A. (**d**) Phosphorylation profiles of Iγ_i3(A) and Iγ_i3(A) T412A, illustrating the isolation of a putative "middle band". The middle band may be a partially phosphorylated band, compared to the upmost phosphorylated band. Bottom arrow indicates the direction of SDS-PAGE.

The apparently discrete bands of phosphorylated states (as opposed to a smear of differentially phosphorylated proteins at various residues) do not necessarily suggest a singular, all-or-none phosphorylation event of the protein molecule. It is equally likely that multiple residues can be the target of regulated phosphorylation pathways, and that phosphorylation could indeed occur in a cooperative fashion. In agreement with this, Iγ_i3 seemed to have at least one extra phosphorylated state, in addition to Iγ_i2's "completely" phosphorylated state and the unphosphorylated state (Figure 8b). A more quantitative comparison between the profiles of Iγ_i3(A) and its T412A mutant, for instance, confirmed this possibility (Figure 8d).

Such a difference suggests that the additional peptide of Iγ_i3, the 26-AA insert near its C-terminus, may be an additional target of phosphorylation *in vivo*. This phenomenon is more thoroughly addressed later in Section 3.3.

3.2.2. Subcellular Localisation

The subcellular localisation of PIP5K Iγ variants was visualised by fluorescence confocal microscopy, in which the plasma membrane-bound fraction (as labelled by Cellmask in a simultaneously recorded channel) was compared to the cytosol. Care was taken not to include the nucleus in the cytosolic measurement. The higher the PM / cytosol ratio, the more PM-targeted the kinase. A PM / cytosol ratio of 1 corresponds to a non-membrane-enriched localisation, as indicated by an orange, dashed line in the quantification panel in relevant figures.

Wild type Iγ_i3(V) and Iγ_i2(V) were to a large extent localised to the PM, with a PM / cytosol ratio around 9–10 (Figure 9a and c). When V443A was introduced, Iγ_i3(A) and Iγ_i2(A) were clearly less PM-associated (Figure 9b and d). This reduction was greater with Iγ_i3. Similarly, direct comparisons using other mutant constructs of Iγ_i2 and Iγ_i3 followed the same pattern, *i.e.*, V443A tended to decrease the PM-association and make the enzyme more cytosolic, all else being equal (*e.g.* D316K in Figure 10 and T412D in Figure 11)[1].

In terms of its contribution to the enzyme's localisation to the membrane, Val^{443} seemed to be a factor independent of other motifs containing mutations. This was also seen in T412D, because it worked in conjunction with T412D to further reduce its already lowered PM localisation from the wild type (Figure 11b). This was paralleled by a similar reduction in PM-association in Iγ_i2, causing Iγ_i3(A) T412D and Iγ_i2(A) T412D to be completely cytosolic(Figure 11b and d).

I deduced that the reason why V443A tended to decrease PM-association was caused by the relative hydrophobicity of these AA residues. The Val^{443} in the wild type was more hydrophobic than alanine (4.2 versus 1.8), and could therefore bind better with the lipid substrates on the PM, as well as associating through hydrophobic interactions with the phospholipid bilayer itself. This impact of the V443A mutation can now be seen to partially explain the previous observation that Iγ_i3(A) tended to be more cytosolic than Iγ_i2(V)[179].

---

[1] The specific behavioural characteristics and significance of D316K and T412D are beyond the scope of the current chapter, and will be discussed in detail later in Chapter 4.
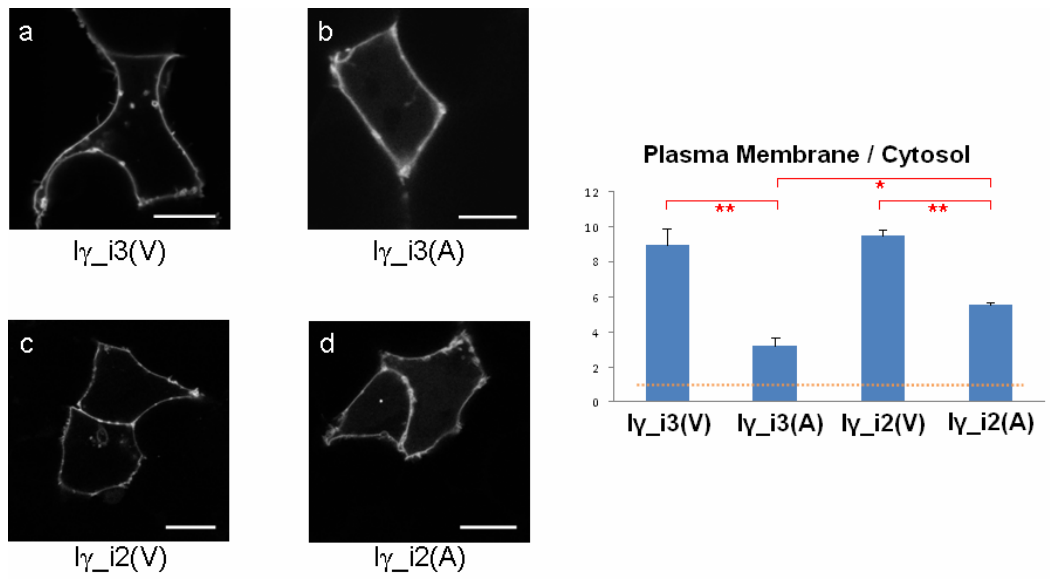
Figure 9 Subcellular localisation of wild type Iγ_i2/3, adjusting for V443A

Typical subcellular localisation of overexpressed GFP-tagged constructs in HEK-293 cells (scale bar = 10 μm). Panel on the right indicates quantified ratio of PM / cytosol fraction. Orange dotted line indicates a cytosolic (non-membrane-enriched) localisation (n = 30, * p < 0.05, ** p < 0.001).
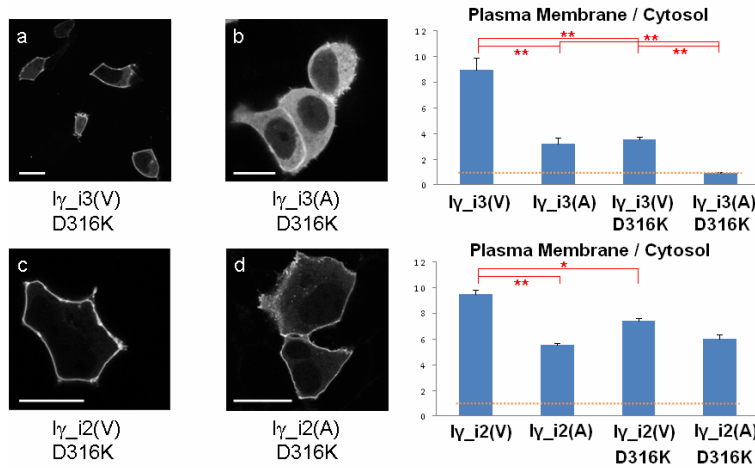
Figure 10 Subcellular localisation of D316K mutants of Iγ_i2/3, adjusting for V443A

Typical subcellular localisation of overexpressed GFP-tagged D316K constructs in HEK-293 cells (scale bar = 10 μm). Panel on the right indicates quantified ratio of PM / cytosol fraction. Orange dotted line indicates a cytosolic (non-membrane-enriched) localisation (n = 30, * p < 0.05, ** p < 0.001).
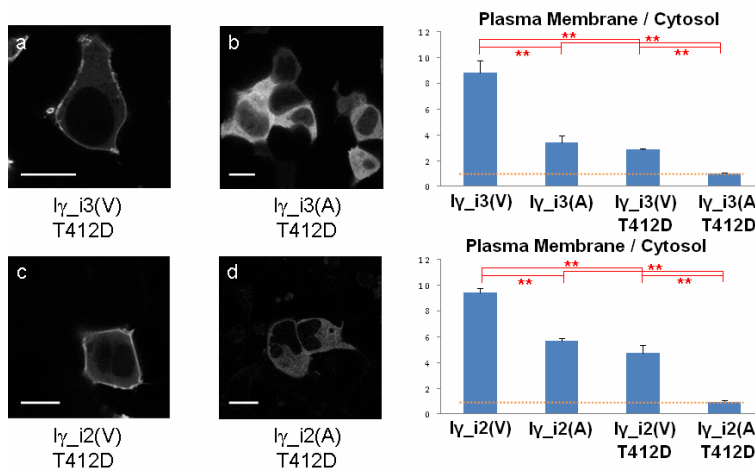
Figure 11 Subcellular localisation of T412D mutants of Iγ_i2/3, adjusting for V443A

Typical subcellular localisation of overexpressed GFP-tagged T412D constructs in HEK-293 cells (scale bar = 10 μm). Panel on the right indicates quantified ratio of PM / cytosol fraction. Orange dotted line indicates a cytosolic (non-membrane-enriched) localisation (n = 30, ** p < 0.001).

However, there are still genuine behavioural differences between equivalent Iγ_i2 and Iγ_i3 constructs, all else being equal. For example, although the kinase-inactive D316K mutants generally exhibited considerably less PM-association (Figure 10a – c), and Iγ_i3(A) D316K was completely cytosolic, Iγ_i2(A) D316K was not different from the active Iγ_i2(A) in its localisation (Figure 10d). That is, rendering the enzyme catalytically inactive had little effect on Iγ_i2, but a profound effect on Iγ_i3. This is examined further in the next Chapter.

3.2.3. Fluorescence Recovery after Photobleaching

Fluorescence recovery after photobleaching (FRAP) is an optical technique capable of quantifying the apparent mobility of a fluorescently labelled molecular probe. In earlier studies, Iγ_i3 (now known to contain the V443A mutation) demonstrated a notably large immobile fraction and slower recovery dynamics when compared to Iγ_i1 and Iγ_i2[179]. The reason for this apparent immobility had not been adressed, but was possibly due to association with unidentified cytoskeleton-related binding partners, which restricted the diffusion of the kinase *in vivo*.

In this study (as well as in [179]), the FRAP method adopted from Brough *et al.*[205] is used to introduce a pulse bleach to the plasma membrane and measure the recovery of the fluorescent protein signal in that region, potentially by means of lateral diffusion within the two dimensional PM surface and/or exchange with adjacent cytosolic compartments. With sophisticated experimental protocols, it is possible to tease apart these two sources of recovery[47], which would be interesting but beyond the scope of the present study. Therefore, only the final level of fluorescence recovery is measured in this study, and used as a general measure of the mobility of membrane-associated PIP5KIγ. As we shall see, some empirical differences exist among different splice variants and mutants of Iγ, which provide informative insight into the behaviour of these constructs (also see more in the Discussions).

Figure 12 shows a typical FRAP analisis using GFP-tagged PIP5KIγ_i2 overexpressed in HEK-293 cells.
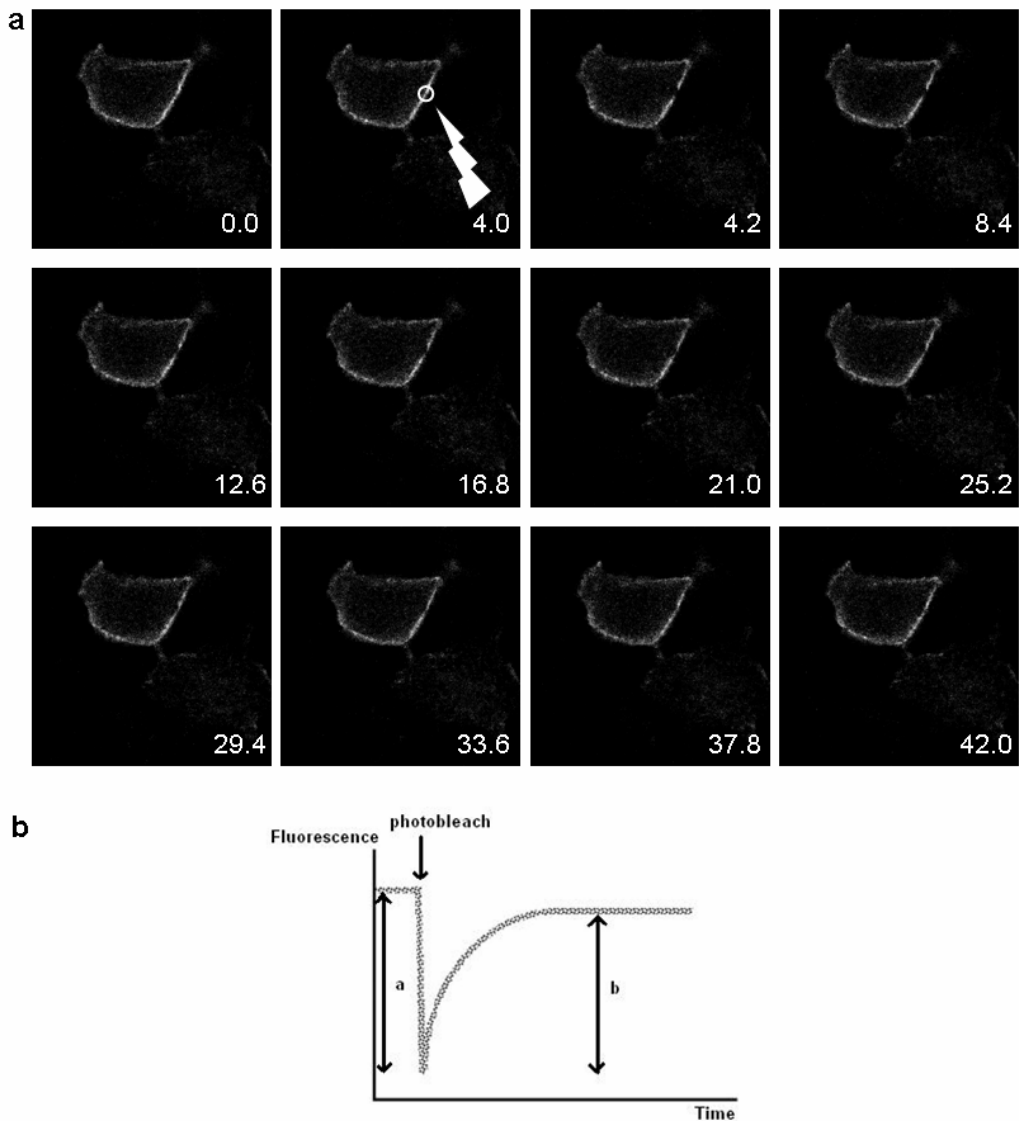
Figure 12 Illustration of the procedure and quantification of FRAP

(**a**) A typical procedure of FRAP, using GFP-tagged PIP5KIγ_i2 overexpressed in HEK-293 cells. Each image is 64.58 μm across, and the time from the start is indicated at the bottom right corner of each frame (in seconds). The lightening arrow in the second frame indicates the spot photobleach at 4 s. (**b**) After adjusting for the background and non-specific loss of signal through time (see Methods), the mobile fraction is calculated as b / a x 100%.

Previous studies[179] showed that when the plasma membrane was bleached by a laser spot, and FRAP was measured as an indication of mobility of the GFP-tagged PIP5Ks, Iγ_i1(V) and Iγ_i2(V) were largely mobile (recovering towards the original baseline over time), whereas Iγ_i3(A) was considerably immobile. When the mutation V443A was corrected back, Iγ_i3(V) was still partially immobile in FRAP, recovering to over 55% under the standard test condition (Figure 13a). This indicated that although the FRAP difference was initially discovered with the V443A mutation, there is still a genuine difference in mobility between Iγ_i3 and its related splice variants once the V443A mutation is corrected.

It is worth notice that the final FRAP recovery observed also depended on the initial extent of bleaching. With a more thorough initial bleach (*e.g.* Figure 13b), the recovery of each isoform was generally lower, and the reverse was true for a weaker bleach (Figure 13c), illustrating how it is important to use a consistent extent of bleaching when comparing different constructs. In this context, the mobility of Iγ_i3 was consistently lower than that of, for instance, Iγ_i1.
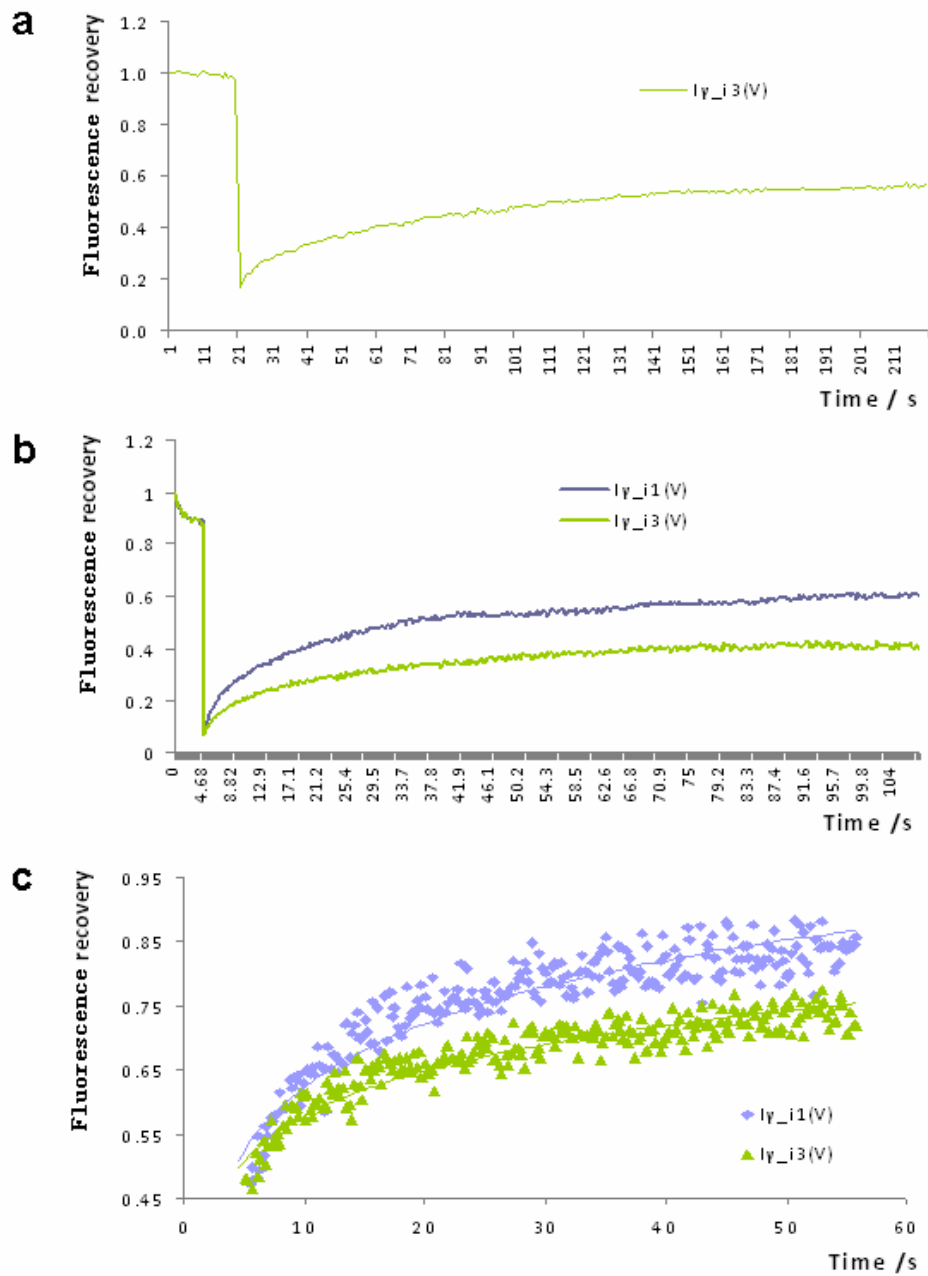
Figure 13 Fluorescence Recovery after Photobleaching of Iγ_i3

GFP-tagged constructs were overexpressed in HEK-293 cells. (**a**) Iγ_i3(V) recovered to 55% of the original level, indicating the presence of an immobile fraction, in agreement with the previous data published by Giudici, 2006. The mobility of Iγ_i3 was consistently lower than that of Iγ_i1 in relative terms, when the initial bleach was deliberately made stronger (**b**) or weaker (**c**). Mean fluorescence intensity is plotted for (**a**) and (**b**) (n = 10), and is used to generate the line of best fit for (**c**) (n = 5).

3.2.4. Lipid Kinase Activity

The lipid kinase activity of various Iγ_i3 constructs was assayed *in vitro*. Using PI4P as the substrate (see Methods), the lipids produced were separated by thin-layer chromatography (TLC), and the [^{32}P]PIP$_2$ produced (identified using a [^{32}P]PIP$_2$ standard run on the same plate) were measured and compared between different constructs, as an indication of their lipid kinase activity. Where the apparent activity slowed down with a longer reaction time, a non-linear fit was applied to the reaction profile, with the equation $y = A \times (1 - e^{-kx})$. The initial rate of reaction was taken for the purpose of comparison. When $x = 0$, the gradient of the curve $dy / dx = A \times k$.

Somewhat surprisingly, the V443A mutation attenuated the Iγ_i3 activity by about 55% (Figure 14). I reasoned that the V443A mutation might make such a difference to the apparent lipid kinase activity *in vitro* was because the interaction with lipid was facilitated by the more hydrophobic Val[443].
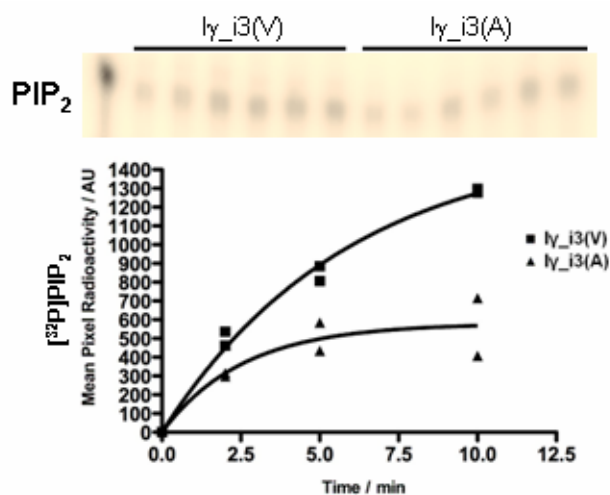
Figure 14 Lipid kinase activity of Iγ_i3(A) was lower than that of Iγ_i3(V)

PI4P micelle was used as the substrate of PIP5KIγ in the lipid kinase assay, with time courses of 2, 5 and 10 minutes. Lipid products were separated by TLC and the [^{32}P]PIP$_2$ level (identified using a radioactive standard, leftmost lane) was measured and compared between constructs (n = 2).

To explore this lipid interaction further, I constructed a more physiological way of presenting the lipid substrates in these *in vitro* assays, to mimic better the membrane environment where the PIP5K enzyme normally sees its substrate. I used a mixture of lipids (PIP_2, PI4P, PI, PE, PC, PS and PA, see Methods) in the form of liposomes.
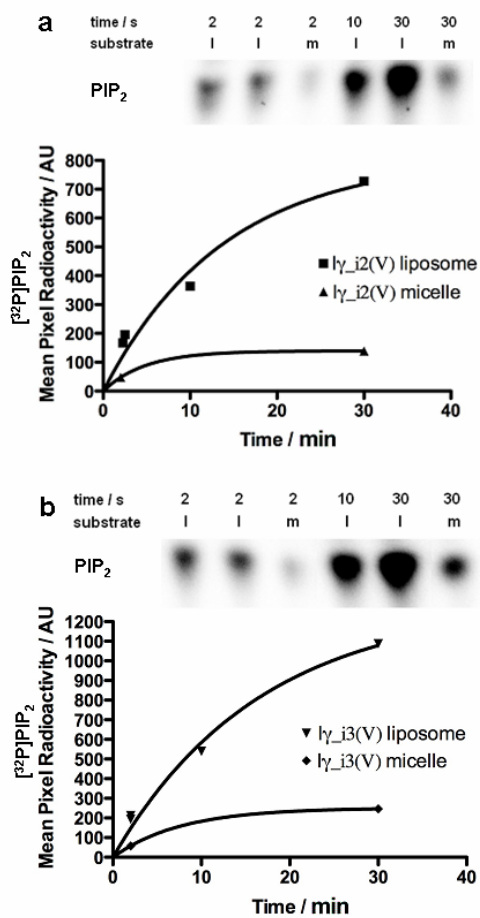
Figure 15 Lipid kinase activity of Iγ_i2/3 using micelle and liposome substrates

In both cases, PI4P was used as the substrate with PA as the activator, for the lipid kinase assay, with time courses 2, 10 and 30 minutes. They were either applied at 10 μM each on their own (micelles, "m"), or at 3.3 μM each with a lipid mixture mimicking the physiological composition of inner cell membrane (liposomes, "l"). The enzymes used were (**a**) Iγ_i2(V) and (**b**) Iγ_i3(V). Lipid products were separated by TLC and the [^{32}P]PIP_2 level was measured and compared.

As shown in Figure 15, the liposome presentation of substrates caused a much higher lipid kinase activity than with the micelle, even though both used PI4P as the substrate and PA as the activator (and note that the PI4P concentration was in fact higher in the micelle composition). This suggests that the PIP5K enzyme has adapted through evolution to function in its physiological environment, *e.g.* in this case sampling lipids anchored in the cell membrane. Therefore, it is important to supply the kinase with a lipid composition as close as possible to that in the cell, in order to interpret meaningfully the enzyme's activity measured in the *in vitro* assay. I therefore adopted the liposome method for all subsequent experiments on the lipid kinase activity.

In order to compare the lipid kinase activity of γ_i3 with that of the other splice variants, I set out to perform assays in parallel, using the lysates of HEK-293 overexpressing the FLAG-tagged enzymes (Figure 16). The relative quantity of enzymes present was assessed by Western blot of the immunoprecipitates, in parallel to those subjected to the kinase assay.

These experiments revealed that Iγ_i3 and Iγ_i2 exhibited the same level of lipid kinase activity *in vitro*, after compensating for the relative quantity of enzymes used. This suggests that the alternative splicing near the C-terminus of PIP5KIγ does not affect the overall structure of the enzyme, or the enzyme's catalytic ability as a lipid kinase.
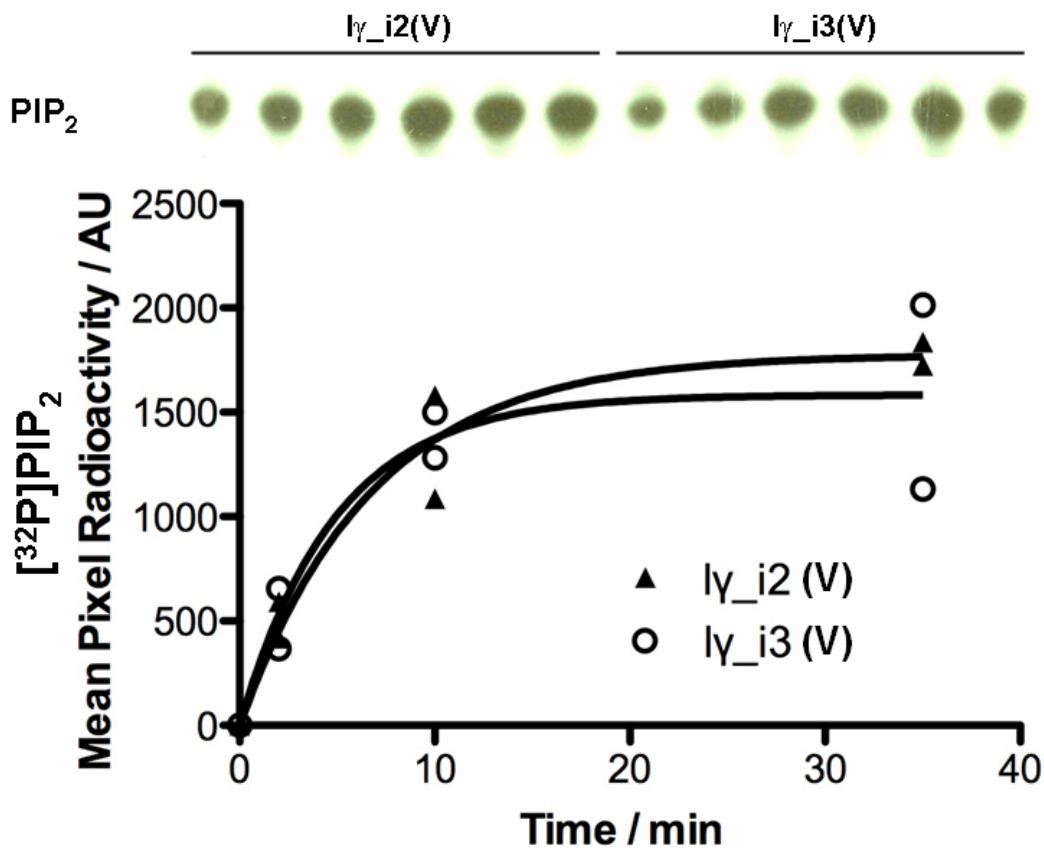
Figure 16 Iγ_i2 and Iγ_i3 exhibited a similar level of lipid kinase activity *in vitro*

The relative quantity of enzymes present was assessed by Western blot of the equivalent immunoprecipitates, in parallel to those subjected to the kinase assay. Wild type Iγ_i2 and Iγ_i3 were assayed in parallel, with time courses 2, 10 and 35 minutes in duplicate. The quantity ratio was 1.2 : 1 from the Western blot. Analyses confirmed that both splice variants of PIP5KIγ exhibited a similar level of lipid kinase activity *in vitro*.

3.2.5. Protein Kinase Activity (Autophosphorylation)

Since PIP5K was also documented to possess protein kinase activity, most likely for autophosphorylation (see Introduction), I also investigated how this might have been changed by the V443A mutation in γ_i3. *In vitro*, the Iγ_i3(A) was only 60% as active as Iγ_i3(V), as a protein kinase (Figure 17a).

I also investigated how the protein kinase activity would be changed by the presence or absence of the 26-AA peptide near the enzyme's C-terminus, that is, how γ_i2 and γ_i3 differed from each other in this aspect.

The lysate containing overexpressed enzyme was first quantified by Western blot (Figure 17b), and then volume-adjusted, in an attempt to use the same amount of enzyme for the kinase assay (Figure 17c). A protein kinase assay was carried out and the ^{32}P incorporation into the enzyme was measured. The Iγ_i3 protein exhibited a 1.5 fold higher autophosphorylation compared to Iγ_i2 (Figure 17d).
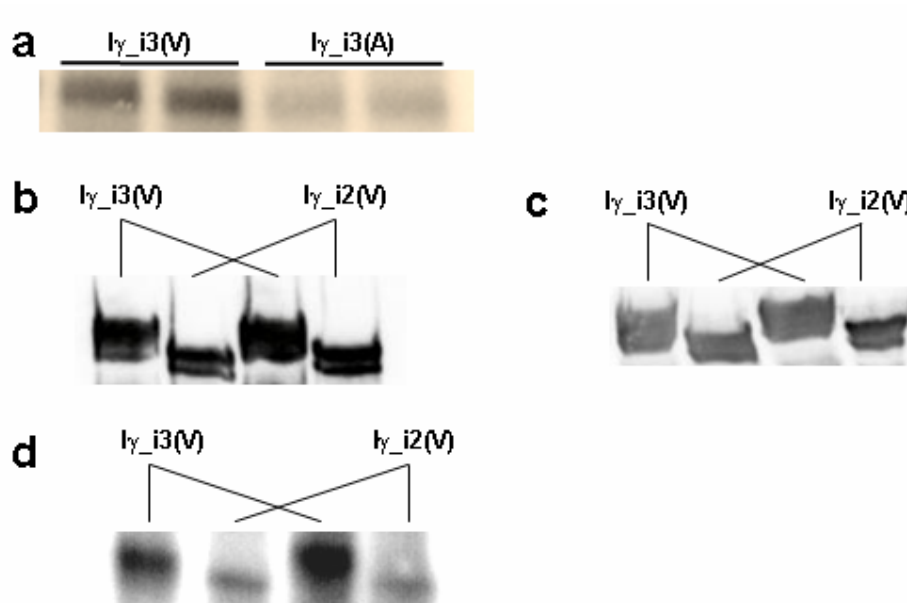
Figure 17 Protein kinase activity of Iγ_i2 and Iγ_i3, adjusting for V443A
(**a**) ^{32}P incorporation into the enzymes in the autophosphorylation assay, visualised by autoradiography of the dried polyacrylamide gel. (**b**) Western blot of the whole HEK-293 lysate overexpressing the FLAG-tagged enzyme. Quantity ratio of Iγ_i3 : Iγ_i2 = 3 : 2. (**c**) Western blot of the equivalent immunoprecipitates subjected to the kinase assay, successfully titrating the quantity ratio to 1: 1. (**d**) Typical ^{32}P incorporation into the enzymes in the autophosphorylation assay, visualised by autoradiography of the dried polyacrylamide gel. Iγ_i3 exhibited a 1.5 fold higher protein kinase activity compared to Iγ_i2, as measured by ^{32}P incorporation (n = 2).

The interpretation of this observation was not immediately clear, given that the two spliceoforms varied only in the C-terminus and the general catalytic ability (at least when measured as lipid kinase activity) was expected to be unchanged. The increased autophosphorylation in Iγ_i3 in the presence of the additional 26-AA insert may suggest that either the insert peptide is a further target of autophosphorylation, or it may serve to interact with other segments within the structure, which would otherwise inhibit autophosphorylation. This would uncover an apparent protein kinase activity of the enzyme by disinhibition.

3.2.6. A Review of the V443A Mutation

The mutation V443A discovered in our original Iγ_i3 constructs, as well as the several corresponding Iγ_i3(V), Iγ_i2(V) and Iγ_i2(A) constructs generated, has given me significant insight into the regulation of PIP5KIγ localisation and activity. It seems that the previously reported profound differences between Iγ_i2 and Iγ_i3[179] were partly due to this V443A mutation in the Iγ_i3 construct used. For example, the Iγ_i3(V) D316K mutant was not completely cytosolic, but remains partly associated with the PM, unlike the cytosolic Iγ_i3(A) D316K mutant reported before (Figure 10a and b).

In general, a PIP5KIγ with Ala^{443} had a more cytosolic (*i.e.*, less PM-bound) localisation than its Val^{443} counterpart. Interestingly, within the range of mutations tested, each of which disrupted different domains of the enzyme, the moderate effect caused by V443A substitution seemed to be similar. That is, V443A substitution seemed to exert an independent influence, leading to a general reduction of PM-association. Many of such changes may be explained by the fact that valine, as one of the most hydrophobic amino acid residues (hydropathy index 4.2), has a much higher hydrophobicity than alanine (hydropathy index 1.8). Therefore, the affinity of Iγ_i3/2(V) to the lipid compositions in the PM was higher than the corresponding Iγ_i3/2(A).

This "off-membrane" effect is particularly intriguing in light of our earlier discussions on multiple, low-affinity membrane-interactions (Section 1.2.2). It may be viewed that when the wild type Val^{443} is present, it increases (albeit minutely) the affinity of the enzyme towards the membrane, and this incremental change is big enough to make certain mutants to go to the membrane, while remaining subthreshold for the others. So, in our hands this V443A mutation turned into a helpful tool to dissect out some of the intrinsic, yet otherwise non-apparent, differences in the PIP5K background.

Moreover, a closer look at AA residue 443 reveals that there may be additional factors. The Val/Ala^{443} site is C-terminal to the activation loop, and is also immediately upstream of a conserved dibasic motif (RK in Figure 6b). The latter motif of two basic residues is important for the PM-localisation and function of Iγ, as revealed by a series of mutagenesis experiments[198]. My results are also consistent with earlier findings identifying residues that were crucial to the activity of PIP5KIβ, homologous to Ser^{440} – Ser^{447} of Iγ[108] (Figure 6b). A truncated Iβ protein ending C-terminally with Ile^{399} retained 100% activity as well as the ability to reorganise actin, whereas Iβ ending with Asn^{392} (lacking the Val^{443}-homologue and dibasic motif mentioned above) was < 5% active, and was unable to reorganise actin. Therefore, I have further established the importance of this region immediately C-terminal to the kinase homology domain in contributions to Iγ's PM-localisation, and have revealed that residue Val^{443} near the dibasic motif may also be crucially implicated in the necessary interactions with the hydrophobic substrate. Therefore, although the Type I activation loop consensus is necessary for correct PM-targeting (see Introduction), other motifs in the rest of the kinase body, such as this one containing Val^{443}, are also required.

To assess whether or not Ala^{443} induced a distortion to the general structure rather than to a specific binding or catalytic site, I compared the lipid kinase activity of Iγ_i3(V) and Iγ_i3(A). Iγ_i3(A) retained only 40% activity compared with Iγ_i3(V) (Figure 14). This result may be explained by the fact that alanine, being considerably less hydrophobic than valine, reduces the efficiency of Iγ_i3's interaction with its lipid substrate, PI4P, near the activation loop. However, the autophosphorylation activity of Iγ_i3(A) was also considerably reduced, to 60% of that of Iγ_i3(V) (Figure

17a). Many more experiments would be required to establish if the lipid and protein kinase changes are significantly different from each other. However, a preliminery argument can be advanced that the protein kinase activity of Iγ_i3 may be impaired by V443A to a lesser extent than the lipid kinase activity because of the location of the Val[443] residue close to the lipid-binding activation loop. The overall behaviour is not explained by previous findings that phosphorylation of the PIP kinase may in some cases be negatively correlated with lipid kinase activity[127, 129].

In conclusion, in addition to weakening lipid-association, V443A may interfere slightly with the general catalytic mechanism of Iγ_i3 as well as its *in vivo* phosphorylation (discussed below), possibly through a non-specific structural disruption. Nonetheless, as we shall see in Chapter 4, I demonstrate that the V443A mutation can be exploited as a helpful (albeit accidental!) tool in exaggerating the effect of certain mutations, and therefore it can shine useful light onto how the physiological functions of PIP5KIγ are performed and regulated.

3.3. Role of the 26-AA Insert of Iγ_i3

As described above, after correcting back the V443A mutation, there were still several genuine functional and behavioural differences between Iγ_i3 and its related spliceoforms, Iγ_i1 and Iγ_i2. These unique characters must be caused by a structural difference between these splice variants, and this must reside in the 26-AA peptide inserted into Iγ_i3 between Exon 16 (the Iγ_i1 "tail") and Exon 18 (the Iγ_i2 "tail"), as illustrated in the Introduction (Figure 5).

Based on experimental evidence and reasoning, I formulated several possible roles of this Iγ_i3-specific insert. This thesis would now address these possibilities in turn.

3.3.1. Potential PIP$_2$-binding Site – the 4R Mutant

It was observed earlier, and this was particularly obvious with the Ala^{443} in place, that the kinase-inactive D316K mutants of both γ_i3 and γ_i2 were completely dephosphorylated (Figure 8c). However, while the Iγ_i3(A) D316K was cytosolic (Figure 10b), Iγ_i2(A) D316K remained appreciably localised on the plasma membrane (Figure 10d). This difference could underlie earlier data indicating that Iγ_i3(A) D316K caused a great reduction in neuronal proliferation, while Iγ_i2(V) D316K did not[179]. Moreover, these data seemed to suggest a unique, specific activity-dependency of Iγ_i3's PM-association, which was not shown by other splice variants.

Since the Asp^{316} position was part of the weak base catalytic mechanism, specifically underlying the enzyme's catalytic capability (as a lipid or protein kinase), the D316K mutation only impaired the kinase activity and spared the lipid binding domains. In other words, the interaction of the D316K mutant with its PI4P substrate should be normal. This effectively ruled out the possibility that the different localisation of D316K was due to its disrupted binding with membrane-associated PI4P.

Clearly, for Iγ_i3 the loss of membrane localisation appears to be associated with a loss of activity in D316K. One possibility was that the enzyme Iγ_i3 needs sufficient PIP$_2$ present on the cell membrane before it could be targeted to and stay on the PM (either directly or via binding PIP$_2$) and that only the active version synthesises enough PIP$_2$ near the enzyme. In order to test this idea, the ideal experiment would be to maintain the apparently normal PIP$_2$ level in the relevant cellular compartments, and observe if the Iγ_i3(A) D316K stayed on the PM. Such a scenario was in fact already tested in an earlier study by Giudici[179], where the γ_i3(A) D316K mutant was co-transfected with active γ_i3 or γ_i2, differentially tagged by GFP and FLAG. Interestingly, the kinase-inactive molecules remained cytosolic, whereas the active enzymes still localised normally to the PM, as if there was no cross-talking. This suggested that it was not the *overall* PIP$_2$ abundance that dictated the enzyme's localisation, but more likely it was the activity specific to each enzyme molecule that determined its own targeting.

I therefore reasoned that the γ_i3's peptide insert could serve as (or as part of) a PIP$_2$-binding site, which binds to the lipid kinase product whenever a PI4P is turned into PIP$_2$ by the same enzyme molecule. Conceivably, the PIP$_2$ produced may be transferred from the catalytic site immediately to this putative binding pocket (formed by the 26-AA peptide), and then expose an *interaction site* with potential binding partners and turn the enzyme into a conformation that was ready to localise to the PM. The converse of this idea is that when the insert has no PIP$_2$ bound, it changes the structure of the enzyme, hence the inactive γ_i3 does not go to the PM as readily as the inactive γ_i2. This would give the γ_i3 splice variant an activity-dependency specific to *each molecule*, which was not seen in γ_i2 or γ_i1.

The hypothesis of a PIP$_2$ binding site in the 26 AA itself was encouraged by the presence of four adjacent arginine residues in the insert (Figure 6c). To test this hypothesis, I engineered a mutant by site-directed mutagenesis, changing all four residues (Arg^{648} to Arg^{651}) into negatively charged glutamate, denoted mutant *4R*. The making of the 4R constructs is summarised later along with other mutageneses in Section 4.1.
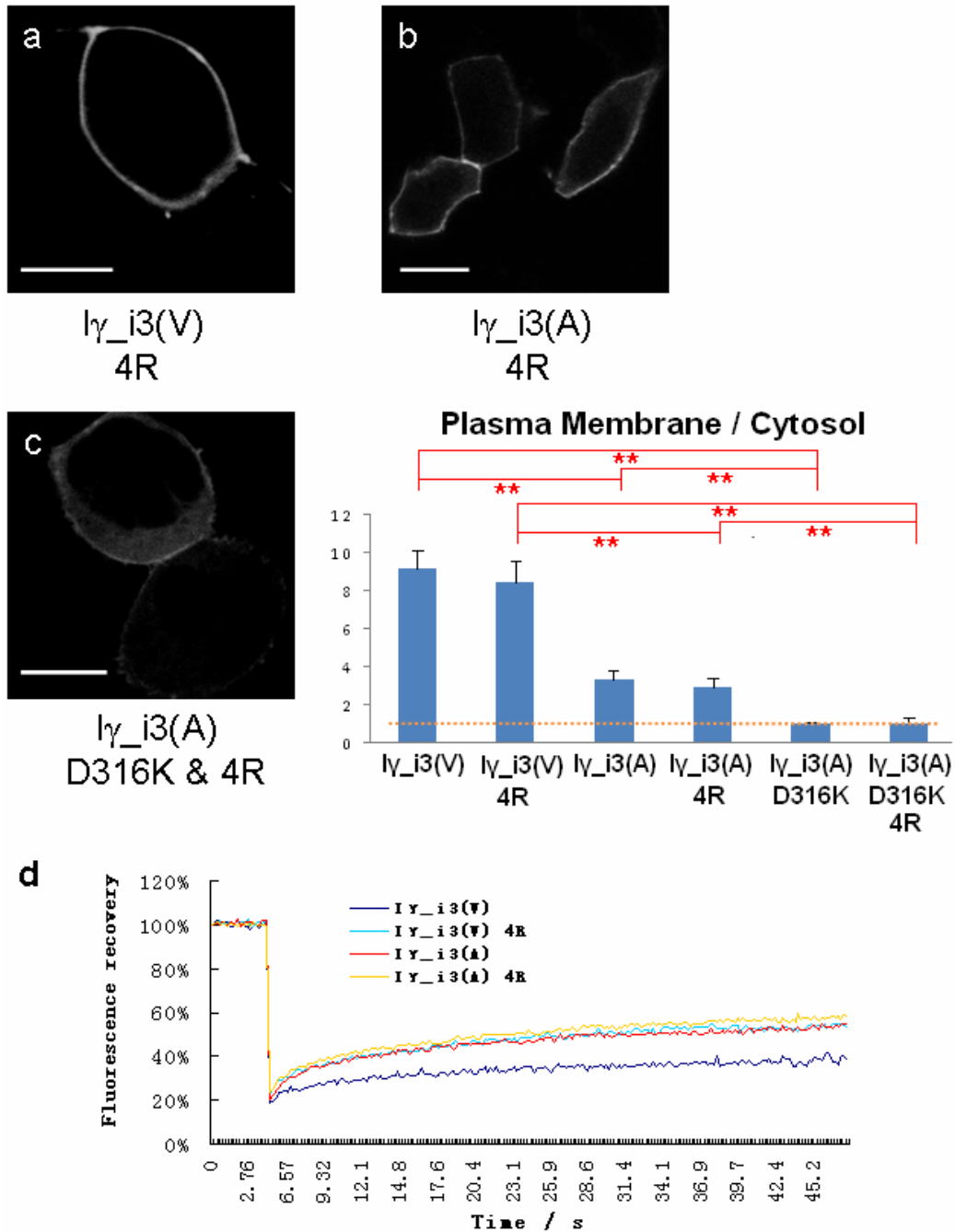
Figure 18 Major characters of the 4R mutants

(**a**) – (**c**) Typical subcellular localisation of overexpressed GFP-tagged 4R constructs in HEK-293 cells (scale bar = 10 μm). Panel on the right indicates quantified ratio of PM / cytosol fraction. Orange dotted line indicates a cytosolic (non-membrane-enriched) localisation (n = 30, ** p < 0.001). (**d**) FRAP behaviour of 4R constructs, mean fluorescence intensity plotted (n = 20).

When introduced alongside D316K, 4R did not make any difference to the cytosolic localisation of γ_i3 (Figure 18c), as expected from the activity-dependency of the PIP$_2$-binding hypothesis above. However, in the active enzyme, the 4R mutation also did not change the original localisation of γ_i3(V) (Figure 18a). In case there was a "ceiling effect" because γ_i3(V) was already maximally PM-bound, I also tested 4R on γ_i3(A), which was localised on the PM to a lower extent. Again, the PM-association was unchanged (Figure 18b). In other words, when the putative PIP$_2$-binding site could no longer bind the PIP$_2$ product, the localisation of γ_i3 was not altered. Nonetheless, the 4R mutation increased the degree of mobility of the enzyme to a greater degree in the presence of Val^{443} (Figure 18d). This would make sense, if the four positively charged arginine residues normally interact and associate with other protein and lipid partners, either specifically (*e.g.* PIP$_2$ as in my hypothesis) or in a general, electrostatic fashion. However, in the absence of an effect on localisation, the interpretation of these data was not immediately clear. Presumably, it still remains a remote chance that the 4R mutation did not impair the PIP$_2$-binding as we expected.

Nevertheless, the above preliminary results seem to suggest that the PIP$_2$-binding hypothesis is probably incorrect.

3.3.2. Potential Phosphorylation Target – the 5P Mutant

As mentioned in the last Section (3.2), the apparently discrete phosphorylated states of PIP5KIγ_i3 *in vivo* do not suggest a singular, all-or-none phosphorylation of the protein molecule. It is more likely that multiple residues may be the target of regulated phosphorylation pathways. Indeed, γ_i3 seemed to have at least one extra phosphorylated state, between the "completely" phosphorylated state and the unphosphorylated state (Figure 8d). Furthermore, the autophosphorylation activity of γ_i3 seemed to be higher than that of γ_i2 (Figure 17c and d), which might suggest that the additional peptide of γ_i3, the 26-AA insert near its C-terminus, could be a target of phosphorylation *in vivo*. Conceivably, the insert itself may contain additional

phosphorylation sites that, together with the sites in common with Iγ_i2, give the larger separation of the "completely phosphorylated" band in Iγ_i3 (Figure 8d).

Various bioinformatics tools were used in an attempt to narrow down the search for potential phosphorylation sites, producing a theoretical prediction of the target S, T and Y residues in the γ_i3 peptide (*e.g.* NetPhos in Figure 19a). In particular, within the 26-AA insert (AAs 637–662), Ser^{646}, Thr^{656} and Ser^{658} were predicted with a superthreshold score above 0.50 (0.990, 0.934 and 0.879, respectively), labelled as highly probable by the program. This result was confirmed by a related, kinase-specific program, NetPhosK[206].

Therefore, although the phosphorylation state observed provides us with some useful information and intriguing correlations with the rest of Iγ_i3 behaviour, the overall phosphosphorylation should not be taken as an entity, and we need to bear in mind the possibility of different combination of residues producing indistinguishable patterns on Western blot.

I sought to address this possibility experimentally by extracting and purifying the overexpressed enzyme from mammalian cells, treating some of it with alkaline phosphatase *in vitro* (which removes all phosphorylation as shown in Figure 8a), and then subjecting both the native (retaining the original phosphorylation pattern) and dephosphorylated protein to mass spectroscopy. This comparison should enable the identification of key AA residues implicated in the phosphorylation *in vivo*. With the use of smaller peptide fragments generated by proteases, we could then dissect out which residues within this 26-AA insert is a genuine phosphorylation target. This would enable us to obtain the fine print of the overall phosphorylation state observed, to distinguish between autophosphorylation and phosphorylation by other proteins, and to determine whether phosphorylation at a certain site is necessary or sufficient for other enzyme behaviours, *e.g.* PM-targeting (see next Chapter).

Protocols were developed and the purification was proven to be possible, either by immunoprecipitation using the anti-FLAG antibody, or by competition using the 3xFLAG peptide. The exact conditions for these protocols to work required a considerable amount of optimisation. For example, with the immunoprecipitation

method, trials were carried out with 3, 6, 10 and 15 washes. When the washes were too few, it was difficult to get rid of the non-specific background; when too many, less and less tagged protein remained on the beads. It was discovered that 6–10 washes produced the best signal to background ratio (Figure 19b). However, after several preliminery trials, it proved difficult to obtain the overexpressed FLAG-tagged PIP5KIγ_i3 at a high enough purity to proceed with.
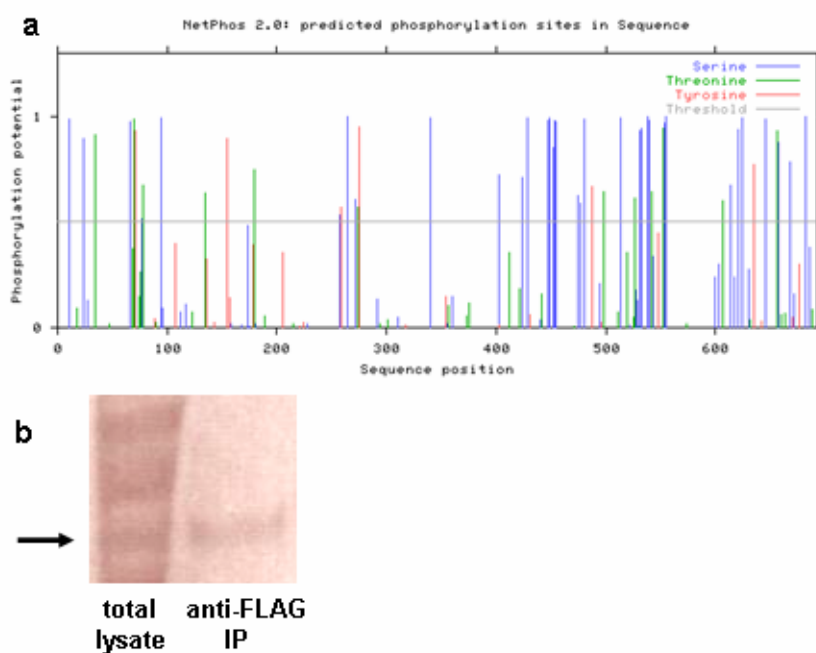
Figure 19 Prediction of phosphorylation sites and Iγ_i3 purification for mass spectroscopy

(**a**) Theoretical prediction of target residues on the γ_i3 peptide by NetPhos, the bottom numbers corresponding to AA numbers in the γ_i3 peptide, and the height of the bars indicating the likelihood of being a phosphorylation site. (**b**) Picture of dried down SDS-PAGE gels, stained with Coomassie blue; arrows indicate the FLAG-tagged γ_i3 band. The enzyme was purified by immunoprecipitation using the anti-FLAG antibody (with 10 washes).

Due to the significant time and resources required by this mass spectroscopy project, and considering the amount of information and analysis involved once the numerous phosphorylation targets were identified, it seemed unrealistic, given the timescale, for the present study to proceed in this direction. Instead, we conceived a simpler way of at least confirming whether or not the 26-AA insert of γ_i3 was a physiological target of phosphorylation.

This method is based on the fact that only certain amino acids could possibly undergo phosphorylation, *i.e.*, serine, threonine and tyrosine. There were five such residues within the 26-AA insert, namely, Tyr^{642}, Ser^{646}, Thr^{656}, Ser^{658} and Thr^{660}. As a proof-of-principle experiment, I mutated all five residues into alanine, denoted mutant *5P*.

The making of the 5P constructs is summarised later along with other mutageneses in Section 4.1.
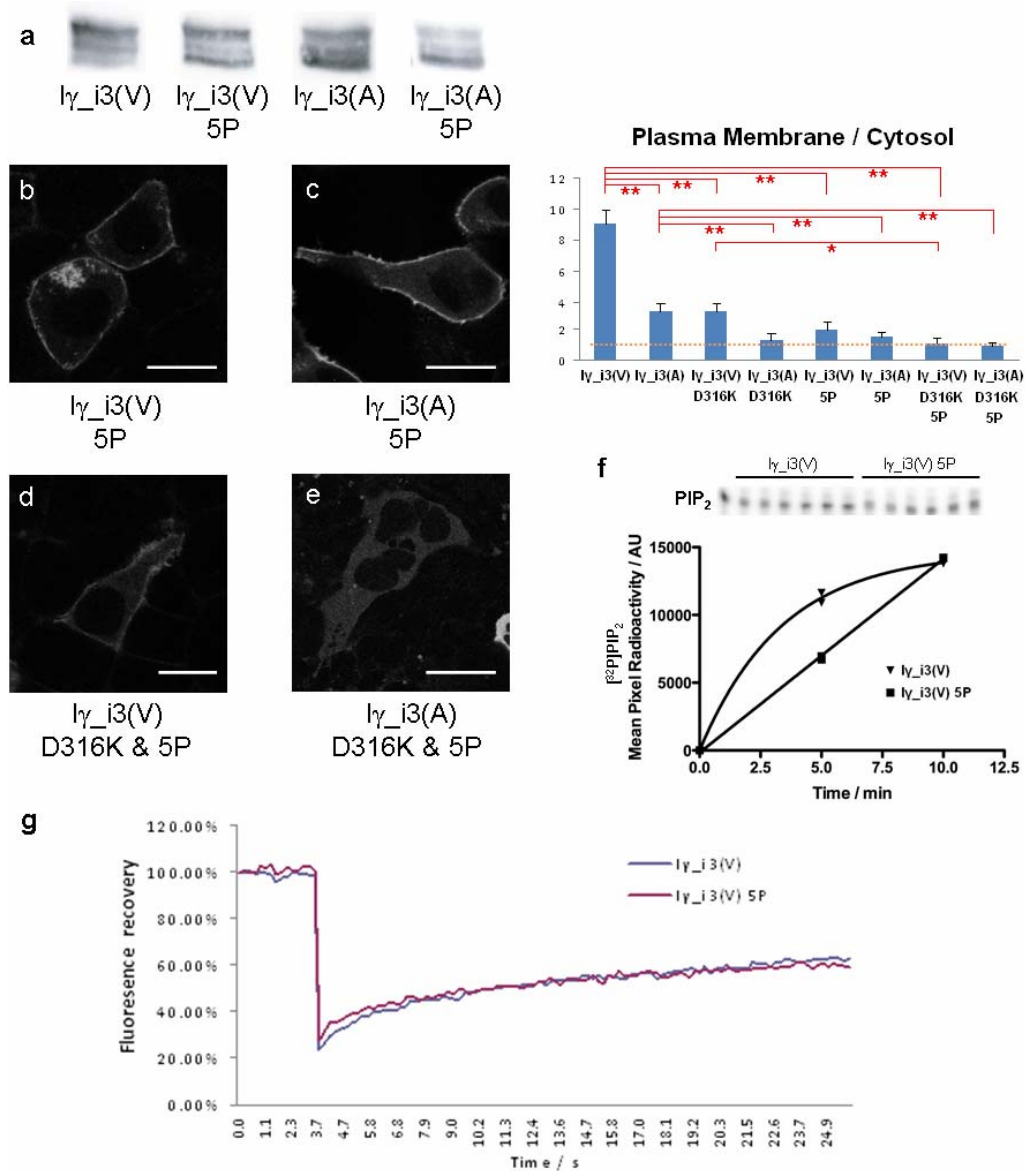
**Figure 20 Major characters of the 5P mutants**

(**a**) Phosphorylation pattern of 5P constructs. (**b**) – (**e**) Typical subcellular localisation of overexpressed GFP-tagged 5P constructs in HEK-293 cells (scale bar = 10 μm). Panel on the right indicates quantified ratio of PM / cytosol fraction. Orange dotted line indicates a cytosolic (non-membrane-enriched) localisation (n = 30, * $p < 0.05$, ** $p < 0.001$). (**f**) Lipid kinase activity of Iγ_i3(V) 5P, with time courses of 5 and 10 minutes. Lipid products were separated by TLC and [^{32}P]PIP$_2$ was measured and compared between constructs (n = 2). (**g**) FRAP mobility of Iγ_i3(V) 5P, mean fluorescence intensity plotted (n = 20).

If any of the five residues were physiological phosphorylation sites, we reasoned that the 5P mutant should eliminate such modification, and consequently the protein should show up as having a smaller separation between the phosphorylated and unphosphorylated bands in SDS-PAGE. In the 5P mutants tested, the separation of the "completely phosphorylated" band from the presumed dephosphorylated band did not decrease (Figure 20a). Furthermore, a hint of the middle band, although fainter, could still be detected.

Interestingly, it was the overall ratio of phosphorylated to unphosphorylated molecules that was reduced. It meant that the insert was not likely to be a direct phosphorylation target *in vivo*, but might cause indirect changes in the enzyme's structure or accessibility to kinases (including its own catalytic core) that would lead to further phosphorylation on the rest of the protein. This alternative theory could explain the fact that 5P slightly reduced the enzyme's efficiency as a lipid kinase, slowing it down even if the overall capacity of catalysis remained comparable to the wild type (Figure 20f). The different kinetics in Figure 20f require confirmation and then more detailed examination before any interpretation can be put on them.

The mutant's mobility was unaffected, measured by FRAP (Figure 20g), while the PM-association of Iγ_i3 constructs appeared to be significantly reduced by 5P, whether the enzyme was active (Figure 20b and c) or inactive (Figure 20d). In fact, such a correlation between PM-association and *in vivo* phosphorylation was frequently observed for PIP5KIγ (see next Chapter), so whether the lower PM-association of 5P was the cause or the result of its reduced phosphorylation is not clear from these data. This topic will be addressed in the next Chapter, when the relationship between different aspects of the enzyme's behaviour is more thoroughly studied.

3.3.3. The C-terminus on Its Own

As a quick experiment to find out whether there was any discernible difference between the C-terminal peptides of γ_i3 and γ_i2 on themselves, *i.e.*, without

potential combinatorial influence from the sophisticated regulatory motifs in the whole protein, we devised a "C_{12}" construct for both splice variants. The C_{12} constructs consisted of the C-terminal portion of the enzyme, starting from Exon 12 (downstream of the activation loop). Perhaps not surprisingly, these constructs failed to be targeted to any compartments and filled the cytosol as a consequence, since the peptides made had no protein backbones to fold onto and therefore were likely unstructured (Figure 21c and d).
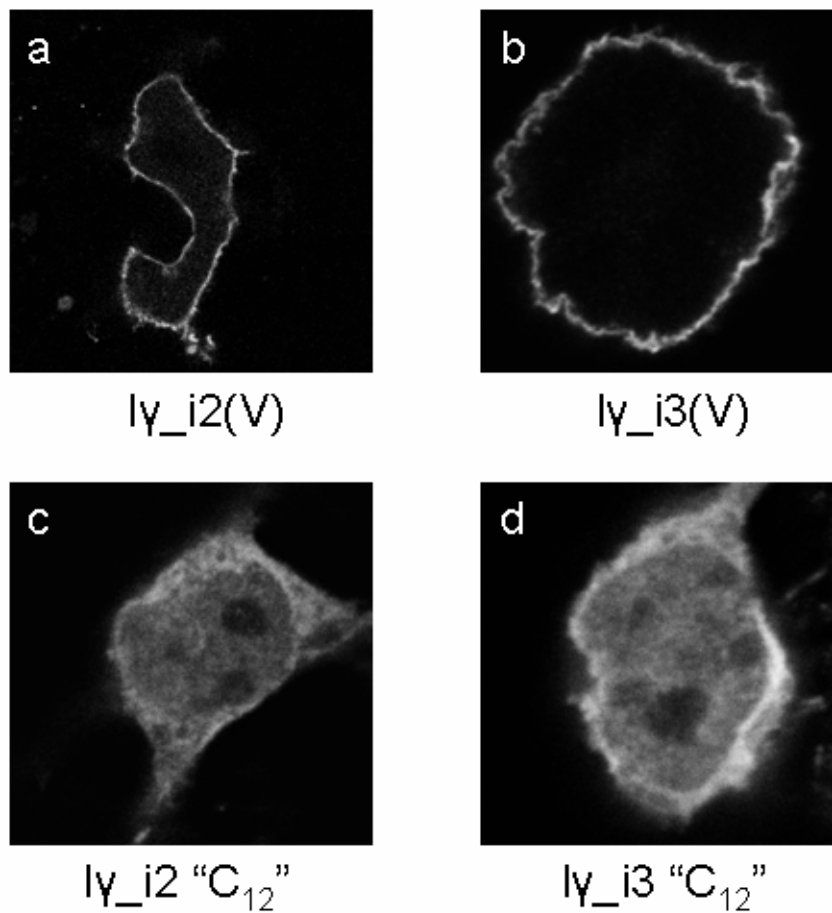
Figure 21 Subcellular localisation of the C-terminal constructs of Iγ_i3/2
Typical immunocytochemical staining of overexpressed FLAG-tagged constructs in HEK-293 cells.

Taken together, the above data most likely indicated that the 26-AA insert of Iγ_i3 was probably not a direct phosphorylation target, nor a PIP$_2$-binding site. A hypothesis for the above data is that the 26-AA insert could impose a structural influence on Iγ_i3, potentially exposing additional AA targets for autophosphorylation. Only when such autophosphorylation takes place could Iγ_i3 be recognised by certain partners, which might then bring the molecule onto the PM. Conversely, in the absence of the insert (*i.e.*, Iγ_i2 and Iγ_i1), the enzyme may have a conformation that is readily accessible by these partners. Such a theory could also explain the observation that the PM-association of Iγ_i3 required the enzyme being active, while on the other hand it was not necessary for the localisation of Iγ_i2.

Without detailed knowledge of the phosphorylation sites, it was far from straight forward to start testing this hypothesis. Nonetheless, we may be able to gain some insight from *in silico* screening of available protein databases. Meanwhile, one further possibility is proposed in the Discussions (Section 7.3.3).

3.3.4. Structural Insights

A preliminary search in the Pfam database[207] identified several features of the peptide insert, which could underlie its interaction with other parts of the protein. For example, part of the insert peptide was matched to a hinged β-pleated sheet in hemopexin, a serum glycoprotein that binds and transports haem. This might imply potential interactions with other peptide motifs, enabling the functions as hypothesised above.

Except for the above finding, however, there were in fact very few hits the online screening produced for the insert peptide on itself, based on sequence homology. This was initially puzzling, until I considered the possibility that the insert may be a "purposely" unstructured peptide through evolution. This refers to protein segments (potentially with certain characteristics) that fail to self-fold into a fixed 3-dimensional structure, sometimes in their native state[208, 209]. The significance of such peptides is only being increasingly understood recently, more frequently

encountered in the eukaryotes[210, 211], primarily as a way of introducing structural disturbance and flexibility to a protein, whereby it gains or loses salient functions. According to the "Protein Trinity Hypothesis", a given native protein can be in any of the ordered, partially ordered or extended forms, and functions can arise from any one of the three forms or from transitions between them[211]. A particularly intriguing example is MARCKS, whose basic effector domain is unstructured, yet binds PIP_2 with very high affinity on the lipid bilayer[50]. This is only explained by the fact that the unstructured effector domain binds several (probably three) PIP_2 molecules to form an electroneutral complex, greatly enhancing its affinity for the PC/PIP_2 membrane, whereas a small basic hydrophilic peptide cannot typically form complexes with more than one PIP_2[212, 213]. In other cases, the structurally disordered peptide domain may form a regulatory sensor, a folding inhibitor, a flexible linker, an entropic spring, or a loose loop prone to protease cleavage, upon which it alters conformation and is able to bind other partners and assume novel functions[208].

4. Results II – Localisation and Regulation of Iγ_i3

4.1. Mutagesis and Subcloning of Constructs

This study designed and generated quite a few mutants, either by site-directed mutagenesis or by subcloning (using restriction digestion followed by ligation). As so many constructs are mentioned in the previous Chapter as well as this, it may be helpful to summarise them here.

4.1.1. Summary of Mutants Used in This Study

A summary of all relevant mutants in the present study is shown in Table 4.

Mutation	Original	Mutated	Note
V443A	Val^{443}	Ala^{443}	Random mutation discovered in our Iγ_i3 constructs, accumulated from the initial cloning into all subsequent mutants made[*]
D316K	Asp^{316}	Lys^{316}	Mutation in the weak base catalytic mechanism of the conserved kinase domain, making the enzyme inactive for both lipid and protein catalysis[*]
K188A	Lys^{188}	Ala^{188}	Mutation in the ATP-binding site of the conserved kinase domain, an alternative way to D316K of making the enzyme catalytically inactive
E410A	Glu^{410}	Ala^{410}	Mutation in the activation loop, significantly reducing Type I lipid kinase activity, and giving rise to considerable Type II activity[130]
T412A	Thr^{412}	Ala^{412}	Mutation in the activation loop, where substitution of threonine into alanine prevents phosphorylation on this residue

T412D	Thr^{412}	Asp^{412}	Mutation in the activation loop, where substitution of threonine into aspartate mimics the effect of constitutive phosphorylation on this residue by negative charge*
5P	Tyr^{642}, Ser^{646}, Thr^{656}, Ser^{658}, Thr^{660}	Ala^{642}, Ala^{646}, Ala^{656}, Ala^{658}, Ala^{660}	Mutation prevents phosphorylation at all five putative phosphorylation targets within the Iγ_i3-specific 26-AA insert*
4R	Arg^{648}, Arg^{649}, Arg^{650}, Arg^{651}	Ala^{648}, Ala^{649}, Ala^{650}, Ala^{651}	Mutation eliminates the positive charges on the basic motif within the Iγ_i3-specific 26-AA insert*
E111L	Glu^{111}	Leu^{111}	Mutation homologous to E61L in rat PIP kinase Iβ, where interaction with Rac is abrogated[138]. Rac is a small monomeric G-protein and a member of the Rho family GTPases, required for plasma membrane-association of Type I PIP kinases
PM	Met^{1}…	Met^{1}Gly^{2} Cys^{3}Ile^{4} Lys^{5}Ser^{6} Lys^{7}Arg^{8} Lys^{9}Asp^{10}…	Mutation adds a 9-AA N-terminal tag from Lyn kinase, responsible for the posttranslational modifications palmitoylation and myristoylation, attaching lipid on the protein and thereby inserting it into the plasma membrane
C$_{12}$	full length	Exons 12–19	Mutation keeps only the C-terminal portion of the enzyme, without the catalytic core or activation loop*

Table 4 Summary of all mutants used in the present study

* indicates mutations that already appeared in the previous Chapter (Results I).

4.1.2. Generation of Mutants by Site-directed Mutagenesis

Typically, the point mutations introduced involved a single amino acid substitution. This was achieved with the help of appropriately designed primer pairs that annealed to both sides of the target site of mutagenesis, flanking the desired sequence to be introduced (Table 5). In the case of multiple amino acid substitutions, *e.g.* the 4R and the 5P mutants, several rounds of site-directed mutagenesis were performed sequentially, to change the residues in smaller, manageable groups. This was because a larger region of mismatch may lead to non-specific or particularly weak binding between the primers and the template. For instance, with the 4R mutants, I originally attempted to mutate all four Arg residues simultaneously. However, the result was negative, prompting me to achieve this by dividing it into two sequential steps, as described above.

Purpose	SDM forward	SDM reverse
A443V	GAGCAGCACGG *T* CTTCCGGAAGAGTTCC	CTTCCGGAAG *A* CCGTGCTGCTCATGAAC
V443A	GTTCATGAGCAGCACGG *C* CTTCCGGAAGAG	GGAACTCTTCCGGAAG *G* CCGTGCTGCTC
D316K	GAGCTTCAAGATAATG *AAG* TACAGCCTGC	CCAGCAGCAGGCTGTA *CTT* CATTATCTTG
5P (1–2)	CGCCCACGGGAGA *GC* CTGGCTTTTC *G* CTCCCCGTCG	CGGCGACGACGGGGAG *C* GAAAAGCCAG *GC* TCTCCCG
5P (3–5)	CGCCGACTGCGGGCCGTG *G* CACCA *GC* CCAC *G* CAGGCGCTCC	CGTCGGTGGGAGCGCCTG *C* GTGG *GC* TGGTG *C* CACGGCCCGC
4R	GGCTTTTCTCTCCC *GAAGAAGAAGAA* CTGCGGGC	CCCGCAG *TTCTTCTTCTTC* GGGAGAGAAAAGCCAG

4R (1–2)	CTTTTCTCTCCC *GAAGAA* CGCCGACTGCG	CAGTCGGCG *TTCTTC* GGGAGAGAAAAGCC
4R (3–4)	CTCTCCCGAAGAA *GAAGA* ACTGCGGGCCG	CACGGCCCGCAGT *TCTTC* TTCTTCGGGAG
E410A	GTTCATCAAGAAGTTAG *C* ACACACCTGG	GGGCCTTCCAGGTGTGT *G* CTAACTTCTTG
T412D	CATCAAGAAGTTAGAACAC *GA* CTGGAAGGCCC	GGACGAGGGCCTTCCAG *TC* GTGTTCTAAC
T412A	CAAGAAGTTAGAACAC *G* CCTGGAAGGCCC	GGACGAGGGCCTTCCAGG *C* GTGTTCTAAC
E111L	GACTTCTATGTGGTG *CTG* AGCATCTTCTTTCCCAG	GAAAGAAGATGCT *CAG* CACCACATAGAAGTCCTGC
PM	(see next section 4.1.3)	

Table 5 Primers for the generation of mutants by site-directed mutagenesis
The nucleotides in *underlined and Italic* font refer to the mismatching region with the template, *i.e.*, the sequence desired after site-directed mutagenesis.

The site-directed mutagenesis typically generated a linear band of double-stranded fragment after PCR, theoretically with a background of the circular plasmid template which may not always be discernible on the gel due to its low concentration. This product was treated *in vitro* with the restriction enzyme *DpnI* to remove the contamination by the methylated DNA of the original plasmid (Figure 22). The remaining product should all contain the desired target sequence, dictated by the primers added. The resultant DNA was transformed into competent bacteria to amplify, and circular plasmids were extracted at the end.
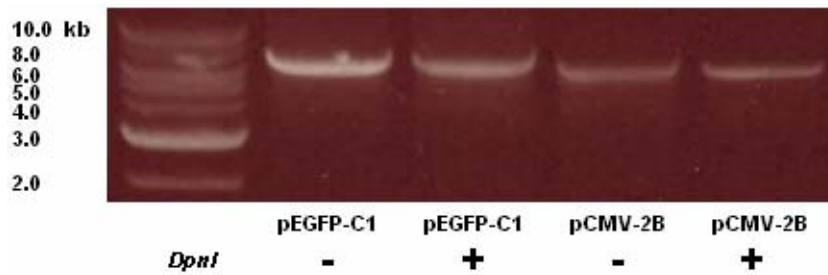
Figure 22 Typical *DpnI* digestion in a site-directed mutagenesis

4.1.3. The Generation of the PM Mutants

I shall later discuss the important significance of the PM construct. Its generation involved the addition of nine amino acids (GCIKRKGKD) from the Lyn kinase onto the N-terminus of the fusion gene (just after the starting methionine). This was quite difficult to achieve, in that the insertion (~ 30 bp) was neither short enough to be achieved by a simple site-directed mutagenesis reaction, nor long enough to be readily ligated as an insertion fragment into the multiple cutting site at the N-terminus of the fusion gene.

Since it was important to ensure that the PM tag only inserted in the correct direction, I decided to utilise two different restriction sites on either side of the potential PM insertion. Based on the existing multiple cutting site within the pEFGP-C1 and pCMV-2B (FLAG) vectors, I chose to introduce *SalI* and *EcoRV*, which were both novel and hence unique in the plasmids. This was important in the plasmid digestion steps later to produce a single backbone. Correspondingly, the *SalI* and *EcoRV* sites were also introduced as the flanking sequences on the primers used for the amplication of the PM-tag, to be digested into the double-cut configuration after PCR purification (Figure 23a).

Unfortunately, the entire fragment of PM-tag (including the flanking restriction sites) was below 40 bp, too short to be amplified by PCR. After a few unsuccessful attempts, an alternative method of making the double-cut PM fragment was tried. I decided to

make two DNA oligomers (as I would do for making ordinary site-directed mutagenesis and sequencing primers), both complementary over the PM sequence and each protruding at one end. When both strands were allowed to denature and remix in an aqueous solution, they should anneal with each other into double-stranded fragments, with both ends in a configuration exactly as if it was cut by the *SalI* and *EcoRV* restriction enzymes (Figure 23b). This new strategy was successful.

The next step was to introduce the same *SalI* and *EcoRV* sites into the PIP5KIγ-containing plasmids, just before the start codon. Using appropriate primers for site-directed mutagenesis on both plasmids, I managed to obtain the plasmids with the desired restriction sites in place. I then proceeded to double digest the plasmids containing the FLAG- or GFP-tagged PIP5KIγ, so that the N-terminus of the fusion gene could accept the PM insert (Figure 23c). The digestion was successful, producing linear backbones of the correct size (Figure 24a and b).

Since the ligation was unidirectional (using two different restriction sites) and hence the cut vector could not reanneal on itself, the phosphatase treatment was optional in this scenario (Figure 23c). The concentration of both the cut backbone and "cut" insert was measured, and titrated in search of an optimised molar ratio (*e.g.* Figure 24c). However, after several attempts, the ligation was not successful, presumably because, again, the insert was too small and consequently the stoichiometric ratio was too extreme to be optimised.
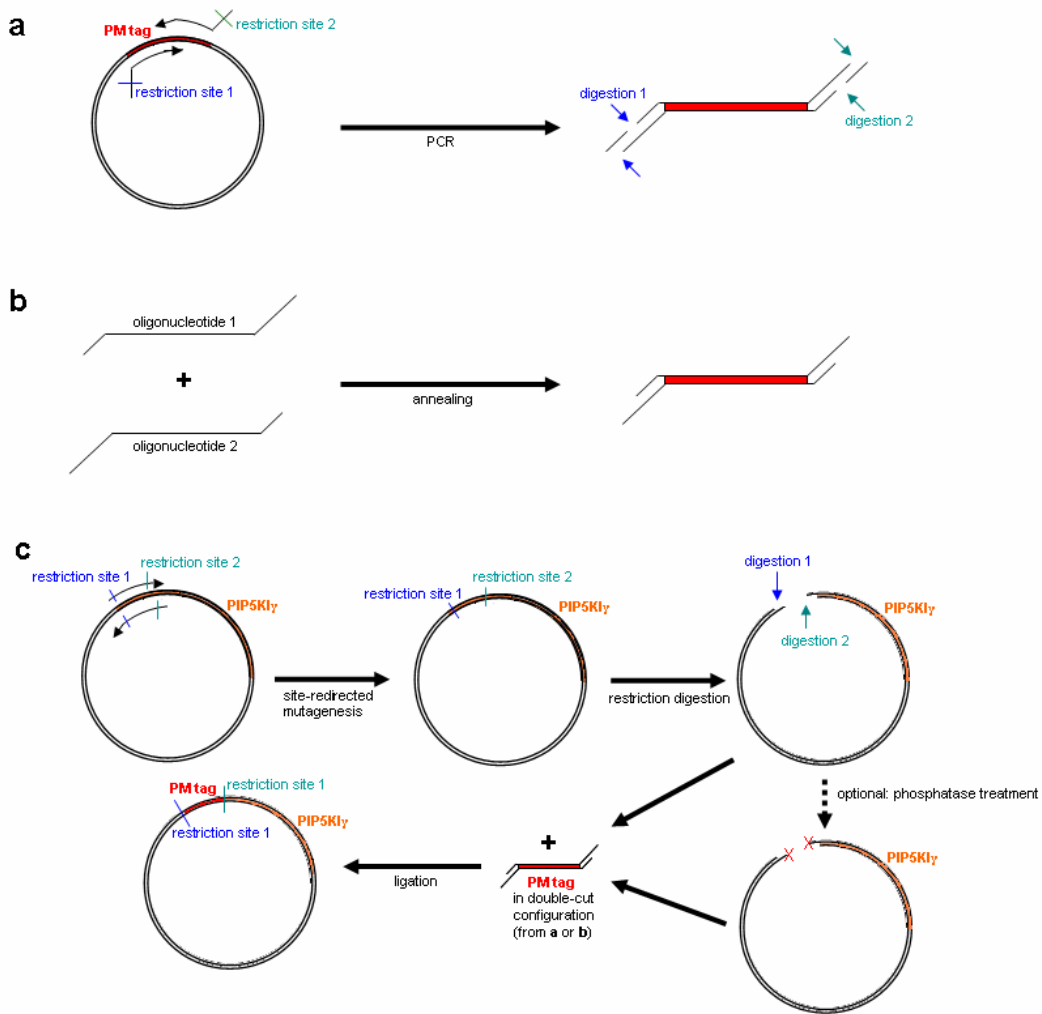
Figure 23 The subcloning scheme of PM-tagged constructs

(**a**) Introducing restriction sites into both end of the PM-tag while cloning it out of an existing vector using normal PCR. This double-stranded fragment may then be cut by corresponding restriction enzymes. (**b**) Two oligonucleotides annealing together to form the double-stranded, cut configuration of the PM-tag. (**c**) Subcloning procedure, making the gene-containing vector available for ligation with the PM insert.
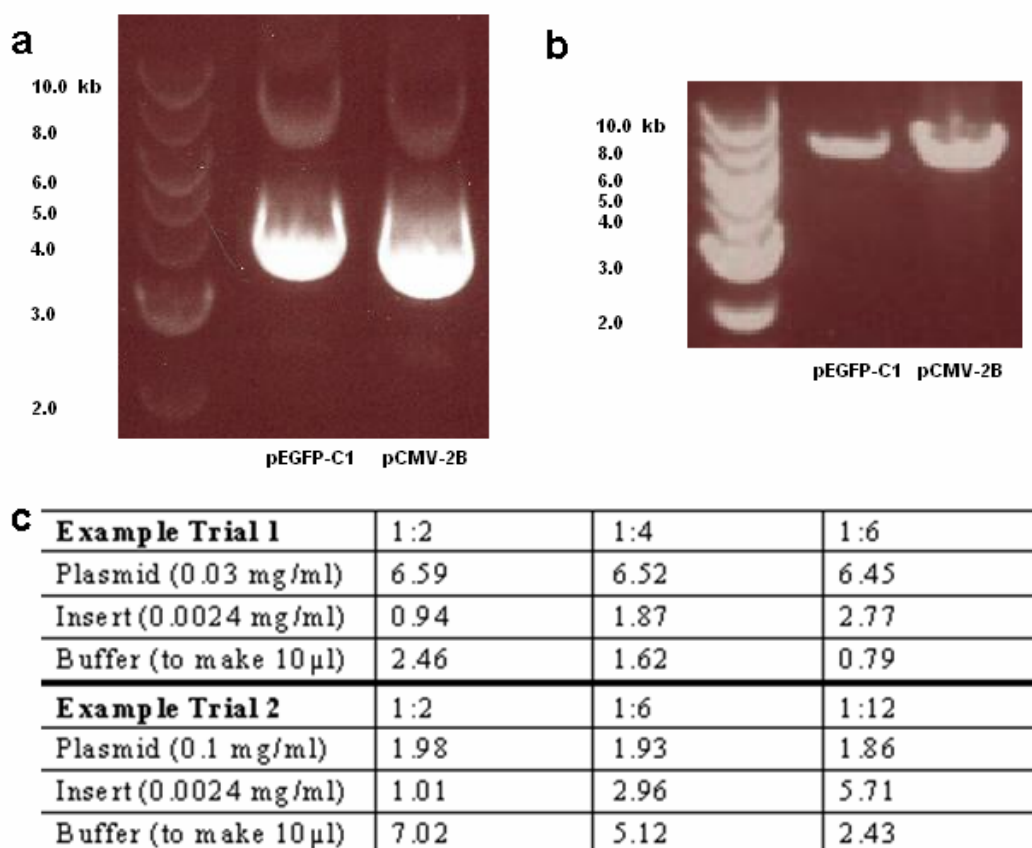
Figure 24 Subcloning of PM-tagged constructs
(**a**) Circular GFP (pEGFP-C1) and FLAG (pCMV-2B) plasmids containing the PIP5KIγ_v3 before digestion. Appropriate restriction sites already introduced into the N-terminus of the fusion gene. (**b**) The same plasmids linearised after restriction digestion. (**c**) Titration of optimal conditions for the ligation of PM insert and plasmid backbones. Top rows indicate the equivalent molar ratio of vector to insert. Values are volumes in μl.

I therefore sought after a different approach to make the PM constructs, by sequential site-directed mutagenesis, as I did for the 4R and 5P mutants. A first trial of two site-directed mutagenesis steps on Iγ_v3(V), each with a relatively lengthy mismatching fragment, proved to work (Table 6). I then obtained the other PM constructs by introducing *e.g.* the V443A and D316K mutations into this PM/GFP- or PM/FLAG-tagged Iγ_v3(V) construct.

Purpose	Mutagenesis (forward)	Mutagenesis (reverse)
PM (1/2) for pEFGP-C1	CGGTCGCCACC *ATGGGATGTATTAAA* GTGAGCAAGGG	CCCTTGCTCAC *TTTAATACATCCCAT* GGTGGCGACCGGTAG
PM (2/2) for pEFGP-C1	CACCATGGGATGTATTAAA *TCAAAAAGGAAAGAC* GTGAGCAAGGG	CTCGCCCTTGCTCAC *GTCTTTCCTTTTTGA* TTTAATACATCCCAT
PM (1/2) for pCMV-2B	CGGCCGCCACC *ATGGGATGTATTAAA* GATTACAAGG	CATCCTTGTAATC *TTTAATACATCCCAT* GGTGGCGGCC
PM (2/2) for pCMV-2B	GCCACCATGGGATGTATTAAA *TCAAAAAGGAAAGAC* GATTACAAGG	CGTCATCCTTGTAATC *GTCTTTCCTTTTTGA* TTTAATACATCCCATGG

Table 6 Primers for the generation of PM mutants by site-directed mutagenesis

The nucleotides in *underlined and Italic* font refer to the mismatching region with the template, *i.e.*, the sequence desired after site-directed mutagenesis.

4.2. Relationship between Kinase Activities and Membrane Localisation

4.2.1. Requirement for Activation Loop Mutants

As described and extensively used in earlier studies[167, 179] as well as the previous Chapter, the Iγ_i3(A) D316K mutant was completely cytosolic, and Iγ_i3(V) D316K mutant was also significantly less PM-bound than the wild type Iγ_i3(V) (Figure 10). The D316K mutation was a widely accepted way of making a dominant negative PIP5KIγ. Asp^{316} is a weak base involved in the general catalytic mechanism, therefore D316K should impair both the lipid kinase and protein kinase activities[127]. Moreover, D316K was unlikely to have caused undesired, non-specific structural

changes to the rest of the enzyme, since K188A, a non-ATP-binding mutant, had independently produced similar effects on cerebellar granular cells in earlier experiments (*e.g.* [179], see Introduction). From these data, one obvious possibility is that lipid kinase activity is required for PM-localisation. However, it was equally likely that autophosphorylation was necessary for PM-targeting, instead of the ability of producing PIP_2 itself. In the D316K mutant, the impairment to these two kinase activities was coupled and therefore non-separable.

In order specifically to impair the enzyme's ability to perform lipid catalysis, while leaving the protein kinase activity intact, the E410A, T412D and T412A mutants were designed, generated and tested. These mutations are all in the activation loop.

4.2.2. Characterisation of the T412A and T412D Mutants

As described in the Introduction (Section 1.3.4), since preliminary results by Giudici on the EH(410,411)AE showed reduced phosphorylation compared to E410A, the immediately adjacent Thr^{412} residue came to our attention. This Thr/Ser residue is completely conserved in the Type I PIP kinase family, which are generally PM-associated. This led us to wonder whether it could be a conserved Thr/Ser phosphorylation site implicated in Iγ_i3's regulation. Two mutants were generated, T412D and T412A, in an attempt to constitute the effect of phosphorylation and dephosphorylation, respectively. Despite certain caveats related to the electrostatic property (see below), this is a well documented and widely adopted method of mimicking amino acid phosphorylation states.
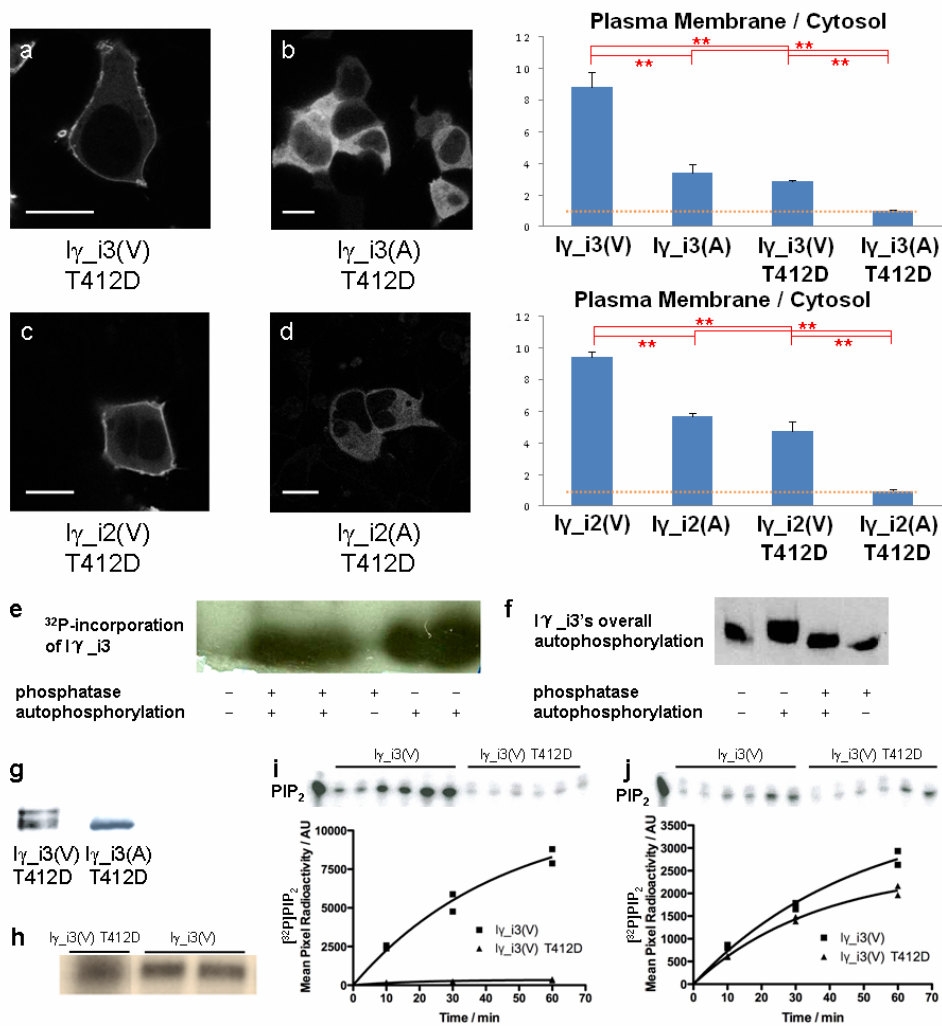
Figure 25 Characterisation of the T412D mutants

(**a**) – (**d**) Typical subcellular localisation of overexpressed GFP-tagged T412D constructs in HEK-293 cells (scale bar = 10 μm). Panel on the right indicates quantified ratio of PM / cytosol fraction. Orange dotted line indicates a cytosolic localisation (n = 30, ** p < 0.001). (**e**) Prior *in vitro* phosphatase treatment of Iγ_i3 did not change their autophosphorylation activity, measured by incorporation of ^{32}P. (**f**) Prior *in vitro* phosphatase treatment of Iγ_i3 decreased its extent of phosphorylation as detected by Western blot. This pattern was only partially restored by subsequent autophosphorylation. (**g**) *In vivo* phosphorylation pattern of the T412D mutants. (**h**) Protein kinase activity of T412D, measured by autoradiography. (**i**) Lipid kinase activity of the T412D mutant (n = 2), substrate presented as liposomes. (**j**) Lipid kinase activity of the T412D mutant, substrate presented as micelles (n = 2). For both (**i**) and (**j**), time courses of 10, 30 and 60 minutes were performed. Lipid products were separated by TLC and [^{32}P]PIP$_2$ was measured and compared between constructs.

Thus, T412D was expected to mimic the effect of phosphorylation on the Thr[412] residue by its negative charge. The T412D mutation significantly reduced the PM-association in Iγ_i3, and these effects were paralleled by similar reductions in PM-association in Iγ_i2, leading to, in the extreme cases, both the Iγ_i3(A) T412D and Iγ_i2(A) T412D being completely cytosolic (Figure 25a – d). Meanwhile, T412D also reduced phosphorylation of both Iγ_i3(V) and (A), to an extent that Iγ_i3(A) T412D was completely dephosphorylated (Figure 25g).

We tested the effect on general dephosphorylation (by phosphatase treatment *in vitro*) on the autophosphorylation activity and the ^{32}P incorporation did not seem to be greatly altered (Figure 25e). Autophosphorylation with non-radioactive ATP had only a minor reversing effect of the dephosphorylation shift on a Western blot (Figure 25f). Importantly, when Iγ_i3(V) T412D was assessed for its autophosphorylation, it was phosphorylated to a comparable extent (after background subtraction) to the wild type (Figure 25h), indicating the integrity of the general kinase structure. In contrast, the lipid kinase activity was specifically impaired by as much as 94%, using the liposome substrate (Figure 25i). Interestingly, when the PI4P substrate was presented in the form of micelles, the lipid kinase activity was much weaker in the wild type and then impaired only slightly in the T412D mutant (Figure 25j), again, illustrating the importance of presenting the substrate in a form better resembling a membrane.

This was encouraging so far, in that all these data are consistent with the idea that Thr[412] could be a target of phosphorylation, which in turn would regulate its behaviour. The fact that parallel effects of T412D were observed in Iγ_i3 and Iγ_i2 was particularly interesting. It suggested that phosphorylation of the conversed Thr/Ser residue in the activation loop may indeed represent a universal mechanism of regulation of Type I PIP kinases, and also this is the first mutation I introduced that appeared to affect Iγ_i2 and Iγ_i3 identically. Potentially, we could even extend our investigation into PIP5KIα and Iβ in the near future to consolidate this finding. To exhaust our knowledge about this potential phosphorylation site, I generated and studied its complementary mutation, T412A.
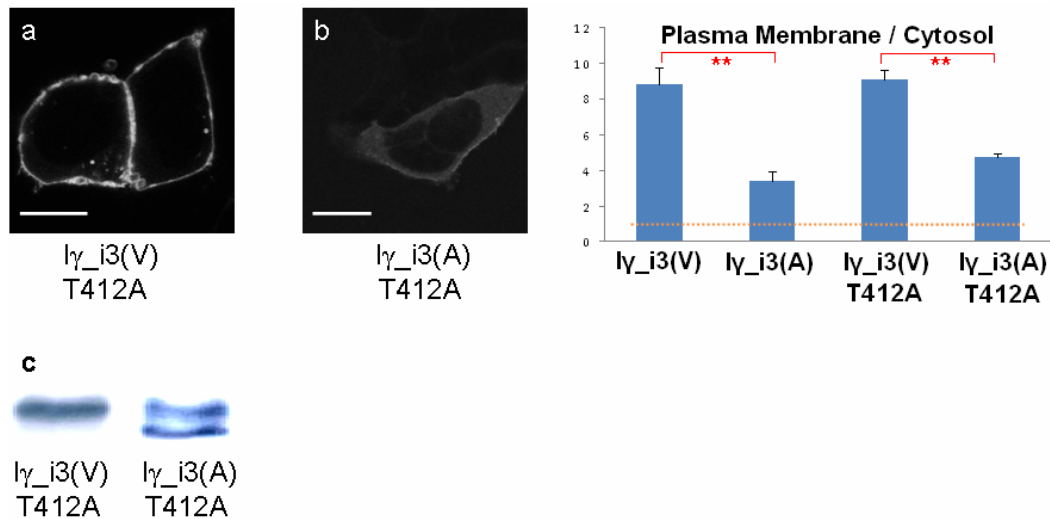
Figure 26 Characterisation of the T412A mutants

(**a**) – (**b**) Typical subcellular localisation of overexpressed GFP-tagged T412A constructs in HEK-293 cells (scale bar = 10 μm). Panel on the right indicates quantified ratio of PM / cytosol fraction. Orange dotted line indicates a cytosolic (non-membrane-enriched) localisation (n = 30, ** p < 0.001). (**c**) *In vivo* phosphorylation pattern of the T412A mutants.

While the lipid kinase activity was similar to the wild type (about 115% from Giudici's unpublished observation), the overall *in vivo* phosphorylation was generally increased, as well as its PM-association. In contrast to T412D, Iγ_i3(A) T412A was more PM-associated than Iγ_i3(A) (perhaps due to alanine being more hydrophobic than threonine) (Figure 26a). Meanwhile, Iγ_i3(V) T412A was similar to Iγ_i3(V) in its localisation (Figure 26b), although this might have been a "ceiling effect" in that Iγ_i3(V) wild type was already near maximally PM-localised, as could be measured using our method. T412A also increased the phosphorylation of both Iγ_i3 constructs, with the most striking effect on the Val[443] construct, where the mutant was completely phosphorylated (Figure 26c).

However, these data raised another question. The crucial difference between the overall phosphorylation profiles of Iγ_i3 and Iγ_i2 (Figure 8) should be recalled. Compared to Iγ_i2, which had one major "fully" phosphorylated band, Iγ_i3 had at

least one additional phosphorylated state, and its "fully" phosphorylated band appeared to have a larger separation from the dephosphorylated band than that of Iγ_i2. With T412A, the putative "partially phosphorylated" band was obviously weakened (Figure 8d), but without a general absence of phosphorylation (indeed, the overall phosphorylation actually increased), indicating that Thr^{412} residue does not itself account for the major phosphorylated bands observed, and suggesting that any phosphorylation on the Thr^{412} residue is a small part of the overall phosphorylation pattern.

Therefore, the effects observed using T412D and T412A could have been indirectly related to phosphorylation, *e.g.* a general, electrostatic effect due to the acidity or hydrophobicity, respectively, of the substituted residue. The decrease in PM-association with T412D may be due to the negative charge on the aspartate residue compared to threonine, decreasing the affinity for the PM. Conversely, the higher hydrophobicity on alanine could have led to the opposite effect of T412A. Similarly, these could produce the observed effects on the lipid kinase activity, given the affinities of the substituted residues to the negatively charged and hydrophobic lipid substrate. Once targeted to the PM, the protein could then be phosphorylated by other kinases on (or near) the membrane, achieving its full phosphorylation pattern *in vivo* at equilibrium (see more studies in Section 4.3).

4.2.3. Characterisation of the E410A Mutant

As described in the Introduction, Glu^{410} is an extremely important residue implicated in the Type I specificity of PIP5KIγ. Its substitution into alanine should impair the PI4P 5-kinase activity of γ_i3 selectively, while sparing the general structure of the enzyme[130].
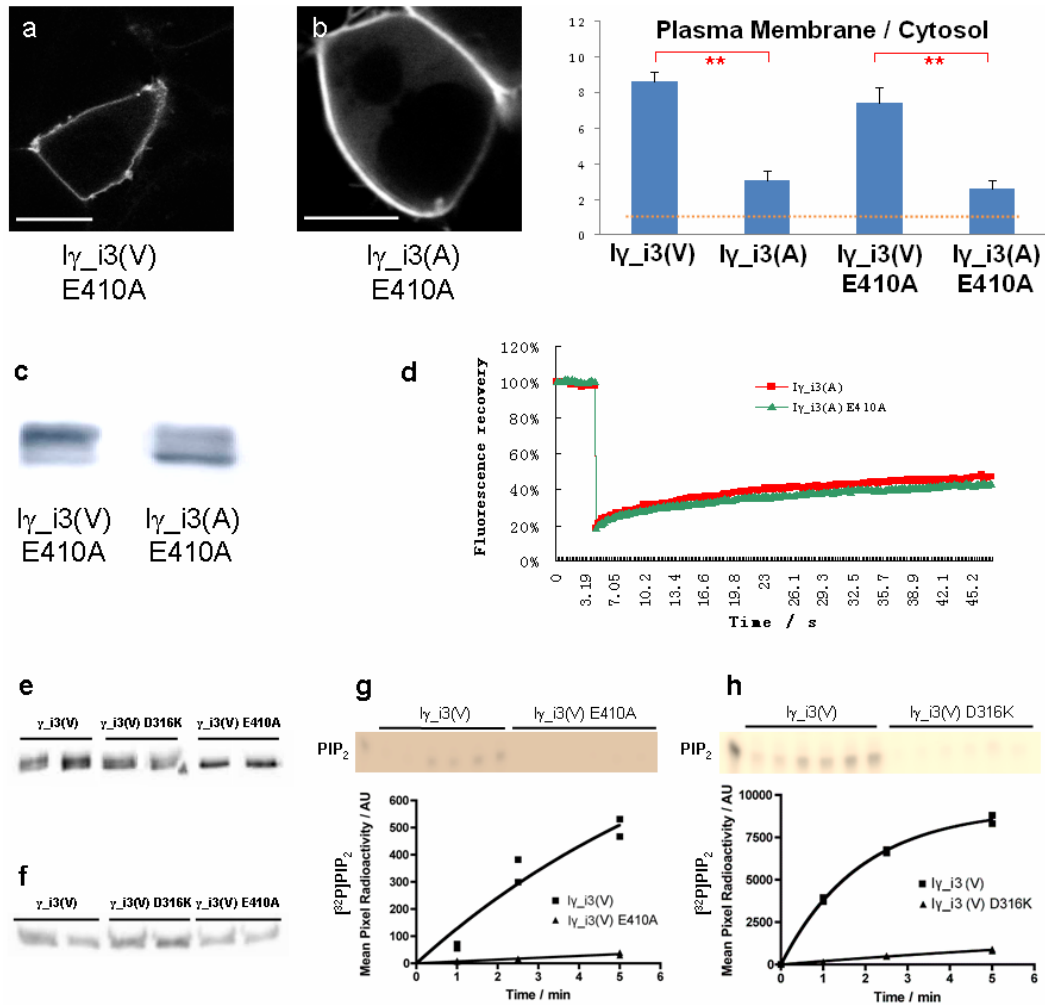
Figure 27 Characterisation of the E410A mutants

(**a**) – (**b**) Typical subcellular localisation of overexpressed GFP-tagged E410A constructs in
HEK-293 cells (scale bar = 10 μm). Panel on the right indicates quantified ratio of PM /
cytosol fraction. Orange dotted line indicates a cytosolic (non-membrane-enriched)
localisation (n = 30, ** p < 0.001). (**c**) *In vivo* phosphorylation pattern of the E410A mutants.
(**d**) FRAP behaviour of the E410A mutant, mean fluorescence intensity plotted (n = 30). (**e**)
Western blot of raw HEK-293 lysate overexpressing the FLAG-tagged constructs. (**f**) Western
blot of the lysate in (**f**) after volume titration and immunoprecipitation using the anti-FLAG
antibody. (**g**) Lipid kinase activity of the E410A mutant (n = 2). (**h**) Lipid kinase activity of
the D316K mutant. For both (**g**) and (**h**), time courses of 1, 2.5 and 5 minutes were performed.
Lipid products were separated by TLC and $[^{32}P]PIP_2$ was measured and compared between
constructs.

In order to compare the degree of impairment of E410A as a kinase-inactive mutant, and to see if it truly reached the lowest activity detectable using the current protocol, the E410A mutant was assayed alongside the wild type and the well established kinase-inactive mutant, D316K. Total lysates were Western blotted in order to determine the relative concentration of the enzyme (Figure 27e), and added in different volumes so the amount of enzyme in the assay was the same across the samples. This was verified by Western blot using the post-immunoprecipitation samples, treated in parallel as the samples submitted to the actual kinase assay (Figure 27f).

The lipid kinase activity of E410A was severely reduced, retaining only a trace amount of residual activity (Figure 27g). This was comparable to the activity of D316K (Figure 27h), confirming that the enzyme was indeed made essentially inactive as a PI4P 5-kinase. This result was consistent with Kunz *et al.*, where the equivalent single AA substitution in Iβ partially impaired the PI4P-binding specificity (and thus made it cytosolic) and also its Type I PIP kinase activity, while giving rise to Type II activity[130].

Strikingly, the localisation of E410A mutants were not significantly different from that of the wild type Iγ_i3 (Figure 27a and b), and they were also phosphorylated to a similar extent (Figure 27c). In addition, the FRAP mobility was indistinguishable from the wild type (Figure 27d).

This collection of observations is potentially interesting. The mutant enzyme is indistinguishable from the wild type in many behavioural aspects (such as *in vivo* phosphorylation, membrane localisation, cytoskeletal association and mobility), but has specifically abolished lipid kinase (PI4P 5-kinase) activity. Given the low levels of PI5P relative to PI4P *in vivo*[95], the Type II (PI5P 4-kinase) activity that it possesses can be regarded as leading to negligible PIP_2 synthesis. As we shall see later in the next section, this mutant has proven to be a key that helped us to exclude several alternative hypotheses regarding the regulation of the enzyme.

To verify whether the E410A mutant had indeed become a Type II, PI5P 4-kinase despite its dramatically reduced Type I activity, I tested its catalytic efficiency by the lipid kinase assay using PI5P as the substrate (instead of PI4P).
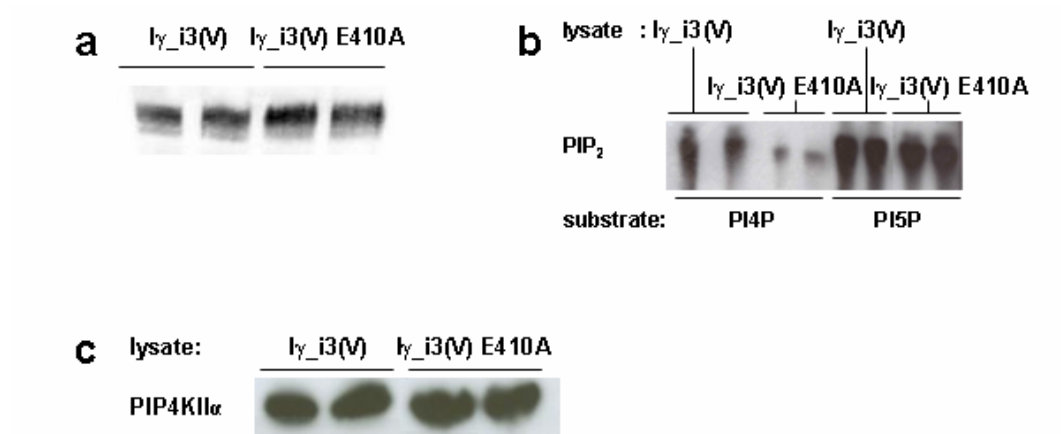
Figure 28 Co-immunoprecipitation of Type II PIP kinase activity with immunopulldown of PIP5KIγ

(**a**) Lysates of overexpressed FLAG-tagged Iγ_i3 and its E410A mutant titrated to the same concentration after anti-FLAG immunoprecipitation. (**b**) Lipid kinase assay of Iγ_i3 and the E410A mutant, each using PI4P and PI5P as the substrate, and PIP$_2$ product measured by autoradiography. (**c**) Western blot using anti-PIP4KIIα antibody, after immunoprecipitation for FLAG-tagged PIP5KIγ and its E410A mutant.

Using the same quantity of enzymes (Figure 28a), the E410A mutant exhibited an almost negligible Type I activity, exactly as described before (Figure 27g). However, in the PIP4K assay (using PI5P as the substrate), both the wild type and mutant enzyme showed the same amount of Type II activity, which was very high even compared to the Type I activity. This was puzzling at first sight, given that although E410A might be expected to assume some PIP4K activity, the wild type PIP5KIγ had always been known as a strictly Type I enzyme.

I reasoned that this could be due to an artefact caused by contaminating Type II enzymes in the immunoprecipitation preparation, since the enzymes were overexpressed in HEK-293, a mammalian strain which could endogenously express PIP4Ks. Indeed, when I Western blotted the PIP5KIγ immunoprecipitate for the presence of PIP4KIIα, the most active[110, 111] and usually predominant isoform of PIP4Ks, both Iγ_i3 and Iγ_i3 E410A pulled down a significant amount of PIP4KIIα (Figure 28c). This co-immunoprecipitation was in agreement with previous findings, where Type I and Type II PIP kinases were observed to associate with each other both *in vivo* and *in vitro*[105]. Therefore, a more appropriate way of detecting the Type II activity of Type I PIP kinases, or *vice versa*, would be to overexpress the protein in a bacterial system, where there was no contamination from other endogenous enzymes, as done in Kunz *et al.*[130].

The fact that wild type and the E410A mutant of Iγ_i3 pulled down the same amount of PIP4KIIα is consistent with the above discussion. It suggests that Type I and II interaction is mediated by interfaces independent of the activation loop, and at the same time confirms that E410A caused minimal disturbance to the general structure of the Iγ_i3 enzyme.

4.2.4. Synoptic Considerations for the Relationship between Kinase Activities and Membrane Localisation

The quantified kinase activities, as individually determined above, are collectively presented in Table 7.

	Lipid Kinase Activity		Protein Kinase Activity	
	Iγ_i3(V)	Iγ_i3(A)	Iγ_i3(V)	Iγ_i3(A)
Wild type	100	45 / 100	100	60 / 100
D316K	4	<1 *	ND	ND
T412D	6	15 *	80	ND
T412A	ND	115 *	ND	ND
E410A	5	5 *	ND	ND

Table 7 Summary of lipid and protein kinase activities of the activation loop mutants
Calculations were based on the raw data shown in the previous figures. Activities of mutants were calculated as a percentage of either Iγ_i3(V) activity (in blue), or Iγ_i3(A) (in red) (n no smaller than 2). Ratios above 10% were approximated to the nearest 5%, for the ease of communication. ND = not determined. * indicates data from previous work (by Giudici, unpublished), from which raw data was not included in the present study.

Putting the T412D and T412A data together suggests that the changes in their lipid kinase activity may have been a direct result of a change in the electrostatic charges of the activation loop. For example, the T412D mutation introduced a negative charge to the activation loop, and this may have imposed electrostatic repulsion and steric hindrance on its substrate-binding, hence lowering the lipid kinase activity. T412A, on the other hand, made the residue slightly more hydrophobic and gave easy access of its lipid substrate to the activation loop. So it could be that the effects on lipid kinase activity were caused by the same factors that altered its PM-association (and overall phosphorylation).

However, the fact that E410A mutants had greatly impaired lipid kinase activity but largely unchanged PM-localisation, phosphorylation and FRAP mobility from the wild type tells us the PM-localisation is not a simple consequence of the lipid kinase activity, nor of the interaction with the hydrophobic substrate. It is important to note here that our observations are consistent with the PIP5KIβ data of Anderson's group[130].

While E410A showed that the PM-association was not necessarily dependent on the lipid kinase activity of Iγ_i3, I showed in the previous Chapter that the localisation of Iγ_i3(A) required its kinase activity in general, as highlighted by the differences between the D316K constructs of Iγ_i3 and Iγ_i2. Given these two findings, the most parsimonious explanation to fit both observations would be: it is the *protein kinase* activity that is implicated at the initial stage of Iγ_i3's membrane localisation. That is, a Iγ_i3 molecule needs to phosphorylate itself (or potentially other protein partners), before it could be targeted to the plasma membrane.

Experimentally, it is difficult, if not impossible, to generate a mutant that specifically impairs the protein kinase activity of the PIP5KIγ, while leaving the lipid kinase activity unaffected. Given that both activities share the same catalytic core underlying the general phosphate-transferring mechanism, it would only be by identifying the amino acid residues that are autophosphorylated and mutating them that this could be achieved. Without the knowledge of target AA residues to mutate, the autophosphorylation of the protein cannot be manipulated in a specific fashion. However, using the mutants affecting either the general kinase activity (D316K) or the lipid-binding site in the activation loop (E410A), I was able to dissect out the differences, and arrive at conclusion that the protein kinase activity was most likely essential for the initial targeting to the PM.

The above conclusion leads to another key question: does membrane localisation lead directly to the rest of the phosphorylation events *in vivo*, as observed by Western blot (*e.g.* Figure 8)? This will be addressed in detail now in the next section.

4.3. Relationship between Membrane Localisation and Phosphorylation

4.3.1. A Meaningful Causal Relationship?

From the wide range of mutants tested above, an intriguing correlation seemed to have emerged, between their *in vivo* phosphorylation state and PM-association. A general pattern could be observed, that the higher the overall phosphorylation, such as in the case of T412A, the more PM-localised the enzyme. The converse cases were observed *e.g.* with the V443A, D316K and T412D mutants.

This, of course, is not a quantitatively precise correlation, and is likely to involve multiple mechanisms of phosphorylation and PM-targeting. For example, Iγ_i3(A) and Iγ_i3(V) D316K had apparently the same PM-bound fraction (Figure 9b and Figure 10a), but slightly different phosphorylation profiles (Figure 8b and c).

Is this apparent correlation a causal relationship? In other words, does phosphorylation help a PIP5KIγ molecule to associate with the PM, or does membrane-associaion lead to its phosphorylation instead? If so, is this causal relationship necessary or sufficient? These were the questions that we were potentially interested in, and to break this cyclic argument, I needed to specifically interfere with one factor and observe its effect on the other.

As discussed in the previous Chapter, without comprehensive knowledge of the target residues implicated in the *in vivo* phosphorylation, it would be difficult to interfere with the phosphorylation pattern *per se*. On the other hand, if I had certain ways of forcing an originally cytosolic enzyme to attach to the membrane, or making an otherwise normal enzyme cytosolic, I would be able to gain insight into the role of membrane localisation in the full phosphorylation of the protein. These experiments were made possible by my PM and E111L mutants, as discussed below.

4.3.2. Forcing a Cytosolic PIP5KIγ onto the Membrane – the PM Mutant

Whether PM-association is sufficient on its own to lead to phosphorylation was an unanswered question, and to address this I used the ten amino acids at the N-terminal motif from the human Lyn kinase (MGCIKRKGKD), which lead to palmitoylation and myristoylation ("PM") *in vivo* that forces the attachment of the fusion protein onto the membrane, regardless of the protein's original localisation[214].
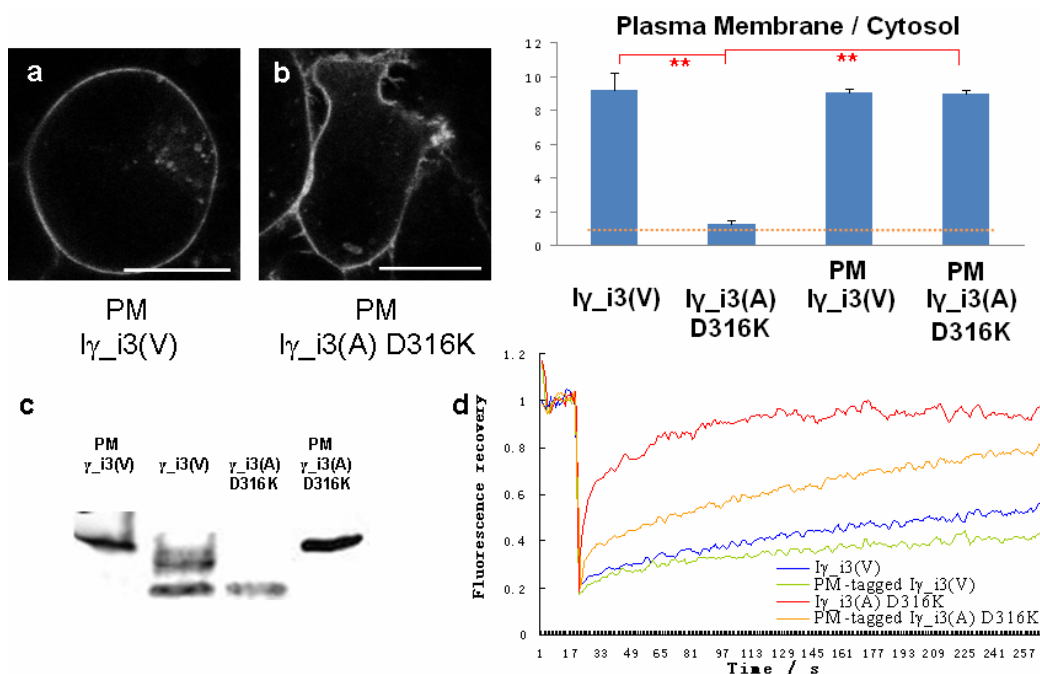
Figure 29 Major characters of the PM mutants

(**a**) and (**b**) Typical subcellular localisation of overexpressed PM- and GFP-tagged constructs in HEK-293 cells (scale bar = 10 μm). Panel on the right indicates quantified ratio of PM / cytosol fraction. Orange dotted line indicates a cytosolic (non-membrane-enriched) localisation (n = 30, ** p < 0.001). (**c**) *In vivo* phosphorylation pattern of the PM mutants. (**d**) FRAP mobility of the PM mutants, mean fluorescence intensity plotted (n = 10).

The PM constructs unfailingly localised to the plasma membrane, as expected (Figure 29). In particular, the normally completely cytosolic Iγ_i3(A) D316K mutant was targeted to the membrane by the PM-tag to an extent comparable to the wild type enzyme on itself. This confirmed that the PM-tag could override other potential regulatory mechanisms and anchor the fusion protein to the plasma membrane as a useful molecular tool, without the need of altering the property of the rest of the protein.

Perhaps not surprisingly, the PM constructs exhibited a lower mobile fraction and slower recovery relative to the enzyme on itself (Figure 29d). This would be due to the fact that the PM-tag was irreversibly attached to the membrane, and therefore the fusion protein could be constricted in its range of diffusion by various lipid compartments, compared to a freely diffusible protein according to the fluid mosaic model. The rate of diffusion was most likely limited by the collision and transient binding of the PM-tag to other components in the lipid bilayer, which should inevitably slow the diffusion down. Moreover, the overexpressed fluorescent enzyme was entirely membrane-bound in this case, therefore the source of recovery was limited to lateral diffusion, with no input from exchanges with the cytosolic proteins[47].

Strikingly, the PM-tagged constructs were all phosphorylated, regardless of their original phosphorylated pattern before PM-targeting (Figure 29c). The most persuasive example was the PM-tagged Iγ_i3(A) D316K, which enabled the protein to be fully phosphorylated, when the Iγ_i3(A) D316K on itself was completely unphosphorylated (Figure 8c). This evidence suggested strongly that the protein kinases that phosphorylate Iγ_i3 *in vivo* are very likely situated on or close to the plasma membrane.

Having stated the above, the membrane association aided by the PM-tag may still be different from that occurring physiologically. For example, the PIP5KIγ may normally be binding to specific proteins (*e.g.* Rac, as discussed in the next section) or to particular lipids on the membrane, instead of anchoring itself randomly in the phospholipid bilayer. The PM-tag may have a different preference for the lipid composition with which it associates, and therefore it could become inserted into a

different compartment or raft (see Introduction). Also, the physiological association of Iγ with the membrane is likely reversible and dynamic, where the equilibrium is determined by the on/off constants of its binding with partners. In contrast, the PM-tag becomes palmitoylated and myristoylated, which in turn leads to irreversible anchoring at the plasma membrane[47]. Nevertheless, given the results above, the membrane localisation was proven to be *sufficient* for achieving the phosphorylation of Iγ_i3.

4.3.3. Forcing a Membrane PIP5KIγ into the Cytosol – the E111L Mutant

Whether or not the membrane localisation is *necessary* for Iγ_i3 phosphorylation was a different question. To address this, I needed to bring a wild type enzyme off the membrane and, without changing anything else, observe its phosphorylation pattern.

It has been documented that a particular glutamate residue (Glu^{61}) before the conserved kinase domain in PIP kinase Iβ was crucially implicated in the association with the monomeric G-protein Rac (a member of the Rho family GTPases)[138]. Extensive data from Halstead *et al.* using mutagenesis, microscopy and co-immunoprecipitation demonstrated conclusively that this glutamate was essential for the binding of PIP5KIβ with Rac. This interaction was abolished when this glutamate was mutated into leucine, and consequently there was no PM-association[138].

Following on from these observations, I therefore generated the equivalent mutant in Iγ_i3, E111L.
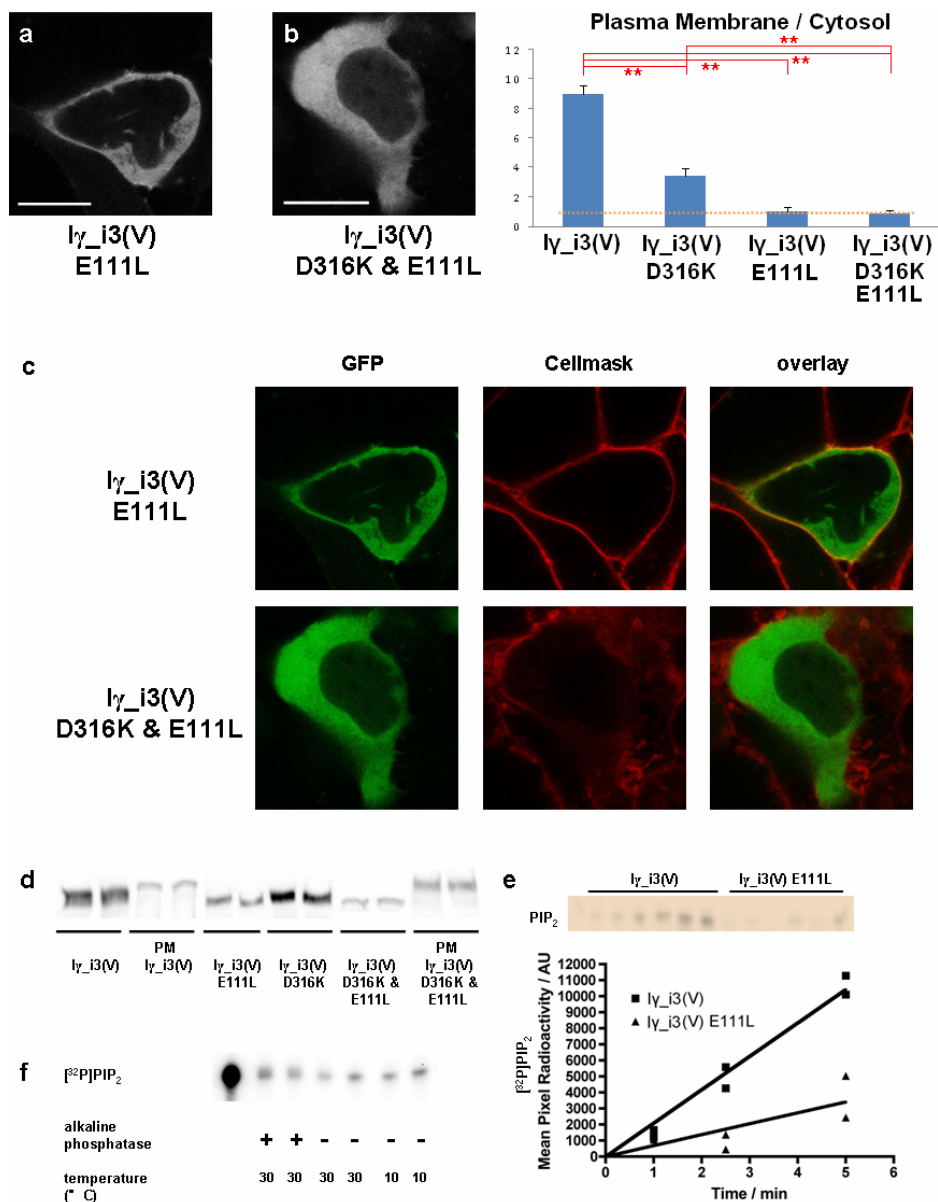
Figure 30 Major characters of the E111L mutants

(**a**) – (**b**) Typical subcellular localisation of overexpressed GFP-tagged E111L constructs in HEK-293 cells (scale bar = 10 μm). Orange dotted line indicates a cytosolic (non-membrane-enriched) localisation (n = 30, ** $p < 0.001$). (**c**) Overlay of GFP (Iγ_i3) and Cellmask channels, where yellow indicated superposition of the green and red signals. (**d**) *In vivo* phosphorylation pattern of the E111L mutants and the PM & E111L double mutants, on a wild type, V443A or D316K enzyme. (**e**) Lipid kinase activity of the E111L mutant, with time courses of 1, 2.5 and 5 minutes. Lipid products were separated by TLC and [^{32}P]PIP$_2$ was measured and compared between constructs (n = 2). (**f**) Alkaline phosphatase treatment and control incubation at 30 °C did not affect the apparent lipid kinase activity *in vitro*.

The E111L mutants turned out to be indeed cytosolic (Figure 30a and b), suggesting that this mutation could prove to be a useful tool to impair the membrane association of Iγ_i3 without altering its other functional motifs.

However, a more detailed examination of the confocal images revealed an important difference between these two constructs. The Iγ_i3(V) D316K & E111L double mutant was cytosolic in the real sense, in that it did not colocalise with any portion of the cell membrane, highlighted by the red Cellmask label. In contrast, the Iγ_i3(V) E111L construct was still partially *present* at the membrane, shown by the yellow superposition with the Cellmask signal. It simply did not *enrich* at the membrane, giving the general impression that it was cytosolic (Figure 30c). Evidently, this fine difference was not picked up by our plasma membrane / cytosol ratio analysis, probably because of the limited resolution of the region-of-interest intensity measurement.

This E111L mutant was nevertheless totally unphosphorylated, similar to D316K, as was the D316K & E111L double mutant (Figure 30d). However, when then tagged with a PM-tag, even the most cytosolic Iγ_i3(A) D316K & E111L became fully phosphorylated (in complete agreement with earlier data, Figure 29), again pointing to plasma membrane association as being the main driver of Iγ phosphorylation.

On a separate note, I tested the E111L mutant as a lipid kinase, and found that its activity was reduced to about 1/3 (Figure 30e). This was unexpected, since the E111L mutation was not supposed to cause disruption to the general structure or any catalysis-related domains of the enzyme. As a control, I investigated whether the overall phosphorylation *per se* (which is abolished in this mutant) could be a cause of the reduction in the lipid kinase activity. It appeared not to be the case, since incubation with alkaline phosphatase *in vitro* (which removed all phosphorylation, see Figure 8a) prior to immunoprecipitation did not alter the activity measured; neither did the pre-incubation temperature have a descernible effect (Figure 30f). It led me to reason that it must be an intrinsic property of E111L, *e.g.* the inability to bind Rac, that caused this reduction. Indeed, Rac has long been identified as an activator in

many phosphoinositide-related pathways, including not only the Type I PIP5K[136], but also *e.g.* the Type II PI4K[75], PI 4,5-kinase, PI 3-kinase and PI 5-kinase[143]. This also indirectly supported the proposed effect of the E111L mutation as to abolish Rac-binding of the kinase.

4.3.4. Rac and Iγ Interaction – Assessed by Co-immunoprecipitation

I tried to see whether the wild type Iγ_i3 and Rac associated *in vivo* and could be co-immunoprecipitated together, and thereby demonstrate that the E111L mutation indeed obliterated (or reduced) such binding.

I first attempted to immunoprecipitate the FLAG-tagged enzymes with anti-FLAG, and detect whether Rac co-immunoprecipitated with various Iγ_i3 constructs. Rac has a molecular weight of 21 kDa. Unfortunately, the light chain of the mouse IgG1 used as the immunoprecipitating antibody (hence remaining in the sample) had a MW of 22 kDa, running at exactly the distance of interest and hence contaminating the Rac signal (Figure 31a). The heavy chain should run at 43.3–55 kDa, and protein G (linked to the sepharose beads for immunoprecipitation) at around 31–34 kDa (apparent in the SDS-PAGE, as reported by the manufacturer, despite its calculated MW of 21.6 kDa). Therefore, the unfortunate recognition of the light chain of the immunoprecipitate/primary antibody imposed a real problem to the studies.

I reasoned that it would be possible to overcome this problem, if the secondary antibody for Western blot only recognised the heavy chain of IgG1, instead of both chains (Figure 31b). I therefore managed to find a secondary antibody against the mouse heavy chain, denoted anti-mouse-IgG1-HC. Using this antibody, the problem above was indeed overcome. The light chain was no longer detected, shown by the anti-FLAG antibody control, and the protein G was not in the way of Rac detection either. This, along with the use of 15% polyacrylamide running gels, was developed into a standard tool for all the future experiments where I was interested in detecting Rac from an immunoprecipitation.

However, even though the immunoprecipitation of γ_i3 constructs worked fine (Figure 31c), the Rac signal itself was not detected in the range of samples tested, including even the wild type Iγ_i3(V) (Figure 31d). The thin band ubiquitiously present in all samples at around 20 kDa was not Rac, as the genuine endogenous Rac signal was controlled for in the total lysate sample running alongside, producing a higher band at exactly 21 kDa, as expected.

This co-immunoprecipitation experiment was repeated for another 4–5 times using the same mild conditions of detergent extraction and minimal number of washes during immunoprecipitation, producing the same negative results on Rac, in spite of normal γ_i3 pull-down. It seemed that the putative association between PIP5KIγ_i3 and E111L may not be strong or long enough for me to detect using the above protocol.

a
Iγ_i3(V) D316K & E111L | PM Iγ_i3(V) D316K | Iγ_i3(V) D316K | Iγ_i3(V) E111L | Iγ_i3(V)

15% polyacrylamide
IP Ab: mouse anti-FLAG
primary Ab: mouse anti-Rac
secondary Ab: goat anti-mouse IgG1

64 kDa
50
36
22
16

b
light chain — heavy chain — light chain

c
Iγ_i3(V) | Iγ_i3(A) E111L | Iγ_i3(A) D316K | PM Iγ_i3(A) D316K & E111L | Iγ_i3(A) D316K & E111L | Iγ_i3(V) D316K & E111L

Iγ_i3 construct →

148 kDa
98

6% polyacrylamide
IP Ab: mouse anti-FLAG
primary Ab: mouse anti-FLAG
secondary Ab: goat anti-mouse IgG1

d
pr. G | anti-FLAG | PM
γ_i3(V) D316K& E111L | γ_i3(A) D316K& E111L | lysate | γ_i3(A) D316K | γ_i3(A) D316K | γ_i3(A) | γ_i3(V) E111L

heavy chain →
protein G →
Rac →

98 kDa
64
50
36
22
16

15% polyacrylamide
IP Ab: mouse anti-FLAG
primary Ab: mouse anti-Rac
secondary Ab: goat anti-mouse IgG1-HC

Figure 31 Rac did not co-immunoprecipitate with PIP5KIγ_i3 using the E2139 antibody
FLAG-tagged Iγ_i3 constructs were overexpressed in HEK-293 cells and extracted. (**a**) Rac
signal had the same apparent MW on the Western blot as the antibody light chain. (**b**)
Schematic illustration of the IgG1 structure. (**c**) Immunoprecipitation of overexpressed Iγ_i3
constructs. (**d**) Western blot using anti-mouse-IgG1-HC, detecting the heavy chain, but not
the light chain, of IgG1. Overexpressed Iγ_i3 constructs were compared with controls (shown
in red), such as the immunoprecipitating anti-FLAG, protein G, as well as total HEK-293
lysate (as a Rac standard).

Potentially, one possibility for such difficulty was that Rac interacted with the N-terminal domains of PIP5KIγ (*e.g.* the motif containing E111L falling back onto its N-terminus in 3D). This would compete with the binding of anti-FLAG antibody to the γ_i3 during the immunoprecipitation. Once the antibody pulls the enzyme down, Rac binding would be lost. As an alternative means of demonstrating this association, I decided to go about it from another direction, immunoprecipitating for the Rac and detecting the FLAG signal on the γ_i3.

The commercial Rac antibody had only been used for Western blot previously, and I had no knowledge whether or how readily it would immunoprecipitate. As a first step, the immunoprecipitation protocol using the anti-Rac antibody was optimised. It appeared that the antibody indeed pulled down Rac. For the following experiments, 1 μl of anti-Rac (in 500 μl PBS, diluted from 0.25 mg/ml, BD Transduction) was used with a standard immunoprecipitation protocol.
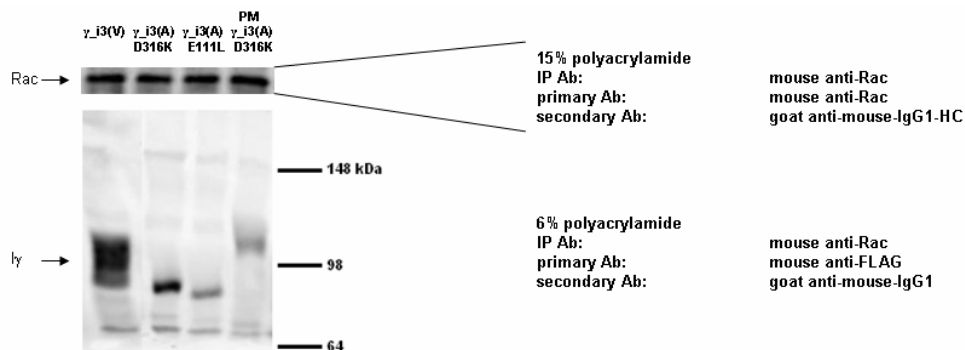
Figure 32 PIP5KIγ_i3 co-immunoprecipitated with Rac using the anti-Rac antibody
Co-immunoprecipitation of Iγ_i3 constructs with Rac, using anti-Rac antibody. FLAG-tagged Iγ_i3 constructs were overexpressed in HEK-293 cells and extracted.

The endogenous Rac was again confirmed to be pulled down by this antibody, in a variety of γ_i3 overexpression lysates tested (Figure 32). When blotted with the anti-

FLAG antibody, the Iγ_i3 signals were successfully detected (Figure 32). The relative position and pattern of phosphorylation were exactly those expected of these constructs, as addressed earlier. Note that with the same amount of overexpression (titrated by volume before the immunoprecipitation), the γ_i3 was most readily immunoprecipitated. The PM construct was immunoprecipitated to a less extent, presumably because the artificial anchoring to specific lipid compartments by the PM-tag hindered the enzyme's interaction with Rac. Moreover, the PM-tag was at the very N-terminus of the fusion protein and hence, if our earlier theory of Rac binding with N-terminus of PIP5KIγ was correct, it could hinder the interaction with Rac *in vivo*. More interestingly, the Iγ_i3(A) D316K mutant was pulled down (although at a lower quantity). This may be because the enzyme was completely cytosolic *in vivo*, and therefore had not much opportunity to sample the membrane-bound Rac, while during the extraction and immunoprecipitation procedure, it came in contact with Rac, and became bound to Rac since its Glu[111] motif was intact. The crucial E111L mutant exhibited greatly impaired binding to Rac, exactly consistent with Halstead *et al.*[138].

I should note that this co-immunoprecipitation was relatively difficult to reproduce and did not work every time I repeated this experiment. Presumably, the binding of γ_i3 and Rac was relatively weak and transient after all, and the association was only clearly revealed when multiple factors in the co-immunoprecipitation were optimal, such as the overexpression level, lysate quality, extraction severity and incubation conditions. In fact, in the original Halstead study, although it was stated that all isoforms of Type I PIP kinase (including Iγ) were confirmed to associate and co-immunoprecipitate with Rac, they only showed data using microscopy, mutagenesis, Rac immunoprecipitation followed by lipid kinase activity assay (as an indication of the presence of the kinase), or co-immunoprecipitation using the more reliable biotin/streptavidin system in the initial immunoprecipitation[138]. Perhaps strikingly in retrospect, similar types of data were shown in earlier studies showing PIP5K association with Rac too[139, 141, 143]. In contrast, co-immunoprecipitation using an anti-Rac antibody, followed by direct detection of PIP5KI on Western blot (as I tried to achieve), was never directly demonstrated. Such difficulty in co-

immunoprecipitation was confirmed by the authors (Divecha, personal communications). This interesting case also reiterates the point that genuine molecular interactions *in vivo*, especially via weak and transient interactions on multiple domains, do not necessarily last strongly or long enough for their association to be reliably detected *in vitro*, which may be required to last *e.g.* longer than 5 seconds[215].

Nevertheless, here I successfully demonstrated the co-immunoprecipitation of membrane-bound PIP5KIγ with endogenous Rac, as well as the greatly reduced binding of the E111L mutant, in a direct and less arbitrary fashion (Figure 32). This is helpful when interpreting the behavioural data of the E111L mutants (Figure 30), which is exactly consistent with this Rac-binding theory.

4.3.5. Synoptic Considerations for the Relationship between Membrane Localisation and Phosphorylation

In summary, I have managed to break the cyclic argument and tease apart the apparent correlation between the observed phosphorylation pattern and the enzyme's membrane localisation. Taken together, these data have demonstrated that the membrane localisation is not only *sufficient*, but also *necessary* for the phosphorylation of Iγ_i3 *in vivo*, independent of the enzyme's catalytic (lipid or protein kinase) activity. In the previous section (4.2), I showed that the membrane-dependent full phosphorylation *in vivo* is likely a downstream process of the protein's initial autophosphorylation (which may be the main arbiter of whether Iγ_i3 associates with the membrane). Once it associates with the membrane, Iγ_i3 becomes further phosphorylated by other protein kinases at or near the membrane. When the protein is unable to associate with the membrane, no discernible phosphorylation takes place, in spite of unaltered functions in all other aspects of the protein.

5. Results III – Discovery and Characterisation of A Novel PIP5KIγ Splice Variant, Iγ_i6

5.1. Discovery of Iγ_v6

In an attempt originally set up to establish a more comprehensive distribution pattern of PIP5KIγ_v3 *in vivo* and to find a mammalian cell line which potentially expressed Iγ_v3 endogenously, I investigated mRNA libraries of different mouse tissues.

Previously, *in situ* hybridisation had shown that Iγ_i3 expression is confined to certain groups of neurons in the brain, such as the cortex, cerebellum, hippocampus, olfactory bulb[167] and the pituitary (primarily in the anterior part, unpublished by Giudici). A mouse cell line available in the Department, AtT-20, is also derived from the anterior pituitary of mice, and could potentially be used as a cell line that expresses endogenous Iγ_v3, if I could confirm the expression in the anterior pituitary. Therefore, the pituitary was my first target in which to look for Iγ_v3. The tissue was dissected, frozen in the RNAlater reagent and extracted for mRNA.

In order to show Iγ_v3 exclusively, *i.e.*, to avoid the products from amplification of Iγ_v1 and Iγ_v2 (which would have resulted from PCR with primers against common sequences of all these spliceoforms), two pairs of primers were designed to specifically pick up Iγ_v3 (A1 and A2 in Figure 33).

Reaction A1 confirmed the existence of γ_v3 in this tissue, with a 353 bp fragment produced as expected. Apparently, using the primer pair against Exons 16 and 19, reaction AC preferentially used γ_v1 as the template over γ_v2 and γ_3 (as could be told from the predicted fragment length), though this did not necessarily indicate a quantitative difference among these splice variants.

The A2 result was more interesting. Besides the predicted band of 319 bp with γ_v3, there was a background smear potentially containing other PCR fragments. This was not expected, since no other mRNA was expected to contain both Exons 16 and 17, except for that of Iγ_v3. The identity of the lowest band just below 300 bp was subjected to sequencing.

a

b

c
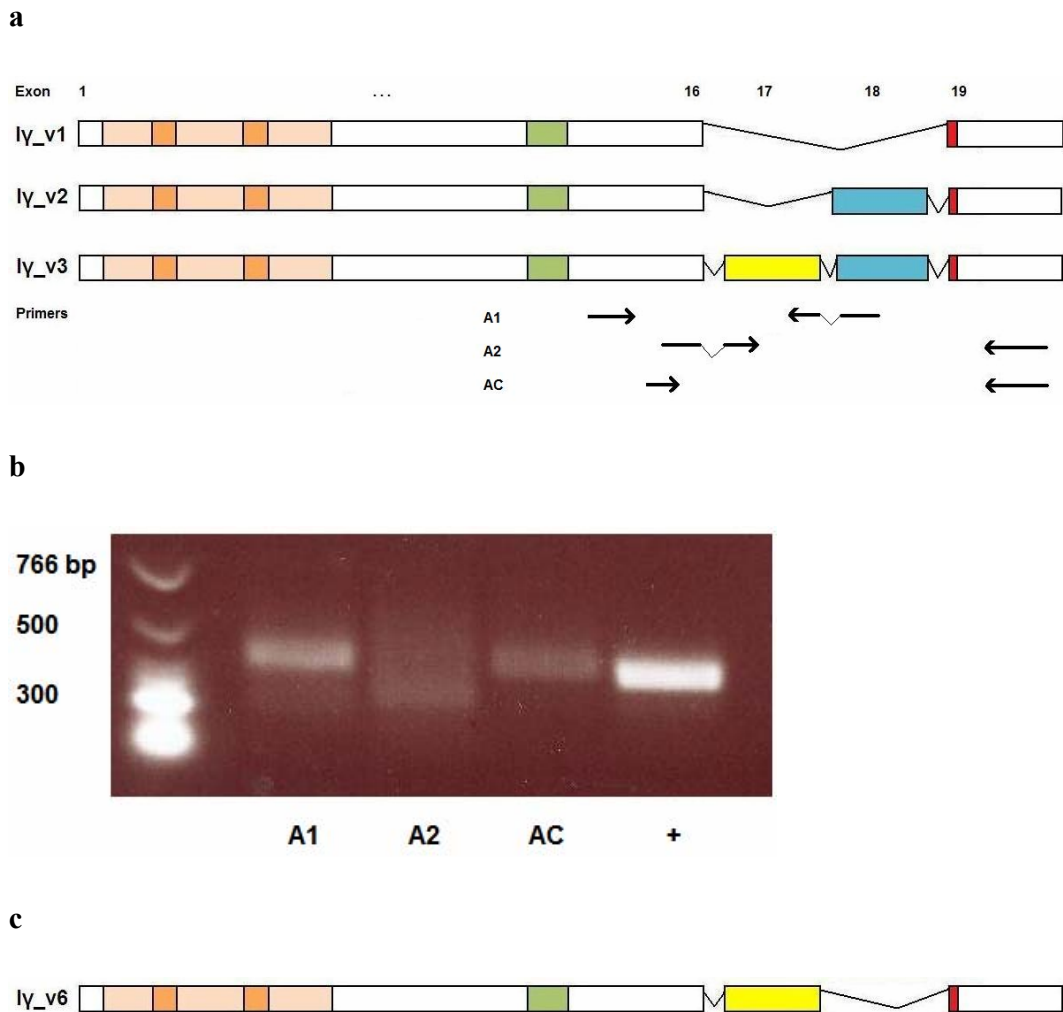
Figure 33 RT-PCR for Iγ_v3 from rat anterior pituitary mRNA

(**a**) PCR scheme. **A1**: forward primer anneals to Exons 13/14, reverse primer against 17/18 (γ_v3 specific), Iγ_v3 product expected at 353 bp. **A2**: forward primer anneals to Exons 16/17 (γ_v3 specific), reverse primer against Exon 19 3' UTR, Iγ_v3 product expected at 319 bp. **AC**: forward primer anneals to Exon 16, reverse primer against Exon 19 3' UTR, Iγ_v3 product expected at 493 bp, but also Iγ_v2 at 415 bp, and Iγ_v1 at 337 bp. +: actin control expected at 323 bp. (**b**) RT-PCR product after agarose gel electrophoresis. A1 and + band sizes were as expected, the main product of AC corresponded to the preferential amplification of γ_v1, and the A2 product consisted of smaller bands besides that expected from Iγ_v3. The lower band was subjected to sequencing and confirmed to be a novel spliceoform, named PIP5KIγ_v6. (**c**) Splicing scheme of the new splice variant, Iγ_v6.

This unexpected band was found to be a novel splice variant of PIP5KIγ. It included Exons 1–16 as all other spliceoforms, followed by the 78-nt Exon 17 (as in γ_v3) and, instead of having Exon 18 (which γ_v2 and γ_v3 have in common), was ligated directly onto Exon 19, the beginning of which is the stop codon TAA. In other words, this novel protein could be described as a truncated version of PIP5KIγ_i3, ending with the 26 AAs that constitute the unique peptide insert of γ_i3.

We named this new spliceform PIP5KIγ_v6, according to the convention that Schill and Anderson suggested[170]. It is interesting that since Exon 17 and Exon 18 (and hence the peptide that they code for) have the same length, Iγ_i6 should have the same molecular weight as Iγ_i2 (around 90 kDa).

It should be noted here that the actin reaction (Lane + in Figure 33b) controlled for the optimisation of the PCR protocol. During subsequent PCR experiments, this positive control was included whenever it was necessary to trouble-shoot a reaction where no amplification product was observed (data not shown). However, in a typical set of reactions using the same condition and mix composition in parallel, the experiments were already internally controlled for, because some reactions showed positive results demonstrating not only the optimisation of the general conditions, but also the availability of PIP5KIγ templates and the specific accessibility by their PIP5KIγ primers.

5.2. Iγ Spliceform Expression Profile in Specific Tissues

Since the Iγ_v2 and Iγ_v6 would produce fragments of the same size in a general PIP5K PCR (*e.g.* AC primers in Figure 33), it left open to other interpretations previous estimates of Iγ variants using similar primers (*e.g.* [167, 170]). Moreover, to study Iγ_v6 further, it was necessary to be able to distinguish between each splice variant unambiguously. I further developed this PCR strategy into a more targeted way of distinguishing between different splice variants, by using primers that annealed to particular spliceoform-specific junctions of exons. This way, I was able to detect the existence of a particular splice variant exclusively.

Figure 34 shows the PCR for specific Iγ splice variants in the anterior and posterior parts of the rat pituitary, as well as AtT-20, the mouse anterior pituitary derived cell line.

a

b
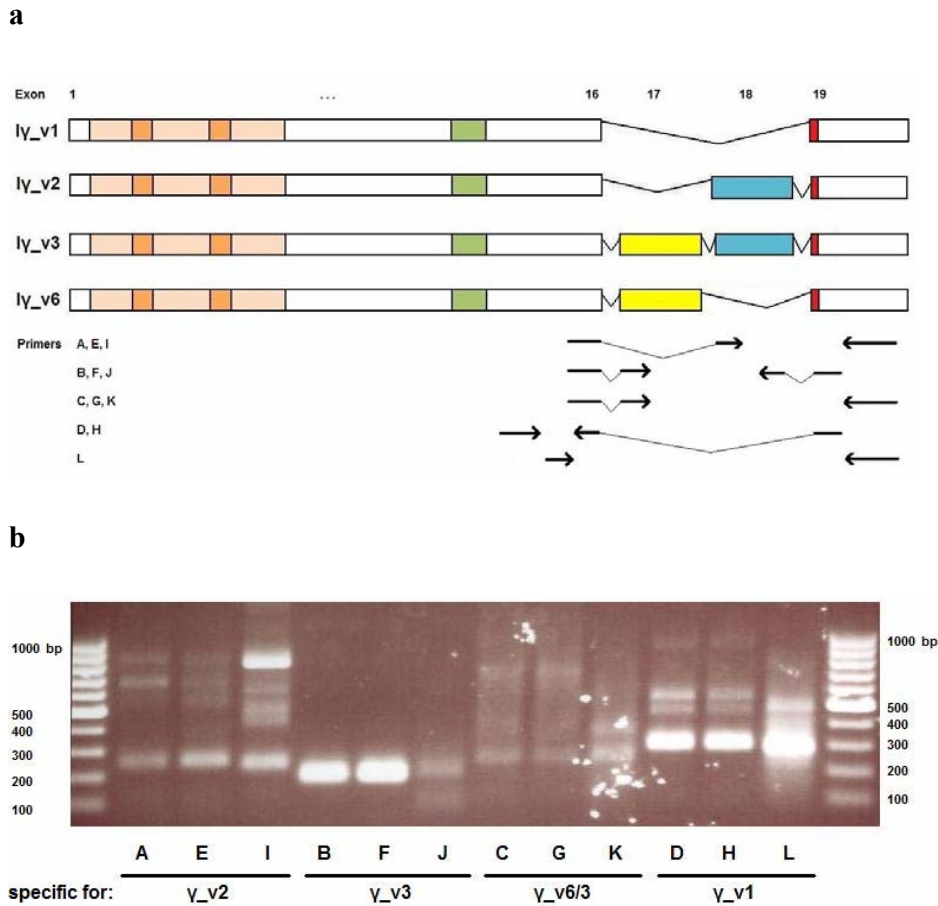
Figure 34 PCR for specific Iγ splice variants in the pituitary and AtT-20 cell line
(**a**) PCR scheme. **A**, **E**, **I**: forward primer anneals to Exons 16/18, reverse against 19, γ_v2 product expected = 243 (rat) or 234 (mouse) bp. **B**, **F**, **J**: forward 16/17, reverse 19/18, γ_v3 product expected = 184 (rat) or 191 (mouse) bp. **C**, **G**, **K**: forward 16/17, reverse 19, γ_v6 product expected = 241 bp, γ_v3 product = 319 bp. **D**, **H**: forward 13/14, reverse 19/16, γ_v1 product expected = 294 bp. **L**: forward 15/16, reverse 19, γ_v1 product = 286 bp, γ_v2/6 product = 364 bp, γ_v3 product = 442 bp. (**b**) PCR product. mRNA template added: **A – D**: anterior pituitary (rat), **E – H**: posterior pituitary (rat), and **I – L**: AtT-20 (mouse anterior pituitary).

121

Relevant bands were sequenced after gel extraction. It was confirmed that γ_v3 was indeed expressed in all of the three sources, *i.e.*, anterior pituitary, posterior pituitary and AtT-20. In addition to the γ_v6 found in the pituitary as described in the previous section, its expression was also confirmed in AtT-20 (band extracted and sequenced).

I extended the search further onto the hippocampus, where Iγ_v3 expression was previously demonstrated[167]. Using specific primers for each splice variant, the existence of each template was verified (Figure 35). Iγ_v1, Iγ_v2 and Iγ_v3 were all confirmed to be present in the rat hippocampal cDNA library. However, The lower band in Lane B corresponded to Iγ_v3 (319 bp), while the upper band was confirmed to be a non PIP kinase product by sequencing. By these criteria, Iγ_v6 is apparently absent from the hippocampus.
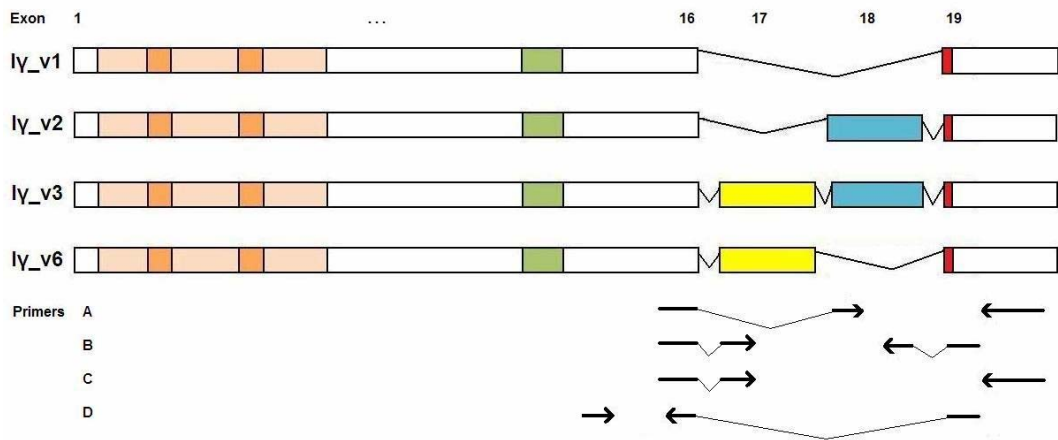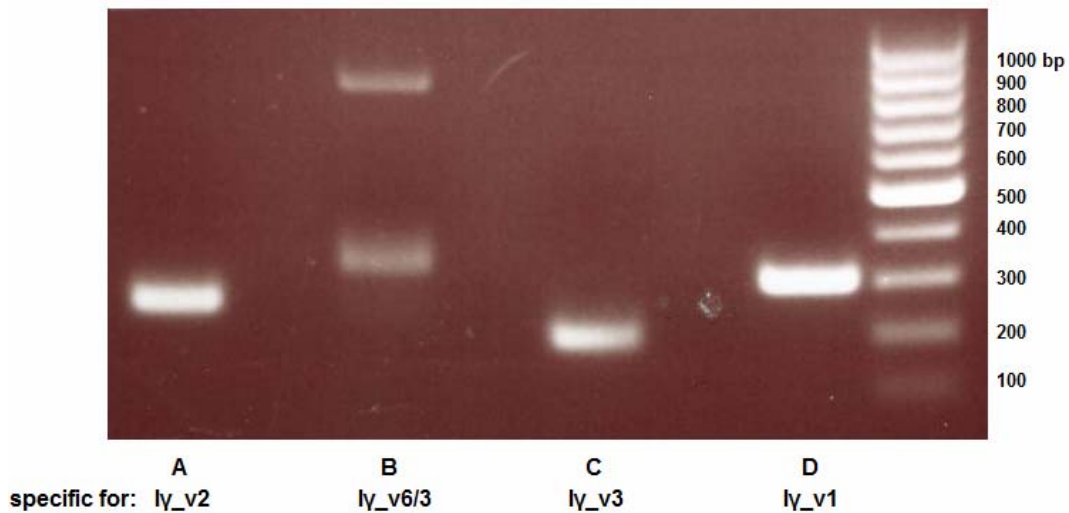
Figure 35 PCR for specific Iγ spliceoforms from rat hippocampus

(**a**) PCR scheme from rat hippocampal cDNA library. Primer pairs used were: **A**: 16/18 and 19, **B**: 16/17 and 19, **C**: 16/17 and 19/18, **D**: 13/14 and 19/16. Expected fragments were 243, 319/241, 184, 294 bp, respectively. (**b**) PCR result. A, C and D fragments were of the lengths expected. The lower band in Lane B corresponded to Iγ_v3 (319 bp), while the upper band was a non PIP kinase product. The band expected using the Iγ_v6 template (241 bp) was absent.

5.3. Tissue Distribution of PIP5KIγ Spliceoforms in Mice – the Updated Picture

In an attempt to repeat Giudici's initial cloning of Iγ_v3 from total mRNA of various tissues of Swiss Webster mice, and to confirm its expression pattern across different tissues, RT-PCR was repeated with the same protocol as in Giudici *et al.* (2004)[167]. With the forward primer spanning the junctions of Exons 15 and 16 (in common of all known Iγ spliceoforms) and the reverse primer complementary to the 3' UTR in Exon 19, the experiment was designed to amplify all PIP5KIγ splice variants.

Reassuringly, the expression pattern observed was identical to the one published by Guidici *et al.*[167] (Figure 36b).

a
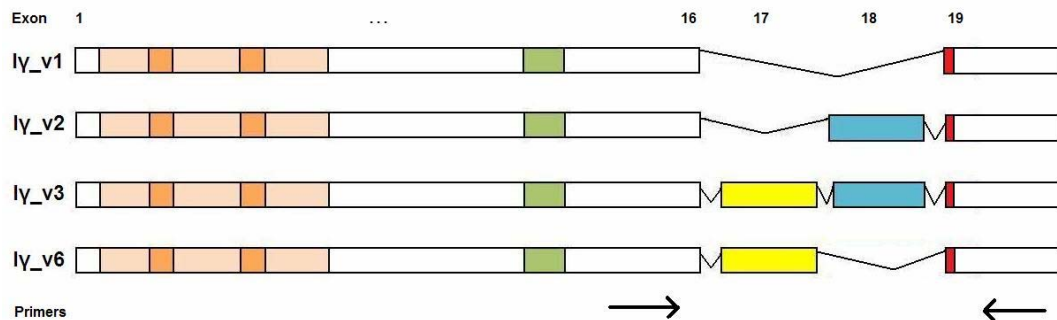
b
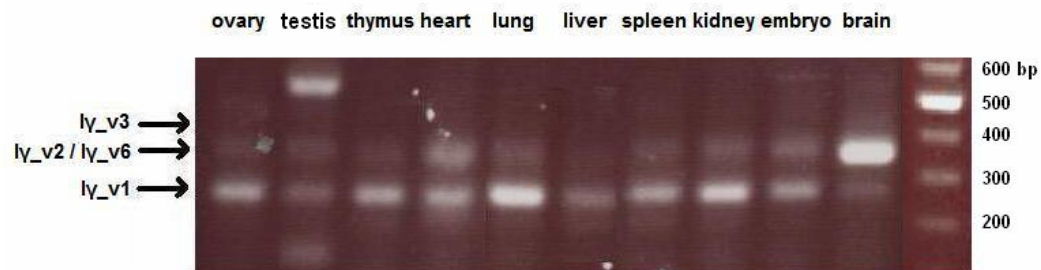
Figure 36 RT-PCR result for general amplification of PIP5KIγ from mouse tissue total mRNA.

(**a**) PCR scheme, forward against Exons 15/16, reverse against Exon 19. (**b**) PCR results consistent with Giudici (2004). Iγ_v3 products were the subsidiary bands just above the Iγ_v2 products, though less obvious due to lower intensity. The very high band in the tescicle lane was confirmed to be a non-PIP5K product. It is worth noting that the middle band was originally considered as the PCR product from Iγ_v2 exclusively. Now we know that the template could have been both Iγ_v2 and Iγ_v6, the novel splice variant discovered in this study.

As mentioned above, this adds complexity to the interpretation of existing evidence on the tissue distribution of Iγ splice variants. For example, in the original RT-PCR experiment[167], the middle lane corresponding to 364 bp had always been considered a segment resulting from the amplification of γ_v2. Now we know that

125

with this choice of primers, the middle lane may well have been the result of the amplification of a mixture of both γ_v2 and γ_ v6, both giving PCR products of the same length. The identity of this middle lane is therefore no longer specific for a particular splice variant.

Therefore, I focussed on the tissue distribution of each splice variant in turn, and performed RT-PCR from the total mRNA of mouse tissues (Figure 37), using specific primers for each splice variant, as described in the previous section.

a
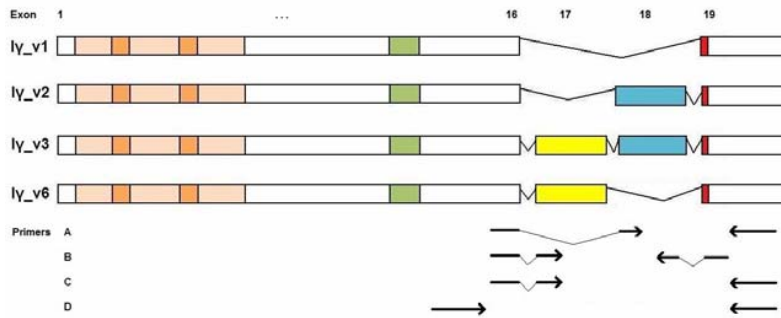
b
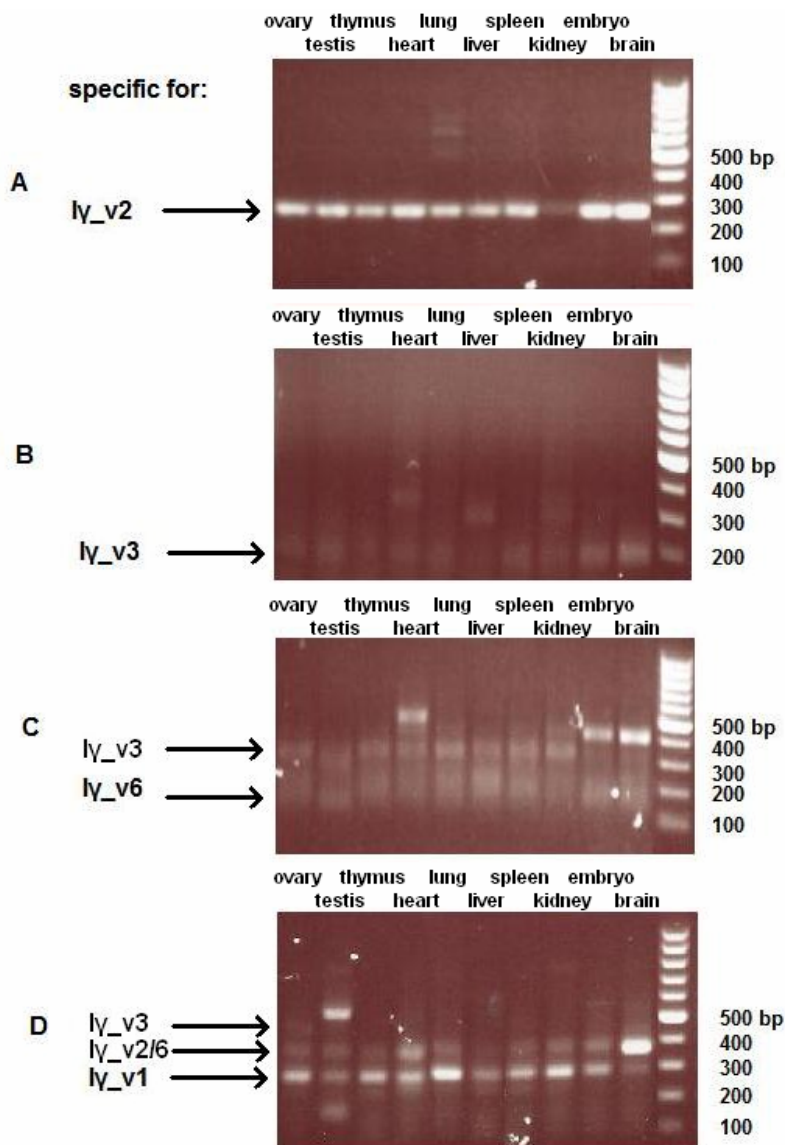
Figure 37 RT-PCR for specific splice variants in mouse tissues

(**a**) PCR scheme, using primers (**A**) 16/18 and 19 for γ_v2 (234 bp), (**B**) 16/17 and 19/18 for γ_v3 (191 bp), (**C**) 16/17 and 19 for γ_v6 (241 bp) and γ_v3 (319 bp), and (**D**) 15/16 and 19 for γ_v1 (286 bp), γ_v2/6 (364 bp) and γ_v3 (442 bp). (**b**) PCR result from the total mRNA of mouse tissues. Note that the Iγ_v3 bands in B and C resembled each other, although it seemed less favourable to be used as the template in reaction D, compared to other splice variants.

It is apparent that the various Iγ splice variants produced fragments at the expected sizes, indicating their presence. Iγ_v2 was present largely ubiquitously throughout different tissues. The pattern of Iγ_v3 expression was similar in Panels B and C, which both resembled that in Giudici *et al.* (2004)[167]. The band separation was probably not clear enough for each product to reflect the original abundance of the mRNA of each spliceoform naturally present, and this PCR protocol is largely qualitative.

I therefore resorted to one more PCR screening (with a larger separation in gel electropheresis). Besides the same paradigm as Panel C in Figure 37, another pair of primers was also designed to specifically detect Iγ_v6, annealing to Exons 15/16 and 19/17, respectively.
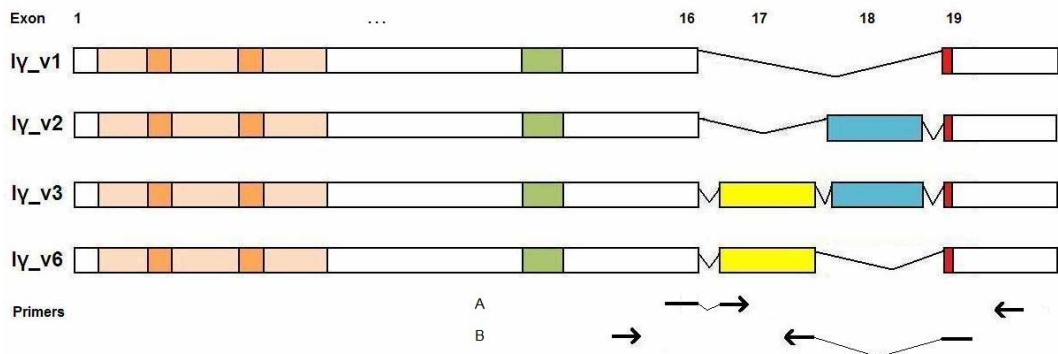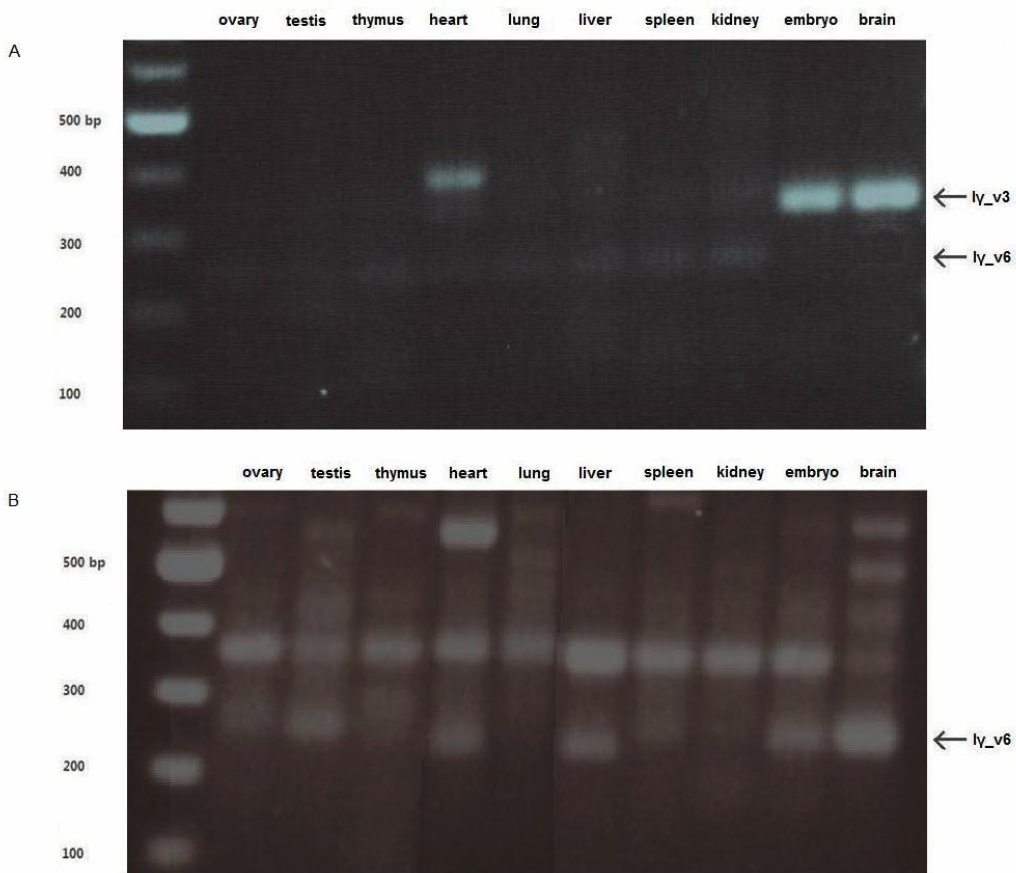
Figure 38 RT-PCR of Iγ_v3 and Iγ_v6 in the mouse tissues

(**a**) PCR scheme using primers (**A**) 16/17 and 19 for γ_v3/6 (318/240 bp), and (**B**) 15/16 and 19/17 for γ_v6 (239 bp). (**b**) PCR result from the total mRNA of mouse tissues.

It appeared that the γ_v3 expression pattern was highest in the brain, as found before.

The 239-bp band from the amplification of γ_v6 in Panel B seemed to be present across different tissue types. In order to verify its identity, the bands from the heart, liver, spleen and kidney were extracted, purified and sequenced. In all these samples tested, the presence of the γ_v6 splice variant was confirmed unambiguously. These data revealed a low but ubiquitous expression of Iγ_v6 across tissues included in the library. The upper bands in Figure 38b (B) did not correspond to any of the other splice variants, and probably resulted from misbinding of primers to other non-PIP5KIγ templates.

5.4. List of Primers Used for Rodent Templates

Below is a list of primers used above, to amplify PIP5KIγ from the rat and the mouse (Table 8).

Organism	Exon(s)	Sequence
mouse	15/16 forward	`GGAGGAGGGTGCAGG AGTGGAGGTC`
mouse	16/17 forward	`CCCTCTACAGACATCTATTTT TTCGCCCATGG`
mouse	19/18 reverse	`CTGCATAGAAGTTA TGTGTCGCTCTCGCCG`
mouse	19/17 reverse	`GGGGACTGCATAGAAGTTA AGTGCCTGTGTGG`
rat	13/14 forward	`GGTACAG GCGGCGTACGCAGTCTTC`
rat	15/16 forward	`GCAGGGTGCAGG AGTGGAGGTTCC`
rat	16 forward	
rat	16/17 forward	`GACATCTATTTT TTCGCCCACGGGAGATAC`
rat	18/19 forward	`GACTGCATAGAAGTTA TGTGTCGCTCTCGCC`
rat	18/17 reverse	`GGTGGG AGCGCCTGTGTGGCTTG`
rat/mouse	16/18 forward	`CAGACATCTATTTT CCCACCGACGAGAGG`
rat/mouse	19/16 reverse	`CAGATTGGGGACTGCATAGAAGTTA AAAATAGATGTCTG`
rat/mouse	19 reverse	`CCGTCAGTGGGAGGGAGAGAACAAG`

Table 8 List of primers used for the amplification of PIP5KIγ from the rodents

The space within sequences illustrates the exon junction.

5.5. Generation of Mammalian Expression Vectors Containing Iγ_i6 and Its Mutants

Having validated that Iγ_i6 was naturally expressed in the cells, I went on to subclone Iγ_i6 that is N-terminally tagged with GFP and FLAG, under the mammalian

promoter pCMV. This would allow me to overexpress Iγ_i6 in *e.g.* HEK-293 and COS-7 cells, and study its features extensively in comparison with the other splice variants.

Usually, a *de novo* cloning project would require us to amplify the Iγ_v6 gene out of a cDNA/mRNA library, clone it into a bacterial expression vector, and then subclone it into a mammalian vector (such as the pCMV-2B and pEGFP-C1 used above). However, an alternative approach was adopted. Since Iγ_i6 only differed from Iγ_i3 by a 26-AA peptide at the very C-terminus of the latter (*i.e.* the Iγ_i2 "tail"), I decided to introduce a stop codon into the spectrum of Iγ_i3 constructs, in order to generate the corresponding Iγ_i6 mutants (Figure 39a).

a Primer	Sequence
forward	CCAAGCCACACAGGCGCT *TAA* ACCGACGGG
reverse	CCAGCTCCTCCCGTCGGT *TTA* AGCGCCTGTG

Iγ_i3   Iγ_i6
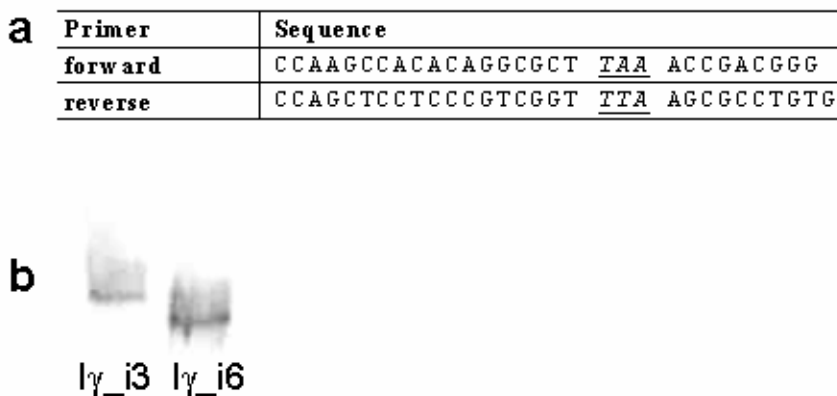
Figure 39 Generation of the Iγ_i6 construct for overrexpression
(**a**) Primers used to introduce by site-directed mutagenesis a stop codon (immediately after Exon 17), illustrated by the *underlined and Italic* font refer to the mismatching region with the template, *i.e.*, the desired sequence. (**b**) Overexpressed FLAG-tagged Iγ_i6 in HEK-293 cells, lysate detected by anti-FLAG antibody in Western blot. The protein band appeared at the correct molecular weight expected for the full length Iγ_i6.

When detected by anti-FLAG antibody in Western blot, the Iγ_i6 band appeared at the correct molecular weight expected of the full length protein, 26 amino acids shorter than Iγ_i3 (Figure 39b).

5.6. Live Imaging of Overexpressed Iγ_i6

The GFP-tagged PIP5KIγ_i6 was overexpressed in COS-7 cells. Like its other spliceoforms, the enzyme seemed to localise primarily to the plasma membrane (Figure 40). Using alternative methods, the localisation of Iγ_i6 is investigated in more detail in later sections.
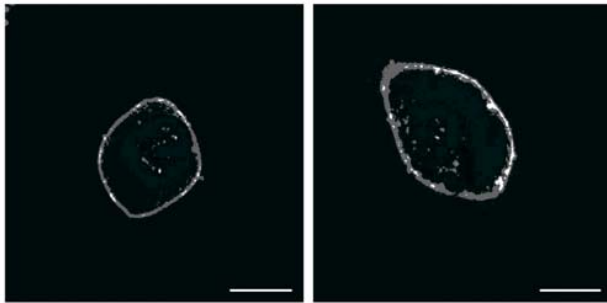
Figure 40 GFP-tagged Iγ_i6 localised to the plasma membrane
Typical subcellular localisation of overexpressed GFP-tagged Iγ_i6 constructs in COS-7 cells (scale bar = 10 μm).

5.7. FRAP Behaviour of Iγ_i6

When assessed by FRAP, Iγ_i6 recovered towards a lower equilibrium level compared to Iγ_i1 and 2, partially resembling Iγ_i3 (Figure 41). This seemed to suggest that the 26-AA insert was at least partially responsible for the observed

immobile fraction of Iγ_i3. These data also suggest that the immobility of Iγ_i3 was not a simple consequence of its larger molecular size compared to Iγ_i2.
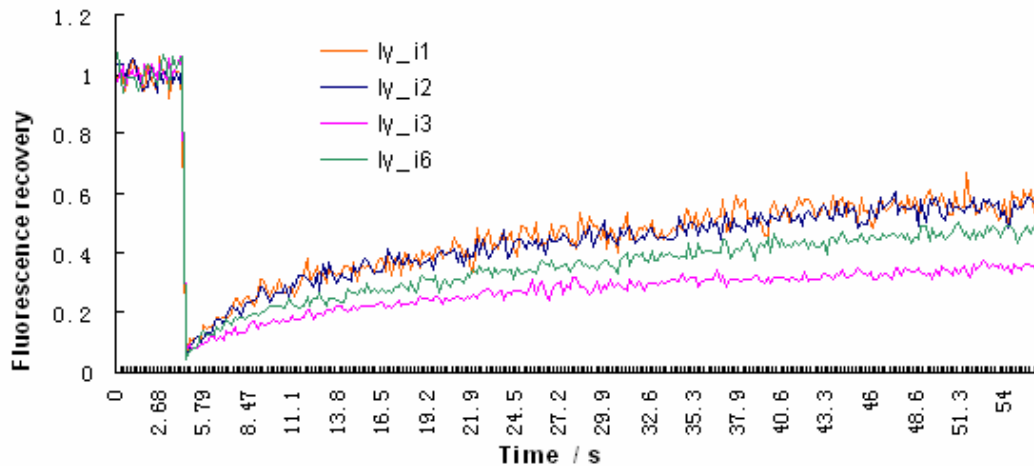
Figure 41 The mobility of Iγ_i6 partially resembled that of Iγ_i3

FRAP behaviour of different splice variants of PIP5KIγ, mean fluorescence intensity plotted (n = 10).

5.8. Subcellular Localisation of Iγ Splice Variants in COS-7 Cells – Assessed by Immunocytochemistry

The subcellular localisation of overexpressed Iγ_i6 was compared between that of the other Iγ splice variants in COS-7 cells. Proteins were N-terminally tagged with either GFP or FLAG, and the tag visualised by immunocytochemistry.

As shown in the previous section (Figure 46) and earlier studies[179], all splice variants of PIP5KIγ displayed similar localisation to the plasma membrane when overexpressed in HEK-293 cells. In contrast, when overexpressed in COS-7 cells, Iγ_i3 was shown to be more internalised than Iγ_i1 and Iγ_i2[179]. However, the

Iγ_i3 construct used is now known to contain the V443A mutation (see Results I); when this was corrected back, the difference between the wild type (Val^{443}) of each splice variant was much less obvious, all constructs now primarily localising to the plasma membrane (Figure 42). Nonetheless, it was interesting to see how Iγ_i6 behaved, since it had the same size (in terms of the primary sequence) as γ_i2, yet possessed the peptide insert of γ_i3, which made γ_i3/6 different from Iγ_i2. In an immunocytochemical staining on COS-7 cells, γ_i6 was shown to have a localisation that was largely membrane-bound, quite similar to the other splice variants (Figure 42).
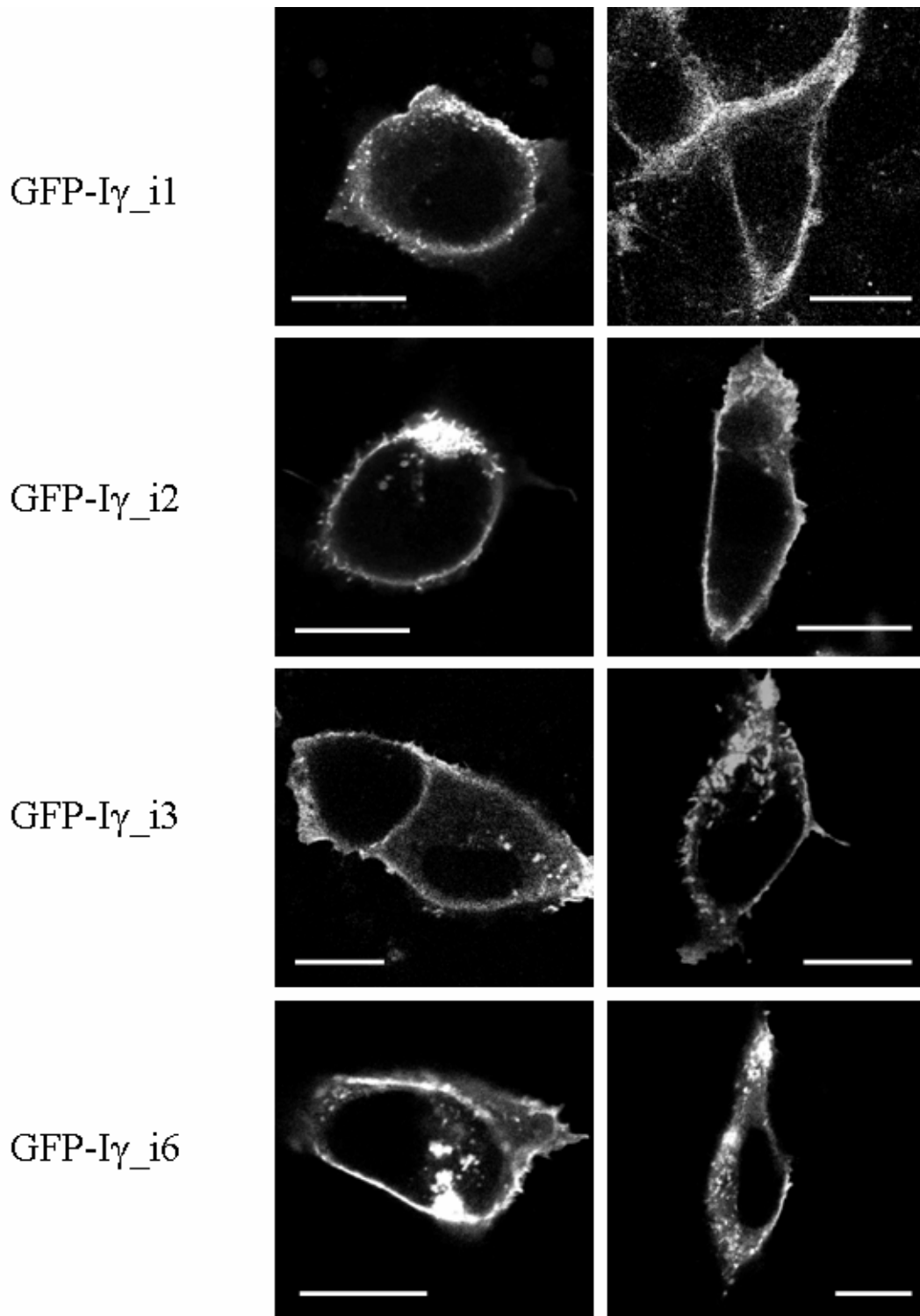
Figure 42 All wild type Iγ splice variants localised similarly in COS-7 cells

Typical subcellular localisation of overexpressed GFP-tagged constructs in COS-7 cells (scale bar = 10 μm). All constructs used contained the wild type Val[443].

5.9. Development of Specific Antibody Against Iγ_i6

In order to be able to detect the endogenous Iγ_i6 at the protein level and perform Western blot, immunocytochemical staining and/or immunoprecipitation, I sought to generate a primary antibody that was raised against the C-terminus of Iγ_i6. This was of course also the unique 26-AA peptide present in Iγ_i3. A rabbit polyclonal antibody, E2139, was developed by our lab (outsourced to NeoMPS), against the C-terminal 16 amino acids on the Iγ_i3/6 peptide insert. The epitope sequence was CRRRRLRAVTPSHTGA.

5.10. Optimisation and Specificity of E2139 for Western Blot

This primary antibody was first tested for Western blot application. Starting from the standard Western blot protocol (see Materials and Methods 2.19), optimisation was carried out testing a range of E2139 concentrations, while keeping the goat anti-rabbit secondary antibody at an established working concentration.

Within the dilution range of 1:20000 – 1:1000 from the stock, the E2139 antibody appeared to work in a concentration-dependent fashion (Figure 43).
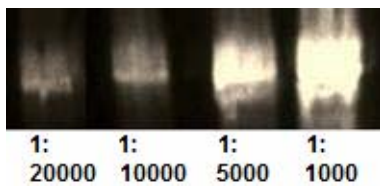
Figure 43 Optimisation of the E2139 antibody

Samples were equal volumes of HEK-293 lysate, overexpressing PIP5KIγ_i6.

In this study, all subsequent Western blots using E2139 were performed according to this optimised protocol, with a 1 hr incubation of E2139 (1:7500, or 1:2500 from the 1:1 glycerol-diluted stock), followed by a 1 hr incubation of HRP-conjugated goat anti-rabbit antibody (1:1000).

There was, however, another concern. The epitope sequence (against which E2139 was raised) was present not only in Iγ_i6, but also in Iγ_i3. The difference was that this peptide was at the very C-terminus of Iγ_i6, while in Iγ_i3 it was followed by the 26-AA tail of Iγ_i2 (compare Figure 33a and c).

I therefore tested the recognition efficacy of Iγ_i3 and Iγ_i6 by E2139 (Figure 44), and found that a stronger signal was generated by the same quantity (assessed by FLAG) of Iγ_i6 versus Iγ_i3.
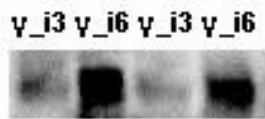
Figure 44 Recognition specificity of E2139 to Iγ_i3 and Iγ_i6
Equal amounts of Iγ_i3 and Iγ_i6 were loaded, as assessed by Western blot using the anti-FLAG antibody.

This result was not very surprising, given the frequent observation that antibodies typically recognise the C-terminus of the antigen much better than an epitope that is more hindered within the peptide sequence (*e.g.* [216]).

Such specificity of E2139 to Iγ_i6 was encouraging, because with a PIP5KIγ signal recognised by E2139 as the primary antibody, we could interpret it as γ_i6, but not γ_i3, with reasonable confidence.

5.11. Optimisation and Specificity of E2139 for Immunocytochemistry

With the antibody E2139 established to recognise Iγ_i6 specifically in Western blot, I moved on to test where it could be used for the same purpose in immunocytochemistry.

The immunocytochemistry typically uses antibody at a much higher concentration (*e.g.* 5x) than that for Western blot. A preliminary staining revealed that using a dilution factor of 1:1000 – 1:100 for primary incubation produced successful staining with a good signal-to-background ratio (Figure 45).
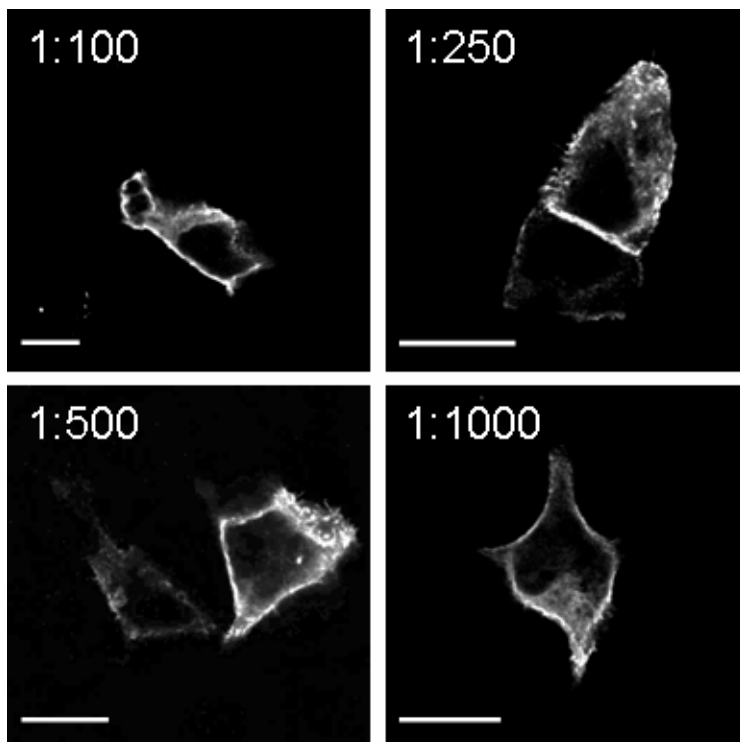
Figure 45 Optimisation of E2139 for immunocytochemistry

Typical immunocytochemical staining of overexpressed FLAG-tagged Iγ_i6 constructs in HEK-293 cells (scale bar = 10 μm), using E2139 as the primary antibody. Ratios indicate dilution factor of the primary antibody incubation.

All subsequent immunocytochemical staining using E2139 was diluted at the optimal ratio of 1:750, to ensure good signal quality.

Since there was not any spliceoform-specific antibody available for PIP5KIγ, this was the first time that it was possible to detect the protein of a Iγ spliceoform directly, without the requirement for a peptide tag. Therefore, I first set out to investigate the reliability of our previously used immunocytochemistry protocols using anti-FLAG staining, and how it overlapped with the E2139 signal (Figure 46).

As essential controls, Figure 46a and b showed that there was no bleed-through of Alexa 555 into the green channel, or the Alexa 488 into the red channel. c and d showed that there was no cross-talk between the mouse anti-FLAG primary and the anti-rabbit secondary, or the rabbit E2139 primary and the anti-mouse secondary antibodies. As an internal control, the negative staining in Panel c also showed that the anti-rabbit secondary by itself did not give rise to any non-specific background.

Figure 46e and f established that the subcellular localisation pattern of overexpressed, FLAG-tagged Iγ_i6 was consistent, whether stained with anti-FLAG or E2139 (against the enzyme's C-terminus itself). This was demonstrated by the yellow overlapping signals in Panels k and l.

In the mean time, I intended to verify that when used for immunocytochemistry, E2139 was still specific for Iγ_i6, as opposed to other Iγ spliceoforms. Figure 46g and h showed that FLAG-tagged Iγ_i1 and Iγ_i2 gave no signal when stained with E2139. However, Panels i and j seemed to suggest that there was some binding of E2139 to Iγ_i3, though the affinity (as shown by green intensity) was much less than that of Iγ_i6 (probably for the same reasons discussed above).
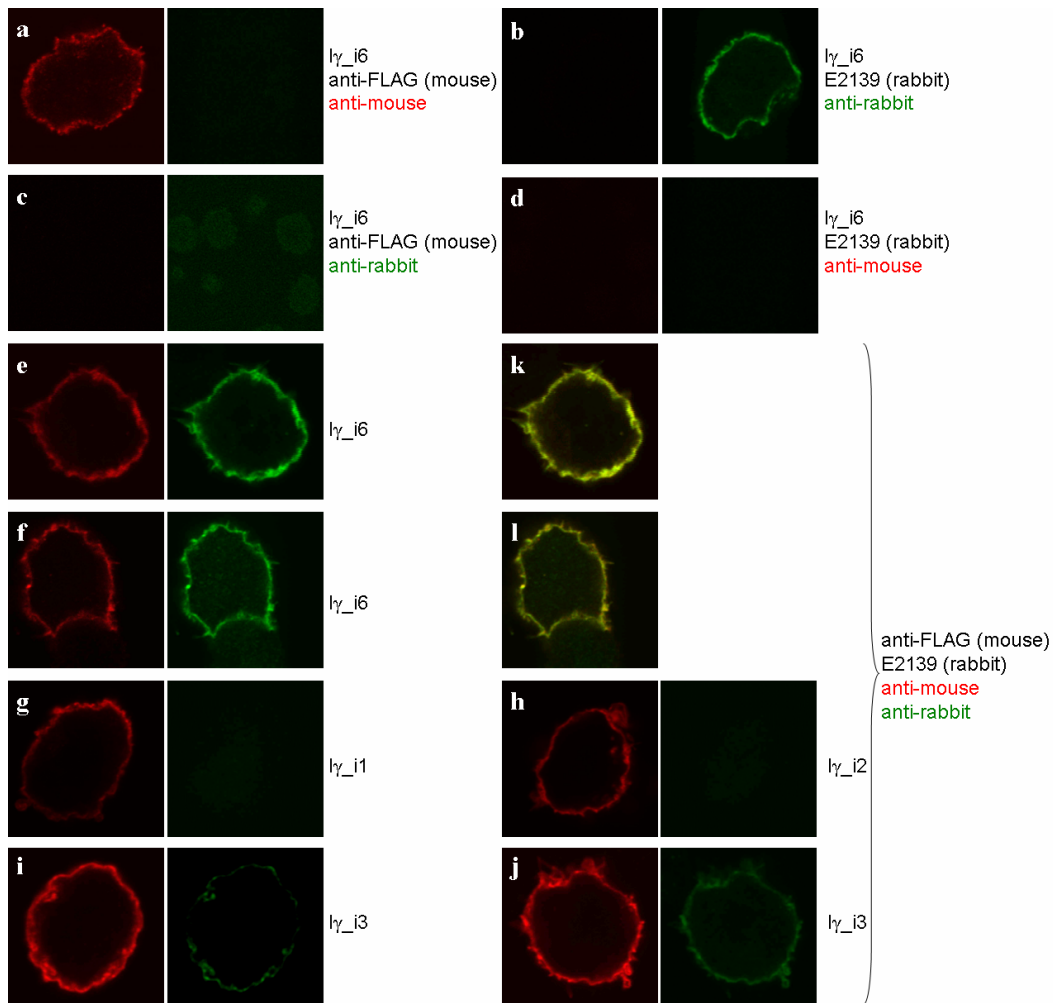
Figure 46 Comparison between E2139 and anti-FLAG staining

Typical confocal images of fixed, permeabilised and stained HEK-293 cells overexpressing PIP5KIγ constructs. Primary antibodies: anti-FLAG was made from the mouse and E2139 from the rabbit. Secondary antibodies (from goat): the anti-mouse antibody was conjugated to Alexa 555 (red) and anti-rabbit conjugated to Alexa 488 (green). Cells overexpressed different constructs and were incubated with different antibody combinations, as indicated on the right hand side of each image. (**a**) – (**j**): left (red) channel = 550–580 nm, right (green) channel = 500–540 nm, excited using a 543 nm laser and an Argon laser filtered at 488 nm, respectively. (**k**) and (**l**) were superimposed images of (**e**) and (**f**), respectively. Image dimensions: 15.4 x 15.4 μm, except (**c**) 38.2 x 38.2 μm.

5.12. Detection of Endogenous Iγ_i6 Protein by Immunohistochemistry

As described above, Iγ_v6 mRNA was confirmed in both the pituitary and the AtT-20 cell line (Sections 5.1 and 5.2). I would therefore like to validate the presence of Iγ_i6 in the pituitary (or other tissues) directly at the protein level.

Using fixed sagittal slices from the mouse brain, I performed immunohistochemistry, in an attempt to detect endogenous Iγ_i6. After several trials, the protocol was optimised, and the E2139 signal could be detected against a relatively low background. Meanwhile, a NeuroTrace marker was included, which highlighted the Nissl body present only in the soma of neurons and hence served as a general neuron label.

Different parts of the brain displayed different levels of staining with E2139. In particular, the signal appeared abundant in certain subclasses of neurons in the cerebral cortex, olfactory bulb, hypothalamus, limbic system and the cerebellum. It was reassuring that the signal was not ubiquitous for all neurons present in the same region (*e.g.* pons, olfactory bulb and prefrontal cortex), suggesting that the staining was epitope-specific.

CB (molecular layer)

CB (Purkinje layer)

CB (granular layer)

medulla

Hpc (CA1)

pons

hypothalamus

frontal cortex

thalamus

Hpc (CA3)

Hpc (DG)

olfactory bulb

143
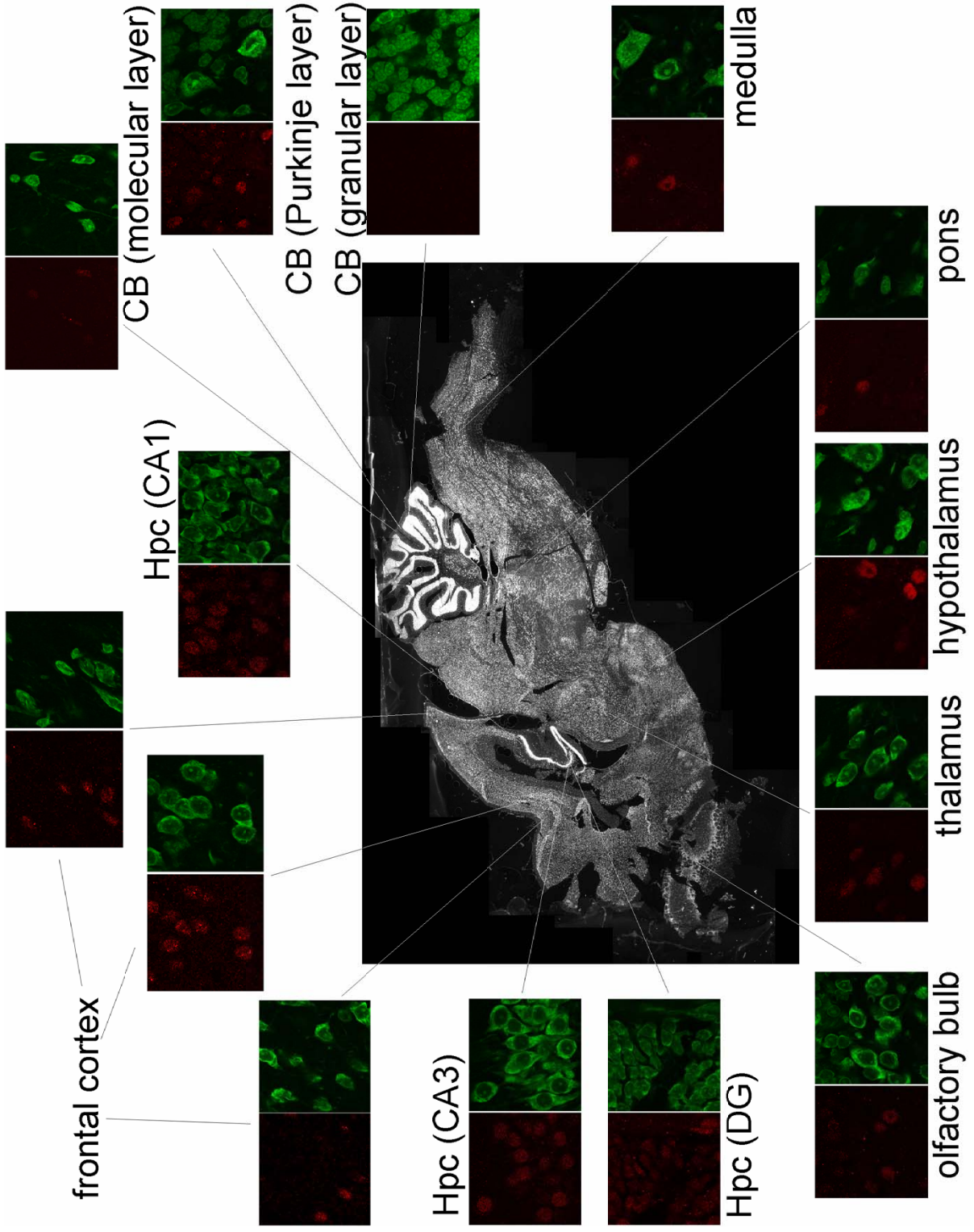
Figure 47 Immunohistochemical staining of the brain using E2139

Images from different regions of the brain (red = E2139 + donkey anti-rabbit secondary, 555 nm; green = NeuroTrace green, 535 nm), mapped onto the sagittal slice. Whole picture was acquired in smaller, overlapping pieces under low magnification fluorescence microscope (visualising the NeuroTrace signal) and joined together afterwards *in silico*. Hpc = hippocampus, DG = dentate gyrus, CB = cerebellum. Scale bar (bottom left) = 1 mm.

However, the positive E2139 signal in various areas of the hippocampus was puzzling. As we saw earlier (Figure 35), the Iγ_v6 is apparently absent in the hippocampus at the mRNA level. This discrepancy could only be explained by the fact that Iγ_i3 was also detected by the E2139 antibody, albeit at a lower efficacy (see above, Figure 44). This means that ultimately, although we have good reasons to assume E2139 detects Iγ_i6 best, due to its uniquely exposed C-terminal epitope, it is impossible to rule out the possibility that some of the signal may also originate from binding with Iγ_i3 in a less specific manner. This preliminary immunohistochemistry work therefore needs careful interpretation at the splice variant level. Nevertheless, it is the first direct demonstration that Iγ_i6 and/or Iγ_i3 is indeed present endogenously at the protein level.

6. Results IV – Confirmation of Iγ_i3 and Iγ_i6 Expression in Humans

6.1. Theoretical Examination of the Human Genome Sequence

The spliceoform Iγ_v3 was discovered by Giudici in our lab from the amplification of a rat hippocampal cDNA library[167], after Ishihara's initial discovery of Iγ_v1 and Iγ_v2 in the rodents[108]. The 26-AA insert near the C-terminus is analogous on the peptide level (but not the DNA level) to an *in silico* translated segment of the human Iγ gene, and therefore it was long assumed that Iγ_v3 should very likely exist in human too, though its expression had never been directly demonstrated. Having characterised the Iγ_i3 and Iγ_i6 constructs from the rodents, I thought it would be interesting and important to investigate whether these two splice variants also existed in humans. This question became especially pertinent in the light of a detailed study on Iγ splicing in humans.

Schill and Anderson[170] performed 3' RACE on the purified mRNA from the mammary epithelial cell line MCF10A, with the forward primer annealing to Exon 16, which all the known PIP5KIγ spliceoforms had in common. These experiments identified bands unexpected by their apparent molecular weight. Subsequent sequencing revealed two novel C-terminal splice variants of Iγ, both sharing the PIP kinase core spanning Exons 1–16, but rejoined onto different, novel downstream exons with unique stop codons within their own 3' UTR. Schill and Anderson named them Iγ_v4 and Iγ_v5, and the novel human exons 16b and 16c, to distinguish them from the original Exon 16 (which they then called 16a).

These novel exons (16b and 16c) were in an exceptionally lengthy region between human Exons 16a and 17 (which exactly corresponded to Exons 16 and 18 in the rodent, see Figure 5, though this interval was much shorter in rodents compared to the human). Therefore, it was impossible to find the counterparts in the mouse genome, homologous to human 16b and 16c. However, theoretical translation of this inter-exonic region in the human Ensembl database and alignment by ClustalW revealed that part of the predicted peptide sequence was highly homologous to the 26-AA

insert of rodent Iγ_v3 (Figure 48a). In fact, a comparison (Figure 48a) revealed that this is exactly the first 26 amino acids of the human Exon 16c!
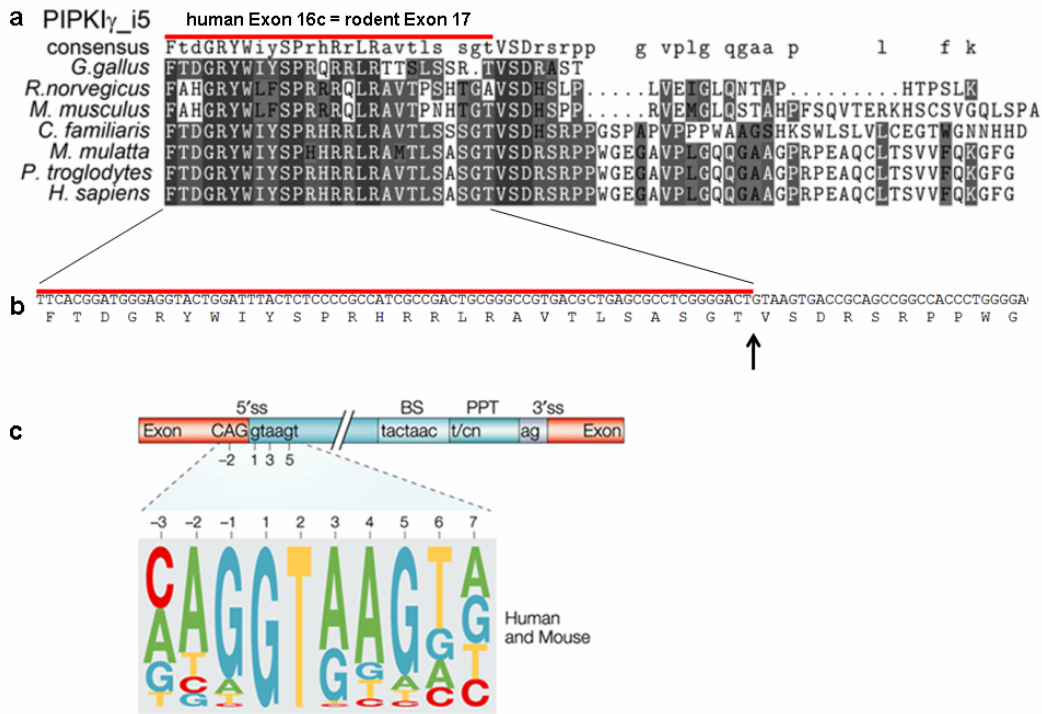
Figure 48 *In silico* **translation of Exon 16c of human PIP5KIγ_i5 and other Iγ orthologues**

(**a**) ClustalW alignment of theoretically translated peptide sequences from the Ensembl genomic database, showing downstream of human Exon 16c. Red line indicates the initial 26 AA, homologous to the rodent Exon 17. (**b**) An illustration of the underlying nucleotide sequence in human Exon 16c. Arrow indicates putative 3' splice site, alternative to that used by PIP5KIγ_i5. (**c**) Example of 5' splice site consensus, size of nucleotide indicating occurance frequency, modified from Ast (2004)[217].

This observation begged the question of whether the DNA sequence underlying the 26-AA peptide insert of the putative human Iγ_v3 might exist as an individual exon,

and also whether the Iγ_v3 splicing configuration actually occurrs in the human. It is plausible, because the sequence at the 3' junction of this putative exon (*i.e.*, the 5' splice site with regard to the next intron), GTAAGT, appears to be a well documented, perfect 5' splice site consensus (Figure 48c)[217, 218]. This site would enable the PIP5KIγ gene to produce the Iγ_v3 splice variant (directly demonstrated at least in the rodents), and this site also appears to be highly conserved across the species, even in the humans, at both the DNA and peptide levels (motif VSD in Figure 48b).

The possibility that the putative human exon in question existed (alongside 16b and 16c) is fascinating, because it means that on the one hand, Exon 16c could be spliced as it is in Iγ_v4 and Iγ_v5, while on the other hand its initial 78 bp could be spliced out as an individual exon, and ligated to the next exon(s) much further downstream to form Iγ_v3. This would be a case of internal splicing, *i.e.* alternative splicing within one exon to produce another smaller, overlapping exon, depending on a different choice of the 5' splice site (named with regard to the *intron*).

In this chapter, I refer to all the exons by their numbering as in the rodent, unless only relevant to the human (Figure 49). That is, I consistently refer to the rodent Exons 18 and 19 as in the above mentioned system, despite the confusing fact that Schill and Anderson[170] named them 17 and 18 instead, respectively.

Figure 49a shows a schematic aligment of all hypothetical PIP5KIγ splice variants that may be present in humans. The putative human Exon 17 (as should exist in Iγ_v3 and Iγ_v6) is depicted in yellow, which exactly corresponds to the beginning 78 bp of Exon 16c, as illustrated in Figure 49b.
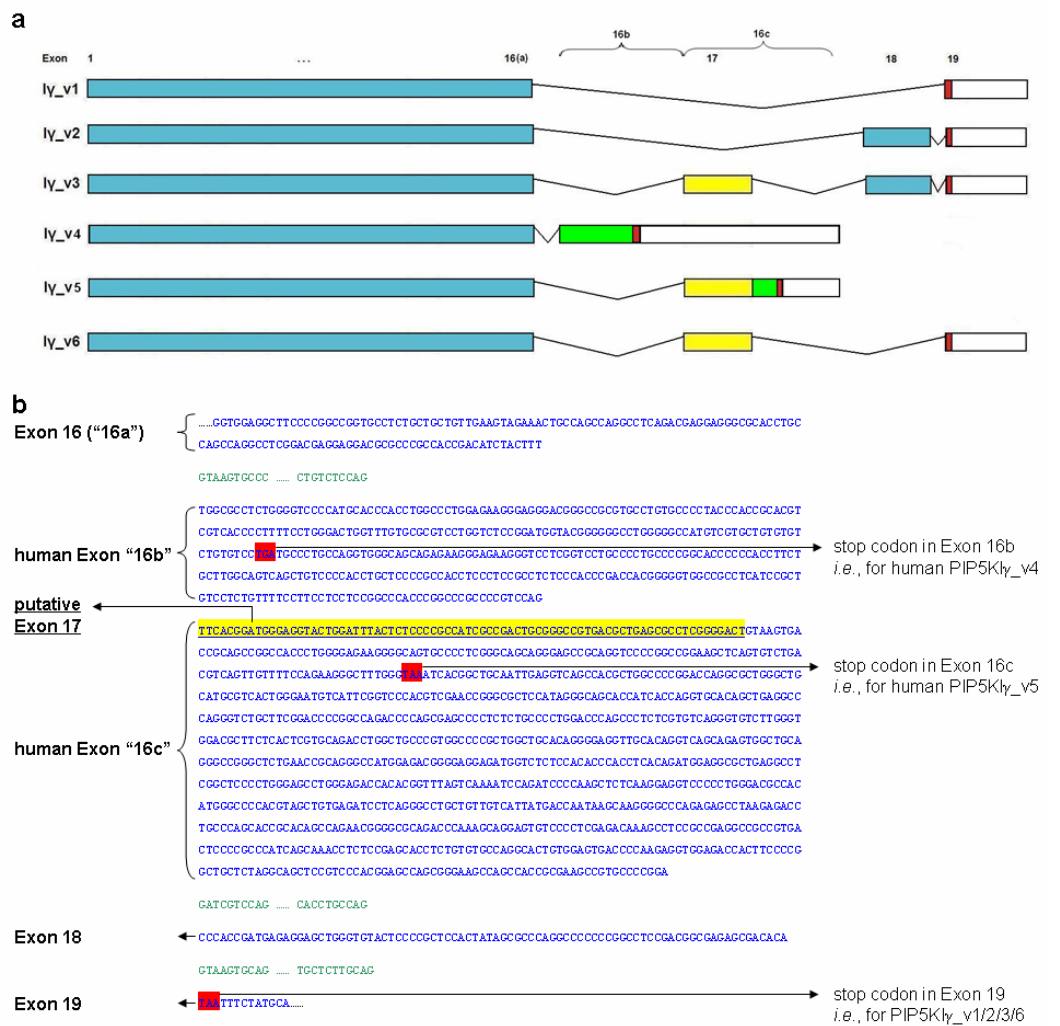
Figure 49 Illustration of the human genomic sequence between Exons 16 and 18
(**a**) Updated alternative splicing scheme of human PIP5KIγ, including the putative splice variants Iγ_v3 and Iγ_v6. The proposed Exon 17 is shown in yellow, with the rest of the 3' tails of Iγ_v4 and Iγ_v5 in green, 3' UTR in white, and other exons in blue. (**b**) Detailed genomic sequence of the human, emphasising the C-terminal sequence of Iγ. Exons are shown in blue, with introns (in the omitted form) in green, alternative stop codons highlighted in red and, again, putative Exon 17 in yellow.

Even though alternative 5' splice sites are known to exist in human and other mammalian genomes[219], the feasibility of the above scenario was not certain and needed to be addressed experimentally.

6.2. Detection of PIP5KIγ_v3 in the Human Brain

Based on our knowledge of Iγ_v3 and Iγ_v6 expression in the rodent brain, as described in the previous chapter as well as previous publications[167], I first investigated a cDNA library of the human brain. PCR was performed to amplify each splice variant of PIP5KIγ, using primers that specifically annealed to the exon junctions, based on the human PIP5KIγ gene sequence (Figure 50). The "Exon 17" counterpart in the human was assumed to be the initial 78 bp of the human Exon 16c (Figure 49b).

a
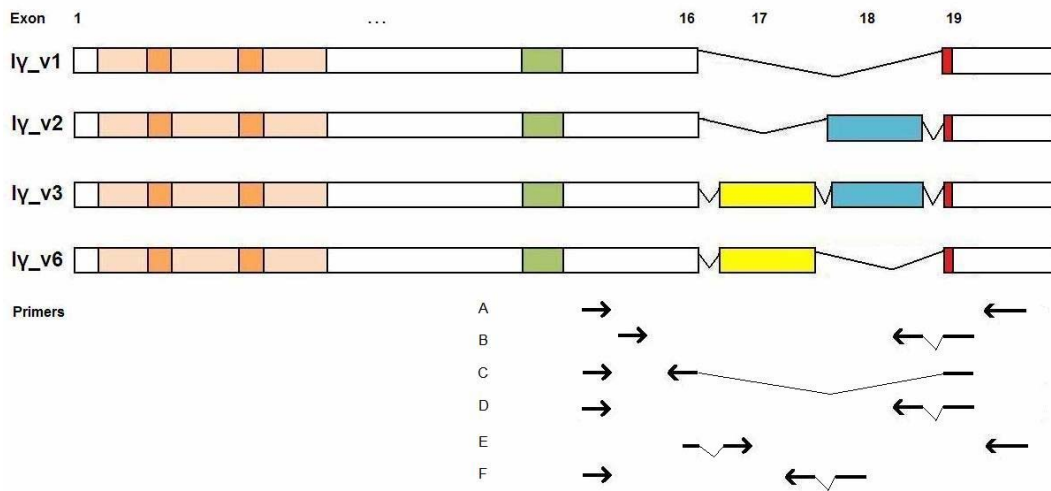
b
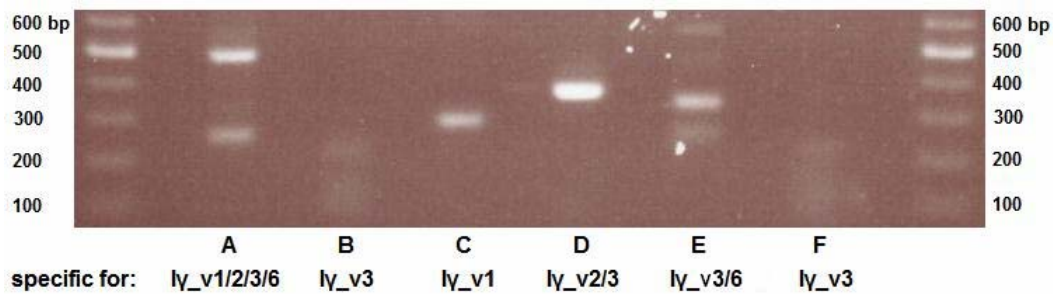
Figure 50 PCR for each Iγ splice variant in the human brain

(**a**) PCR scheme. Primers used were: **A**: 14/15 and 19 for Iγ_v1/2/3/6 (404/482/560/482 bp),
B: 16/17 and 19/18 for Iγ_v3 (199 bp), **C**: 14/15 and 19/16 for Iγ_v1 (268 bp), **D**: 14/15 and
19/18 for Iγ_v2/3 (354/432 bp), **E**: 16/17 and 19 for Iγ_3/6 (327/249 bp), **F**: 14/15 and 18/17
for Iγ_v3 (343 bp). (**b**) PCR result from the human brain cDNA library.

The PCR products from Figure 50 were extracted, purified and sequenced. The 482-
bp band in A and 354-bp band in D were confirmed to be fragments of Iγ_v2.

Importantly, the 199-bp band in B and 327-bp in E were confirmed to be fragments of
Iγ_v3. This means that the initial 78 bp of human Exon 16c is indeed an exon in its

own right, and in at least certain tissues (*e.g.* the brain) it could be spliced out in the same fashion as the rodent Exon 17. This exon, ligated between Exons 16 and 18, forms the human version of Iγ_v3. In other words, Iγ_i3 was demonstrated to be expressed in the human.

6.3. Detection of PIP5KIγ_v6 in the Human Brain

In Figure 50, the lower, 249-bp band in Lane E corresponded to the molecular weight of the PCR product from Iγ_v6, but the gel extract was not pure enough to be sequenced unambiguously. I therefore repeated this PCR, and sequenced the 249 bp product (Figure 51).
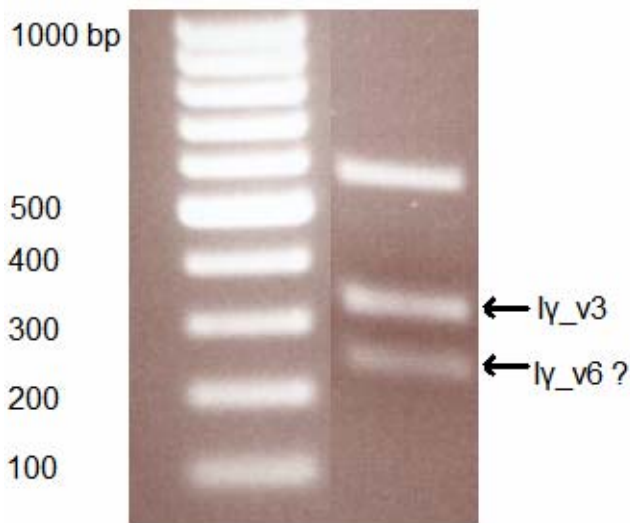
Figure 51 Amplification of Iγ_v3 and Iγ_v6 in the human brain
PCR result from the human brain cDNA library, as in Reaction E of Figure 50. The upper band was not a PIP kinase product. The middle band of 327 bp was confirmed previously to be a Iγ_v3 product. The lower band of 249 bp was sequenced.

151

Somewhat surprisingly, the band in question was in fact not from Iγ_v6, but a product also containing some sequence of Exon 18. Moreover, because the primers used were Exons 16/17 and 19, a product containing Exon 18 in addition should in fact be Iγ_v3, giving the middle band of 327 bp (Figure 51). The lower band corresponded to a product that was 78 bp shorter, which was puzzling at first sight.

A sequencing of these bands revealed that this product was in fact the result of promiscuous binding of the forward primer onto the Iγ_v2 cDNA in the templates. The 3' half of the forward primer did not exactly anneal with the start of Exon 18, but its 5' half was already annealed to the end of Exon 16; despite the mismatch on the 3' end, the PCR reaction was able to proceed, giving the rest of the Exon 18, all the way through to the reverse primer binding site within Exon 19. Since Exons 17 and 18 were of the same size, the product appeared as a Iγ_v6 band on the gel.

Presumably, the concentration of Iγ_v6 was not as high as Iγ_v2 in the brain, and/or its structural conformation was not readily accessible for this particular set of human primers to anneal to. As a result, I needed to find another means of detecting Iγ_v6 unambiguously, in case it was truly present.

Another pair of primers was used for amplifying Iγ_v6 more specifically (that is, even exclusively to Iγ_v3). The forward primer spanned Exons 14/15, whereas the reverse annealed to Exons 19/17 (Figure 52). Only Iγ_v6 should be picked up by these primers as a genuine template, producing a fragment of 349 bp.

a

b
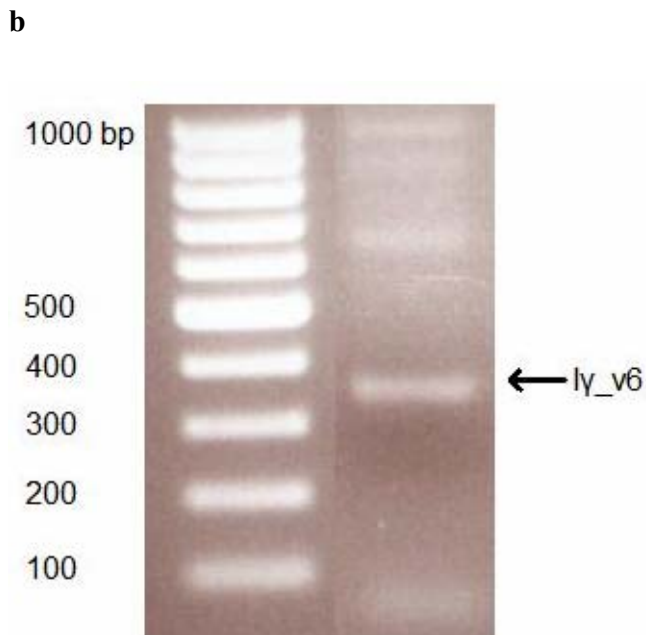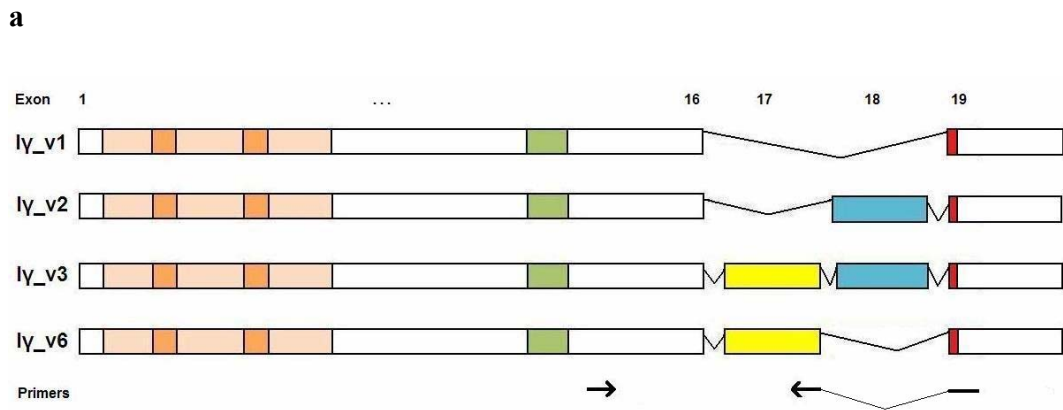
Figure 52 Iγ_v6-specific amplification from the human brain

(**a**) PCR scheme. Primers used were 14/15 and 19/17, for amplifying Iγ_v6 specifically, producing a 349 bp fragment. (**b**) PCR result from the human brain cDNA library.

The 349 bp band from Figure 52b was extracted, and sequencing revealed its identity to be Iγ_v6. The product consisted of the forward primer site in Exon 14, followed by Exons 15, 16, 17 and 19, all the way through to the reverse primer binding site. Iγ_v6 was thus experimentally confirmed to be expressed in humans.

6.4. Expression Profile of PIP5KIγ Spliceoforms in Human Tissues

With the splice variants Iγ_v3 and Iγ_v6 directly demonstrated in humans for the first time and the presence of the equivalent "Exon 17" established, I next sought to reveal the tissue distribution of the different PIP5KIγ spliceoforms in humans, especially Iγ_v3/6 (Figure 53).

a

b
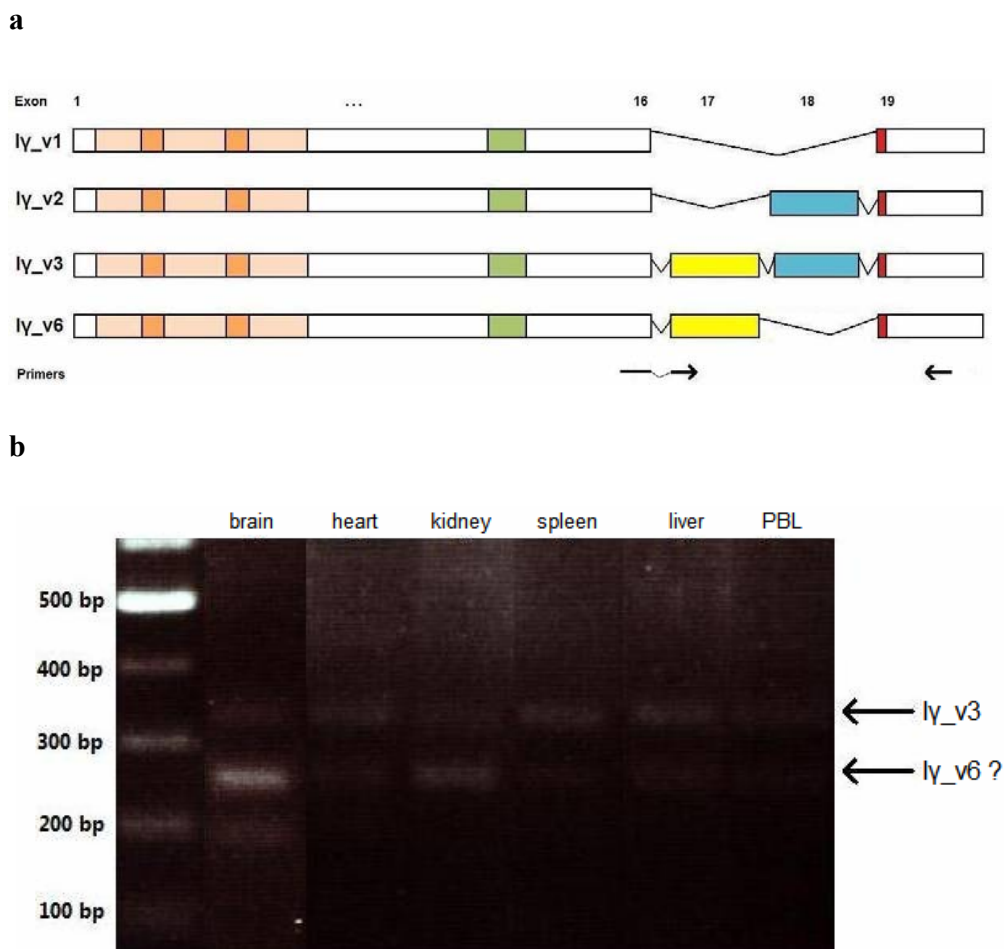
Figure 53 Amplification of Iγ_v3 and Iγ_v6 in human tissues

(**a**) PCR scheme, forward primer spanned Exons 16/17, reverse Exon 19, for the amplification of Iγ_v3 and Iγ_v6 producing bands of 327 and 249 bp, respectively. (**b**) PCR result from the cDNA library of human tissues.

The band sizes corresponded correctly to the scenario of Iγ_v3/6 amplification. Sequencing revealed that the Iγ_v3 bands were genuine, whereas the apparent Iγ_v6 bands were actually, once again, mis-primed PCR products of Iγ_v2. This was exactly the same case as described before for the PCR from the human brain cDNA library (Figure 51), where promiscuous binding of the forward primer to Iγ_v2 masked any potential Iγ_v6 detection.

To overcome this problem, an alternative PCR paradigm was adopted. To match the same reverse primer, a new primer was designed to anneal within Exon 17 itself, therefore preventing any potential PCR elongation in the case of mismatch. Using these primer sets, I expected to see products of both γ_v3 and γ_v6 if they both existed.
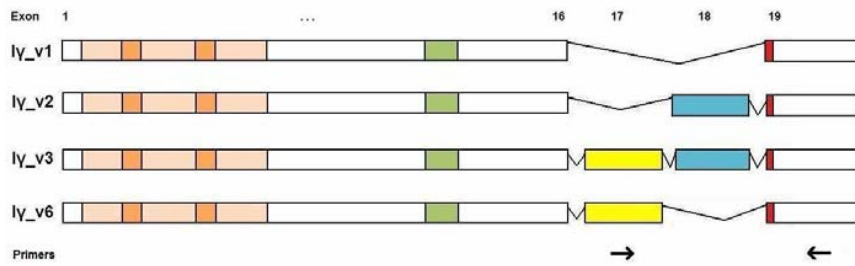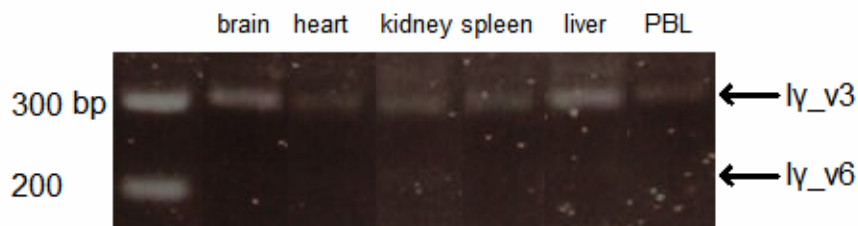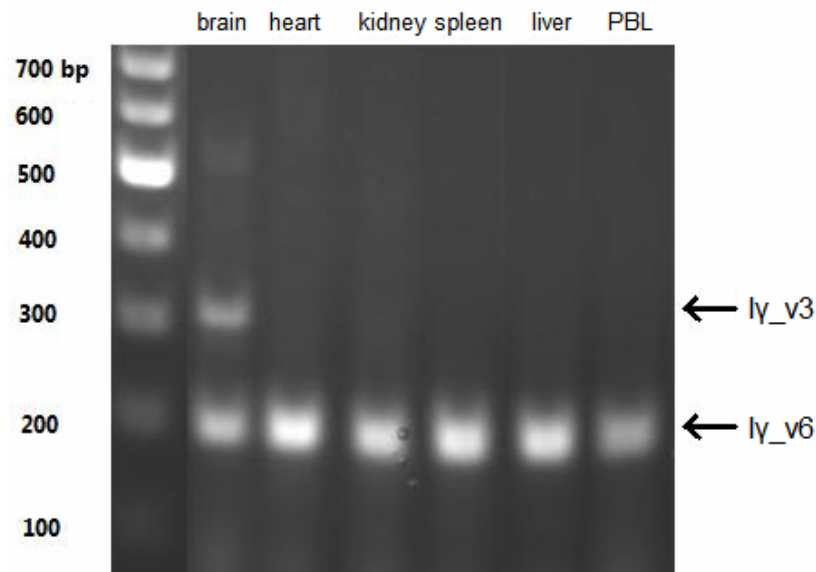
Figure 54 Amplification of Iγ_v3 and Iγ_v6 in human tissues (second trial)
(**a**) PCR scheme. Primers used were 17 and 19, for amplifying both Iγ_v3 and Iγ_v6,
producing 299 and 221 bp fragments, respectively. (**b**) PCR result from the cDNA library of
human tissues. (**c**) PCR result with 10x concentrated primers, which increased the ratio of
Iγ_v6 recognition over Iγ_v3 dramatically.

Though the 221-bp bands were not very strong in intensity (Figure 54b), the shape of the band was discernible enough to be extracted from the gel, at least in the lanes of the brain, heart, kidney and liver. Sequencing result of all these samples confirmed the existence of the Iγ_v6 splice variant in the human.

In trouble-shooting the conditions for using these primers, I discovered that if the primer concentration (of both the forward and reverse primers) was raised to 2 µM each (10x of the 0.2 µM as in the standard protocol, see Methods), the ratio of Iγ_v6 amplification over Iγ_v3 was increased dramatically (Figure 54c), while Iγ_v3 was still expressed most strongly in the brain. Since the forward primer only recognised Exon 17, the 221-bp band could not possibly be produced by mismatching to any template other than γ_v6 itself. This result, confirmed by sequencing, provided further evidence for the widespread existence of γ_v6 in humans.

The change between Figure 54b and c was very interesting, but the comparison between γ_v3 and γ_v6 cannot be quantitatively accurate, and so conclusions about the relative levels of the splice variants much await more detailed studies with quantitative real-time PCR.

In conclusion, I have confirmed the existence of both Iγ_v3 and Iγ_v6 in the human. Not only is this interesting in the light of the co-existence of γ_v4 and γ_v5 in the human (overlapping in their exon sequences with Exon 17), but it also adds to our knowledge base about alternative 5' splice site exons. This is the second most important alternative splicing mechanism to exon-skipping[220], and creates typically subtle changes in mRNA (instead of retention or omission of much longer nucleotide sequences), and these may play decisive roles in development and human diseases (*e.g.* [221]).

This study extends (if not potentially completes) our knowledge of PIP5KIγ spliceoforms that exist in the human, potentially in a spectrum of tissue types and at different developmental stages (Figure 55). The alternative splicing profile as proposed at the start of this chapter is proven to be correct (Figure 49a). Indeed, Iγ_i3/6 and Iγ_i4/5 expression may be differentially regulated under specific

signalling pathways, and the global alternative splicing profile, just like transcription profiles, can reflect the tissue identity in mammalian cells[222].
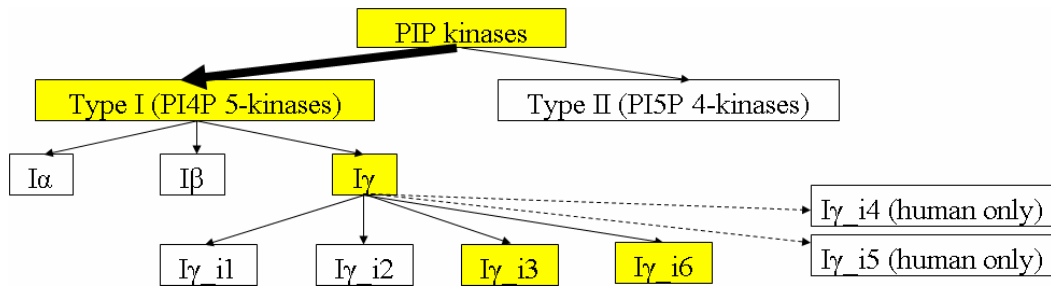
Figure 55 Updated picture of PIP5KIγ splice variants in the human

6.5. *List of Primers Used for Human Templates*

Below is a summary list of primers used in this Chapter, for the amplification of PIP5KIγ from the human (Table 9).

Exon(s)	Sequence
14/15 forward	GACAGGATGGCAG GCCGCAGGAGGAG
16/17 forward	GCCACCGACATCTACTTT TTCACGGATGGGAGGTAC
17 forward	GATTTACTCTCCCCGCCATCGCCGAC
17 reverse	CAGTCGGCGATGGCGGGG
16c reverse	GCTGCGGTCACTTAC AGTCCCCGAG
18/17 reverse	CTCTCATCGGTGGG AGTCCCCGAGGC
19/16 reverse	GGGCTGCATAGAAATTA AAAGTAG
19/17 reverse	GGGCTGCATAGAAATTA AGTCCCCGAGGCGC
	CGGGGGCTGCATAGAAATTA AGTCCC
19/18 reverse	GGGGGCTGCATAGAAATTA TGTGTCG
	GCTGCATAGAAATTA TGTGTCGCTCTCGCCGTCG
19 reverse	CATCCGTGCAGGGGGAGGACGAG
	GGAGCAGAAGTGGAGCTCGGCTCTGG

Table 9 List of primers used for the amplification of PIP5KIγ from the human

The space within sequences illustrates the exon junction.

7. Further Discussions and Remarks

7.1. Discoveries and Conclusions from This Study

In this study, I have to a significant degree reconciled the behavioural differences between Iγ_i2 and Iγ_i3, and attributed part of this to the previously undiscovered V443A mutation in our Iγ_i3 constructs. The Iγ_i3-specific 26-AA insert does not seem to be a simple PIP$_2$-binding or phosphorylation site, as revealed by the 4R and 5P mutants, respectively.

The localisation of Iγ_i3, but not Iγ_i1 or Iγ_i2, is activity-dependent, and independent of PI4P-binding. The lipid kinase activity *per se* of Iγ_i3 is not implicated in the enzyme's localisation and phosphorylation, unlike initially speculated[167, 179]. Rather, the membrane localisation may be autophosphorylation-dependent, and this in turn is both necessary and sufficient for the enzyme to achieve its apparently full phosphorylation pattern *in vivo*, while at the membrane.

Along with Iγ_v3, a novel splice variant has been discovered to exist in both rodents and humans. Their tissue expression profiles have been addressed at the mRNA level, and preliminary data have also been obtained on the Iγ_i6 protein's possible endogenous distribution, both subcellularly and in tissues (*e.g.* the brain). Importantly, the co-existence of both splice variants with Iγ_i4 and Iγ_i5 presents an interesting case of overlapping exons (by alternative 5' splice sites) in humans.

7.2. Useful Experimental Tools Developed During This Study

Several useful tools and methods have been developed that are not only beneficial to this study, but also for future investigations. For example, the activation loop mutants (E410A, T412D, T412A) specifically impair the enzyme's substrate-binding and lipid kinase activity, while leaving the protein kinase activity unaltered, and this is a step forward from the previously used D316K (and K188A) mutants. The PM and E111L

mutants provide a way of directly interferering with the enzyme's subcellular localisation, forcing it on or off the plasma membrane, while leaving other properties largely unchanged. The V443A (as well as the reciprocal A443V) mutation can be used as another tool that subtly decreases (or increases) the enzyme's affinity for the plasma membrane, independently of other regulatory mechanisms, and hence helps to reveal behavioural differences that are otherwise not immediately apparent.

The discovery and cloning of Iγ_i6 is a significant advance. The range of Iγ_i1/2/3/6 expression vectors we now have is a comprehensive toolbox for investigating the functions of the 26-AA peptides, corresponding to either Exon 17 (Iγ_i3/6 insert) or Exon 18 (Iγ_i2 tail). This, perhaps with the help of my 4R and 5P mutants, will likely give new insights into the significance of Iγ's C-terminal variations.

The specifically developed antibody against Iγ_i3's 26-AA insert (E2139) has been optimised and with refinement may become a tool to investigate the subcellular and tissue distribution of endogenous Iγ_i6, as well as its phosphorylation pattern or other association properties using Western blot.

Furthemore, a protocol for co-immunoprecipitating PIP5Ks with Rac has been devised and optimised, which detects the endogenous protein association directly using Western blot for the first time, free of contaminating signals from the antibodies. This may be useful for future studies on PIP5K's membrane dynamics, as well as binding partner identification.

7.3. Potential Future Directions

Here I briefly discuss several potential directions for future experiments, to follow up on the present study. Should time and resources permit, they may provide important insight into the functions and regulatons of PIP5Ks.

7.3.1. Significance of Alternative Splicing

Based on our current picture of Iγ's alternative splicing, we can perceive Iγ_i1/2/3/6 as an elegant 2 x 2 matrix regarding their usage of the C-terminal peptide (Iγ_i4/5 are human-specific and hence not considered here). In other words, the gene can have on its C-terminus (following Exon 16) either no further peptide (Iγ_i1), or the 26-AA from Exon 17 (Iγ_i6), or the 26-AA from Exon 18 (Iγ_i2), or both (Iγ_i3). We now know that both 26-AA peptides may be included independently of the other.

We already know that the C-terminus of Iγ_i2 is implicated in certain functions *e.g.* talin-binding (see Introduction), and that the Iγ_i3-specific 26-AA insert conveys other unique properties *e.g.* possible autophosphorylation-dependency of membrane localisation. In response to different developmental or physiological stimuli, alternative splicing may give rise to functional deiversity at the protein level, in the important signalling and metabolic pathways regulated by PIP5KIγ. Combined with the tissue distribution of these different splice variants, it would be interesting to know whether the alternative splicing profile (*i.e.*, presence or absence of either of the 26-AA peptides) dictates a tissue identity or fate during development, *e.g.* whether the Iγ_i3 insert is physiologically relevant to neuron development. It is therefore also important to understand the functions and regulations of Iγ_i6.

Ultimately, it would be interesting to better characterise the alternative splicing profile of Iγ, and determine whether Iγ_i3, Iγ_i6 and the more ubiquitous spliceoform Iγ_i2 may be expressed in the same neuron *in vivo*, for example by using single-cell PCR.

7.3.2. Back to the Neurons

We have examined and discussed many aspects of PIP5KIγ_i3's behaviour in HEK-293 cells. While HEK-293 is a convenient mammalian expression system that allows easy maintenance and transfection, and provides informative insight into the physiological Iγ_i3 in the nervous system, it is still considerably different from the neurons.

In the near future, the subcellular localisation of Iγ_i3 and its effect on proliferation should be tested on neuronal cultures. Regions in the cerebellum and cerebral cortex, especially the forebrain, have been demonstrated to express Iγ_i3[167]. Existing primary culturing techniques of cerebellar granule cells[167] will be a convenient way of achieving that. We would like to test whether Iγ_i3(V) D316K, a true dominant negative enzyme as opposed to Iγ_i3(A) D316K as reported before[167], also significantly compromises neuronal survival and alters their morphology compared to Iγ_i2(V) D316K. Since Iγ_i3(V) D316K and Iγ_i3(A) D316K have different subcellular localisations, this would address the question whether this detrimental effect of Iγ_i3(A) is due to the 26-AA insert, or the cytosolic distribution which potentially interferes with the cytoskeleton. The PM-tagged Iγ_i3(A) D316K, which is still catalytically inactive but is now membrane-bound, can also help in this context, *e.g.* to address whether the inactive enzyme strips the Rac off the membrane, which might lead to physiological consequences.

Presumably, an inducible overexpression system (such as the tet-on/off system[223, 224] or the Rapalogue-inducible FKBP/FRB dimerisation system[225]) may be helpful. It will be useful to transfect the neurons at the time of plating, but turn on the desired gene expression only when the primary culture has been properly developed into the suitable confluence and neurite connections. This would then eliminate any potential side effects caused by other PIP5KIγ-sensitive factors during development (because of prolonged exposure to the overexpressed transgene), but not Iγ itself in the functional neuron.

7.3.3. Another Hypothesis on the Enzyme's Activity-dependent Localisation

We have seen that the Iγ_i3 localisation is dependent on its activity. Another perhaps remote possibility underlying this would be that a molecule of PIP5KIγ_i3 binds PI4P on the endomembrane in the cytoplasm (*e.g.* Golgi or cytoplasmic vesicles), turns it into PIP_2, and then gets associated with the PM while the PIP_2 product itself becomes

inserted in the PM. This mechanism would also be protein molecule-specific, consistent with previous findings[179]. Of course, from the E410A data we know that the substrate binding does not affect Iγ_i3's steady state localisation, but this may not have been a limiting factor in the above proposed mechanism, which is nevertheless activity-dependent. However, this hypothesis may not be very physiologically feasible, if we agree to the current evidence that most of the substrate PI4P is in fact already in the PM[68], and not just only in the Golgi, as people initially considered.

One way of testing this hypothesis may be to make a tandem construct of two Iγ_i3, one active and one inactive, linked together. The localisation of such a conjugate protein would inform us whether the previously observed cytosolic localisation of inactive Iγ_i3 was because it simply did not have the mechanism to insert into the membrane, or whether it was positively retained in the cytoplasm (as would be explained by the above hypothesis, where inactive enzyme remains bound to uncatalysed PI4P in the cytosol).

7.3.4. Phosphorylation Site Identification

There are many aspects of the *in vivo* phosphorylation pattern that we did not understand. The "overall" phosphorylation is likely to be an ensemble of multiple phosphorylation events, potentially in a cooperative manner. This is complicated by the fact that some phosphorylations may not actually cause a mobility shift in SDS-PAGE, and are hence not detectable using our method. It is not known what sites are involved in the phosphorylation of wild type Iγ_i2 or Iγ_i3, except for the very few residues identified in particular kinase pathways, which when impaired still leave the overall phosphorylation pattern largely unchanged[164]. On that note, it is not clear which kinase pathways converge onto PIP5KIγ to produce the overall phosphorylation under different circumstances, or whether part of the *in vivo* phosphorylation observed is due to autophosphorylation.

A two-dimension gel (based on *e.g.* protein mass, protein complex mass in the native state or isoelectric point) may be able to tease apart the originally inseparable

phosphorylation band, into multiple states arising from modifications at different combinations of residues[226, 227]. Moreover, we may consider the possibility of identifying these sites systematically, for example, by mass spectroscopy or *in vivo* incubation with radioactive ATP followed by Edman sequencing[228-232].

7.3.5. Autophosphorylation or Cross Phosphorylation

The autophosphorylation activity that we have observed is clearly dependent on the enzyme's catalytic ability, as revealed by the D316K (and K188A) mutants. However, a remote possibility to explain the above phenomenon may be that the enzyme is co-immunoprecipitated with another enzyme partner from the mammalian cell lysate, which is activated by the PIP5Ks and then phosphorylates PIP5Ks in return.

This caveat may be overcome by using recombinant proteins made by a bacterial expression vector. However, a negative result from the subsequent autophosphorylation assay does not necessarily validate the above hypothesis. The protein may not have folded properly, acquired the appropriate post-translational modifications or, indeed, pulled down other co-factors that are absent from the bacteria, which do not phosphorylate the PIP5K directly but serve as activators (*e.g.* Rac, as demonstrated in this study).

7.3.6. Structural Model

So far, although some structural features are known for PIP4KIIβ with emphasis on the catalytic and dimerisation mechanism[98], there are no good crystal structure of Type I PIP kinases available. *De novo* prediction is limited in its reliability and accuracy[233]. Even though homology or comparative modelling is possible nowadays through programs such as Swiss-Model, M4T, 3D-JIGSAW and I-TASSER, the homology between Type I and Type II PIP kinases is largely conserved

only over the catalytic core of the enzymes. The C-terminal portion of the protein is unstructured in the published IIβ model, making it meaningless to simulate the C-terminal structure of PIP5KIγ by homology, where the Iγ_i3-specific insert also happens to be.

Ultimately, a good crystal structure of PIP5KIγ (and its different splice variants) would be tremendously helpful, in verifying my "natively disordered domain" hypothesis of the Iγ_i3-specific insert, and elucidating how the enzyme functions are regulated physiologically.

7.3.7. Immobility and Insolubility

In this study, we have tacitly used FRAP as a general indicator of PIP5K's mobility on the plasma membrane, which was helpful as far as providing an empirical method of assessing the differential behaviours of different constructs. Because of the incomplete recovery and possibly multiple PM-binding states of Iγ_i3, its mobility was not easily characterised in terms of diffusion and time constants, but may instead be described by the mobile fraction and half time of recovery as in [205]. A similar method used by Dr Luisa Giudici (unpublished) was Triton X-100 solubility, where Iγ_i3 constructs tended to be more insoluble than their Iγ_i2 counterparts.

We do not yet know exactly what specific factors underly these behaviours, and whether they are attributable to associations with lipid rafts, actin cytoskeleton or other binding partners. Time permitting, a screen of binding partners may be helpful for addressing this question, using *e.g.* electron microscopy, high performance liquid chromatography (HPLC), co-immunoprecipitation or yeast two-hybrid systems.

8. Appendix – Sequence Alignments

```
MELEVPDEAESAEAGAVTAEAAWSAESGAAAGMTQKKAILAEAPLVTGQPGPGHGKKLGH 60
MELEVPDEAESAEAGAVTAEAAWSAESGAAAGMTQKKAGLAEAPLVTGQPGPGHGKKLGH 60
MELEVPDEAESAEAGAVPSEAAWAAESGAAAGLAQKKAAPTEVLSMTAQPGPGHGKKLGH 60
*****************.:****:*********::****   :*.  :*.***********

RGVDASGETTYKKTTSSTLKGAIQLGIGYTVGNLSSKPERDVLMQDFYVVESIFFPSEGS 120
RGVDASGETTYKKTTSSTLKGAIQLGIGYTVGNLSSKPERDVLMQDFYVVESIFFPSEGS 120
RGVDASGETTYKKTTSSTLKGAIQLGIGYTVGHLSSKPERDVLMQDFYVVESIFFPSEGS 120
********************************:***************************

NLTPAHHFQDFRFKTYAPVAFRYFRELFGIRPDDYLYSLCNEPLIELSNPGASGSVFYVT 180
NLTPAHHFQDFRFKTYAPVAFRYFRELFGIRPDDYLYSLCNEPLIELSNPGASGSVFYVT 180
NLTPAHHFQDFRFKTYAPVAFRYFRELFGIRPDDYLYSLCNEPLIELSNPGASGSLFYVT 180
*******************************************************:****

SDDEFIIKTVMHKEAEFLQKLLPGYYMNLNQNPRTLLPKFYGLYCVQSGGKNIRVVVMNN 240
SDDEFIIKTVMHKEAEFLQKLLPGYYMNLNQNPRTLLPKFYGLYCVQSGGKNIRVVVMNN 240
SDDEFIIKTVMHKEAEFLQKLLPGYYMNLNQNPRTLLPKFYGLYCVQSGGKNIRVVVMNN 240
************************************************************

VLPRVVKMHLKFDLKGSTYKRRASKKEKEKSLPTYKDLDFMQDMPEGLLLDSDTFGALVK 300
VLPRVVKMHLKFDLKGSTYKRRASKKEKEKSLPTYKDLDFMQDMPEGLLLDSDTFGALVK 300
ILPRVVKMHLKFDLKGSTYKRRASKKEKEKSFPTYKDLDFMQDMPEGLLLDADTFSALVK 300
:*****************************:*****************:***.****

TLQRDCLVLESFKIMDYSLLLGVHNIDQQERERQAEGAQSKADEKRPVAQKALYSTAMES 360
TLQRDCLVLESFKIMDYSLLLGVHNIDQQERERQAEGAQSKADEKRPVAQKALYSTAMES 360
TLQRDCLVLESFKIMDYSLLLGVHNIDQHERERQAQGAQSTSDEKRPVGQKALYSTAMES 360
****************************:******:****.:******.***********

IQGGAARGEAIETDDTMGGIPAVNGRGERLLLHIGIIDILQSYRFIKKLEHTWKALVHDG 420
IQGGAARGEAIETDDTMGGIPAVNGRGERLLLHIGIIDILQSYRFIKKLEHTWKALVHDG 420
IQGGAARGEAIESDDTMGGIPAVNGRGERLLLHIGIIDILQSYRFIKKLEHTWKALVHDG 420
************:***********************************************

DTVSVHRPSFYAERFFKFMSSTVFRKSSSLKSSPSKKGRG-ALLAVKPLGPTAAFSASQI 479
DTVSVHRPSFYAERFFKFMSSTVFRKSSSLKSSPSKKGRG-ALLAVKPLGPTAAFSASQI 479
DTVSVHRPSFYAERFFKFMSNTVFRKNSSLKSSPSKKGRGGALLAVKPLGPTAAFSASQI 480
********************.*****.************* *******************

PSEREDVQYDLRGARSYPTLEDEGRPDLLPCTPPSFEEATTASIATTLSSTSLSIPERSP 539
PSEREDVQYDLRGARSYPTLEDEGRPDLLPCTPPSFEEATTASIATTLSSTSLSIPERSP 539
PSEREEAQYDLRGARSYPTLEDEGRPDLLPCTPPSFEEATTASIATTLSSTSLSIPERSP 540
*****:.*****************************************************

SDTSEQPRYRRRTQSSGQDGRPQEEL-HAEDLQKITVQVEPVCGVGVVVPKEQGAGVEVP 598
SDTSEQPRYRRRTQSSGQDGRPQEEP-HAEDLQKITVQVEPVCGVG-VVPKEEGAGVEVP 597
SETSEQPRYRRRTQSSGQDGRPQEEPPAEEDLQQITVQVEPACSVEIVVPKEEDAGVEAS 600
*:*********************     ****:*******.*.*   *****:.****..

PSGASAAATVEVDAAS--QASEPASQASDEEDAPSTDIYFFAHGRYWLFSPRRRRLRAVT 656
PCGASAAASVEIDAAS--QASEPASQASDEEDAPSTDIYFFAHGRYWLFSPRRRQLRAVT 655
PAGASAAVEVETASQASDEEGAPASQASDEEDAPATDIYFFTDGRYWIYSPRHRRLRAVT 660
*.*****. **   : :   :  . ************:******:.****::***:*:*****

PSHTGAPTDERSWVYSPLHYSAR--PASDGESDT 688
PNHTGTPTDERSWVYSPLHYSAR--PASDGESDT 687
LSASGTPTDERSWVYSPLHYSAQAPPASDGESDT 694
  .:*:*****************:  *********
```

ClustalW alignment between rat (purple), mouse (orange) and human (green) sequences of PIP5KIγ. ***** represents AA identity and dots AA similarity.

```
----------------MATPGNLGSSVLAS------------------------KTKTKKKHFVAQKVKLFRASDPLLSVLMWGVNHSINELSHVQIPVMLMPDDFKAYS---KIKVD 75
----------MSSNCTSTTAVAVAPLSAS------------------------KTKTKKKHFVCQKVKLFRASEPILSVLMWGVNHTINELSNVPVPVMLMPDDFKAYS---KIKVD 80
----------MASSSVPPATVSAATAGPGP--------------------GFGFASKTKKKHFVQQKVKVFRAADPLVGVFLWGVAHSINELSQVPPPVMLLPDDFKASS---KIKVN 85
--------------------MSSAAENGEAA--------------------PGK---------QNEEKTYKKTASSAIKGAIQLGIGYTVGNLTSKPERDVLMQDFYVVES---VFLPS 67
MELEVPDEAESAEAGAVPSEAAWAAESGAAAGLAQKKAAPTEVLSMTAQPGPGHGKKLGHRGVDASGETTYKKTTSSTLKGAIQLGIGYTVGHLSSKPERDVLMQDFYVVES---IFFPS 117
MASASSGPSSSVGFSSFDPAVPSCTLSSASG-------IKRFMASEVPYASGMPIKKIGHRSVDSSGETTYKKTTSSALKGAIQLGITHTVGSLSTKPERDVLMQDFYVVES---IFFPS 110
----------MAAPSPGPREVLAPSPEAGCR--------------------------AVTSSRRGLLWRLRDKQSRLGLFEISPGHELHGMTCMMQAGLWAATQVSMDHPPTGPPSR 81
                .     . : .:  . ::  ::  ::     :

N-HLFNKENMPSHFKFKEYCPMVFRNLRERFGIDDQDFQNSLTRS-APLPNDSQARSGARFHTSYDKRYIIKTITSEDVAEMHNILKKYHQYIVECHGITLLPQFLGMYRLNVD-GVEIY 192
N-HLFNKENLPSRFKFKEYCPMVFRNLRERFGIDDQDYQNSVTRS-APINSDSQGRCGTRFLTTYDRRFVIKTVSSEDVAEMHNILKKYHQFIVECHGNTLLPQFLGMYRLTVD-GVETY 197
N-HLFHRENLPSHFKFKEYCPQVFRNLRDRFGIDDQDYLVSLTRN-PPSESEG---SDGRFLISYDRTLVIKEVSSEDIADMHSNLSNYHQYIVKCHGNTLLPQFLGMYRVSVD-NEDSY 199
EGSNLTPAHHYPDFRFKTYAPLAFRYFRELFGIKPDDYLYSICSE-PLIELSNPGASGSLFFVTSDDEFIIKTVQHKEAEFLQKLLPGYYMNLNQNP-RTLLPKFYGLYCMQSG-GINIR 184
EGSNLTPAHHFQDFRFKTYAPVAFRYFRELFGIRPDDYLYSLCNE-PLIELSNPGASGSLFYVTSDDEFIIKTVMHKEAEFLQKLLPGYYMNLNQNP-RTLLPKFYGLYCVQSG-GKNIR 234
EGSNLTPAHHYNDFRFKTYAPVAFRYFRELFGIRPDDYLYSLCSE-PLIELCSSGASGSLFYVSSDDEFIIKTVQHKEAEFLQKLLPGYYMNLNQNP-RTLLPKFYGLYCVQAG-GKNIR 227
DDFSEVLTQVHEGFELGTLAGPAFAWLRRSLGLAEEDYQAALGPGGPYLQFLSTSKSKASFFLSHDQRFFLKTQGRREVQALLAHLPRYVQHLQRHP-HSLLARLLGVHSLRVDRGKKTY 200
  :        :     *.:   .  .* :*  :*:  :*:  ::         .   .     *     . ::*    .:    *   *   .    :**.:: *::  . . .

VIVTRNVFSHRLSVYRKYDLKGSTVAREASDK-EKAKELPTLKDNDFINEGQK-IYIDDNNKKVFLEKLKKDVEFLAQLKLMDYSLLVGIHDVERAEQEEVECEENDGEEEGESDGT--- 307
MVVTRNVFSHRLTVHRKYDLKGSTVAREASDK-EKAKDLPTFKDNDFLNEGQK-LHVGEESKKNFLEKLKRDVEFLAQLKIMDYSLLVGIHDVDRAEQEEMEVEERAEDEECENDGVGG- 314
MLVMRNMFSHRLPVHRKYDLKGSLVSREASDK-EKVKELPTLKDMDFLNKNQK-VYIGEEEKKIFLEKLKRDVEFLVQLKIMDYSLLLGIHDIIRGSEPEEEAPVREDESEVDGDCSLTG 317
IVVMNNVLPRSMRMHFTYDLKGSTYKRRASRK-EREKSNPTFKDLDFLQDMHEGLYFDTETYNALMKTLQRDCRVLESFKIMDYSLLLGIHFLDHSLKEKEEETPQNVPDAKRTGMQK-- 301
VVVMMNNILPRVVKMHLKFDLKGSTYKRRASKK-EKEKSFPTYKDLDFMQDMPEGLLLDADTFSALVKTLQRDCLVLESFKIMDYSLLLGVHNIDQHERERQAQGAQSTSDEKRPVGQK-- 351
IVVMNNLLPRSVKMHIKYDLKGSTYKRRASQK-EREKPLPTFKDLDFLQDIPDGLFLDADMYNALCKTLQRDCLVLQSFKIMDYSLLMSIHNIDHAQREPLSSETQYSVDTRRPAPQK-- 344
FIVMQSVFYPAGRISERYDIKGCEVSRWVDPAPEGSPLVLVLKDLNFQGKTIN----LGPQRSWFLRQMELDTTFLRELNVLDYSLLIAFQRLHEDERGPGSS--------------- 299
.:*  ..::   :    :*:**.   *  ..  *        . ** :*  .    :   .:  .:: *   .*  .::::*****:..:  : .  .

-----HPVGTPPDSPGNTLNSSPPLAPGEFDPNIDVYGIKCHENSPRKEVYFMAIIDILTHYDAKKKAAHAAKTVKHGAGAEISTVNPEQYSKRFLDFIGHILT--------------- 406
--NLLCSYGTPPDSPGNLLSFPRFFGPGEFDPSVDVYAMKSHESSPKKEVYFMAIIDILTPYDTKKKAAHAAKTVKHGAGAEISTVNPEQYSKRFNEFMSNILT--------------- 416
PPALVGSYGTSPEGIGGYIHSHRPLGPGEFESFIDVYAIRSAEGAPQKEVYFMGLIDILTQYDAKKKAAHAAKTVKHGAGAEISTVHPEQYAKRFLDFITNIFA--------------- 421
-----VLYSTAMESIQGPGKSG---DGIITENPDTMGGIPAKSHRGELLLLFMGIIDILQSYRLMKKLEHSWKALVYDG-DTVSVHRPSFYADRFLKFMNSRVFKKIQALKASPSKK-RC 411
-----ALYSTAMESIQGGAARG---EAIESD--DTMGGIPAVNGRGERLLLHIGIIDILQSYRFIKKLEHTWKALVHDG-DTVSVHRPSFYAERFFKFMSNTVFRKNSSLKSSPSKKGRG 460
-----ALYSTAMESIQGEARRG---GTMETD--DHMGGIPARNSKGERLLLYIGIIDILQSYRFVFKLEHSWKALVHDG-DTVSVHRPGFYAERFQRFMCNTVFKKIP-LKPSPSKKFRS 452
------LIFRTARSVQGAQSPEESRAQNRRLLPDAPNALHILDGPEQR--YFLGVVDLATVYGLRKRLEHLWKTLRYPG-RTFSTVSPARYARRLCQWVEAHTE--------------- 394
          . . .             .:  .:   .:.::*:    *   *: *  *:: :  .   .*.  *  *: *:  ::

-----------------------------------------------------------------------------------------------------------------------
-----------------------------------------------------------------------------------------------------------------------
-----------------------------------------------------------------------------------------------------------------------
NSIAALK---ATSQEIVSSISQEWKDEKRDLLTEGQSFSSLDEEALGSRHRPDLVPSTPSLFEAAS---LATTISSSSLYVNEHYP--------HDRPTLYSNSKGLP----------- 505
GALLAVKPLGPTAAFSASQIPSEREEAQYDLRG-ARSYPTLEDEG-----RPDLLPCTPPSFEEATTASIATTLSSTSLSIPERSPSETSEQPRYRRRTQSSGQDRGPQEEPPAEEDLQQ 574
GSSSFSRR-AGSSGNSCITYQPSVSGEHKAQVTTKAEVEPGVHLGR------PDVLPQTPPLEEISE----GSPIPDPSFSPLVGET---------LQMLTT--------------- 533
```

```
-----------------------------------------------------------------------------------  PIP4KIIα
-----------------------------------------------------------------------------------  PIP4KIIβ
-----------------------------------------------------------------------------------  PIP4KIIγ
---------SSSTFTLEEGTIYLTAEPN----TLEVQ----------------DDNASVLDVYL------------------------ 540  PIP5KIβ
ITVQVEPACSVEIVVPKEEDAGVEASPAGASAAVEVETASQASDEEGAPASQASDEEDAPATDIYFPTDERSWVYSPLHYSAQAPPASDGESDT 668  PIP5KIγ
---------STTLEKLEVAESEFTH--------------------------------------------------------------- 549  PIP5KIα
-----------------------------------------------------------------------------------  PIP5KL1
```

ClustalW alignment of all human PIP kinase paralogue sequences. From top to bottom in each panel: PIP4KIIα, PIP4KIIβ, PIP4KIIγ, PIP5KIβ, PIP5KIγ, PIP5KIα, PIP5KL1. ***** represents AA identity and dots AA similarity.

9. References

1. Momose, G., *On the Inositol of Brain and its Preparation.* Biochem J, 1916. **10**(1): p. 120-5.
2. Needham, J., *Studies on Inositol: The Synthesis of Inositol in the Animal Body.* Biochem J, 1924. **18**(5): p. 891-904.
3. Streb, H., R.F. Irvine, M.J. Berridge, and I. Schulz, *Release of Ca2+ from a nonmitochondrial intracellular store in pancreatic acinar cells by inositol-1,4,5-trisphosphate.* Nature, 1983. **306**(5938): p. 67-9.
4. Agranoff, B.W., *Cyclitol confusion.* Trends Biochem Sci, 1978. **3**: p. N283-5.
5. Irvine, R.F., *Inositide evolution - towards turtle domination?* J Physiol, 2005. **566**(Pt 2): p. 295-300.
6. Berridge, M.J. and R.F. Irvine, *Inositol trisphosphate, a novel second messenger in cellular signal transduction.* Nature, 1984. **312**(5992): p. 315-21.
7. Nishizuka, Y., *Turnover of inositol phospholipids and signal transduction.* Science, 1984. **225**(4668): p. 1365-70.
8. Wymann, M.P. and L. Pirola, *Structure and function of phosphoinositide 3-kinases.* Biochim Biophys Acta, 1998. **1436**(1-2): p. 127-50.
9. Janmey, P.A., W. Xian, and L.A. Flanagan, *Controlling cytoskeleton structure by phosphoinositide-protein interactions: phosphoinositide binding protein domains and effects of lipid packing.* Chem Phys Lipids, 1999. **101**(1): p. 93-107.
10. Itoh, T. and T. Takenawa, *Phosphoinositide-binding domains: Functional units for temporal and spatial regulation of intracellular signalling.* Cell Signal, 2002. **14**(9): p. 733-43.
11. Powner, D.J., R.M. Payne, T.R. Pettitt, M.L. Giudici, R.F. Irvine, and M.J. Wakelam, *Phospholipase D2 stimulates integrin-mediated adhesion via phosphatidylinositol 4-phosphate 5-kinase Igamma b.* J Cell Sci, 2005. **118**(Pt 13): p. 2975-86.
12. Di Paolo, G. and P. De Camilli, *Phosphoinositides in cell regulation and membrane dynamics.* Nature, 2006. **443**(7112): p. 651-7.
13. Kanaho, Y., K. Nakayama, M.A. Frohman, and T. Yokozeki, *Regulation of phosphatidylinositol 4-phosphate 5-kinase activity by partner proteins.* Methods Enzymol, 2007. **434**: p. 155-69.
14. Lassing, I. and U. Lindberg, *Specific interaction between phosphatidylinositol 4,5-bisphosphate and profilactin.* Nature, 1985. **314**(6010): p. 472-4.
15. Janmey, P.A. and T.P. Stossel, *Modulation of gelsolin function by phosphatidylinositol 4,5-bisphosphate.* Nature, 1987. **325**(6102): p. 362-4.
16. Rozelle, A.L., L.M. Machesky, M. Yamamoto, M.H. Driessens, R.H. Insall, M.G. Roth, K. Luby-Phelps, G. Marriott, A. Hall, and H.L. Yin, *Phosphatidylinositol 4,5-bisphosphate induces actin-based movement of raft-enriched vesicles through WASP-Arp2/3.* Curr Biol, 2000. **10**(6): p. 311-20.
17. Gilmore, A.P. and K. Burridge, *Regulation of vinculin binding to talin and actin by phosphatidyl-inositol-4-5-bisphosphate.* Nature, 1996. **381**(6582): p. 531-5.

18. van Rheenen, J. and K. Jalink, *Agonist-induced PIP(2) hydrolysis inhibits cortical actin dynamics: regulation at a global but not at a micrometer scale.* Mol Biol Cell, 2002. **13**(9): p. 3257-67.

19. Hilgemann, D.W. and R. Ball, *Regulation of cardiac Na+,Ca2+ exchange and KATP potassium channels by PIP2.* Science, 1996. **273**(5277): p. 956-9.

20. Liscovitch, M., V. Chalifa, P. Pertile, C.S. Chen, and L.C. Cantley, *Novel function of phosphatidylinositol 4,5-bisphosphate as a cofactor for brain membrane phospholipase D.* J Biol Chem, 1994. **269**(34): p. 21403-6.

21. Itoh, T., S. Koshiba, T. Kigawa, A. Kikuchi, S. Yokoyama, and T. Takenawa, *Role of the ENTH domain in phosphatidylinositol-4,5-bisphosphate binding and endocytosis.* Science, 2001. **291**(5506): p. 1047-51.

22. Ford, M.G., B.M. Pearse, M.K. Higgins, Y. Vallis, D.J. Owen, A. Gibson, C.R. Hopkins, P.R. Evans, and H.T. McMahon, *Simultaneous binding of PtdIns(4,5)P2 and clathrin by AP180 in the nucleation of clathrin lattices on membranes.* Science, 2001. **291**(5506): p. 1051-5.

23. Tucker, W.C., J.M. Edwardson, J. Bai, H.J. Kim, T.F. Martin, and E.R. Chapman, *Identification of synaptotagmin effectors via acute inhibition of secretion from cracked PC12 cells.* J Cell Biol, 2003. **162**(2): p. 199-209.

24. Raucher, D., T. Stauffer, W. Chen, K. Shen, S. Guo, J.D. York, M.P. Sheetz, and T. Meyer, *Phosphatidylinositol 4,5-bisphosphate functions as a second messenger that regulates cytoskeleton-plasma membrane adhesion.* Cell, 2000. **100**(2): p. 221-8.

25. Lemmon, M.A., *Membrane recognition by phospholipid-binding domains.* Nat Rev Mol Cell Biol, 2008. **9**(2): p. 99-111.

26. Jones, D.R., M.A. Sanjuan, and I. Merida, *Type Ialpha phosphatidylinositol 4-phosphate 5-kinase is a putative target for increased intracellular phosphatidic acid.* FEBS Lett, 2000. **476**(3): p. 160-5.

27. Anderson, R.A., I.V. Boronenkov, S.D. Doughman, J. Kunz, and J.C. Loijens, *Phosphatidylinositol phosphate kinases, a multifaceted family of signaling enzymes.* J Biol Chem, 1999. **274**(15): p. 9907-10.

28. Singer, S.J. and G.L. Nicolson, *The fluid mosaic model of the structure of cell membranes.* Science, 1972. **175**(23): p. 720-31.

29. Stier, A. and E. Sackmann, *Spin labels as enzyme substrates. Heterogeneous lipid distribution in liver microsomal membranes.* Biochim Biophys Acta, 1973. **311**(3): p. 400-8.

30. Hui, S.W. and D.F. Parsons, *Direct observation of domains in wet lipid bilayers.* Science, 1975. **190**(4212): p. 383-4.

31. Rothman, J.E. and J. Lenard, *Membrane asymmetry.* Science, 1977. **195**(4280): p. 743-53.

32. Simons, K. and D. Toomre, *Lipid rafts and signal transduction.* Nat Rev Mol Cell Biol, 2000. **1**(1): p. 31-9.

33. Brown, D.A. and E. London, *Structure and function of sphingolipid- and cholesterol-rich membrane rafts.* J Biol Chem, 2000. **275**(23): p. 17221-4.

34. Waugh, M.G., S. Minogue, D. Chotai, F. Berditchevski, and J.J. Hsuan, *Lipid and peptide control of phosphatidylinositol 4-kinase IIalpha activity on Golgi-endosomal Rafts.* J Biol Chem, 2006. **281**(7): p. 3757-63.

35. Minogue, S., K.M. Chu, E.J. Westover, D.F. Covey, J.J. Hsuan, and M.G. Waugh, *Relationship between phosphatidylinositol 4-phosphate synthesis,*

membrane organization, and lateral diffusion of PI4KIIalpha at the trans-Golgi network. J Lipid Res, 2010. **51**(8): p. 2314-24.

36. Waugh, M.G., S. Minogue, J.S. Anderson, M. dos Santos, and J.J. Hsuan, *Signalling and non-caveolar rafts.* Biochem Soc Trans, 2001. **29**(Pt 4): p. 509-11.

37. Waugh, M.G. and J.J. Hsuan, *Preparation of membrane rafts.* Methods Mol Biol, 2009. **462**: p. 403-14.

38. Gylfason, G.A., E. Knutsdottir, and B. Asgeirsson, *Isolation and biochemical characterisation of lipid rafts from Atlantic cod (Gadus morhua) intestinal enterocytes.* Comp Biochem Physiol B Biochem Mol Biol, 2009. **155**(1): p. 86-95.

39. Waugh, M.G., K.M. Chu, E.L. Clayton, S. Minogue, and J.J. Hsuan, *Detergent-free isolation and characterization of cholesterol-rich membrane domains from trans-Golgi network vesicles.* J Lipid Res, 2010. **52**(3): p. 582-9.

40. Cayrol, R., A.S. Haqqani, I. Ifergan, A. Dodelet-Devillers, and A. Prat, *Isolation of human brain endothelial cells and characterization of lipid raft-associated proteins by mass spectroscopy.* Methods Mol Biol, 2011. **686**: p. 275-95.

41. Mihailescu, M., R.G. Vaswani, E. Jardon-Valadez, F. Castro-Roman, J.A. Freites, D.L. Worcester, A.R. Chamberlin, D.J. Tobias, and S.H. White, *Acyl-chain methyl distributions of liquid-ordered and -disordered membranes.* Biophys J, 2011. **100**(6): p. 1455-62.

42. Rao, W., R.E. Isaac, and J.N. Keen, *An analysis of the Caenorhabditis elegans lipid raft proteome using geLC-MS/MS.* J Proteomics, 2011. **74**(2): p. 242-53.

43. Anderson, R.G. and K. Jacobson, *A role for lipid shells in targeting proteins to caveolae, rafts, and other lipid domains.* Science, 2002. **296**(5574): p. 1821-5.

44. Kenworthy, A., *Peering inside lipid rafts and caveolae.* Trends Biochem Sci, 2002. **27**(9): p. 435-7.

45. Munro, S., *Lipid rafts: elusive or illusive?* Cell, 2003. **115**(4): p. 377-88.

46. Morone, N., C. Nakada, Y. Umemura, J. Usukura, and A. Kusumi, *Three-dimensional molecular architecture of the plasma-membrane-associated cytoskeleton as reconstructed by freeze-etch electron tomography.* Methods Cell Biol, 2008. **88**: p. 207-36.

47. Hammond, G.R., Y. Sim, L. Lagnado, and R.F. Irvine, *Reversible binding and rapid diffusion of proteins in complex with inositol lipids serves to coordinate free movement with spatial information.* J Cell Biol, 2009. **184**(2): p. 297-308.

48. McLaughlin, S., J. Wang, A. Gambhir, and D. Murray, *PIP(2) and proteins: interactions, organization, and information flow.* Annu Rev Biophys Biomol Struct, 2002. **31**: p. 151-75.

49. Dietrich, U., P. Kruger, and J.A. Kas, *Structural investigation on the absorption of the MARCKS peptide on anionic lipid monolayers - effects beyond electrostatic.* Chem Phys Lipids, 2011.

50. Arbuzova, A., L. Wang, J. Wang, G. Hangyas-Mihalyne, D. Murray, B. Honig, and S. McLaughlin, *Membrane binding of peptides containing both basic and aromatic residues. Experimental studies with peptides corresponding to the scaffolding region of caveolin and the effector region of MARCKS.* Biochemistry, 2000. **39**(33): p. 10330-9.

51. Golebiewska, U., M. Nyako, W. Woturski, I. Zaitseva, and S. McLaughlin, *Diffusion coefficient of fluorescent phosphatidylinositol 4,5-bisphosphate in the plasma membrane of cells.* Mol Biol Cell, 2008. **19**(4): p. 1663-9.

52. Swierczynski, S.L. and P.J. Blackshear, *Membrane association of the myristoylated alanine-rich C kinase substrate (MARCKS) protein. Mutational analysis provides evidence for complex interactions.* J Biol Chem, 1995. **270**(22): p. 13436-45.

53. McLaughlin, S. and D. Murray, *Plasma membrane phosphoinositide organization by protein electrostatics.* Nature, 2005. **438**(7068): p. 605-11.

54. Tall, E.G., I. Spector, S.N. Pentyala, I. Bitter, and M.J. Rebecchi, *Dynamics of phosphatidylinositol 4,5-bisphosphate in actin-rich structures.* Curr Biol, 2000. **10**(12): p. 743-6.

55. Stauffer, T.P., S. Ahn, and T. Meyer, *Receptor-induced transient reduction in plasma membrane PtdIns(4,5)P2 concentration monitored in living cells.* Curr Biol, 1998. **8**(6): p. 343-6.

56. Varnai, P. and T. Balla, *Visualization of phosphoinositides that bind pleckstrin homology domains: calcium- and agonist-induced dynamic changes and relationship to myo-[3H]inositol-labeled phosphoinositide pools.* J Cell Biol, 1998. **143**(2): p. 501-10.

57. Laux, T., K. Fukami, M. Thelen, T. Golub, D. Frey, and P. Caroni, *GAP43, MARCKS, and CAP23 modulate PI(4,5)P(2) at plasmalemmal rafts, and regulate cell cortex actin dynamics through a common mechanism.* J Cell Biol, 2000. **149**(7): p. 1455-72.

58. Watt, S.A., G. Kular, I.N. Fleming, C.P. Downes, and J.M. Lucocq, *Subcellular localization of phosphatidylinositol 4,5-bisphosphate using the pleckstrin homology domain of phospholipase C delta1.* Biochem J, 2002. **363**(Pt 3): p. 657-66.

59. Parmryd, I., J. Adler, R. Patel, and A.I. Magee, *Imaging metabolism of phosphatidylinositol 4,5-bisphosphate in T-cell GM1-enriched domains containing Ras proteins.* Exp Cell Res, 2003. **285**(1): p. 27-38.

60. Pike, L.J. and L. Casey, *Localization and turnover of phosphatidylinositol 4,5-bisphosphate in caveolin-enriched membrane domains.* J Biol Chem, 1996. **271**(43): p. 26453-6.

61. Levine, T.P. and S. Munro, *The pleckstrin homology domain of oxysterol-binding protein recognises a determinant specific to Golgi membranes.* Curr Biol, 1998. **8**(13): p. 729-39.

62. Godi, A., P. Pertile, R. Meyers, P. Marra, G. Di Tullio, C. Iurisci, A. Luini, D. Corda, and M.A. De Matteis, *ARF mediates recruitment of PtdIns-4-OH kinase-beta and stimulates synthesis of PtdIns(4,5)P2 on the Golgi complex.* Nat Cell Biol, 1999. **1**(5): p. 280-7.

63. Jones, D.H., J.B. Morris, C.P. Morgan, H. Kondo, R.F. Irvine, and S. Cockcroft, *Type I phosphatidylinositol 4-phosphate 5-kinase directly interacts with ADP-ribosylation factor 1 and is responsible for phosphatidylinositol 4,5-bisphosphate synthesis in the golgi compartment.* J Biol Chem, 2000. **275**(18): p. 13962-6.

64. Helms, J.B., K.J. de Vries, and K.W. Wirtz, *Synthesis of phosphatidylinositol 4,5-bisphosphate in the endoplasmic reticulum of Chinese hamster ovary cells.* J Biol Chem, 1991. **266**(32): p. 21368-74.

65. Osborne, S.L., C.L. Thomas, S. Gschmeissner, and G. Schiavo, *Nuclear PtdIns(4,5)P2 assembles in a mitotically regulated particle involved in pre-mRNA splicing.* J Cell Sci, 2001. **114**(Pt 13): p. 2501-11.

66. Cockcroft, S. and M.A. De Matteis, *Inositol lipids as spatial regulators of membrane traffic.* J Membr Biol, 2001. **180**(3): p. 187-94.

67. Sasaki, T., J. Sasaki, Y. Kaneyasu, and S. Suzuki, *[Compartmentalization of phosphatidylinositol 4, 5-bisphosphate].* Rinsho Byori, 2006. **54**(1): p. 45-50.

68. Hammond, G.R., G. Schiavo, and R.F. Irvine, *Immunocytochemical techniques reveal multiple, distinct cellular pools of PtdIns4P and PtdIns(4,5)P(2).* Biochem J, 2009. **422**(1): p. 23-35.

69. Kwiatkowska, K., *One lipid, multiple functions: how various pools of PI(4,5)P(2) are created in the plasma membrane.* Cell Mol Life Sci, 2010. **67**(23): p. 3927-46.

70. De Matteis, M.A. and G. D'Angelo, *The role of the phosphoinositides at the Golgi complex.* Biochem Soc Symp, 2007(74): p. 107-16.

71. Roy, A. and T.P. Levine, *Multiple pools of phosphatidylinositol 4-phosphate detected using the pleckstrin homology domain of Osh2p.* J Biol Chem, 2004. **279**(43): p. 44683-9.

72. Balla, A., G. Tuymetova, A. Tsiomenko, P. Varnai, and T. Balla, *A plasma membrane pool of phosphatidylinositol 4-phosphate is generated by phosphatidylinositol 4-kinase type-III alpha: studies with the PH domains of the oxysterol binding protein and FAPP1.* Mol Biol Cell, 2005. **16**(3): p. 1282-95.

73. Balla, A., Y.J. Kim, P. Varnai, Z. Szentpetery, Z. Knight, K.M. Shokat, and T. Balla, *Maintenance of hormone-sensitive phosphoinositide pools in the plasma membrane requires phosphatidylinositol 4-kinase IIIalpha.* Mol Biol Cell, 2008. **19**(2): p. 711-21.

74. Wang, Y.J., J. Wang, H.Q. Sun, M. Martinez, Y.X. Sun, E. Macia, T. Kirchhausen, J.P. Albanesi, M.G. Roth, and H.L. Yin, *Phosphatidylinositol 4 phosphate regulates targeting of clathrin adaptor AP-1 complexes to the Golgi.* Cell, 2003. **114**(3): p. 299-310.

75. Wei, Y.J., H.Q. Sun, M. Yamamoto, P. Wlodarski, K. Kunii, M. Martinez, B. Barylko, J.P. Albanesi, and H.L. Yin, *Type II phosphatidylinositol 4-kinase beta is a cytosolic and peripheral membrane protein that is recruited to the plasma membrane and activated by Rac-GTP.* J Biol Chem, 2002. **277**(48): p. 46586-93.

76. Stefan, C.J., A.G. Manford, D. Baird, J. Yamada-Hanff, Y. Mao, and S.D. Emr, *Osh proteins regulate phosphoinositide metabolism at ER-plasma membrane contact sites.* Cell, 2011. **144**(3): p. 389-401.

77. Thompson, G.A., Jr., *Special roles of inositol lipids in cell signaling and metabolic regulation.* Prog Lipid Res, 1994. **33**(1-2): p. 129-35.

78. Martin, T.F., *Phosphoinositides as spatial regulators of membrane traffic.* Curr Opin Neurobiol, 1997. **7**(3): p. 331-8.

79. Rameh, L.E., A. Arvidsson, K.L. Carraway, 3rd, A.D. Couvillon, G. Rathbun, A. Crompton, B. VanRenterghem, M.P. Czech, K.S. Ravichandran, S.J. Burakoff, D.S. Wang, C.S. Chen, and L.C. Cantley, *A comparative analysis of the phosphoinositide binding specificity of pleckstrin homology domains.* J Biol Chem, 1997. **272**(35): p. 22059-66.

80. Kavran, J.M., D.E. Klein, A. Lee, M. Falasca, S.J. Isakoff, E.Y. Skolnik, and M.A. Lemmon, *Specificity and promiscuity in phosphoinositide binding by pleckstrin homology domains.* J Biol Chem, 1998. **273**(46): p. 30497-508.

81. Lemmon, M.A. and K.M. Ferguson, *Signal-dependent membrane targeting by pleckstrin homology (PH) domains.* Biochem J, 2000. **350 Pt 1**: p. 1-18.

82. Lemmon, M.A., K.M. Ferguson, R. O'Brien, P.B. Sigler, and J. Schlessinger, *Specific and high-affinity binding of inositol phosphates to an isolated pleckstrin homology domain.* Proc Natl Acad Sci U S A, 1995. **92**(23): p. 10472-6.

83. Hirose, K., S. Kadowaki, M. Tanabe, H. Takeshima, and M. Iino, *Spatiotemporal dynamics of inositol 1,4,5-trisphosphate that underlies complex Ca2+ mobilization patterns.* Science, 1999. **284**(5419): p. 1527-30.

84. Fukuda, M., J. Aruga, M. Niinobe, S. Aimoto, and K. Mikoshiba, *Inositol-1,3,4,5-tetrakisphosphate binding to C2B domain of IP4BP/synaptotagmin II.* J Biol Chem, 1994. **269**(46): p. 29206-11.

85. Cullen, P.J., J.J. Hsuan, O. Truong, A.J. Letcher, T.R. Jackson, A.P. Dawson, and R.F. Irvine, *Identification of a specific Ins(1,3,4,5)P4-binding protein as a member of the GAP1 family.* Nature, 1995. **376**(6540): p. 527-30.

86. Quinn, K.V., P. Behe, and A. Tinker, *Monitoring changes in membrane phosphatidylinositol 4,5-bisphosphate in living cells using a domain from the transcription factor tubby.* J Physiol, 2008. **586**(Pt 12): p. 2855-71.

87. Arbuzova, A., K. Martushova, G. Hangyas-Mihalyne, A.J. Morris, S. Ozaki, G.D. Prestwich, and S. McLaughlin, *Fluorescently labeled neomycin as a probe of phosphatidylinositol-4, 5-bisphosphate in membranes.* Biochim Biophys Acta, 2000. **1464**(1): p. 35-48.

88. Hammond, G.R., S.K. Dove, A. Nicol, J.A. Pinxteren, D. Zicha, and G. Schiavo, *Elimination of plasma membrane phosphatidylinositol (4,5)-bisphosphate is required for exocytosis from mast cells.* J Cell Sci, 2006. **119**(Pt 10): p. 2084-94.

89. Balla, T., T. Bondeva, and P. Varnai, *How accurately can we image inositol lipids in living cells?* Trends Pharmacol Sci, 2000. **21**(7): p. 238-41.

90. Szymanska, E., A. Sobota, E. Czurylo, and K. Kwiatkowska, *Expression of PI(4,5)P2-binding proteins lowers the PI(4,5)P2level and inhibits FcgammaRIIA-mediated cell spreading and phagocytosis.* Eur J Immunol, 2008. **38**(1): p. 260-72.

91. Levine, T.P. and S. Munro, *Targeting of Golgi-specific pleckstrin homology domains involves both PtdIns 4-kinase-dependent and -independent components.* Curr Biol, 2002. **12**(9): p. 695-704.

92. Godi, A., A. Di Campli, A. Konstantakopoulos, G. Di Tullio, D.R. Alessi, G.S. Kular, T. Daniele, P. Marra, J.M. Lucocq, and M.A. De Matteis, *FAPPs control Golgi-to-cell-surface membrane traffic by binding to ARF and PtdIns(4)P.* Nat Cell Biol, 2004. **6**(5): p. 393-404.

93. Bazenet, C.E., A.R. Ruano, J.L. Brockman, and R.A. Anderson, *The human erythrocyte contains two forms of phosphatidylinositol-4-phosphate 5-kinase which are differentially active toward membranes.* J Biol Chem, 1990. **265**(29): p. 18012-22.

94.   Loijens, J.C. and R.A. Anderson, *Type I phosphatidylinositol-4-phosphate 5-kinases are distinct members of this novel lipid kinase family.* J Biol Chem, 1996. **271**(51): p. 32937-43.

95.   Rameh, L.E., K.F. Tolias, B.C. Duckworth, and L.C. Cantley, *A new pathway for synthesis of phosphatidylinositol-4,5-bisphosphate.* Nature, 1997. **390**(6656): p. 192-6.

96.   Zhang, X., J.C. Loijens, I.V. Boronenkov, G.J. Parker, F.A. Norris, J. Chen, O. Thum, G.D. Prestwich, P.W. Majerus, and R.A. Anderson, *Phosphatidylinositol-4-phosphate 5-kinase isozymes catalyze the synthesis of 3-phosphate-containing phosphatidylinositol signaling molecules.* J Biol Chem, 1997. **272**(28): p. 17756-61.

97.   Halstead, J.R., M. Roefs, C.D. Ellson, S. D'Andrea, C. Chen, C.S. D'Santos, and N. Divecha, *A novel pathway of cellular phosphatidylinositol(3,4,5)-trisphosphate synthesis is regulated by oxidative stress.* Curr Biol, 2001. **11**(6): p. 386-95.

98.   Rao, V.D., S. Misra, I.V. Boronenkov, R.A. Anderson, and J.H. Hurley, *Structure of type IIbeta phosphatidylinositol phosphate kinase: a protein kinase fold flattened for interfacial phosphorylation.* Cell, 1998. **94**(6): p. 829-39.

99.   Boronenkov, I.V. and R.A. Anderson, *The sequence of phosphatidylinositol-4-phosphate 5-kinase defines a novel family of lipid kinases.* J Biol Chem, 1995. **270**(7): p. 2881-4.

100.   Grishin, N.V., *Phosphatidylinositol phosphate kinase: a link between protein kinase and glutathione synthase folds.* J Mol Biol, 1999. **291**(2): p. 239-47.

101.   Galiano, F.J., E.T. Ulug, and J.N. Davis, *Overexpression of murine phosphatidylinositol 4-phosphate 5-kinase type Ibeta disrupts a phosphatidylinositol 4,5 bisphosphate regulated endosomal pathway.* J Cell Biochem, 2002. **85**(1): p. 131-45.

102.   Stephens, L.R., K.T. Hughes, and R.F. Irvine, *Pathway of phosphatidylinositol(3,4,5)-trisphosphate synthesis in activated neutrophils.* Nature, 1991. **351**(6321): p. 33-9.

103.   Morris, J.B., K.A. Hinchliffe, A. Ciruela, A.J. Letcher, and R.F. Irvine, *Thrombin stimulation of platelets causes an increase in phosphatidylinositol 5-phosphate revealed by mass assay.* FEBS Lett, 2000. **475**(1): p. 57-60.

104.   Clarke, J.H., A.J. Letcher, S. D'Santos C, J.R. Halstead, R.F. Irvine, and N. Divecha, *Inositol lipids are regulated during cell cycle progression in the nuclei of murine erythroleukaemia cells.* Biochem J, 2001. **357**(Pt 3): p. 905-10.

105.   Hinchliffe, K.A., M.L. Giudici, A.J. Letcher, and R.F. Irvine, *Type IIalpha phosphatidylinositol phosphate kinase associates with the plasma membrane via interaction with type I isoforms.* Biochem J, 2002. **363**(Pt 3): p. 563-70.

106.   Payrastre, B., M. Nievers, J. Boonstra, M. Breton, A.J. Verkleij, and P.M. Van Bergen en Henegouwen, *A differential location of phosphoinositide kinases, diacylglycerol kinase, and phospholipase C in the nuclear matrix.* J Biol Chem, 1992. **267**(8): p. 5078-84.

107.   Shibasaki, Y., H. Ishihara, N. Kizuki, T. Asano, Y. Oka, and Y. Yazaki, *Massive actin polymerization induced by phosphatidylinositol-4-phosphate 5-kinase in vivo.* J Biol Chem, 1997. **272**(12): p. 7578-81.

108. Ishihara, H., Y. Shibasaki, N. Kizuki, T. Wada, Y. Yazaki, T. Asano, and Y. Oka, *Type I phosphatidylinositol-4-phosphate 5-kinases. Cloning of the third isoform and deletion/substitution analysis of members of this novel lipid kinase family.* J Biol Chem, 1998. **273**(15): p. 8741-8.

109. Ciruela, A., K.A. Hinchliffe, N. Divecha, and R.F. Irvine, *Nuclear targeting of the beta isoform of type II phosphatidylinositol phosphate kinase (phosphatidylinositol 5-phosphate 4-kinase) by its alpha-helix 7.* Biochem J, 2000. **346 Pt 3**: p. 587-91.

110. Wang, M., N.J. Bond, A.J. Letcher, J.P. Richardson, K.S. Lilley, R.F. Irvine, and J.H. Clarke, *Genomic tagging reveals a random association of endogenous PtdIns5P 4-kinases IIalpha and IIbeta and a partial nuclear localization of the IIalpha isoform.* Biochem J, 2010. **430**(2): p. 215-21.

111. Clarke, J.H., P.C. Emson, and R.F. Irvine, *Localization of phosphatidylinositol phosphate kinase IIgamma in kidney to a membrane trafficking compartment within specialized cells of the nephron.* Am J Physiol Renal Physiol, 2008. **295**(5): p. F1422-30.

112. Botelho, R.J., M. Teruel, R. Dierckman, R. Anderson, A. Wells, J.D. York, T. Meyer, and S. Grinstein, *Localized biphasic changes in phosphatidylinositol-4,5-bisphosphate at sites of phagocytosis.* J Cell Biol, 2000. **151**(7): p. 1353-68.

113. Fairn, G.D., K. Ogata, R.J. Botelho, P.D. Stahl, R.A. Anderson, P. De Camilli, T. Meyer, S. Wodak, and S. Grinstein, *An electrostatic switch displaces phosphatidylinositol phosphate kinases from the membrane during phagocytosis.* J Cell Biol, 2009. **187**(5): p. 701-14.

114. Buser, C.A., C.T. Sigal, M.D. Resh, and S. McLaughlin, *Membrane binding of myristylated peptides corresponding to the NH2 terminus of Src.* Biochemistry, 1994. **33**(44): p. 13093-101.

115. Berg, H.C. and E.M. Purcell, *Physics of chemoreception.* Biophys J, 1977. **20**(2): p. 193-219.

116. Lagerholm, B.C. and N.L. Thompson, *Theory for ligand rebinding at cell membrane surfaces.* Biophys J, 1998. **74**(3): p. 1215-28.

117. Kholodenko, B.N., J.B. Hoek, and H.V. Westerhoff, *Why cytoplasmic signalling proteins should be recruited to cell membranes.* Trends Cell Biol, 2000. **10**(5): p. 173-8.

118. Adam, G. and M. Delbruck, *Reduction of dimensionality in biological diffusion processes.* Structural Chemistry and Molecular Biology, 1968: p. 198-25.

119. Willars, G.B., S.R. Nahorski, and R.A. Challiss, *Differential regulation of muscarinic acetylcholine receptor-sensitive polyphosphoinositide pools and consequences for signaling in human neuroblastoma cells.* J Biol Chem, 1998. **273**(9): p. 5037-46.

120. Grondin, P., M. Plantavid, C. Sultan, M. Breton, G. Mauco, and H. Chap, *Interaction of pp60c-src, phospholipase C, inositol-lipid, and diacyglycerol kinases with the cytoskeletons of thrombin-stimulated platelets.* J Biol Chem, 1991. **266**(24): p. 15705-9.

121. Schmidt, M., C. Nehls, U. Rumenapp, and K.H. Jakobs, *m3 Muscarinic receptor-induced and Gi-mediated heterologous potentiation of phospholipase*

C stimulation: role of phosphoinositide synthesis. Mol Pharmacol, 1996. **50**(4): p. 1038-46.

122.   Schmidt, M., M. Frings, M.L. Mono, Y. Guo, P.A. Weernink, S. Evellin, L. Han, and K.H. Jakobs, *G protein-coupled receptor-induced sensitization of phospholipase C stimulation by receptor tyrosine kinases.* J Biol Chem, 2000. **275**(42): p. 32603-10.

123.   Saito, K., K.F. Tolias, A. Saci, H.B. Koon, L.A. Humphries, A. Scharenberg, D.J. Rawlings, J.P. Kinet, and C.L. Carpenter, *BTK regulates PtdIns-4,5-P2 synthesis: importance for calcium signaling and PI3K activity.* Immunity, 2003. **19**(5): p. 669-78.

124.   Cochet, C., O. Filhol, B. Payrastre, T. Hunter, and G.N. Gill, *Interaction between the epidermal growth factor receptor and phosphoinositide kinases.* J Biol Chem, 1991. **266**(1): p. 637-44.

125.   Minogue, S., M.G. Waugh, M.A. De Matteis, D.J. Stephens, F. Berditchevski, and J.J. Hsuan, *Phosphatidylinositol 4-kinase is required for endosomal trafficking and degradation of the EGF receptor.* J Cell Sci, 2006. **119**(Pt 3): p. 571-81.

126.   Pan, W., S.C. Choi, H. Wang, Y. Qin, L. Volpicelli-Daley, L. Swan, L. Lucast, C. Khoo, X. Zhang, L. Li, C.S. Abrams, S.Y. Sokol, and D. Wu, *Wnt3a-mediated formation of phosphatidylinositol 4,5-bisphosphate regulates LRP6 phosphorylation.* Science, 2008. **321**(5894): p. 1350-3.

127.   Itoh, T., H. Ishihara, Y. Shibasaki, Y. Oka, and T. Takenawa, *Autophosphorylation of type I phosphatidylinositol phosphate kinase regulates its lipid kinase activity.* J Biol Chem, 2000. **275**(25): p. 19389-94.

128.   Vancurova, I., J.H. Choi, H. Lin, J. Kuret, and A. Vancura, *Regulation of phosphatidylinositol 4-phosphate 5-kinase from Schizosaccharomyces pombe by casein kinase I.* J Biol Chem, 1999. **274**(2): p. 1147-55.

129.   Park, S.J., T. Itoh, and T. Takenawa, *Phosphatidylinositol 4-phosphate 5-kinase type I is regulated through phosphorylation response by extracellular stimuli.* J Biol Chem, 2001. **276**(7): p. 4781-7.

130.   Kunz, J., A. Fuelling, L. Kolbe, and R.A. Anderson, *Stereo-specific substrate recognition by phosphatidylinositol phosphate kinases is swapped by changing a single amino acid residue.* J Biol Chem, 2002. **277**(7): p. 5611-9.

131.   Chong, L.D., A. Traynor-Kaplan, G.M. Bokoch, and M.A. Schwartz, *The small GTP-binding protein Rho regulates a phosphatidylinositol 4-phosphate 5-kinase in mammalian cells.* Cell, 1994. **79**(3): p. 507-13.

132.   Amano, M., K. Chihara, K. Kimura, Y. Fukata, N. Nakamura, Y. Matsuura, and K. Kaibuchi, *Formation of actin stress fibers and focal adhesions enhanced by Rho-kinase.* Science, 1997. **275**(5304): p. 1308-11.

133.   Oude Weernink, P.A., P. Schulte, Y. Guo, J. Wetzel, M. Amano, K. Kaibuchi, S. Haverland, M. Voss, M. Schmidt, G.W. Mayr, and K.H. Jakobs, *Stimulation of phosphatidylinositol-4-phosphate 5-kinase by Rho-kinase.* J Biol Chem, 2000. **275**(14): p. 10168-74.

134.   van Horck, F.P., E. Lavazais, B.J. Eickholt, W.H. Moolenaar, and N. Divecha, *Essential role of type I(alpha) phosphatidylinositol 4-phosphate 5-kinase in neurite remodeling.* Curr Biol, 2002. **12**(3): p. 241-5.

135.   Hartwig, J.H., G.M. Bokoch, C.L. Carpenter, P.A. Janmey, L.A. Taylor, A. Toker, and T.P. Stossel, *Thrombin receptor ligation and activated Rac uncap*

actin filament barbed ends through phosphoinositide synthesis in permeabilized human platelets. Cell, 1995. **82**(4): p. 643-53.

136. Tolias, K.F., J.H. Hartwig, H. Ishihara, Y. Shibasaki, L.C. Cantley, and C.L. Carpenter, *Type Ialpha phosphatidylinositol-4-phosphate 5-kinase mediates Rac-dependent actin assembly.* Curr Biol, 2000. **10**(3): p. 153-6.

137. Doughman, R.L., A.J. Firestone, M.L. Wojtasiak, M.W. Bunce, and R.A. Anderson, *Membrane ruffling requires coordination between type Ialpha phosphatidylinositol phosphate kinase and Rac signaling.* J Biol Chem, 2003. **278**(25): p. 23036-45.

138. Halstead, J.R., N.E. Savaskan, I. van den Bout, F. Van Horck, A. Hajdo-Milasinovic, M. Snell, W.J. Keune, J.P. Klooster, P.L. Hordijk, and N. Divecha, *Rac controls PIP5K localisation and PtdIns(4,5)P2 synthesis, which modulates vinculin localisation and neurite dynamics.* J Cell Sci, 2010.

139. Chao, W.T., A.C. Daquinag, F. Ashcroft, and J. Kunz, *Type I PIPK-alpha regulates directed cell migration by modulating Rac1 plasma membrane targeting and activation.* J Cell Biol, 2010. **190**(2): p. 247-62.

140. Kost, B., E. Lemichez, P. Spielhofer, Y. Hong, K. Tolias, C. Carpenter, and N.H. Chua, *Rac homologues and compartmentalized phosphatidylinositol 4, 5-bisphosphate act in a common pathway to regulate polar pollen tube growth.* J Cell Biol, 1999. **145**(2): p. 317-30.

141. Oude Weernink, P.A., K. Meletiadis, S. Hommeltenberg, M. Hinz, H. Ishihara, M. Schmidt, and K.H. Jakobs, *Activation of type I phosphatidylinositol 4-phosphate 5-kinase isoforms by the Rho GTPases, RhoA, Rac1, and Cdc42.* J Biol Chem, 2004. **279**(9): p. 7840-9.

142. Ren, X.D., G.M. Bokoch, A. Traynor-Kaplan, G.H. Jenkins, R.A. Anderson, and M.A. Schwartz, *Physical association of the small GTPase Rho with a 68-kDa phosphatidylinositol 4-phosphate 5-kinase in Swiss 3T3 cells.* Mol Biol Cell, 1996. **7**(3): p. 435-42.

143. Tolias, K.F., L.C. Cantley, and C.L. Carpenter, *Rho family GTPases bind to phosphoinositide kinases.* J Biol Chem, 1995. **270**(30): p. 17656-9.

144. Honda, A., M. Nogami, T. Yokozeki, M. Yamazaki, H. Nakamura, H. Watanabe, K. Kawamoto, K. Nakayama, A.J. Morris, M.A. Frohman, and Y. Kanaho, *Phosphatidylinositol 4-phosphate 5-kinase alpha is a downstream effector of the small G protein ARF6 in membrane ruffle formation.* Cell, 1999. **99**(5): p. 521-32.

145. Brown, F.D., A.L. Rozelle, H.L. Yin, T. Balla, and J.G. Donaldson, *Phosphatidylinositol 4,5-bisphosphate and Arf6-regulated membrane traffic.* J Cell Biol, 2001. **154**(5): p. 1007-17.

146. Krauss, M., M. Kinuta, M.R. Wenk, P. De Camilli, K. Takei, and V. Haucke, *ARF6 stimulates clathrin/AP-2 recruitment to synaptic membranes by activating phosphatidylinositol phosphate kinase type Igamma.* J Cell Biol, 2003. **162**(1): p. 113-24.

147. Wong, K.W. and R.R. Isberg, *Arf6 and phosphoinositol-4-phosphate-5-kinase activities permit bypass of the Rac1 requirement for beta1 integrin-mediated bacterial uptake.* J Exp Med, 2003. **198**(4): p. 603-14.

148. Divecha, N., M. Roefs, A. Los, J. Halstead, A. Bannister, and C. D'Santos, *Type I PIPkinases interact with and are regulated by the retinoblastoma susceptibility gene product-pRB.* Curr Biol, 2002. **12**(7): p. 582-7.

149. Boronenkov, I.V., J.C. Loijens, M. Umeda, and R.A. Anderson, *Phosphoinositide signaling pathways in nuclei are associated with nuclear speckles containing pre-mRNA processing factors.* Mol Biol Cell, 1998. **9**(12): p. 3547-60.

150. Vann, L.R., F.B. Wooding, R.F. Irvine, and N. Divecha, *Metabolism and possible compartmentalization of inositol lipids in isolated rat-liver nuclei.* Biochem J, 1997. **327 (Pt 2)**: p. 569-76.

151. Payrastre, B., K. Missy, S. Giuriato, S. Bodin, M. Plantavid, and M. Gratacap, *Phosphoinositides: key players in cell signalling, in time and space.* Cell Signal, 2001. **13**(6): p. 377-87.

152. Powner, D.J. and M.J. Wakelam, *The regulation of phospholipase D by inositol phospholipids and small GTPases.* FEBS Lett, 2002. **531**(1): p. 62-4.

153. Exton, J.H., *Regulation of phospholipase D.* FEBS Lett, 2002. **531**(1): p. 58-61.

154. Ishihara, H., Y. Shibasaki, N. Kizuki, H. Katagiri, Y. Yazaki, T. Asano, and Y. Oka, *Cloning of cDNAs encoding two isoforms of 68-kDa type I phosphatidylinositol-4-phosphate 5-kinase.* J Biol Chem, 1996. **271**(39): p. 23611-4.

155. Homma, K., S. Terui, M. Minemura, H. Qadota, Y. Anraku, Y. Kanaho, and Y. Ohya, *Phosphatidylinositol-4-phosphate 5-kinase localized on the plasma membrane is essential for yeast cell morphogenesis.* J Biol Chem, 1998. **273**(25): p. 15779-86.

156. Desrivieres, S., F.T. Cooke, P.J. Parker, and M.N. Hall, *MSS4, a phosphatidylinositol-4-phosphate 5-kinase required for organization of the actin cytoskeleton in Saccharomyces cerevisiae.* J Biol Chem, 1998. **273**(25): p. 15787-93.

157. Carvajal, J.J., M.A. Pook, M. dos Santos, K. Doudney, R. Hillermann, S. Minogue, R. Williamson, J.J. Hsuan, and S. Chamberlain, *The Friedreich's ataxia gene encodes a novel phosphatidylinositol-4- phosphate 5-kinase.* Nat Genet, 1996. **14**(2): p. 157-62.

158. Jenkins, G.H., P.L. Fisette, and R.A. Anderson, *Type I phosphatidylinositol 4-phosphate 5-kinase isoforms are specifically stimulated by phosphatidic acid.* J Biol Chem, 1994. **269**(15): p. 11547-54.

159. Chao, W.T., F. Ashcroft, A.C. Daquinag, T. Vadakkan, Z. Wei, P. Zhang, M.E. Dickinson, and J. Kunz, *Type I phosphatidylinositol phosphate kinase beta regulates focal adhesion disassembly by promoting beta1 integrin endocytosis.* Mol Cell Biol, 2010. **30**(18): p. 4463-79.

160. Padron, D., Y.J. Wang, M. Yamamoto, H. Yin, and M.G. Roth, *Phosphatidylinositol phosphate 5-kinase Ibeta recruits AP-2 to the plasma membrane and regulates rates of constitutive endocytosis.* J Cell Biol, 2003. **162**(4): p. 693-701.

161. Wang, L., G. Li, and S. Sugita, *A central kinase domain of type I phosphatidylinositol phosphate kinases is sufficient to prime exocytosis: isoform specificity and its underlying mechanism.* J Biol Chem, 2005. **280**(16): p. 16522-7.

162. Wang, Y., R.I. Litvinov, X. Chen, T.L. Bach, L. Lian, B.G. Petrich, S.J. Monkley, D.R. Critchley, T. Sasaki, M.J. Birnbaum, J.W. Weisel, J. Hartwig, and C.S. Abrams, *Loss of PIP5KIgamma, unlike other PIP5KI isoforms,*

impairs the integrity of the membrane cytoskeleton in murine megakaryocytes. J Clin Invest, 2008. **118**(2): p. 812-9.

163.   Volpicelli-Daley, L.A., L. Lucast, L.W. Gong, L. Liu, J. Sasaki, T. Sasaki, C.S. Abrams, Y. Kanaho, and P. De Camilli, *Phosphatidylinositol-4-phosphate 5-kinases and phosphatidylinositol 4,5-bisphosphate synthesis in the brain.* J Biol Chem, 2010. **285**(37): p. 28708-14.

164.   Ling, K., R.L. Doughman, V.V. Iyer, A.J. Firestone, S.F. Bairstow, D.F. Mosher, M.D. Schaller, and R.A. Anderson, *Tyrosine phosphorylation of type Igamma phosphatidylinositol phosphate kinase by Src regulates an integrin-talin switch.* J Cell Biol, 2003. **163**(6): p. 1339-49.

165.   Wenk, M.R., L. Pellegrini, V.A. Klenchin, G. Di Paolo, S. Chang, L. Daniell, M. Arioka, T.F. Martin, and P. De Camilli, *PIP kinase Igamma is the major PI(4,5)P(2) synthesizing enzyme at the synapse.* Neuron, 2001. **32**(1): p. 79-88.

166.   Di Paolo, G., H.S. Moskowitz, K. Gipson, M.R. Wenk, S. Voronov, M. Obayashi, R. Flavell, R.M. Fitzsimonds, T.A. Ryan, and P. De Camilli, *Impaired PtdIns(4,5)P2 synthesis in nerve terminals produces defects in synaptic vesicle trafficking.* Nature, 2004. **431**(7007): p. 415-22.

167.   Giudici, M.L., K.A. Hinchliffe, and R.F. Irvine, *Phosphatidylinositol phosphate kinases.* J Endocrinol Invest, 2004. **27**(6 Suppl): p. 137-42.

168.   Wang, Y., L. Lian, J.A. Golden, E.E. Morrisey, and C.S. Abrams, *PIP5KI gamma is required for cardiovascular and neuronal development.* Proc Natl Acad Sci U S A, 2007. **104**(28): p. 11748-53.

169.   Graveley, B.R., *Alternative splicing: increasing diversity in the proteomic world.* Trends Genet, 2001. **17**(2): p. 100-7.

170.   Schill, N.J. and R.A. Anderson, *Two novel phosphatidylinositol-4-phosphate 5-kinase type Igamma splice variants expressed in human cells display distinctive cellular targeting.* Biochem J, 2009. **422**(3): p. 473-82.

171.   Di Paolo, G., L. Pellegrini, K. Letinic, G. Cestra, R. Zoncu, S. Voronov, S. Chang, J. Guo, M.R. Wenk, and P. De Camilli, *Recruitment and regulation of phosphatidylinositol phosphate kinase type 1 gamma by the FERM domain of talin.* Nature, 2002. **420**(6911): p. 85-9.

172.   Ling, K., R.L. Doughman, A.J. Firestone, M.W. Bunce, and R.A. Anderson, *Type I gamma phosphatidylinositol phosphate kinase targets and regulates focal adhesions.* Nature, 2002. **420**(6911): p. 89-93.

173.   Sun, Y., K. Ling, M.P. Wagoner, and R.A. Anderson, *Type I gamma phosphatidylinositol phosphate kinase is required for EGF-stimulated directional cell migration.* J Cell Biol, 2007. **178**(2): p. 297-308.

174.   Bairstow, S.F., K. Ling, X. Su, A.J. Firestone, C. Carbonara, and R.A. Anderson, *Type Igamma661 phosphatidylinositol phosphate kinase directly interacts with AP2 and regulates endocytosis.* J Biol Chem, 2006. **281**(29): p. 20632-42.

175.   Nakano-Kobayashi, A., M. Yamazaki, T. Unoki, T. Hongu, C. Murata, R. Taguchi, T. Katada, M.A. Frohman, T. Yokozeki, and Y. Kanaho, *Role of activation of PIP5Kgamma661 by AP-2 complex in synaptic vesicle endocytosis.* EMBO J, 2007. **26**(4): p. 1105-16.

176.   Ling, K., S.F. Bairstow, C. Carbonara, D.A. Turbin, D.G. Huntsman, and R.A. Anderson, *Type Igamma phosphatidylinositol phosphate kinase modulates*

adherens junction and E-cadherin trafficking via a direct interaction with mu 1B adaptin. J Cell Biol, 2007. **176**(3): p. 343-53.

177.   Kahlfeldt, N., A. Vahedi-Faridi, S.J. Koo, J.G. Schafer, G. Krainer, S. Keller, W. Saenger, M. Krauss, and V. Haucke, *Molecular basis for association of PIPKI gamma-p90 with clathrin adaptor AP-2.* J Biol Chem, 2010. **285**(4): p. 2734-49.

178.   Kim, H., R. Klein, J. Majewski, and J. Ott, *Estimating rates of alternative splicing in mammals and invertebrates.* Nat Genet, 2004. **36**(9): p. 915-6; author reply 916-7.

179.   Giudici, M.L., K. Lee, R. Lim, and R.F. Irvine, *The intracellular localisation and mobility of Type Igamma phosphatidylinositol 4P 5-kinase splice variants.* FEBS Lett, 2006. **580**(30): p. 6933-7.

180.   Bondeva, T., L. Pirola, G. Bulgarelli-Leva, I. Rubio, R. Wetzker, and M.P. Wymann, *Bifurcation of lipid and protein kinase signals of PI3Kgamma to the protein kinases PKB and MAPK.* Science, 1998. **282**(5387): p. 293-6.

181.   Kim, C., N.H. Xuong, and S.S. Taylor, *Crystal structure of a complex between the catalytic and regulatory (RIalpha) subunits of PKA.* Science, 2005. **307**(5710): p. 690-6.

182.   Wybenga-Groot, L.E., B. Baskin, S.H. Ong, J. Tong, T. Pawson, and F. Sicheri, *Structural basis for autoinhibition of the Ephb2 receptor tyrosine kinase by the unphosphorylated juxtamembrane region.* Cell, 2001. **106**(6): p. 745-57.

183.   Goldberg, J., A.C. Nairn, and J. Kuriyan, *Structural basis for the autoinhibition of calcium/calmodulin-dependent protein kinase I.* Cell, 1996. **84**(6): p. 875-87.

184.   de Pereda, J.M., K.L. Wegener, E. Santelli, N. Bate, M.H. Ginsberg, D.R. Critchley, I.D. Campbell, and R.C. Liddington, *Structural basis for phosphatidylinositol phosphate kinase type Igamma binding to talin at focal adhesions.* J Biol Chem, 2005. **280**(9): p. 8381-6.

185.   Ferguson, K.M., M.A. Lemmon, J. Schlessinger, and P.B. Sigler, *Structure of the high affinity complex of inositol trisphosphate with a phospholipase C pleckstrin homology domain.* Cell, 1995. **83**(6): p. 1037-46.

186.   Ma, A.D., L.F. Brass, and C.S. Abrams, *Pleckstrin associates with plasma membranes and induces the formation of membrane projections: requirements for phosphorylation and the NH2-terminal PH domain.* J Cell Biol, 1997. **136**(5): p. 1071-9.

187.   Yagisawa, H., K. Sakuma, H.F. Paterson, R. Cheung, V. Allen, H. Hirata, Y. Watanabe, M. Hirata, R.L. Williams, and M. Katan, *Replacements of single basic amino acids in the pleckstrin homology domain of phospholipase C-delta1 alter the ligand binding, phospholipase activity, and interaction with the plasma membrane.* J Biol Chem, 1998. **273**(1): p. 417-24.

188.   Baraldi, E., K. Djinovic Carugo, M. Hyvonen, P.L. Surdo, A.M. Riley, B.V. Potter, R. O'Brien, J.E. Ladbury, and M. Saraste, *Structure of the PH domain from Bruton's tyrosine kinase in complex with inositol 1,3,4,5-tetrakisphosphate.* Structure, 1999. **7**(4): p. 449-60.

189.   Harlan, J.E., P.J. Hajduk, H.S. Yoon, and S.W. Fesik, *Pleckstrin homology domains bind to phosphatidylinositol-4,5-bisphosphate.* Nature, 1994. **371**(6493): p. 168-70.

190. Isakoff, S.J., T. Cardozo, J. Andreev, Z. Li, K.M. Ferguson, R. Abagyan, M.A. Lemmon, A. Aronheim, and E.Y. Skolnik, *Identification and analysis of PH domain-containing targets of phosphatidylinositol 3-kinase using a novel in vivo assay in yeast.* EMBO J, 1998. **17**(18): p. 5374-87.

191. Gaullier, J.M., A. Simonsen, A. D'Arrigo, B. Bremnes, H. Stenmark, and R. Aasland, *FYVE fingers bind PtdIns(3)P.* Nature, 1998. **394**(6692): p. 432-3.

192. Wurmser, A.E., J.D. Gary, and S.D. Emr, *Phosphoinositide 3-kinases and their FYVE domain-containing effectors as regulators of vacuolar/lysosomal membrane trafficking pathways.* J Biol Chem, 1999. **274**(14): p. 9129-32.

193. Fruman, D.A., L.E. Rameh, and L.C. Cantley, *Phosphoinositide binding domains: embracing 3-phosphate.* Cell, 1999. **97**(7): p. 817-20.

194. Misra, S. and J.H. Hurley, *Crystal structure of a phosphatidylinositol 3-phosphate-specific membrane-targeting motif, the FYVE domain of Vps27p.* Cell, 1999. **97**(5): p. 657-66.

195. Sbrissa, D., O.C. Ikonomov, and A. Shisheva, *Phosphatidylinositol 3-phosphate-interacting domains in PIKfyve. Binding specificity and role in PIKfyve. Endomembrane localization.* J Biol Chem, 2002. **277**(8): p. 6073-9.

196. Heo, W.D., T. Inoue, W.S. Park, M.L. Kim, B.O. Park, T.J. Wandless, and T. Meyer, *PI(3,4,5)P3 and PI(4,5)P2 lipids target proteins with polybasic clusters to the plasma membrane.* Science, 2006. **314**(5804): p. 1458-61.

197. Kunz, J., M.P. Wilson, M. Kisseleva, J.H. Hurley, P.W. Majerus, and R.A. Anderson, *The activation loop of phosphatidylinositol phosphate kinases determines signaling specificity.* Mol Cell, 2000. **5**(1): p. 1-11.

198. Arioka, M., S. Nakashima, Y. Shibasaki, and K. Kitamoto, *Dibasic amino acid residues at the carboxy-terminal end of kinase homology domain participate in the plasma membrane localization and function of phosphatidylinositol 5-kinase gamma.* Biochem Biophys Res Commun, 2004. **319**(2): p. 456-63.

199. Turina, P. and R.A. Capaldi, *ATP binding causes a conformational change in the gamma subunit of the Escherichia coli F1ATPase which is reversed on bond cleavage.* Biochemistry, 1994. **33**(47): p. 14275-80.

200. Kong, X., X. Wang, S. Misra, and J. Qin, *Structural basis for the phosphorylation-regulated focal adhesion targeting of type Igamma phosphatidylinositol phosphate kinase (PIPKIgamma) by talin.* J Mol Biol, 2006. **359**(1): p. 47-54.

201. Gaudette, D.C. and B.J. Holub, *Effect of genistein, a tyrosine kinase inhibitor, on U46619-induced phosphoinositide phosphorylation in human platelets.* Biochem Biophys Res Commun, 1990. **170**(1): p. 238-42.

202. Barsukov, I.L., A. Prescot, N. Bate, B. Patel, D.N. Floyd, N. Bhanji, C.R. Bagshaw, K. Letinic, G. Di Paolo, P. De Camilli, G.C. Roberts, and D.R. Critchley, *Phosphatidylinositol phosphate kinase type 1gamma and beta1-integrin cytoplasmic domain bind to the same region in the talin FERM domain.* J Biol Chem, 2003. **278**(33): p. 31202-9.

203. Lee, S.Y., S. Voronov, K. Letinic, A.C. Nairn, G. Di Paolo, and P. De Camilli, *Regulation of the interaction between PIPKI gamma and talin by proline-directed protein kinases.* J Cell Biol, 2005. **168**(5): p. 789-99.

204. Clarke, J.H., M. Wang, and R.F. Irvine, *Localization, regulation and function of type II phosphatidylinositol 5-phosphate 4-kinases.* Adv Enzyme Regul, 2009. **50**(1): p. 12-8.

205. Brough, D., F. Bhatti, and R.F. Irvine, *Mobility of proteins associated with the plasma membrane by interaction with inositol lipids.* J Cell Sci, 2005. **118**(Pt 14): p. 3019-25.

206. Blom, N., T. Sicheritz-Ponten, R. Gupta, S. Gammeltoft, and S. Brunak, *Prediction of post-translational glycosylation and phosphorylation of proteins from the amino acid sequence.* Proteomics, 2004. **4**(6): p. 1633-49.

207. Finn, R.D., J. Mistry, J. Tate, P. Coggill, A. Heger, J.E. Pollington, O.L. Gavin, P. Gunasekaran, G. Ceric, K. Forslund, L. Holm, E.L. Sonnhammer, S.R. Eddy, and A. Bateman, *The Pfam protein families database.* Nucleic Acids Res, 2010. **38**(Database issue): p. D211-22.

208. Dunker, A.K., J.D. Lawson, C.J. Brown, R.M. Williams, P. Romero, J.S. Oh, C.J. Oldfield, A.M. Campen, C.M. Ratliff, K.W. Hipps, J. Ausio, M.S. Nissen, R. Reeves, C. Kang, C.R. Kissinger, R.W. Bailey, M.D. Griswold, W. Chiu, E.C. Garner, and Z. Obradovic, *Intrinsically disordered protein.* J Mol Graph Model, 2001. **19**(1): p. 26-59.

209. Linding, R., L.J. Jensen, F. Diella, P. Bork, T.J. Gibson, and R.B. Russell, *Protein disorder prediction: implications for structural proteomics.* Structure, 2003. **11**(11): p. 1453-9.

210. Ward, J.J., J.S. Sodhi, L.J. McGuffin, B.F. Buxton, and D.T. Jones, *Prediction and functional analysis of native disorder in proteins from the three kingdoms of life.* J Mol Biol, 2004. **337**(3): p. 635-45.

211. Romero, P., Z. Obradovic, and A.K. Dunker, *Natively disordered proteins: functions and predictions.* Appl Bioinformatics, 2004. **3**(2-3): p. 105-13.

212. Wang, J., A. Arbuzova, G. Hangyas-Mihalyne, and S. McLaughlin, *The effector domain of myristoylated alanine-rich C kinase substrate binds strongly to phosphatidylinositol 4,5-bisphosphate.* J Biol Chem, 2001. **276**(7): p. 5012-9.

213. Wang, J., A. Gambhir, G. Hangyas-Mihalyne, D. Murray, U. Golebiewska, and S. McLaughlin, *Lateral sequestration of phosphatidylinositol 4,5-bisphosphate by the basic effector domain of myristoylated alanine-rich C kinase substrate is due to nonspecific electrostatic interactions.* J Biol Chem, 2002. **277**(37): p. 34401-12.

214. Teruel, M.N., T.A. Blanpied, K. Shen, G.J. Augustine, and T. Meyer, *A versatile microporation technique for the transfection of cultured CNS neurons.* J Neurosci Methods, 1999. **93**(1): p. 37-48.

215. Schmiedeberg, L., P. Skene, A. Deaton, and A. Bird, *A temporal threshold for formaldehyde crosslinking and fixation.* PLoS One, 2009. **4**(2): p. e4636.

216. Kohno, T., Y. Nakano, N. Kitoh, H. Yagi, K. Kato, A. Baba, and M. Hattori, *C-terminal region-dependent change of antibody-binding to the Eighth Reelin repeat reflects the signaling activity of Reelin.* J Neurosci Res, 2009. **87**(14): p. 3043-53.

217. Ast, G., *How did alternative splicing evolve?* Nat Rev Genet, 2004. **5**(10): p. 773-82.

218. Shapiro, M.B. and P. Senapathy, *RNA splice junctions of different classes of eukaryotes: sequence statistics and functional implications in gene expression.* Nucleic Acids Res, 1987. **15**(17): p. 7155-74.

219. Bortfeldt, R., S. Schindler, K. Szafranski, S. Schuster, and D. Holste, *Comparative analysis of sequence features involved in the recognition of tandem splice sites.* BMC Genomics, 2008. **9**: p. 202.

220. Sugnet, C.W., W.J. Kent, M. Ares, Jr., and D. Haussler, *Transcriptome and genome conservation of alternative splicing events in humans and mice.* Pac Symp Biocomput, 2004: p. 66-77.

221. Hutton, M., C.L. Lendon, P. Rizzu, M. Baker, S. Froelich, H. Houlden, S. Pickering-Brown, S. Chakraverty, A. Isaacs, A. Grover, J. Hackett, J. Adamson, S. Lincoln, D. Dickson, P. Davies, R.C. Petersen, M. Stevens, E. de Graaff, E. Wauters, J. van Baren, M. Hillebrand, M. Joosse, J.M. Kwon, P. Nowotny, L.K. Che, J. Norton, J.C. Morris, L.A. Reed, J. Trojanowski, H. Basun, L. Lannfelt, M. Neystat, S. Fahn, F. Dark, T. Tannenberg, P.R. Dodd, N. Hayward, J.B. Kwok, P.R. Schofield, A. Andreadis, J. Snowden, D. Craufurd, D. Neary, F. Owen, B.A. Oostra, J. Hardy, A. Goate, J. van Swieten, D. Mann, T. Lynch, and P. Heutink, *Association of missense and 5'-splice-site mutations in tau with the inherited dementia FTDP-17.* Nature, 1998. **393**(6686): p. 702-5.

222. Pan, Q., O. Shai, C. Misquitta, W. Zhang, A.L. Saltzman, N. Mohammad, T. Babak, H. Siu, T.R. Hughes, Q.D. Morris, B.J. Frey, and B.J. Blencowe, *Revealing global regulatory features of mammalian alternative splicing using a quantitative microarray platform.* Mol Cell, 2004. **16**(6): p. 929-41.

223. Gossen, M. and H. Bujard, *Tight control of gene expression in mammalian cells by tetracycline-responsive promoters.* Proc Natl Acad Sci U S A, 1992. **89**(12): p. 5547-51.

224. Gossen, M., S. Freundlieb, G. Bender, G. Muller, W. Hillen, and H. Bujard, *Transcriptional activation by tetracyclines in mammalian cells.* Science, 1995. **268**(5218): p. 1766-9.

225. Inoue, T., W.D. Heo, J.S. Grimley, T.J. Wandless, and T. Meyer, *An inducible translocation strategy to rapidly activate and inhibit small GTPase signaling pathways.* Nat Methods, 2005. **2**(6): p. 415-8.

226. Aebersold, R.H., J. Leavitt, R.A. Saavedra, L.E. Hood, and S.B. Kent, *Internal amino acid sequence analysis of proteins separated by one- or two-dimensional gel electrophoresis after in situ protease digestion on nitrocellulose.* Proc Natl Acad Sci U S A, 1987. **84**(20): p. 6970-4.

227. Yamagata, A., D.B. Kristensen, Y. Takeda, Y. Miyamoto, K. Okada, M. Inamatsu, and K. Yoshizato, *Mapping of phosphorylated proteins on two-dimensional polyacrylamide gels using protein phosphatase.* Proteomics, 2002. **2**(9): p. 1267-76.

228. Sickmann, A., M. Mreyen, and H.E. Meyer, *Identification of modified proteins by mass spectrometry.* IUBMB Life, 2002. **54**(2): p. 51-7.

229. Mann, M. and O.N. Jensen, *Proteomic analysis of post-translational modifications.* Nat Biotechnol, 2003. **21**(3): p. 255-61.

230. Loyet, K.M., J.T. Stults, and D. Arnott, *Mass spectrometric contributions to the practice of phosphorylation site mapping through 2003: a literature review.* Mol Cell Proteomics, 2005. **4**(3): p. 235-45.

231. Blackburn, K. and M.B. Goshe, *Challenges and strategies for targeted phosphorylation site identification and quantification using mass spectrometry analysis.* Brief Funct Genomic Proteomic, 2009. **8**(2): p. 90-103.

232. Zhao, J., T.H. Patwa, M. Pal, W. Qiu, and D.M. Lubman, *Analysis of protein glycosylation and phosphorylation using liquid phase separation, protein microarray technology, and mass spectrometry.* Methods Mol Biol, 2009. **492**: p. 321-51.

233. Zhang, H., T. Zhang, K. Chen, K.D. Kedarisetti, M.J. Mizianty, Q. Bao, W. Stach, and L. Kurgan, *Critical assessment of high-throughput standalone methods for secondary structure prediction.* Brief Bioinform, 2011.